Tertiary and carboniferous magmatism around Lundy Island and the outer Bristol Channel - a geophysical and geochemical perspective

Thesis

TERTIARY AND CARBONIFEROUS MAGMATISM AROUND LUNDY ISLAND AND THE OUTER BRISTOL CHANNEL - A GEOPHYSICAL AND GEOCHEMICAL PERSPECTIVE

A thesis presented for the degree of
Doctor of Philosophy

by

CLIVE LYNTON ROBERTS
B.A. (Hons) Open, 1986

Department of Earth Sciences,

The Open University

November, 1996

RESEARCH DEGREES CENTRE

LIBRARY AUTHORISATION FORM

Please return this form to the The Research Degrees Centre with the two bound copies of your thesis to be deposited with the University Library.
All students should complete Part 1. Part 2 only applies to PhD students.

Student: CLIVE L. ROBERTS PI: L0104805

Degree: PhD

Thesis title: TERTIARY + CARBONIFEROUS MAGMATISM AROUND LUNDY ISLAND AND THE OUTER BRISTOL CHANNEL

Part 1 Open University Library Authorisation [to be completed by all students]

I confirm that I am willing for my thesis to be made available to readers by the Open University Library, and that it may be photocopied, subject to the discretion of the Librarian.

Signed: Clive Roberts Date: 28/4/98

Part 2 British Library Authorisation [to be completed by PhD students only]

If you want a copy of your PhD thesis to be available on loan to the British Library Thesis Service as and when it is requested, you must sign a British Library Doctoral Thesis Agreement Form. Please return it to the Research Degrees Centre with this form. The British Library will publicise the details of your thesis and may request a copy on loan from the University Library. Information on the presentation of the thesis is given in the Agreement Form.

The University has agreed that your participation in the British Library Thesis Service should be voluntary. Please tick either (a) or (b) to indicate your intentions.

[a] ☑ I am willing for the Open University to loan the British Library a copy of my thesis. A signed Agreement Form is attached.

[b] ☐ I do not wish the Open University to loan the British Library a copy of my thesis.

Signed: Clive Roberts Date: 28/4/98

ABSTRACT

The British Tertiary Volcanic Province comprises central volcanic complexes with positive gravity and magnetic anomalies, some centres associated with both large volumes of continental flood basalts and regional dyke swarms. The Lundy Island is the southernmost expression of Tertiary volcanism and consists of granite intruded by around 200 dykes and associated with positive gravity and magnetic anomalies. The Lundy Dyke Swarm comprises basalt/dolerite and trachyte to rhyolite intrusions within host Tertiary granite (58.7 ± 1.6 Ma) and Devonian sediments. Outcrops of dykes are confined to coastal exposures on Lundy as they are veneered by peat over most of the island. Dykes present paired magnetic anomaly profiles, which allows their trends to be determined by proton magnetometry. The dykes have a radial disposition superimposed on a ENE-WSW regional trend. Anisotropy of magnetic susceptibility studies indicate that magma for the radial component was emplaced at shallow to moderate inclinations, suggesting a relatively shallow origin near to the western border of Lundy Island. The regional component was emplaced at shallow to sub-horizontal angles, suggesting lateral movement of magma from a possible source 12 km to the northwest.

Geochemical signatures indicate that the Lundy Dyke Swarm was transitional between plume-related magmatism and partial melting of the lithospheric mantle, the magma being stored in several small storage bodies at differing depths in the upper continental crust, rather than in one large magma chamber. Basic dykes at Lee Bay (60 ± 0.6 to 63.1 ± 0.7 Ma) pre-date the Lundy Dyke Swarm and were derived from a discrete magma chamber, possibly near to Morte Point. Conversely, other dykes in North Devon (Fremington dyke - 292.4 ± 1.7 Ma; Horse-Shoe Rocks - 339.6 ± 7.4 Ma) are not directly related to Tertiary magmatism, even though the Horse-Shoe Rocks have a Tertiary palaeomagnetic overprint.

The Lundy Igneous Complex (comprising granite, dykes and sub-surface basic rocks) is situated close to the intersection of the Variscan Front and the Welsh Caledonides massif where the continental thickness is between 25 and 27 km. Emplacement of magma was assisted by the heavily fractured nature of the host sediments. However, a large positive gravity anomaly to the northwest of Lundy Island does not have a corresponding magnetic anomaly and so is interpreted as the response to relatively dense uplifted basement in the Lundy Horst rather than a large volume of basic rocks. Thus, the Lundy Igneous Complex probably did not produce sub-aerial volcanic activity, as pressure in the magma chamber would not have exceeded the overlying lithostatic load, despite the fractured nature of the host rocks.

TABLE OF CONTENTS

Chapter 1: INTRODUCTION - THE BRITISH TERTIARY VOLCANIC PROVINCE (BTVP)

1.1 Introduction 1
1.1.1 The timing of Tertiary volcanism 3
1.1.2 Physical setting of the BTVP 4
1.1.3 Geophysical Investigations within the BTVP 5
1.1.4 Geochemistry of Tertiary magmatism 7
1.2 Regional Geological Relationships 8
1.2.1 Geology of North Devon 12
1.2.1.1 The sedimentary record 12
1.2.1.1 The igneous record 15
1.2.2 The Bristol Channel area 16
1.2.2.1 Tertiary sediments 17
1.2.3 The Lundy Igneous Complex 18
1.2.3.1 The Lundy Granite 18
1.2.3.2 The Lundy Dyle Suite 21
1.2.4 Structural development in the Bristol Channel 22
1.2.5 Geophysical investigations in the Lundy area 23
1.3 Outline of present work 24
1.3.1 Structure of the thesis 24
1.3.2 Aims and objectives 25

Chapter 2: METHODOLOGY

2.1 Field Techniques 26
2.1.1 Mapping of field relations (dykes) on Lundy 26
2.1.2 Mapping of field relations (joints) 26
2.1.3 Proton magnetometry 27
2.2 Laboratory-based Magnetic Techniques 32
2.2.1 Magnetic susceptibility 32
2.2.2 Anisotropy of magnetic susceptibility (AMS) of dykes 33
2.2.3 Curie temperature determinations and hysteresis loops 39
2.2.4 Natural remanent magnetization (NRM) 40
2.3 Computer Modelling 41
2.3.1 Gravity and magnetic data 41
2.3.2 Modelling of gravity data 44
2.3.3 Modelling of magnetic data 48
2.4 Laboratory-based Geochemistry Techniques 49
2.4.1 Rock sampling and transmitted light petrographic survey 52
2.4.2 Sample preparation for geochemical studies 52
2.4.3 X-ray fluorescence (XRF) analysis 53
2.4.3.1 Sample preparation 53
2.4.3.2 Instrumentation 54
2.4.4 $^{40}Ar/^{39}Ar$ dating method 54

Chapter 3: THE LUNDY DYKE SWARM AND NORTH DEVON

3.1 Introduction 56
3.2 Field Observations 56
3.2.1 Dip and strikes of dykes 56
3.2.2 Direction of flow indicators in dykes 61
3.3 Field-related Magnetic Observations 68
3.3.1 Magnetic anomaly profiles on Lundy Island 68
3.3.2 Natural remanent magnetization (NRM) of dykes 71

3.3.2.1 Lee Bay dykes 73
3.3.2.2 Horse-Shoe Rocks 75
3.3.2.3 Fremington dyke 77
3.3.3 Koenigsberger ratio and modelling of individual dykes 77
3.3.4 Computer modelling of individual dykes 79
3.3.4.1 Reversely magnetized dykes 82
3.3.4.2 Normally magnetized dykes 82
3.3.5 Implied field relations of dykes on Lundy Island 83
3.4 Physical Properties of Dykes and Intrusions 88
3.4.1 Magnetic granulometry from hysteresis loops 88
3.4.1.1 Hysteresis loops from Lundy and Lee Bay 90
3.4.2 Curie temperature determinations 92
3.4.2.1 The Lee Bay dyke assemblage 92
3.4.2.2 The Lundy dyke association 94
3.4.3 Anisotropy of magnetic susceptibility (AMS) 95
3.4.3.1 Magnetic anisotropy in volcanic rocks 98
3.4.3.2 AMS results for the Lundy Dyke Swarm 99
3.4.3.3 Interpretation of results 104

Chapter 4: GEOCHEMISTRY OF ROCKS FROM NORTH DEVON AND LUNDY ISLAND

4.1 Introduction 107
4.2 Petrography 108
4.2.1 Dykes of Lundy Island 109
4.2.2 The Lee Bay mini-dyke association 111
4.2.3 The Horse-Shoe Rocks 115
4.2.4 The Fremington dyke 116
4.3 The Role of Weathering 119
4.4 Ages of the Rocks 120
4.4.1 The Ar-Ar dating method 121
4.4.2 New Ar-Ar data 123
4.4.2.1 Ages of dykes at Lee Bay 124
4.4.2.2 Age of the Horse-Shoe rocks 128
4.4.2.3 Age of the Fremington dyke 131
4.5 Whole Rock Major Element Geochemistry 135
4.5.1 Lundy Island 135
4.5.2 Lee Bay 140
4.5.3 The Horse-Shoe Rocks 141
4.5.4 Fremington dyke 142
4.6 Trace Element Geochemistry 144
4.6.1 Lundy Island 144
4.6.2 Lee Bay 149
4.6.3 Permo-Carboniferous rocks 151
4.7 Petrogenesis of Tertiary rocks in North Devon 154

Chapter 5: REGIONAL GEOPHYSICAL MODELLING

5.1 Introduction 162
5.2 Regional Magnetic Data 162
5.2.1 Data reduction 163
5.2.2 Aeromagnetic anomaly map of the outer Bristol Channel 165
5.3 Regional Gravity Data 171
5.3.1 Reduction of data 173
5.3.1.1 Latitude corrections 173
5.3.1.2 Free-air corrections 174
5.3.1.3 Bouguer corrections 175
5.3.1.4 Terrain corrections 175
5.3.1.5 Eötvös correction 176
5.3.2 Bouguer gravity anomaly map 176

5.3.3 The regional gravity field 180
5.4 Computer Modelling of Geophysical Data 181
5.4.1 Theoretical responses to magnetic models 183
5.4.1.1 The Morte Point anomaly 183
5.4.1.2 Magnetic anomalies near to Lundy Island 186
5.4.2 Theoretical responses to gravity models 191
5.4.2.1 Modelling around the Lundy horst 193
5.5 Summary of Magnetic and Gravity models 200

Chapter 6: IMPLICATIONS FOR LUNDY VOLCANO AND TERTIARY MAGMATISM IN SOUTH-WEST ENGLAND

6.1 Introduction 202
6.1.1 Geochemical constraints on the origin of the Lundy magmas 203
6.2 Physical Setting of Magmatism 208
6.2.1 Discrepancies in geophysical modelling 208
6.2.2 Relationships between dykes and volcano 215
6.2.3 Lundy Volcano? 216
6.3 Tectonic Framework of the Lundy Igneous Complex 218
6.3.1 Implications of the early Tertiary stress regimes on the Lundy Igneous Complex 219
6.3.2 Magmatic activity and the Variscan Orogeny 221
6.3.3 Igneous activity and the Icelandic plume 223
6.3.4 The siting of the Lundy Igneous Complex 226

References 228
Appendices 247

LIST OF FIGURES

Figure 1.1:	Intrusive centres and dykes within the British Tertiary Volcanic Province	2
Figure 1.2:	Simplified geological map of the Outer Bristol Channel	9
Figure 1.3:	Geological summary map of North Devon	10
Figure 1.4:	Geology of Lundy Island	20
Figure 2.1:	Location of the magnetic reconnaissance survey on Lundy Island	30
Figure 2.2:	AMS sample localities in North Devon	34
Figure 2.3:	AMS sample localities on Lundy Island	35
Figure 2.4:	Errors at cross-over points from the gravity survey in the Bristol Channel	42
Figure 2.5:	Ship-borne gravity sample lines in the Bristol Channel	45
Figure 2.6:	Flight lines for the aeromagnetic survey in the Bristol Channel	46
Figure 2.7:	XRF sample localities in North Devon	50
Figure 2.8:	XRF sample localities on Lundy Island	51
Figure 3.1:	Location of igneous rocks in North Devon	57
Figure 3.2:	Location of reference points on Lundy Island	58
Figure 3.3:	Thickness of dykes on Lundy Island	59
Figure 3.4:	Dip of dykes on Lundy Island	60
Figure 3.5:	Strike of dykes on Lundy Island	61
Figure 3.6:	Reconnaissance magnetic survey on Lundy Island	70
Figure 3.7:	Zijderveld diagram for dyke CK21 from Lee Bay	74
Figure 3.8:	Zijderveld diagram for specimen HSR1 from the Horse-Shoe Rocks	76
Figure 3.9:	Paired anomaly profile of a dyke on Ackland's Moor, Lundy Island	78
Figure 3.10:	The Peters' half-slope interpretation method	81
Figure 3.11:	Theoretical magnetic responses	81
Figure 3.12:	Magnetic surveying strategies on Lundy Island	84
Figure 3.13:	Implied field relations on Lundy Island	85
Figure 3.14:	Some characteristics of dyke morphology	86
Figure 3.15:	Typical hysteresis loop for basic rocks on Lundy Island	89
Figure 3.16:	Domain state diagram for rocks from Lee Bay and Lundy Island	91
Figure 3.17:	Thermo-magnetic curve for dyke CK21 from Lee Bay	93
Figure 3.18:	Thermo-magnetic curves for dykes from Lundy Island	95
Figure 3.19:	The susceptibility ellipsoid	97
Figure 3.20:	AMS plot of the Lundy Dyke Swarm	101
Figure 3.21:	Alternative AMS plot for the Lundy Dyke Swarm	101
Figure 3.22:	AMS results for the Lundy Dyke Swarm	103
Figure 4.1:	The inverse isochron method (Turner, 1971)	124
Figure 4.2:	Total argon isotope composition for dykes at Lee Bay	125
Figure 4.3:	Argon isotope composition and age of three plagioclase separates from dyke CK21	127
Figure 4.4:	Argon isotope composition and age of three plagioclase separates from dyke CK30	127
Figure 4.5:	Argon isotope composition and age of two plagioclase separates from the Horse-Shoe Rocks	129

Figure 4.6: Theoretical isotope composition diagram for hydrothermally altered Tertiary rocks 130
Figure 4.7: Age determination for the Fremington dyke 132
Figure 4.8: Chemical classification of a) Tertiary and b) Permo-Carboniferous rocks 136
Figure 4.9: Classification of transitional basalts 137
Figure 4.10: CIPW classification of rocks from North Devon 138
Figure 4.11: Major element variation with Tertiary rocks from Lundy and Lee Bay 139
Figure 4.12: Major element variation within Permo-Carboniferous rocks from North Devon 143
Figure 4.13: Trace element geochemistry in Tertiary rocks from Lundy Island and North Devon 145
Figure 4.14: Trace element composition of dykes from Lundy Island 147
Figure 4.15: Spidergram plot of three sub-groups of dykes from Lundy Island 148
Figure 4.16: Trace element geochemistry from the Lee Bay dykes 150
Figure 4.17: Data from Figure 4.16 normalized to Lun 62 150
Figure 4.18: Trace element geochemistry in the Horse-Shoe Rocks and Fremington dyke 152
Figure 4.19: Trace element compositions in the Horse-Shoe Rocks 153
Figure 4.20: Trace element concentrations in the Fremington dyke 153
Figure 4.21: Comparative spidergram plot for different tectonic settings 155
Figure 4.22: MORB discrimination ratios 156
Figure 4.23: Plot of rare earth elements for North Devon 158
Figure 4.24: Continental crust compositions 158

Figure 5.1: Magnetic anomaly map for the Outer Bristol Channel 166
Figure 5.2: Magnetic anomaly map for the Morte Point area 167
Figure 5.3: Magnetic anomaly map for the Lundy area 169
Figure 5.4: Magnetic signature across the linear magnetic anomaly near Lundy Island 170
Figure 5.5: Magnetic anomalies in the Lundy area viewed towards the northeast 172
Figure 5.6: Bouguer gravity anomaly map for the Outer Bristol Channel 178
Figure 5.7: Regional Bouguer anomaly map for Southeast England 179
Figure 5.8: Crustal thickness around Great Britain 182
Figure 5.9: Theoretical model for the magnetic anomaly at Morte Point 184
Figure 5.10: Theoretical magnetic model along grid line 214 187
Figure 5.11: Theoretical magnetic model along grid line 210 189
Figure 5.12: Theoretical magnetic model along grid line 206 190
Figure 5.13: Model for residual gravity anomalies in the Lundy horst 194
Figure 5.14: Alternative model for residual gravity anomalies in the Lundy horst 195
Figure 5.15: Second model for residual gravity anomalies in the Lundy horst 197
Figure 5.16: Alternative model for residual gravity anomalies in Figure 5.15. 198

Figure 6.1 Idealized cartoon of differing sources of dykes in the Palaeogene 207
Figure 6.2: Bouguer anomaly contours maps for the Lundy area 210
Figure 6.3: Sources of the Lundy Dyke Swarm 213
Figure 6.4: Idealized palaeo-reconstruction of the Icelandic plume prior to break-up of the North Atlantic 214
Figure 6.5: Thickness of partial melt generated by decompression melting of upwelling asthenosphere 225

LIST OF PHOTOGRAPHS

Photo 3.1:	Zonation in dyke CK31 from Lee Bay	64
Photo 3.2:	Zonation in dyke CK21 from Lee Bay	64
Photo 3.3:	Fingers in QB2 from Quarry Beach, Lundy Island	66
Photo 3.4:	Elliptical vesicles in QB2 from Quarry Beach, Lundy Island	66
Photo 3.5:	Foreign xenocryst in chilled margin of BW2 from Brazen Ward, Lundy Island	67
Photo 3.6:	Abrupt bends in dykes from Lametry Beach, Lundy Island	67
Photo 4.1:	Coarse grained dolerite from Lundy Island (BW2) with subophitic texture	110
Photo 4.2:	Fine-grained dolerite from Lundy Island (QB1)	110
Photo 4.3:	Rounded plagioclase phenocryst from CK30, Lee Bay	112
Photo 4.4:	Relatively fresh Mg-rich olivine phenocryst in CK30, Lee Bay	112
Photo 4.5:	Rounded and embayed plagioclase phenocryst from CK30, Lee Bay	113
Photo 4.6:	Rounded clinopyroxene phenocryst in CK30, Lee Bay	113
Photo 4.7:	Fresh clinopyroxene in the Horse-Shoe Rocks	117
Photo 4.8:	Feldspar crystals in the Horse-Shoe Rocks	117
Photo 4.9:	Groundmass minerals in Frem 2, Fremington	118
Photo 4.10:	Buchite structure in xenolithic fragment in Frem 4, Fremington	118

LIST OF TABLES

Table 1.1:	The sedimentary sequence in North Devon	11
Table 3.1:	Site-mean directions for some centres within the BTVP	72
Table 3.2:	Results of mean palaeomagnetic directions for Lee Bay	73
Table 3.3:	Palaeomagnetic directions for the Horse-Shoe Rocks	75
Table 3.4:	Categories of AMS classification in the Lundy Dyke Swarm	102
Table 4.1:	Summary of geochronological relationships of igneous rocks in North Devon	134
Table 4.2:	Characteristic large cation abundances (ppm) for OIB and MORB	159
Table 4.3:	Average large cation abundances (ppm) for Lee Bay and Lundy dolerites	159
Table 5.1:	Density values in Southwest England and the Bristol Channel	192
Table 5.2:	Densities of rocks from Lundy Island	192

CHAPTER 1

THE BRITISH TERTIARY VOLCANIC PROVINCE AND RELATIONSHIPS TO LUNDY

1.1 INTRODUCTION

The British Tertiary Volcanic Province (BTVP) marks one of the most dramatic events in the recent geological history in the British Isles, when large volumes of predominantly tholeiitic basalts of comparatively uniform composition were erupted from fissures over a relatively large continental area. Such continental flood basalt (CFB) eruptions are not seen at the present time, but have occurred at least 15 times worldwide in the geological record from the Late Precambrian to Quaternary. The BTVP produced a thickness of up to about 2,000 m of volcanic rocks over an area of just over 1 x 10^6 km^2 (Basaltic Volcanism Study Project, 1981; Wilson, 1993). In fact, the total volume of igneous rock produced throughout the North Atlantic region as continental rifting proceeded during the early Tertiary, including igneous provinces in the Faeroes and Greenland, has been estimated at 10 million km^3 by White *et al.* (1987).

CFB eruptions are therefore of considerable importance as crust-forming events. They are characterized by rapid eruptions of plateau lavas over a relatively short period of time, indicating that considerable volumes of magma must have been available at relatively shallow depths. The majority of CFB provinces are associated with passive continental margins (Morgan, 1983) and either just pre-date or are contemporaneous with continental separation in various geographic locations. There has been much debate about the role of continental rifting and mantle plume activity with respect to the BTVP, but the actual processes by which the large volume of magma evidenced in outcrop could have been produced are still not fully understood.

Within the BTVP, volcanism was most intense in the Inner Hebrides and neighbouring northwest Scottish mainland, but also extended into Northern Ireland and the Outer Hebrides (Figure 1.1). Intrusive Tertiary episodes also invaded northeast England,

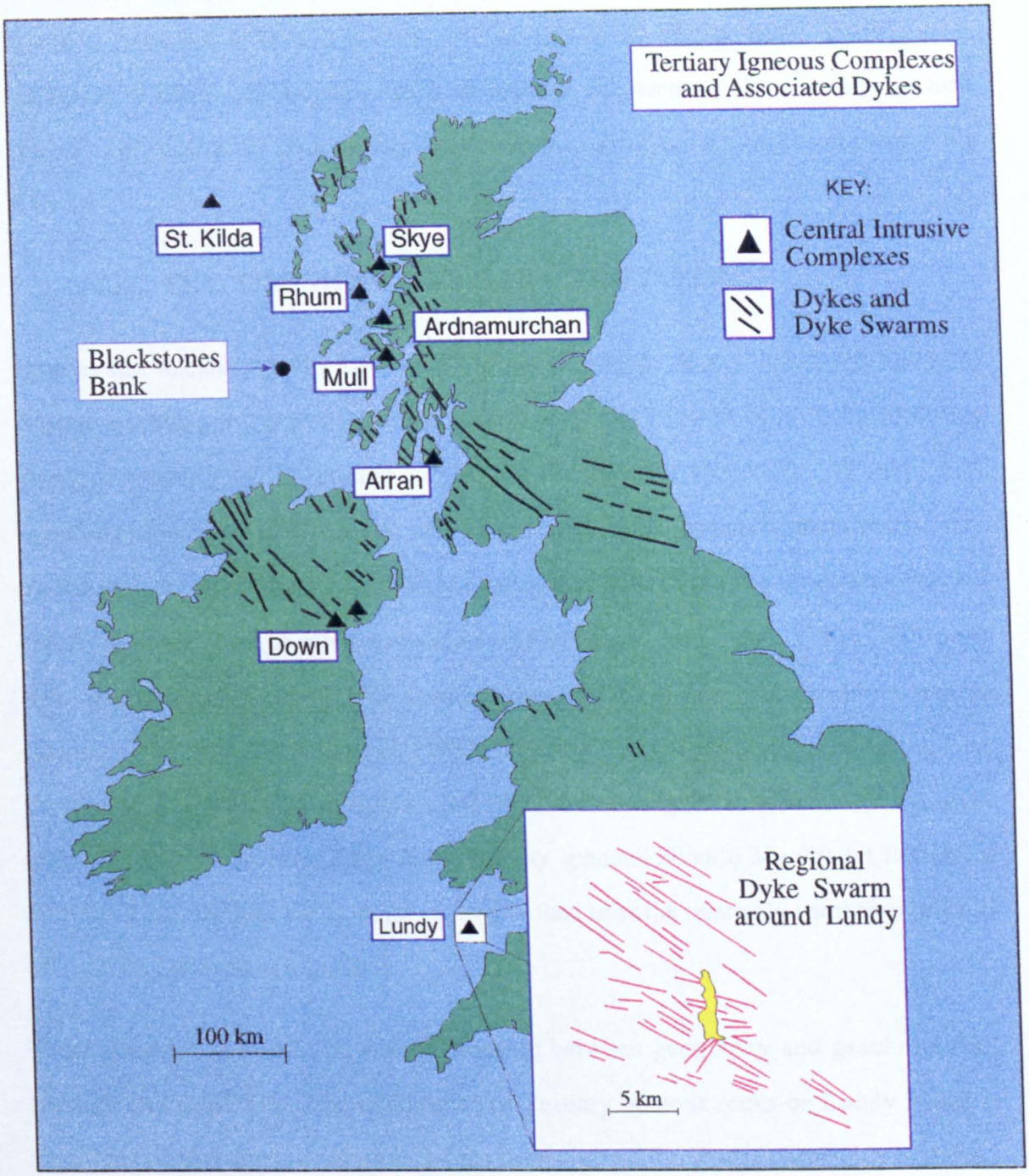

Figure 1.1: Intrusive centres and dykes within the British Tertiary Volcanic Province. Information on the off-shore dykes around the coastof Lundy within the inset is taken from Hains *et al.* (1983) and is based on magnetic evidence rather than submarine outcrops. The remaining dykes are are taken from Emeleus (1982) and Emeleus and Gyopari (1992). It should be noted that not all Tertiary dykes can be shown on the scale of this map. Nevertheless, a NW-SE trend is apparent in the main. The Blackstones Bank is a submarine central complex.

southern Scotland, North Wales, the English Midlands, Eire and the Lundy area. One of the most relevant questions to ask is therefore "Was there a Tertiary volcano where Lundy Island is now and if so, did it ever produce sub-aerial eruptions?" Further, it is important to know why Lundy is such an isolated occurrence. In that context, how typical or atypical is the Lundy complex with respect to other Tertiary centres within the BTVP?

1.1.1 THE TIMING OF TERTIARY VOLCANISM

Igneous and volcanic activity associated with the BTVP are closely linked to the onset of oceanic spreading in the North Atlantic, which is usually taken as being initiated during magnetic anomaly 24, i.e. around 55 - 56 Ma (Berggren *et al.*, 1985). Mussett *et al.* (1988) concluded that most volcanic activity occurred within the approximate interval 63 - 52 Ma with the peak of activity at 59 Ma, whilst the bulk of plateau lavas were erupted before the main onset of off-shore volcanism (White and McKenzie, 1988). Thus, the bulk of activity within the BTVP occurred marginally before ocean spreading started. Harrison (1982) and Durant *et al.* (1982) noted that rarer igneous activity in the Late Cretaceous within the eastern Atlantic and Blackstones complex formed the earliest rocks in the BTVP. Apart from Skye where activity spanned about 6 Ma (59.3 ± 0.7 Ma to 53.5 ± 0.4 Ma; Dickin, 1981), other centres formed over the relatively short time interval of 1 - 3 Ma (Mussett *et al.*, 1988).

There does not appear to be any relationship between geography and geochronology throughout the BTVP. The occurrence of Tertiary igneous rocks on Lundy Island is significant in that although these rocks pre-date many of the Tertiary centres in northwest Scotland and Northern Ireland (see section 1.2.3), Lundy is situated a considerable distance to the south. Reverse magnetic polarity dominates in the province as a whole, but in several centres both normal and reverse polarities have been reported (Wilson *et al.*, 1972; Dagley *et al.*, 1987; Mussett *et al.*, 1987). This indicates that volcanism straddled at least two magnetic reversals. As Mussett *et al.* (1976) reported both normal and reversely magnetized dykes on Lundy Island, this conclusion holds for the Lundy Igneous Complex.

In general, plateau lavas preceded the development of basic central intrusive complexes which in turn preceded the granite intrusions. However, dyke intrusion appears to have occurred throughout the lifetime of specific volcanic centres (Gass and Thorpe, 1980; Emeleus and Gyopari, 1992). Few dykes are seen cutting the granites of volcanic centres in northwest Scotland and so these granites must represent a late stage in the evolution of each centre. Conversely, the Lundy granites are cut by numerous dykes indicating different age relationships between dyke and host compared to their Scottish counterparts. The sequence of events for Tertiary magmatism in the Lundy area was therefore different from other Tertiary centres and signifies its evolutionary history as a distinct phenomenon.

1.1.2 PHYSICAL SETTING OF THE BTVP

BTVP centres were formed within a continental plate some 200 - 800 km to the south and southeast of the emergent Mid-Atlantic Ridge (MAR) in the North Atlantic. The centres are presently located along a crude north-south axis between about 5° and 6° 30'W within a rectangular box some 1,200 km north-south and 100 km east-west (Gass and Thorpe, 1980). Fitton *et al.* (1996) completed a palaeo-reconstruction of BTVP volcanic activity and concluded that the original palaeo-longitude of the centres would have been between 38° and 43°W just prior to continental break-up. However, there are no recorded major structural features within Precambrian, Caledonian, Variscan or Alpine trends with a north-south lineament to suggest a link for the siting of volcanism, although many centres do lie close to northeast-southwest trending faults.

England (1988) reviewed the form and trends of major dyke swarms in the BTVP to derive information on early Tertiary stress regimes and reiterated that the dominant northwest-southeast alignment of dykes was indicative of northeast-southwest directed extension. Emeleus and Gyopari (1992) reviewed the effects of lithospheric attenuation that accompanied extension. Anderson and Dunham (1966), Morrison *et al.* (1985) and Bell and Emeleus (1988) all emphasized that the repeated penetration of the continental crust by dykes of mantle-derived magmas was the main mode of igneous activity. The nature of the continental basement in northwest Scotland, through which magma

migrated, is therefore important. From northwest Scotland to the Southern Uplands, the basement consists of granulite-facies Lewisian gneisses overlain by lower grade amphibolite-facies Lewisian gneisses with superficially lying Moine schists in northwest Scotland (Dunning, 1985).

The nature of basement rocks in Southern Britain and the Lundy area in particular is much more uncertain. Hampton and Taylor (1983) concluded that there was no isotopic evidence for an ancient Precambrian basement (> 1200 Ma) under southern Britain. Within southwest England, part of the basement may consist of the Start schists and Eddystone gneisses (Edmonds *et al.* 1975; Brooks *et al.*, 1993), but Dunning (1985) considered that much of the deeper basement was formed by accretionary processes in the late Precambrian and early Cambrian. In this model, the basement was argued to consist of volcanic formations overlying low-grade metasediments of the kind presently cropping out in Anglesey, although some microplates of basement, e.g. similar to the Rosslare Complex in Southern Ireland, could also be incorporated. This is in agreement with Bamford *et al.* (1976) who determined that the ancient basement of northwest Scotland does not extend southward into southern Britain.

This is significant because potential contamination of magma moving through the crust is governed by the nature of the host rocks, so possible modification of magma by assimilation is likely to be different in southwest England with respect to other areas within the BTVP. Basement rocks in the outer Bristol Channel may thus have more in common with metasediments than with the Lewisian gneisses of northwest Scotland. Unfortunately, there is no corroborative evidence from deep boreholes in Southwest England to indicate the nature of basement rocks.

1.1.3 GEOPHYSICAL INVESTIGATIONS WITHIN THE BTVP

Much of the detail on the deep structure of central complexes within the BTVP has come from studies of the gravitational field. McQuillin and Tuson (1963) completed a detailed survey over Arran and Rhum, whilst Bott and Tuson (1973) offered a correlation between the centres of Skye, Mull and Ardnamurchan. McQuillin *et al.* (1975) also

surveyed the submarine Blackstones Bank complex. The main feature of all these surveys over Tertiary central complexes is that of a conspicuous positive Bouguer anomaly, usually having a crude circular form and overlying the central aspect of the complexes. The anomalies have been interpreted in terms of each central complex being underpinned by a considerable mass of dense rock in the range 3.0 - 3.3 Mg m^{-3}, i.e. gabbro or peridotite. Such masses would have an overall cylindrical form or at least a steep-sided morphology and probably extend down to 12 km through the upper crust. Bott and Tuson (1973) indicate that the masses could be up to 20 km in diameter. Bott and Tantrigoda (1987) emphasized the superficial extent of granites associated with many of the complexes by only being able to model up to a 2 km depth for their thickness.

Centres within the BTVP are also characterized by coincident magnetic anomalies of an approximately circular form, which would be expected if centres are underlain by a large cylindrical mass of basic or ultrabasic rock. Examination of the circular magnetic anomalies may offer further definition to the structure of central complexes. However, Bott and Tantrigoda (1987) noted that a complicated array of a number of magnetic anomalies was coincident with a circular gravity anomaly of + 50 mGal. Variation in the levels of magnetization were mostly due to several intrusive phases, some of which may have affected previous intrusions. Brown and Mussett (1976) showed that both positive and negative magnetic anomalies could be detected over the Skye central complex, a feature not associated with other Tertiary centres. They interpreted these anomalies as indicating that at least two discrete magma chambers fed the Skye volcano. Further, as the polarity of the anomalies straddled a magnetic reversal, the age of each magma chamber must be different and so the volcano demonstrated an evolutionary history for its plumbing system.

Linear and elongate magnetic anomalies have been demonstrated in off-shore environments (Caston, 1975; Ofoegbu and Bott, 1985; Kirton and Donato, 1985) and interpreted as dykes and dykes swarms. Profiles across linear magnetic anomalies on land have also been recorded to reveal the presence of basic dykes (Robson, 1964; Strangeway, 1965; Sowerbutts, 1987; Titman *et al.*, 1989; Gibson and Lyle, 1993).

Although such anomalies cannot indicate Tertiary magmatism by their field signature alone, the magnetic profiles can add a great deal of information on the extent and sub-surface distribution of dykes, provided at least some form of ground truthing is available. Ground based surveys generally provide higher amplitude anomalies than aeromagnetic surveys and both positive and negative Tertiary anomalies have been recorded.

1.1.4 GEOCHEMISTRY OF TERTIARY MAGMATISM

There have been a great deal of geochemical data gathered from the BTVP and these have been summarized in Thompson (1982), Thompson *et al.* (1983), Hawkesworth and Norry (1983), Bell and Harris (1986), Morton and Parsons (1988) and Emeleus and Gyopari (1992). Thompson *et al.* (1972) had earlier established that the Plateau Lavas on Skye could be broadly subdivided into an undersaturated, Ne-normative basalt-hawaiite-mugearite-benmoreite trend and a saturated basalt-trachyte trend, but that these two groups were by far the most prominent in the Skye Main Lava Series (SMLS). Similar rock suites were described within the Mull Plateau Group (MPG) by Skelhorn (1974) and Emeleus (1982).

Morrison *et al.* (1985) also emphasized the similarity to evolutionary trends on Skye but noted that the MPG was a discrete geochemical unit. The use of isotope geochemistry to highlight the petrogenetic history of basic rocks in the SMLS and ultrabasic rocks in the Cuillin Central Complex was undertaken by Thirlwall and Jones (1983). They interpreted the isotope data in terms of mixing between two end-members of North Atlantic mantle and the local Archaean granulite-facies crust (Lewisian basement) with variation in the relative effects and roles of crustal contamination, fractional crystallization and differing degrees of partial melting in the mantle.

Granites within the BTVP have also been extensively studied by Jassim (1970) and Bell (1982) amongst others and reviewed by Bell and Harris (1986). Peraluminous, metaluminous and peralkaline epigranites have been noted in Skye with a range of petrographic characteristics. The relative contributions of extensive crystal fractionation of basalt and partial melting of the underlying crust to the formation of the granites has

been debated by Moorbath and Bell (1965), Moorbath and Welke (1969) and Dickin (1981). It seems that the consensus of opinion on the formation of granitic magma has moved away from partial melting of Lewisian gneisses alone by transfer of heat from an intrusive magma to both crustal and mantle sources as significant contributors, mainly on the evidence of isotope geochemistry.

The use of geochemistry, then, to derive geological information on both processes that helped to form igneous rocks and on geochemical variations in the rocks themselves has been fundamental in understanding and deciphering the record of igneous and volcanic rocks within the BTVP. Whilst most of the volcanism in the BTVP was relatively short lived, understanding how magmatic sources and formative processes have varied with respect to both time and changing tectonic conditions is important for characterizing the history and nature of the province as a whole.

1.2 REGIONAL GEOLOGICAL RELATIONSHIPS

Figure 1.2 is a simplified geological map of the Outer Bristol Channel region that demonstrates overall relationships between the main geological units. Information on the different rock types and varying lithostratigraphic units have been determined mostly by sea-floor grabbing and shallow marine boreholes. Deeper borehole information from discrete locations in the Bristol Channel has been derived from drilling operations by oil companies. The most relevant ones for this thesis are shown on Figure 1.2.

The main rock types surrounding Lundy Island in the Lundy horst (see section 1.2.3) and underlying Mesozoic and Cenozoic sediments throughout the Bristol Channel are described as undivided Carboniferous and Devonian sediments (Hains *et al.*, 1983). More refined definition is not available at present, but the geology of these units must be closely related to known outcrops in the North Devon area. It is thus important to consider the nature and extent of potential host rocks around the Lundy area before considering the geology of Lundy Island itself. Although it is even more important to consider source rocks, there is limited information available (cf. section 1.1.2).

Figure 1.2: Simplified geological map of the Outer Bristol Channel area.
Off-shore dykes around Lundy Island are based on magnetic evidence (Hains et al., 1983). SLZ represents the NW-SE trending Sticklepath-Lustleigh Fault Zone, HSR and SBB represent the sub-marine Horse-Shoe and Stanley Bank Basin respectively. The Main Bristol Channel Basin trends E-W and is contained within post-Palaeozoic sediments. White areas indicate land.

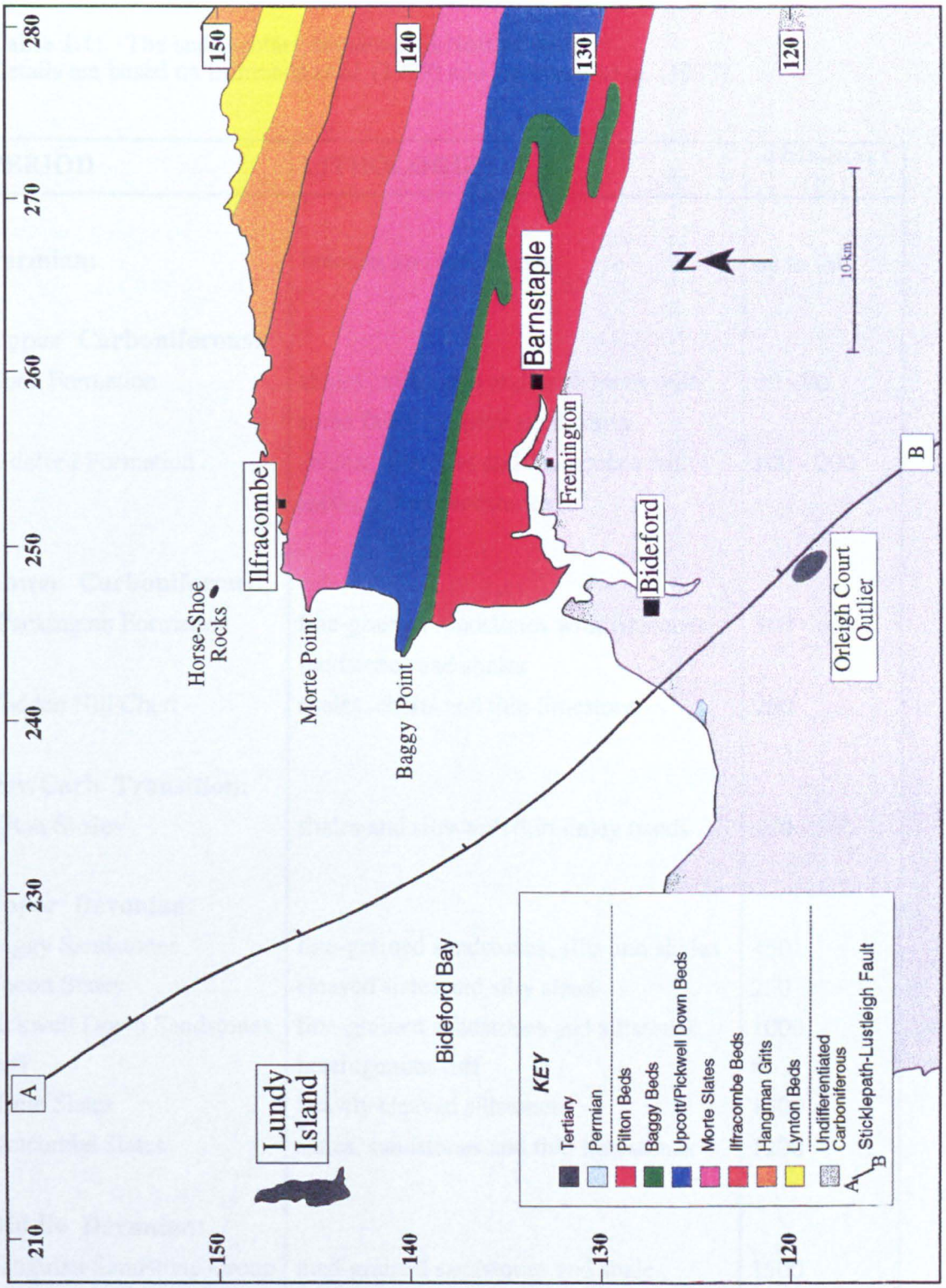

Figure 1.3: Geological summary map of North Devon.
To assist clarity, Carboniferous rocks have been not been sub-divided. Based on Woodland (1977), Brown (1980a, 1980b) and Brown (1982). The geology of Lundy Island is given with more detail in Figure 1.4. The age of the Horse-Shoe rocks is discussed in section 4.4.2.2.

Table 1.1: The sedimentary sequence in North Devon.
Details are based on Edmonds *et al.* (1979) and Edmonds *et al.* (1985).

PERIOD	LITHOLOGIES	Thickness (m)
Permian:	breccias and sandstones	up to 90
Upper Carboniferous:		
Bude Formation	shales , siltstones and mudstones with some fairly massive sandstones	50 - 90
Bideford Formation	shales, siltstones and mudstones with med-grained sandstones	100 - 200
Lower Carboniferous:		
Crackington Formation	fine-grained sandstones with siltstones, mudstones and shales	300 - 600
Codden Hill Chert	shales, cherts and thin limestones	250
Dev/Carb Transition:		
Pilton Shales	shales and silts with thin limey bands	500 - 600
Upper Devonian:		
Baggy Sandstones	fine-grained sandstones, silts and shales	450
Upcott Slates	cleaved slates and silty slates	250
Pickwell Down Sandstones	fine-grained sandstones and siltstones,	1000
Tuff	heterogenous tuff	8
Morte Slates	heavily cleaved siltstones	1500
Ilfracombe Slates	slates, sandstones and thin limestones	1200
Middle Devonian:		
Hangman Sandstone Group	med-grained sandstones and shale alternations with some conglomerates containing igneous clasts	1500
Lower Devonian:		
Lynton Slates	med-grained sandstones with mudstones and siltstones	300 - 400

1.2.1 GEOLOGY OF NORTH DEVON

The North Devon mainland is nearer to Lundy Island than the South Wales coastline (cf. Figure 1.2) and is made up of Devonian rocks to the north with younger Carboniferous rocks cropping out further south towards mid-Devon. Figure 1.3 shows the geological relationships between the main stratigraphic units. The strike of the rocks is between east-west and northwest-southeast throughout much of North Devon, thus rocks that crop out in North Devon can also probably be found to the west near to Lundy Island itself, although Figure 1.2 indicates that precise classification of the submarine rocks in this area is not sufficiently detailed to sub-divide the sediments into litho-stratigraphic units. Also, detailed correlation of sediments on opposite sides of the Sticklepath-Lustleigh Fault is unclear for the Upper Palaeozoic in Bideford Bay.

1.2.1.1 The Sedimentary Record

Devonian rocks in North Devon are represented mostly by a conformable 5000 m thick series of markedly tectonized coarse-grained sandstones, siltstones and shales, with occasional deltaic incursions and rarer limestone bands (Edmonds *et al.*, 1985). The oldest beds exposed, the Lynton Slates, are along the North Devon coastline and are of probable late Emsian age, i.e the top of the Lower Devonian. They are made up of fine to medium-grained grey sandstones, mudstones and siltstones, between 300 and 400 m in thickness. Simpson (1964) inferred that they accumulated in a shallow sea, based mainly on sedimentological and palaeontological evidence. These are superseded by the Hangman Sandstone Group, a series of medium-grained arenaceous deposits with alternating shales or slates and minor intercalations of pebble beds and conglomerates. The whole group is up to 1500 m thick (Tunbridge, 1986) and can be interpreted in terms of non-marine fluviatile systems with the development of infrequent estuaries and fan-deltas (Lane, 1965). Tunbridge (1977, 1986) identified acid tuffs and lavas amongst pebble clasts within the Rawns Formation, a localized division of the Hangman Sandstone Group. Palaeocurrent measurements and the sub-angular to angular characteristics of the clasts were thought to indicate an origin to the north, possibly in the region of the present day Bristol Channel. The sediments may be

associated with a temporary emergent activation of the Bristol Channel Landmass in the Middle Devonian before its main palaeogeographic influence of an upstanding ridge of land in the Silesian (Leeder, 1992).

The sediments comprising the poorly fossiliferous Ilfracombe Slates, which supersede the Hangman Sandstone Group, indicate a change to marine conditions following a general marine transgression. Evans (1922) detailed the stratigraphy of this 1216 m thick group of alternating slates, sandstones and thin limestones, although Holwill *et al.* (1969) recognized three main parts with sandstones characterizing the Lower and Upper Divisions with mainly limestones and slates in the Middle Division. Overlying these, the Morte Slates, believed by Dineley (1992) to represent the lowest formation within the Upper Devonian, are typically smooth silvery to greenish grey siltstones around 1500 m in thickness. They have been heavily cleaved, which has destroyed much of the fossil evidence, but the entire sequence was probably deposited in a shallow water environment, such as a pro-delta or delta platform (Edmonds *et al.*, 1979). The Pickwell Down Sandstones overlie the Morte Slates and contain around 1000 m of purple, red, brown and greenish fine-grained laminated siltstones and sandstones. Current bedding is common and depositional environments probably varied from rivers and lakes to deltas and lagoons (Rogers, 1926). The base of the Group is marked by a keratophyric tuff, persistently 8 m thick in outcrop, implicitly indicating a contemporaneous volcanic origin (Edmonds *et al.* 1985). An earlier description of a water-sorted volcanic ash with fish remains (Rogers, 1926) is thus disputed.

The top of the Devonian is marked by the heavily cleaved Upcott Slates (around 250 m thick), a cream/grey to green/purple formation of slates and silty slates, and by almost 450 m of the Baggy Sandstones, a group of interbedded fine-grained sandstones, siltstones and shales. Goldring (1971) made a detailed analysis of the Baggy Sandstones in North Devon and concluded that they broadly represent a marine sequence with occasional fresh or brackish water sediments. The fossiliferous Pilton Shales are a group of shales and siltstones with thin limey bands and lenses, measuring about 500 to 600 m in thickness, that mark the transition from Devonian into Carboniferous.

It thus follows that most of the Devonian strata in north Devon can be interpreted as near-shore marine sediments for the most part, indicating a relatively stable land mass to the north with a marginally fluctuating east-west shoreline somewhere in the present day Bristol Channel and deeper water to the south-west for much of the Devonian (Tunbridge, 1983 and 1986). There is no direct outcrop evidence of Lower Old Red Sandstone rocks, Lower Palaeozoic units or indeed Precambrian basement within the land area, although all are seen in outcrop within Glamorgan and West Dyfed to the north of the Bristol Channel. However, Allen (1979) inferred terrestrial coastal plain deposits would form sub-crops in north Devon throughout the Gedinnian and Siegenian, based on borehole information obtained in southern England and outcrops in south Devon. Dineley (1992) noted the virtual lack of volcanic units in north Devon, relative to the widespread occurrences in Cornwall and south Devon. The precise nature of the basement beneath North Devon is thus unclear, but is likely to be different from the Lewisian and Torridonian basement of North Scotland (Richey, 1937; Emeleus, 1982).

The lowermost beds in the Lower Carboniferous continue with the Pilton Shales and are overlain by a total thickness of around 250 m in the Codden Hill Chert, a succession of shales, cherts and thin lenticular limestones. This unit is the local equivalent of the Culm Measures, which attain greater thickness further to the south as deeper-water turbidites (Leeder, 1992). The Namurian is represented by the Crackington Formation in North Devon, a 300 to 600 m thick collection of grey fine-grained sandstones within a succession of siltstones, mudstones and shales. The junction with the overlying Westphalian units is confused and much of the basal Bideford Formation is similar to the Crackington Formation. However, the occurrence of fine to medium-grained feldspathic sandstones along prominent ridges in outcrop and a more advanced fossil assemblage led De Raaf *et al.* (1965) to differentiate the Northam Formation (430 m) and Abbotsham Formation (360 m) as distinct from the older Crackington Formation. Edmonds *et al.* (1979) proposed both be amalgamated into the Bideford Formation. The Westphalian sequence is completed by the Bude Formation, comprised of thickly bedded and massive sandstones with thinner sandstones, siltstones, mudstones and shales. This sequence varies from about 50 m of deltaic sediments in the north to about 1300 m of turbidites in

the south. The whole Carboniferous sequence occupies an asymmetric east-west trending syncline with a steeper northerly-dipping limb, but the effects of repetition from folding and faulting are not fully known (Kelling and Collinson, 1992).

The only sedimentary Mesozoic rocks present at outcrop on land in North Devon are the breccias and sandstones of presumed Permian age (Edmonds *et al.*, 1979) in a small faulted outlier to the west of the Sticklepath Fault on the shoreline of Bideford Bay. Prentice (1960) has earlier argued that the original Permian cover may once have been much more extensive, as a belt of red-stained strata occurs within the superficial aspects of Carboniferous rocks. McFarlane (1955) suggested Permian sandstones might be present beneath Northam Burrows, an area of Pleistocene aeolian sands, based on a seismic refraction survey.

1.2.1.2 The Igneous Record

Apart from the Lundy Igneous Complex (see section 1.2.3), few known igneous outcrops are seen on land in North Devon. Dewey (1910) described a greenish-brown minette dyke with calcite-filled amygdales and quartzitic xenoliths at Fremington Pill (Figure 1.2) and inferred a Permian age on the basis of its similarity to post-granitic dykes in Cornwall. Although weathered spheroidal masses with exfoliating crusts were noted, fresh grey-blue cores were observed in some broken spheroids. Hawkes (1985) described the dyke as an autolytic kersantite lamprophyre with altered olivine phenocrysts set in a matrix of oligoclase, biotite, secondary chlorite and carbonate, with abundant grains of accessory limonite. Rounded aggregates of quartz and calcite up to 5 mm across were noted, sometimes weathered out to leave small vesicles, and an affinity with Permian lamprophyric and basic volcanic rocks to the north and east of Dartmoor was indicated.

Arber (1911) first recorded three greenstone dykes at Lee Bay (Figure 1.2) in the littoral zone of the foreshore. Blundell (1957) obtained palaeomagnetic data from one of the dykes, described as a dolerite, and reported a dip of - 51° for its stable magnetic remanence. Similarity to palaeomagnetic dips on Lundy Island was postulated as

evidence of a common link between the two dyke localities and comparisons with Tertiary basalts in Northern Ireland led to the hypothesis of a probable Eocene age for the Lee Bay dyke. Edmonds *et al.* (1979) reported that the dykes were only visible when a very low tide coincided with a suitable disposition of shingle, but did not offer any petrographic descriptions. It is not known whether these dykes are the only representatives of basic dykes of the North Devon coast. The Horse-Shoe Rocks are a submarine outcrop of slightly sheared and metamorphosed dolerites about 5 km northwest of Ilfracombe (Donovan *et al.*, 1971), although Donovan *et al.* (1961) had earlier described angular fragments from a dredged haul over the rocks as mostly carbonated lamprophyric rocks. An assumed Upper Palaeozoic age was adopted by both. Brooks and Thompson (1973) disputed references to the possible spilitic nature of the rocks (Donovan *et al.* 1971) and favoured a Tertiary age whilst noting a low amplitude negative magnetic anomaly over the rocks.

1.2.2 BRISTOL CHANNEL AREA

The geology of the floor of the Bristol Channel has been detailed by Lloyd (1963), Lloyd *et al.* (1973), Doré (1976), Kamerling (1979) and Hains *et al.* (1983). Donovan *et al.* (1961) had first noted that Upper Palaeozoic rocks crop out continuously on the sea floor from the North Devon coastline around Hartland Point to Lundy Island and eastwards to the Ilfracombe area. Owen (1971) inferred a localized horst from the outcrop pattern around the Lundy area. However, Lloyd *et al.* (1973) completed an extensive sampling study of the Inner and Middle Bristol Channel westwards as far as Lundy Island and recorded 1.85 km of Mesozoic sediments unconformably overlying Palaeozoic rocks, the entire Permian sequence not being represented here. They also recognized two major WNW-ESE trending synclines within the Mesozoic sediments arranged *en échelon* with a minor intervening pericline, and Palaeozoic rocks to the north in both Swansea and Carmarthen Bays beneath a thin Pleistocene veneer. The Triassic is represented by a sequence of red silty clays, sandstones, grey shales and buff siltstones indicative of essentially terrestrial and hypersaline environments. The entire stratigraphic column of the Jurassic from Hettangian shales to Portlandian sandstone is present, but dominated by

argillaceous sediments. Evans (1973) refined the structure and stratigraphy in the syncline by mapping an east-west zone of strike faulting, the Bristol Channel Fault Zone (BCFZ), along the northern limb.

Some further definition in the overall structural configuration of the Bristol Channel was achieved by modelling seismic refraction surveys (Brooks and James, 1975; Brooks and Al-Saadi, 1977; Mechie and Brooks, 1984). Brooks and James (1975) implied 2.1 km of Mesozoic sediments with seismic velocities between 2.97 and 4.2 km s^{-1} overlying Devonian rocks with velocities of 4.7 to 4.8 km s^{-1}, whilst also modelling over 1 km southerly downthrow within the BCFZ. Brooks and Al-Saadi (1977) noted overlapping seismic velocity ranges within the main Upper Palaeozoic rock types and concluded that definition of the concealed Lower Palaeozoic sequence could be severely complicated, but broadly concurred with previous interpretations of Mesozoic sequences. Mechie and Brooks (1984) described a Lower Palaeozoic or Precambrian supra-basement facies with a seismic velocity of 5.5 to 5.6 km s^{-1} at a depth of about 2 km and showing a general thickening to around 6 km below North Devon. A Precambrian crystalline basement is correlated with a 6.2 km s^{-1} refractor, dipping southerly from about 6 km depth to the north of the Bristol Channel to almost 8 km depth along the North Devon coastline.

1.2.2.1 Tertiary Sediments

Tertiary sediments are located in basins (Figure 1.2) to the east of Lundy Island in the Stanley Bank Basin (SBB) and to the west and northwest of Lundy Island in the Main Bristol Channel Basin (MBCB). Kamerling (1979) reported that Tertiary sediments were only thinly developed in the MBCB, but the Stanley Bank Basin was described by Fletcher (1975a) who cored a succession of silts, mudstones, lignite clays and lignites of middle to upper Oligocene age. Although Brooks and James (1975) suggested that there may be up to 340 m of Tertiary sediments in the basin from seismic refraction evidence, Fletcher (1975a) indicated that the deepest sample core had only penetrated 33.85 m down through the top of the sequence. Thus there is clearly a considerable thickness of possible Tertiary sediment of undetermined age in the basin. Edwards and Freshney (1982) correlated the known stratigraphical sequence and

depositional environment in the SBB with the upper part of the Tertiary succession in the Petrockstowe Basin (located on the line of the Sticklepath-Lustleigh Fault in mid-Devon) and concluded that the SBB deposits had a continental aspect similar to the clays, sands, gravels and minor lignites contained within the basin (Freshney *et al.*, 1979). Edwards and Freshney (1982) interpreted the environment of deposition in the Petrockstowe Basin as cyclic between a meandering river to that of an overbank floodplain or backswamp nature to a low energy lacustrine setting. In this respect, deposition in the SBB was probably controlled by a river flowing northeasterly along the Sticklepath-Lustleigh Fault (Figure 1.2). A brief marine incursion was noted by Fletcher (1975b) very near to the top of the sequence, i.e. probably upper Oligocene in age. Davies (1987) refined the detail in the SBB using seismic stratigraphy and highlighted three facies. These were described as a widespread floodplain facies overlying a braided sand/gravel channel network with a rarer facies of alluvial channels and bars overlying the other two facies.

1.2.3 THE LUNDY IGNEOUS COMPLEX

The Lundy Igneous Complex (LIC) is composed of mainly (~ 90%) granite and basic to acid dykes emplaced within the Devonian sediments. Figure 1.4 shows the geology of the island and relationship with host sediments.

1.2.3.1 The Lundy Granite

The geology of the LIC has been described in detail by Dollar (1941) and Edmonds *et al.* (1979), where Dollar (1941) identified two main types of medium to coarse-grained feldspar magacrystic biotite/muscovite granites. The earlier G1 granite was considered to be a more homogenous megacrystic granite than the later G2 granite, which contained small phenocrysts of bipyramidal quartz and feldspar in a finer matrix and had a mottled appearance. A late stage fine-grained G3 granite was noted to cut both G1 and G2 granites. Edmonds *et al.* (1979) recorded a NNE-SSW possibly faulted junction between granite and host rocks with xenoliths of sediment incorporated into the granite up to 20 m away from the contact. Evans and Thompson (1979) assigned the sediments to the Pilton Shales as outcrops on Lundy are broadly along strike of

counterparts on the North Devon mainland, whereas Dollar (1941) assumed a correlation with the Morte Slates based on lithological similarities.

Thorpe *et al.* (1990) agreed with Edmonds *et al.* (1979) that the evidence for separate G1 and G2 granites on Lundy was inadequate in that no clear contacts could be discriminated in the field and asserted that there were no whole-rock geochemical distinctions between the two granites. Thorpe *et al.* (1990) concluded that trace element data (Rb, Y, Nb) from the granites demonstrated some affinities with syn-collision and within-plate granites and that Sr isotope data indicated a significant crustal component in petrogenesis. They thus proposed that the Lundy granite was derived from a parental magma with both crustal and mantle-derived components.

Stone (1988) analyzed rimmed garnets in the Lundy granite and revealed that they have a dominantly almandine (~ 85%) component with spessartine (~ 15%) the most important minor component. From a comparison with almandine-rich garnets in other intermediate to acid magmas, Stone (1988) argued that the garnets may represent "restite" material formed during magma generation at ~ 18 km depth. Charoy (1986) had earlier deduced a similar depth for the formation of the older Carnmenellis granite (part of the Devonian/Carboniferous Cornubian batholith) by partial melting of pelitic gneisses, which led Thorpe *et al.* (1990) to invoke their model of a mixed crust/mantle origin for the Lundy granite, although they emphasized the evidence for high-level emplacement of the latter.

The Lundy granite has been dated by various authors at 52 - 57 Ma using whole-rock, K-Ar, Ar-Ar and Rb-Sr methods (Dodson and Long, 1962; Miller and Fitch, 1962; Fitch *et al.*, 1969; Institute of Geological Sciences, 1981). However, a new Rb-Sr whole-rock isochron calculated by Thorpe *et al.* (1990) revealed an age of 58.7 ± 1.6 Ma for the Lundy granite with an initial $^{87}Sr/^{86}Sr$ ratio of 0.715 ± 0.006. This date was argued to have a higher precision and accuracy than previous dates and thus provides a probable maximum age for the complex. Hence, it is interesting to note that emplacement of the Lundy granite may have significantly predated the opening of the North Atlantic (cf. section 1.1.1) by around 2-3 Ma.

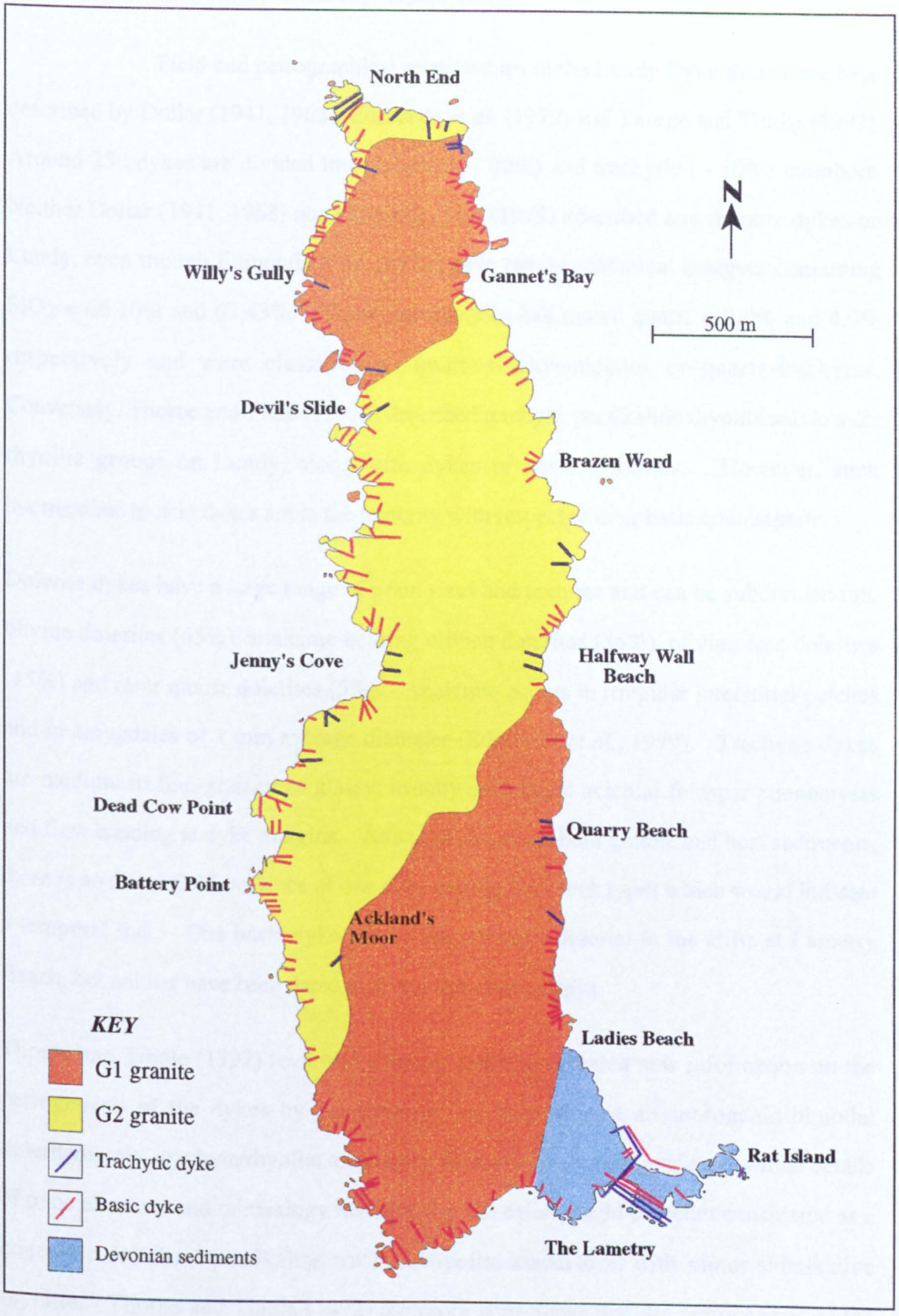

Figure 1.4: Geology of Lundy Island.
As many of the dykes are seen in vertical cliffs, the apparent lateral persistence is schematic only. The G3 granite forms thin sheets and has omitted for clarity. See text for further description of Devonian sediments. Rhyolitic dykes have also been omitted, as they do not present a magnetic field signature and consequently have not been studied in this thesis. After Dollar (1941).

1.2.3.2 The Lundy Dyke Suite

Field and petrographical relationships in the Lundy Dyke Suite have been described by Dollar (1941, 1968), Edmonds *et al.* (1979) and Thorpe and Tindle (1992). Around 250 dykes are divided into doleritic (~ 90%) and trachytic (~ 10%) members. Neither Dollar (1941, 1968) nor Edmonds *et al.* (1979) described any rhyolite dykes on Lundy, even though Edmonds *et al.* (1979) gave two geochemical analyses containing SiO_2 = 66.10% and 67.43%. These two samples had modal quartz = 2.0% and 4.0% respectively and were classified as quartz-trachyandesites or quartz-trachytes. Conversely, Thorpe and Tindle (1992) described trachyte, peralkaline rhyolite and low-Zr rhyolite groups on Lundy, along with dykes of basic affinities. However, such intermediate to acid dykes are in the minority with respect to their basic counterparts.

Dolerite dykes have a large range of grain sizes and textures and can be subdivided into olivine dolerites (45%), analcime-bearing olivine dolerites (35%), olivine-free dolerites (15%) and rarer quartz dolerites (5%). Analcime occurs in irregular interstitial patches and in amygdales of 1 mm average diameter (Edmonds *et al.*, 1979). Trachytic dykes are medium to fine-grained or glassy, usually with small acicular feldspar phenocrysts and flow banding at dyke margins. Although dykes cut both granite and host sediments, there is no direct field evidence of one dyke cutting both rock types which would indicate a temporal link. One basic dyke can be seen to cut a dolerite in the cliffs at Lametry Beach, but neither have been dated to reveal age relationships.

Thorpe and Tindle (1992) reviewed existing data and revealed new information on the petrogenesis of the dykes by determining that they formed an anorogenic bimodal dolerite/basalt - trachyte/rhyolite association from major element evidence, whilst details of trace elements and mineralogy revealed that the dykes might be better considered as a cogenetic dolerite - peralkaline trachyte/rhyolite association with minor subalkaline rhyolite. Thorpe and Tindle (1992) therefore considered that the petrogenesis of the Lundy dyke association could be interpreted in terms of extensive fractional crystallization of a basaltic magma in a magma chamber of complex geometry below the presently exposed Lundy granite. This conclusion echoes the hypothesis of Thorpe and Tindle

(1991), who stated that the rapid high-level emplacement of the basic to acid dykes into the Lundy granite was consistent with the formation and development of a substantial composite bimodal basalt-trachyte/rhyolite volcano centred somewhere close to Lundy Island. In this context, Lundy volcano would have been the southernmost volcano in the BTVP and could have deposited sub-aerial material over substantial parts of Southwest England.

As the dykes are emplaced into granite as well as sediments on Lundy Island (cf. section 1.2.3.1), they clearly post-date the Lundy granite (58.7 ± 1.6 Ma; Thorpe *et al.*, 1990). K/Ar dates for the dykes were reported in the range 44.6 to 54.3 Ma by Mussett *et al.* (1976), although Mussett *et al.* (1988) indicate an Ar/Ar age of 56.4 ± 0.3 Ma for one of the dykes. The dykes may thus have been emplaced relatively soon after the granite solidified. Mussett *et al.* (1988) suggested that the apparent protracted period of activity (54 - 45 Ma) could be an artefact of argon loss or perhaps variable initial argon (Mellor and Mussett, 1975) and is a problematical feature of many Tertiary dykes. A detailed chronology for emplacement of the dykes is therefore unavailable. As the range of published ages (cf. Table 4.1) from a relatively small set of samples (cf. sections 4.1 and 4.2) appears to span 8-9 Ma, it is also unclear whether basic dykes preceded or post-dated the trachytic intrusions, or indeed to what extent they were contemporaneous. Blundell (1957) and Mussett *et al.* (1976) both indicated a lower Tertiary age for the dykes cutting both granite and host sediments based on palaeomagnetic data. This evidence was important in deducing that all dykes on Lundy are related.

1.2.4 STRUCTURAL DEVELOPMENT IN THE BRISTOL CHANNEL

The Outer Bristol Channel is situated between terrains of the Welsh Caledonides to the north and the Cornubian massif to the south. Hancock *et al.* (1983) outlined the formation of NW-SE fault zones within the Cornubian massif during the late Stephanian (upper Carboniferous) when dextral offsets were established, followed later by deposition of Mesozoic sediments in E-W fault-controlled subsiding rift systems (Hart, 1982). Dearman (1963) and Shearman (1967) determined that Tertiary strike-slip

faulting in North Devon was dextral, but Arthur (1982, 1983) considered that major Tertiary sinistral faulting occurred on the established NW-SE fault zones. This was reiterated by Holloway and Chadwick (1986) who described the creation of on-shore Tertiary sedimentary basins as pull-apart basins with rhomboidal centres.

However, the major structural development in the Lundy area has been the formation of the Lundy Rhomb Horst (Arthur, 1989). Following 28 - 40 km of left-stepping sinistral faulting on the Sticklepath Fault in the Palaeogene, the 4 km deep Lundy Pull-Apart Basin was established. In subsequent Cenozoic times, the basin was inverted by around 12 km of left-stepping dextral faulting on the same fault zone to produce the Lundy Rhomb Horst. The net effect is that the rhomb horst has been uplifted by around 2 km with respect to rocks outside the rhomboid and faulted to the north, east, west and (inferred) south, to leave anomalous Palaeozoic strata within the southern margin of the Bristol Channel Basin. This graben/horst relationship was controlled by the interaction and reactivation of Variscan subduction-related E-W thrusts and a NW-SE transform fault system.

1.2.5 GEOPHYSICAL INVESTIGATIONS IN THE LUNDY AREA

The use of seismic refraction and seismic reflection studies as tools for determining stratigraphical and structural relationships has already been discussed in section 1.2.2. Otherwise, Lundy Island itself is associated with both positive and negative magnetic anomalies (cf. Figure 5.1). Blundell (1957) noted that the Lundy granite was very weakly magnetized which led Burley (1979) to deduce that the source of the positive magnetic anomaly over the southern end of the island was probably due to a deeper igneous origin rather than caused by outcropping sediments. Conversely, Cornwell (1971) considered the anomaly was due to the Lundy granite itself. Magnetic anomalies to the west of the island have not been previously interpreted. Cornwell (1971) interpreted a 30 km linear magnetic anomaly trending NW-SE to the northwest of Lundy Island as the response to a reversely magnetized Tertiary dyke or dyke swarm dipping steeply to the southwest and closely approaching the sea floor. Edmonds *et al.* (1979) report a personal communication with Mr. S. R. Winter and Professor M. Brooks, who

measured both normal and reversely magnetized submarine dykes off the coast of Lundy Island with anomalies up to + 250 nT. Hains *et al.* (1983) interpreted this information in terms of a dominant NW-SE regional dyke swarm (Figure 1.1).

Bott *et al.* (1958) completed the first gravity survey on Lundy Island and interpreted a positive gravity anomaly over the granite as indicating a genetically related basic mass underlying the island. Brooks and Thompson (1973) completed a comprehensive marine gravity survey around Lundy in the Outer Bristol Channel and derived an arcuate positive Bouguer anomaly within the Lundy Horst region with a high of + 53 mgal to the northwest of Lundy Island. The gravity anomalies were reported to be superimposed on a strong regional gradient of + 0.38 mgal km^{-1} to the west, which revealed a residual anomaly of + 23 mgal after its removal. They interpreted this as being indicative of an underlying, major basic intrusion at shallow depth with a maximum thickness of between 2.5 km and 4.0 km and lying in the area to the west and northwest of Lundy Island, but in some way related to movement along the Sticklepath Fault Zone to the east of Lundy. Structural weakness associated with the fault may thus have allowed relatively easy access for the basic magma through the continental crust. However, Brooks and Thompson (1973) did not fully elaborate on the contemporaneous relationship between basic magma and fault. Brooks (1973) considered that the basic intrusion was similar to other Tertiary igneous centres in northwest Scotland and related their collective form to an underlying hot spot. The idea of similarity was a major factor in leading Thorpe and Tindle (1991, 1992) to develop their hypothesis on the formation of a Lundy volcano.

1.3 OUTLINE OF PRESENT WORK

1.3.1 STRUCTURE OF THE THESIS

This thesis builds on research initiated by Dr. R. Thorpe of the Open University into the sub-surface form of the Lundy Igneous Complex. In particular, it uses both geophysical and geochemical information to investigate the nature and extent of igneous rocks in the study area, using these data to model the sub-surface geological relationships in the

Lundy Horst area. However, the distinction between granite host and the small number of rhyolite dykes is geophysically difficult and so no attempt is made to model rhyolite dykes. The underlying theme of the thesis is that Lundy Island may have been the site of a large composite volcano (Thorpe and Tindle, 1991) and evidence will be presented in a logical and sequential manner to examine this fundamental hypothesis.

Chapter 2 deals with the methodology employed in both sample and data collection. Chapter 3 contains new geochemical data to supplement the sampling of Thorpe and Tindle (1992). This information provides new insights into the existing data set on Lundy Island, provides new Ar-Ar dates for related dykes on the North Devon mainland and describes geochemical relationships between all basic rocks in the area. Chapter 4 addresses the field relations of the Lundy Dyke Swarm and contains the results of various laboratory experiments carried out to identify the magnetic properties of the dykes themselves. Chapter 5 describes existing gravity and magnetic data and re-processed gravity data to introduce the results of new computer modelling procedures as an alternative to models already published. Chapter 6 synthesizes and correlates both new and published data into a new model for Tertiary magmatism in the Bristol Channel area.

1.3.2 AIMS AND OBJECTIVES

1. To use proton magnetometry on Lundy Island to establish a) the existence, position and trend of the dykes where outcrop is absent and b) whether dykes cropping out in the eastern cliffs extend through the island to crop out in the western cliffs
2. To perform physical and magnetic properties experiments on dyke samples to study the source and level of magnetism and to investigate anisotropic relations.
3. To study major and minor geochemical features in the dykes and to correlate details with counterparts in North Devon and to date them by Ar-Ar methods.
4. To model both gravity and magnetic regional data and to study the deep structure of the area.
5. To integrate all the geophysical and geochemical information into a new model for Tertiary magmatism in the Outer Bristol Channel and to comment on the potential existence of a Lundy volcano.

CHAPTER 2

METHODOLOGY

2.1 FIELD TECHNIQUES

2.1.1 MAPPING OF FIELD RELATIONS (DYKES) ON LUNDY

Dykes are very poorly exposed over the flat, planed island surface due to a thin veneer of vegetation and superficial cover. The solid geology is restricted to discrete outcrops of granite and old quarry workings around the coastal sidelands. It is therefore not possible to record trends of dykes by conventional means over most of the island, but there is total exposure of the solid geology in the coastal cliffs and along foreshore beaches so that, although access is difficult for the most part, dips and strikes of dykes can be recorded with relative ease. These were measured with a standard geological Silva compass/clinometer at suitable locations around the island to give a geographic range of all dykes. Where access to coastal exposures was denied from the top of the island, landings were either made by swimming ashore from a small boat or by landing the boat itself. All measurements were taken over three two-week field trips to the island.

2.1.2 MAPPING OF FIELD RELATIONS (JOINTS)

Joint orientations were established in the field using conventional geological techniques. Where joint surfaces were sub-planar or within very coarse grained granite, several measurements of dip and strike were made and an average determined. Joints were assessed as systematic or non-systematic and grouped into individual joint sets. Types of joint style, joint-system architecture and spatial relationships between neighbouring joint planes were also determined in the field. A dispersion angle of 10^{o} for a spread of joints in a particular group was used to differentiate between two joint sets with small dihedral angles between them and a small joint spectra of orientations about a mean axis. Where possible, joint planes were examined for lineations and other indicators of relative displacement. The presence of gouge with, or without, brecciated fragments was taken to be indicative of fault movement and recorded.

2.1.3 PROTON MAGNETOMETRY

All magnetic surveying was carried out using the methodology of Breiner (1973) and a Geometrics 816 proton magnetometer, which measures the total magnetic field at any location. The sensing device for this instrument is a bottle of organic liquid, containing a large supply of hydrogen atoms, with a copper coil encompassing the liquid. The hydrogen nucleus (a proton) acts as a dipole and possesses a small magnetic moment, which normally aligns itself parallel to the external geomagnetic field. When a current (about 1 A) is passed through the coil, a strong internal magnetic field is created parallel to the long axis of the bottle, ideally perpendicular to the geomagnetic field, and the protons align themselves in this new direction. When the current is switched off, the internal magnetic field is negated and the protons re-align themselves parallel to the external geomagnetic field by precessing about the new direction. The frequency of this precession (f) is around 2kHz and given by

$$f = \frac{\gamma_p \mathbf{B}_e}{2\pi} \qquad \text{equation 2.1}$$

where γ_p = the gyromagnetic ratio of the proton (a known constant) and $\mathbf{B}_e$ = the total geomagnetic field strength or magnetic flux (Kearey and Brooks, 1984). $\mathbf{B}_e$ is thus directly proportional to f, which can be measured by the magnetometer. The value of magnetic flux is displayed in nanoteslas (nT) with a precision of ± 1 nT, each reading taking about 5 s to complete.

The bottle was attached to a 3 m pole and held at arm's length during operation to minimize interference from the power source (strapped to the operator's chest) and from influential soil artefacts, e.g. buried metal objects. The operator also discards all magnetic objects, such as rucksacks and watches. To ensure parity of measurement, each reading was taken with the pole vertical and an arbitrary mark on the bottle oriented to magnetic north. On Lundy, the inclination of the geomagnetic field at the present time is about 66° downwards with declination about 6°W (pers. comm. Dave McCann, BGS Geophysics Group). When the pole was vertical, the magnetic field induced by the

copper coil in the bottle was also vertical and about 24° away from the geomagnetic field. Angular differences up to 90° were tested in a magnetically quiet area for significant errors in reading the field strength. However, a 24° angular difference was found to be sufficient to allow proton precession and hence allow the maximum value of the total field strength to be measured by the magnetometer.

To correct for diurnal drift, a base station (Marisco) was established over a granite outcrop in a magnetically quiet area, where magnetic readings varied by only ± 5 nT over a 5 m radius. Repeated readings were usually taken every 30 minutes at Marisco base on magnetically quiet days (Q days) increasing to every 15 minutes on more noisy days, a second operator using a different Geometrics 816 proton magnetometer was required for this task. Kearey and Brooks (1984) define an amplitude of 20-80 nT as acceptable variation in a 24 hour period on Q days and up to 1000 nT on disturbed days, when all magnetic surveying should be discontinued. An average of three readings was taken at each time interval with repeatability to within ± 2 nT for each set of readings. When work was being undertaken at large distances from Marisco base, the standard method of looping to intermediary base stations enabled magnetic readings to be taken and corrected for diurnal drift. This method also monitored for any unusual magnetic activity, e.g. solar flares or sudden impulses, which could have affected readings over relatively short periods and rendered magnetic surveying ineffective. Whenever the peak amplitude of diurnal drift exceeded an arbitrary 80 nT per working day, readings were deemed unreliable and magnetic surveying was abandoned until the disturbance settled down to normal levels.

Data for more precise diurnal corrections were obtained from Hartland Observatory, under the control of the Automatic Remote Geomagnetic Observatory System (ARGOS). Here, fluxgate magnetometers measure the north (X), east (Y) and vertical (Z) components of the earth's magnetic field every 10 s, the samples then being processed to produce minute values and hourly mean values. Minute values are used in daily magnetograms, which display variations in declination (D), horizontal intensity (**H**) and vertical intensity (**Z**) every minute over a 24 hour period, whilst hourly mean values are

computed from minute values. Proton magnetometers measure the total intensity of the field (**B**) once per hour and provide baseline reference measurements. However, for this research, the total field intensity was calculated from **H** and **Z** values for 5 minute intervals throughout the surveying period, diurnal drift then being plotted graphically.

During the main periods of magnetic surveying on Lundy, the times of all magnetic observations were noted along with the magnetic value itself. This allowed the level of diurnal drift to be recorded whilst magnetic surveying proceeded, thus affording constant monitoring of when surveying should be temporarily suspended in times of anomalously high magnetic activity. Correlations with absolute observations at Hartland Observatory not only allowed the level of magnetic disturbance during the surveying period to be recorded to a higher degree of accuracy, but also provided detail on the level of magnetic activity during the times surveying was halted. As Hartland Observatory is only 25 km to the south-southeast of Lundy, it was assumed that magnetic changes on Lundy Island would be almost identical to changes at the Observatory itself.

An initial reconnaissance of the island was undertaken in June 1991 to highlight the background signature and to delineate areas of interest. Two traverses from the south to north end were completed, one on each side of the island (Figure 2.1), with total field readings taken every 5 m and diurnal drift monitored by looping to temporary base stations (Breiner, 1973). The orientation of the reconnaissance lines was approximately north-south so that profiles were aligned with the Earth's magnetic field, facilitating interpretation of the underlying geology. In some areas man-made artefacts, such as walls and electric fences which may have created spurious readings, made it desirable for the profiles to be oblique so that possible interference to magnetic readings might be avoided.

Anomalous signatures were noted as possibly representing the position of magnetic rocks and marked on the ground with a flag. Ten separate flagged positions were magnetically surveyed every 1 m for a distance of 50 m to the north and south of the flag and hand augering up to a depth of 3 m over each magnetic 'high' explored the underlying geology to eliminate non-geological causes.

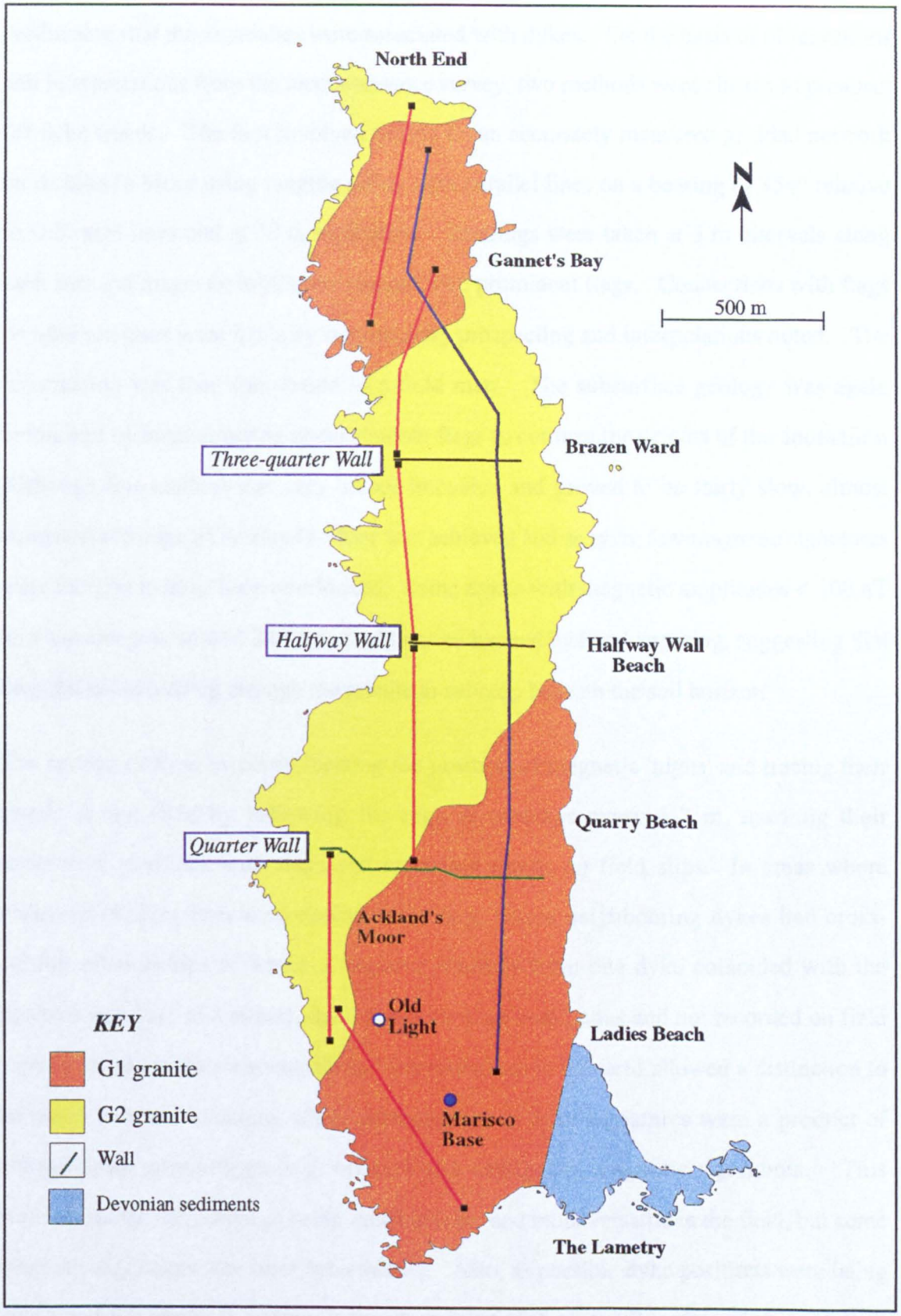

Figure 2.1: Magnetic reconnaissance survey on Lundy Island.
The blue line represents a traverse up the main track. Results from the red traverse are presented in Figure 3.4. Marisco base was used as the main monitoring station for diurnal drift.

In each case, magnetic signatures could be related to particular geological features and confirming that the anomalies were associated with dykes. On the basis of observations and interpretations from the reconnaissance survey, two methods were chosen to prospect for dyke trends. The first involved setting up an accurately measured gridded network on Ackland's Moor using ranging poles, with parallel lines on a bearing of 354° relative to O.S. grid lines and at 30 m separation. Readings were taken at 5 m intervals along each line and magnetic high spots marked with prominent flags. Connections with flags on adjacent lines were made by intermediary prospecting and interpolations noted. The information was then transferred to a field map. The subsurface geology was again monitored by hand augering under random flags to confirm the origins of the anomalies. Although this method was very labour intensive and proved to be fairly slow, almost complete coverage of Ackland's Moor was achieved and as such, few magnetic signatures were thought to have been overlooked. Some dykes with magnetic amplitudes < 100 nT and wavelengths around 30-40 m could not be located by hand augering, suggesting that they did not extend up through the granite to subcrop beneath the soil horizon.

The second method involved locating the position of magnetic 'highs' and tracing their trends in the field by following the highest readings every 1-2 m, marking their successive positions with flags and recording trends on field slips. In areas where magnetic profiles interfered destructively (e.g. where neighbouring dykes had cross-cutting relationships or where a negative anomaly from one dyke coincided with the positive signature of another), dyke positions were ambiguous and not recorded on field slips to avoid erroneous conclusions. Interpolations in the field allowed a distinction to be made between locations where interruptions to dyke signatures were a product of normal dyke morphology (e.g. off-lap) and ambiguous magnetic signatures. This method had the advantage of being much quicker and more versatile in the field, but some magnetic signatures may have been missed. Also, as possible dyke positions were being noted and not absolute values, it was less important to monitor diurnal drift at such frequent intervals. For both methods, trends and map positions were recorded using triangulation techniques with a siting compass. Prominent buildings and positive features of relief were utilized as suitable directional indicators.

The total time spent on proton magnetometry was seven field weeks, assisted for two weeks by twelve members of the Open University Geological Society, who acted as field assistants for the second method.

2.2 LABORATORY-BASED MAGNETIC TECHNIQUES

2.2.1 MAGNETIC SUSCEPTIBILITY

243 oriented and non-oriented core samples from the study area were measured for magnetic susceptibility on a standard AC Bartington susceptibility bridge with an operating frequency of 4.7 kHz in an applied magnetic field of 300 μT and sensitivity of 1.2×10^{-5}. The bridge, which is housed at the Institute of Rock Magnetism (IRM), University of Minnesota, has an estimated calibration accuracy of ± 5% (Dr.C.Hunt, pers. comm.). Samples, and hence susceptibilities, were standardized to 8 cm^3 to ensure parity and measured in one session, with time of measurement also noted. The drift was monitored every 5 minutes with a standard sample of known bulk susceptibility 0.8256 (SI units), apparent values being graphically recorded, so that corrections with respect to time for other measured cores might be facilitated.

100 random cores from the sample collection were re-measured on a comparable Bartington bridge in the Geophysics Laboratory at the Open University to test repeatability of measurements. Regular monitoring for instrument drift was undertaken by the same method with a control core of known intermediate susceptibility (0.0752, SI units), measured at the University of Liverpool with an estimated accuracy of ± 1% (Dr. Hazel Rymer, pers. comm.). Comparability of data between the two laboratories was found to be good, with the IRM bridge mostly measuring susceptibilities up to 2.1% higher than the Open University bridge. This method also served to test absolute accuracy of instrumentation relative to known sources, both bridges measuring to within ± 1.5% after corrections for drift.

2.2.2 ANISOTROPY OF MAGNETIC SUSCEPTIBILITY (AMS) OF DYKES

The low field magnetic susceptibility anisotropy of 152 oriented cores from 42 dykes, including 38 dykes on Lundy Island, was measured at room temperature in the Institute for Rock Magnetism, University of Minnesota using an in-house designed and constructed susceptibility anisotropy bridge, called the "Roly Poly". The dykes were doleritic and trachytic in composition, as rhyolites were not sampled due to their low magnetic susceptibility (by around four orders of magnitude lower than the dolerites and trachytes). Figures 2.2 and 2.3 show the locations of dykes.

The bridge uses AC current with an operating frequency of 750 Hz, has a sensitivity of 1.2×10^{-6} SI and operates in a self adjusting magnetic field, according to the signal strength of the specimen; this can be as high as 1 mT for magnetically weak specimens or as low as 0.01 mT for strong specimens. The majority of the 152 specimens were measured in a magnetic field of 0.1 mT, which is equal to twice the strength of the earth's magnetic field, with some weaker specimens of intermediate composition measured in a field of 1 mT. The field is applied by a pair of Helmholtz coils, with an internal diameter of 80 mm, producing a virtually uniform field throughout the specimen volume. The apparatus automatically compensates for drift

Cores and hence susceptibility values, were standardized to a volume of 8 cm^3 to ensure parity and measured in a magnetically screened environment to eliminate laboratory 'noise'. When a rock sample was placed inside the measuring cylinder of the Roly Poly, a fractional change of inductance was induced in the coil. This change was directly proportional to the bulk susceptibility and the volume ratio of the specimen to air space (Fuller, 1967). Measurement was computer controlled and during each measurement cycle, the specimen was rotated 360^o in a plane perpendicular to the long axis of the measuring cylinder for 3 different positions, designed to represent 3 orthogonal planes.

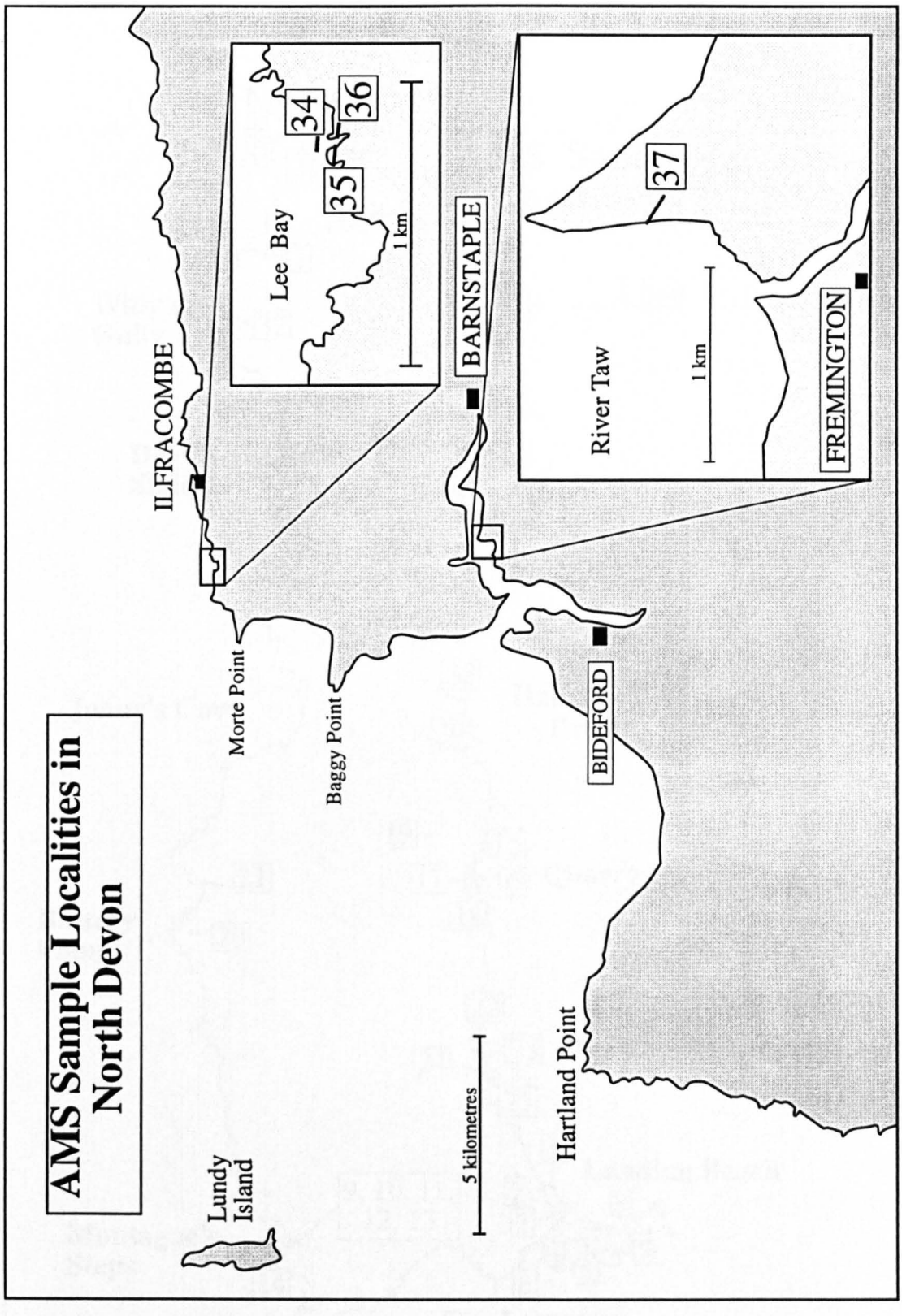

Figure 2.2: AMS sample localities in North Devon.
AMS = anisotropy of magnetic susceptibility (as described in section 2.2.2). Dyke numbers correspond to data presented in Appendix A2.

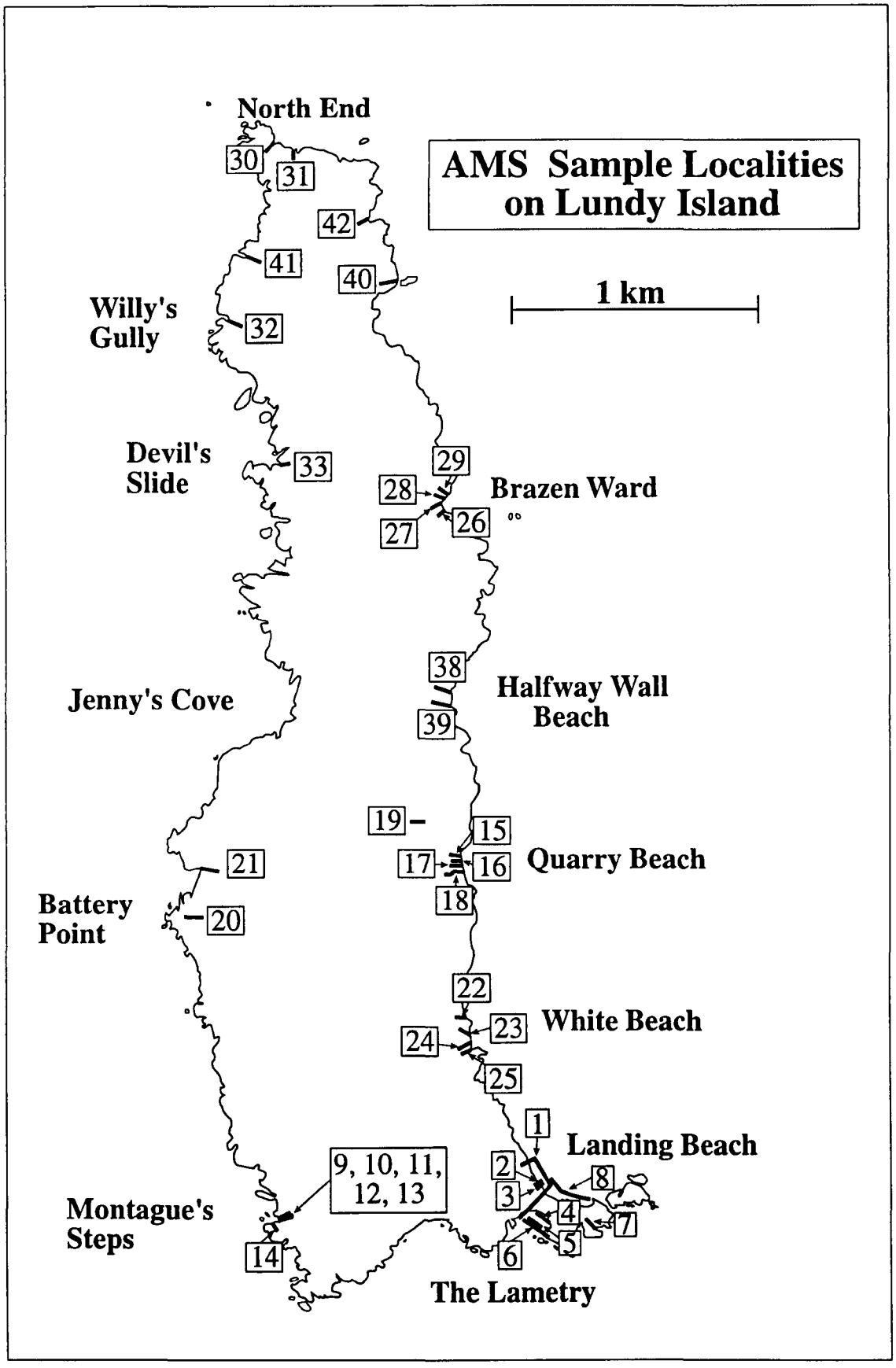

Figure 2.3: AMS sample localities on Lundy Island.
Sample localities correspond to data sample numbers presented in Appendix A2. Dolerite dykes at localities 7, 31 40 and 42 were excessively weathered and did not reveal reliable susceptibility results (cf. section 4.4.3.2).

The stepper motor paused for a fraction of a second every 1.8°, allowing a measurement to be made using one or more AC cycles. Thus, during 360° rotation, 200 directional susceptibility measurements were made. This was repeated for the other two positions, yielding a total of 600 directional susceptibility measurements at 1.8° intervals in 3 orthogonal planes. A least squares best-fit triaxial ellipsoid was then calculated by the computer using in-house dedicated software.

The repeatability of data sets was initially tested by measuring 5 randomly chosen cores from the sample set and duplicating the measuring cycle for N = 1, 2 & 3. This test revealed differences of less than 4° in declination and 2° in inclination for directional measurements in all five specimens, larger errors probably being caused by small variations in core shape giving small departures from the standard core volume. Determinations were thus considered to be reasonably precise, due to the large number of readings in each measurement cycle, and on this basis, one measurement cycle was chosen as suitable for each specimen. Each cycle was completed in 12 minutes. Output from the bridge was fed into an in-house computer program and the principal components and properties calculated.

The main susceptibility tensor is described within a Cartesian axis system, in which the components of the symmetric, second rank tensor are given by k_{ij} ($k_{ij} = k_{ji}$), where i =1,2,3 and j =1,2,3 (Hrouda, 1982). The tensor thus has the form -

$$\begin{matrix} k_{11} & k_{12} & k_{13} \\ k_{21} & k_{22} & k_{23} \\ k_{31} & k_{32} & k_{33} \end{matrix} \qquad \text{equation 2.2}$$

The components k_{11}, k_{22} and k_{33} represent the principal susceptibilities and form the magnitude ellipsoid (Nagata, 1964), which can be derived from four measurements at 45° intervals in three orthogonal planes. The residual susceptibility was obtained from the difference between measured and best-fit susceptibilities (measured to six significant figures) and the root mean square (RMS) calculated from the relationship -

$$\frac{\text{(RMS residual k)}}{\text{(RMS measured k)}} \times 100\% \qquad \text{equation 2.3}$$

Values < 1% were taken to indicate an accurate representation of the AMS tensor. After correction for field sampling orientations, the magnitude and direction (in terms of declination and inclination) of the principal susceptibilities are given for each sample, where K1 = direction of maximum susceptibility, K2 = direction of intermediate susceptibility and K3 = direction of minimum susceptibility. The average bulk susceptibility in SI units is the arithmetic mean of the principal susceptibilities (Nagata, 1964; Janák, 1965), so

$$K_{mean} = \frac{K_1+K_2+K_3}{3} \qquad \text{equation 2.4}$$

Susceptibilities usually have a lognormal distribution pattern for a series of rocks (Mussett *et al.*, 1976; Tarling, 1983), thus the average susceptibility is more accurately represented by the geometric (log) mean. However, as Tarling and Hrouda (1993) observe, where data are of the same order of magnitude, the arithmetic mean only slightly exceeds the geometric mean and so the arithmetic mean is adopted in this thesis

The magnitude of anisotropy is calculated by the relationship between maximum and minimum susceptibilities, termed the anisotropy degree (P_2) by Nagata (1964) and is shown as

$$P_2 = \frac{K_1}{K_3} \qquad \text{equation 2.5}$$

Similarly, the normalized anisotropy degree (Owens, 1974) is given by

$$H = \frac{K_1 - K_3}{K_{mean}} \qquad \text{equation 2.6}$$

Tarling and Hrouda (1993) indicate that these two parameters may be misleading, in that a wide range of susceptibilities may occur within a single rock type and that comparability of arithmetic values in a lognormal distribution is inappropriate. Furthermore, the intermediate susceptibility (K_2) does not take part in the calculations, and so they recommend that the corrected anisotropy degree, as developed by Jelinek (1981), should be adopted.

This is given by -

$$P_J = \exp\sqrt{\{2[(\eta_1-\eta_m)^2+(\eta_2-\eta_m)^2+(\eta_3-\eta_m)^2]\}} \quad \text{equation 2.7}$$

where, $\eta_1 = \ln K_1$, $\eta_2 = \ln K_2$, $\eta_3 = \ln K_3$ and $\eta_m = (\eta_1+\eta_2+\eta_3)/3$. This relationship involves all the parameters used in the geometric mean, but is based on the logarithmic values of susceptibility, which is more meaningful in lognormal distributions, and has been adopted in this thesis.

The software also calculates other parameters, in terms of the shape of the anisotropy ellipsoid. Lineation (P_1) as formulated by Balsley and Buddington (1960) and foliation (P_3) given by Stacey *et al.* (1960) are determined by

$$P_1 = \frac{K_1}{K_2} \quad \text{equation 2.8}$$

$$P_3 = \frac{K_2}{K_3} \quad \text{equation 2.9}$$

Similar properties are also presented by considering differences between K_1, K_2 and K_3 and attempting to normalize data relative to the geometric mean susceptibility. The normalized lineation (L) and normalized foliation (F) were both proposed by Khan (1962) and are given as

$$L = \frac{K_1 - K_2}{K_{mean}} \qquad F = \frac{K_2 - K_3}{K_{mean}} \quad \text{equation 2.10}$$

However, Tarling and Hrouda (1993) consider that such geometric formulae not only mis-represent the lognormal characteristics of susceptibility data, but are also open to confusion whilst comparing data and terminology by different authorities, resulting in potential excessive misunderstandings in data interpretation. They thus recommend that the shape parameter (T) introduced by Jelinek (1981) and discussed by Hrouda (1982) be adopted, given by

$$T = \left[\frac{2(\eta_2 - \eta_3)}{(\eta_1 - \eta_3)}\right] - 1 \quad \text{equation 2.11}$$

In practical terms, this is more usefully written as -

$$T = \frac{\left(\ln \frac{K_1}{K_2} - \ln \frac{K_2}{K_3}\right)}{\left(\ln \frac{K_1}{K_2} + \ln \frac{K_2}{K_3}\right)} \qquad \text{equation 2.12}$$

In this form, the relationship still involves all three principal susceptibilities, but results in a more balanced spread of values for the susceptibility ellipsoid shape than P_2 (Tarling and Hrouda, 1993). Values of $T = 0 < T \leq 1$ correspond to oblate ellipsoids, whereas values of $T = -1 \leq T < 0$ correspond to prolate shapes and values of $T \approx 0$ relate to neutral ellipsoids. This parameter is chosen as the preferred shape parameter in this thesis.

2.2.3 CURIE TEMPERATURE DETERMINATIONS AND HYSTERESIS LOOPS

18 whole rock crushed samples of basic intrusions were analysed on a vibrating sample magnetometer (Princetown Measurements VSM) with a published sensitivity of 2×10^{-8} Am^2 at the Institute of Rock Magnetism (University of Minnesota) to measure hysteresis loops and determine Curie temperatures. The VSM operates by vibrating a prepared sample perpendicular to an applied magnetic field, which is formed by a pair of 6 cm electromagnets, and the resultant magnetic flux changes are detected by a pair of sensing coils. These changes are proportional to the magnetic moment of the sample, which is interpreted by the operating software and recorded at averaging time constants from 10 ms to 10 s.

Hysteresis loops were initially obtained from samples with an applied field between +1000 mT and -1000 mT at ambient room temperatures and with a time constant of 100 ms in a 15 minute total sweep time for each sample. Output to a standard A4 plotter was configured so that the Y-axis displayed magnetization and the X-axis displayed the magnetic field. All data were normalised to correct for paramagnetic behaviour as the field increased. The saturation field (H_{sat}) was found to be between 150 mT and 300 mT for initial samples, and so the maximum applied field was reduced to 450 mT to prevent excessive paramagnetic effects.

The parameters determined by the operating software from the completed hysteresis loops were (i) the saturation magnetization (M_{sat}), which indicates when the sample is magnetically saturated, (ii) the saturation remanence (M_r), which is the magnetization present when the field is reduce to zero, (iii) the coercivity of remanence (H_c), which is the field when the induced magnetization is reduced to zero and (iv) the coercivity of remanence (H_{cr}), which is the reverse field that reduces M_r to zero when applied and then removed.

Curie temperature determinations were undertaken from ambient room temperatures up to 650 °C in an applied field of 350 mT. This level appeared sufficient to bring about magnetic saturation by the results of the hysteresis loops and, using helium gas as a confining medium to inhibit oxidation of minerals, each run took approximately 1.5 hours to complete. The heating leg was completed in 35 minutes, the cooling leg taking around 55 minutes to return to ambient room temperatures. Data output was controlled by a dedicated computer program into a graphical display of saturation magnetization (M_s) plotted against temperature (°C), with statistically derived heating leg Curie points and cooling leg Curie points also displayed. Temperature accuracies are to within ± 0.75% of the displayed temperature and M_s to within $\pm 5 \times 10^{-5}$ Am^2kg^{-1}.

2.2.4. NATURAL REMANENT MAGNETIZATION (NRM)

NRM measurements were taken from nine oriented cores of basic dykes at the Palaeomagnetism Laboratory, University of Plymouth, using a Molspin MS2 magnetometer and a Digico alternating field (AF) demagnetizer. The former rotates the sample about a vertical axis at approximately 7 rotations per second and measures the magnetization (J) in a theoretically zero magnetic field to a sensitivity within 0.02 - 0.05 mAm^{-1}. Six independent sample orientations, pre-determined by the operating software and designed to represent three orthogonal planes, were used in each measuring cycle. Calibration of the magnetometer was undertaken by measuring a standard sample of known magnetization, J = 339 mA m^{-1}, after each measurement by rotating the measuring cylinder slightly until a value of 339 mAm^{-1} ± 0.5 mAm^{-1} was obtained.

Isolation of primary NRM characteristics was obtained by selective removal of secondary remanence, as indicated in Tarling (1983), in a series of demagnetization procedures using an AF demagnetizer with an operating frequency of 50 Hz. For each specimen, demagnetization treatment was carried out in a 15-step sequence, the peak field being set at 0, 3, 5, 7, 10, 20, 30, 40, 50, 60, 70, 80, 90 and 100 mT, in which the specimen was rotated about 2 axes to ensure uniform demagnetization. The sinusoidal waveform of the alternating magnetic field had a linear decay rate with respect to time, expressed by four selectable values, which were 0.004 mT $cycle^{-1}$, 0.008 mT $cycle^{-1}$, 0.016 mT $cycle^{-1}$ and 0.032 mT $cycle^{-1}$. Lower values relate to lower peak fields and higher values to higher peak fields. Specimens were measured on the Molspin magnetometer after each demagnetization step and results entered into "DATAIN", a software programme developed by Prof. D. Tarling, to prepare data in a suitable format for analysis by "PILOT" software, also developed by the same author.

2.3 COMPUTER MODELLING

2.3.1 GRAVITY AND MAGNETIC DATA

Processed gravity and magnetic data were generously made available by Dr. Ian Smith, Regional Geophysics Group, British Geological Society, Keyworth. The area involved was defined by the British National Grid (BNG) as 100-300 km East and 100-200 km North of the BNG origin, namely the outer Bristol Channel and bordering land areas. Marine gravity surveys within the defined area were undertaken by Brooks and Thompson (1973) and Davey (1970), both in conjunction with the Marine Geophysics Group of the IGS. The survey of Brooks and Thompson (1973) covers the area to the east of 4° 00'W and north of 51° 00'N (geographic co-ordinates) and was completed mainly by a series of east-west sampling traverses at 5 km intervals and north-south traverses at 12 km separation. Stations were mostly sampled every 1 to 2 km with an average accuracy of ± 0.55 mGal, determined by analysis of gravity values at traverse line intersections and data were calibrated relative to the IGF reference base station in Cardiff Docks. The survey of Davey (1970) concentrated to the west of 4° 00'W.

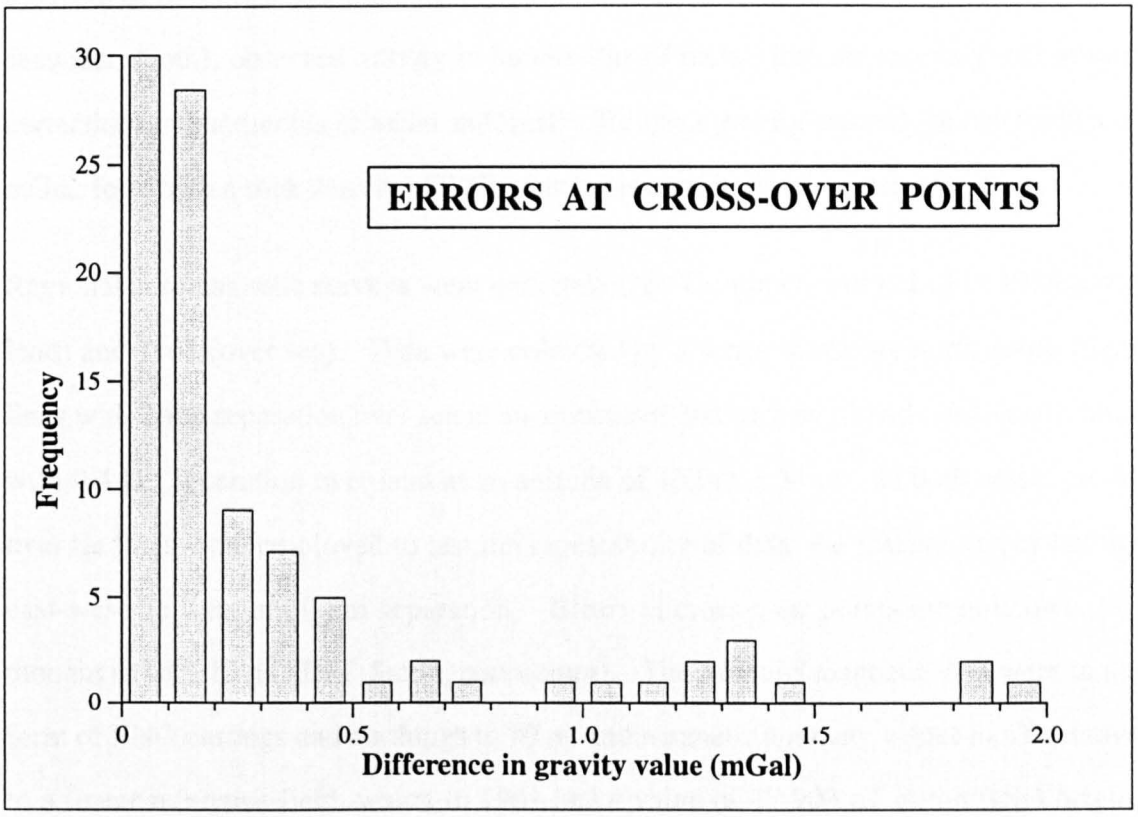

Figure 2.4: Errors at cross-over points from the gravity survey in the Bristol Channel.
Errors have been determined by comparing the Bouguer gravity anomaly values for two gravity stations on different sample lines providing that both stations are located within 100 m of each other. The rationale for this method assumes that gravity anomaly values will not vary much over a distance of 100 m, which was chosen as the minimum inter-station distance to provide the maximum number of cross-over data points without introducing unnecessary error. A separation of 50 m did not give enough data points to reveal reliable statistical information. Gravity sample lines are given in Figure 2.5.

Figure 2.4 displays the cross-over errors in the supplied gravity data by comparing the values at all gravity stations within 100 m of each other, 1.9% being the largest. Errors between 0.9 and 1.9% occurred in areas of relatively high magnetic relief and so may be partly due to variations in the magnetic signature. There is thus good agreement with the errors published by Brooks and Thompson (1973). The supplied gravity data were in the form of BNG eastings and northings to 10 m, station elevation in decimetres (equal to seawater depth), observed gravity in hundredths of mGal, free air anomaly and terrain corrections in hundredths of mGal and finally, Bouguer gravity anomaly in hundredths of mGal, for which a rock density of 2.67 gcm^{-3} was used in the Bouguer correction.

Regional aeromagnetic surveys were undertaken by Hunting Surveys Ltd in 1958 (over land) and 1961 (over sea). Data were collected by a series of mainly north-south flight lines with 2 km separation over sea at an altitude of 305 m ± 46 m and north-south lines with 0.4 km separation over land at an altitude of 152 m ± 30 m. In both cases, cross-over tie lines were employed to test the repeatability of data, the marine survey having east-west tie lines at 10 km separation. Errors at cross-over points are unknown, but thought to be ≤ 10 nT (Dr.I. Smith, pers comm). The supplied magnetic data were in the form of BNG eastings and northings to 10 m, and magnetic anomaly values in nT relative to a linear reference field, which in 1961 had a value of 47 903 nT at the BNG origin, increasing by 2.17 $nTkm^{-1}$ northwards and decreasing by 0.26 $nTkm^{-1}$ eastwards (Burley, 1979).

Aeromagnetic anomaly maps were constructed using UNIMAP 2000 (part of the UNIRAS suite of computer graphics packages). To obtain maximum effectiveness, the gravity data file was first read into the computer and then a small window of data processed prior to computation. The relevant study area was between 110 000 mN and 200 000 mN, and 130 000 mE and 260 000 mE (BNG co-ordinates). This block was chosen as a representative geographic coverage of the sampling area, i.e. Lundy Island and North Devon, whilst also allowing a regional perspective of the Lundy Igneous Complex to be considered. The maximum number of grid cells (X-axis 200, Y-axis 200) allowed for interpolation was chosen so as to minimize the spiky appearance of contoured

anomaly maps. Identical co-ordinates were chosen for the magnetic data as the gravity data and a similar rationale was applied.

The contoured gravity data constitute a Bouguer anomaly map using 5456 data points; Figure 2.5 records the location of ship sampling lines. This map was contoured at 1 mGal intervals to allow accurate derivation of anomaly values along any traverses needed for modelling procedures. Larger contour intervals may potentially introduce errors when interpolating values between isogals. A magnetic anomaly map was similarly contoured at 5 nT intervals from 4912 data points; Figure 2.6 shows the survey flight lines. In this case, 5 nT was chosen as large enough to provide useful magnetic detail throughout the region, but not so small as to inhibit definition of contours in areas of high magnetic relief. Experimentation with plotting indicated that for contour intervals < 5 nT, transposing magnetic anomaly data from traverses proved difficult and led to erroneous profiles.

2.3.2 MODELLING OF GRAVITY DATA

Gravmag, a highly interactive 2.5D gravity and magnetic modelling program (Pedley, 1991), was chosen to model the deep geological structure in the study area. This allows the user to rapidly construct and edit realistic geological models, and has been designed to maximize the degree of interaction. A PC version of the software, which is compatible with the main frame parent program, allows modelling to be carried out at different sites, increasing accessibility to modelling procedures. Two dimensional observed gravity anomaly profiles, i.e. anomaly amplitude with respect to horizontal distance, used by Gravmag during program operation were derived from the Bouguer anomaly map of the region, see 2.3.1, which was plotted onto A1 size paper to facilitate accurate interpretation of the gravity signature.

The program calculates the gravitational effect of a variable number of polygons, each of which is modifiable in terms of shape and physical properties. A comparison is then made with the observed gravity profile and a visual display of observed, calculated and residual fields is produced along with a 2D section of the constructed model.

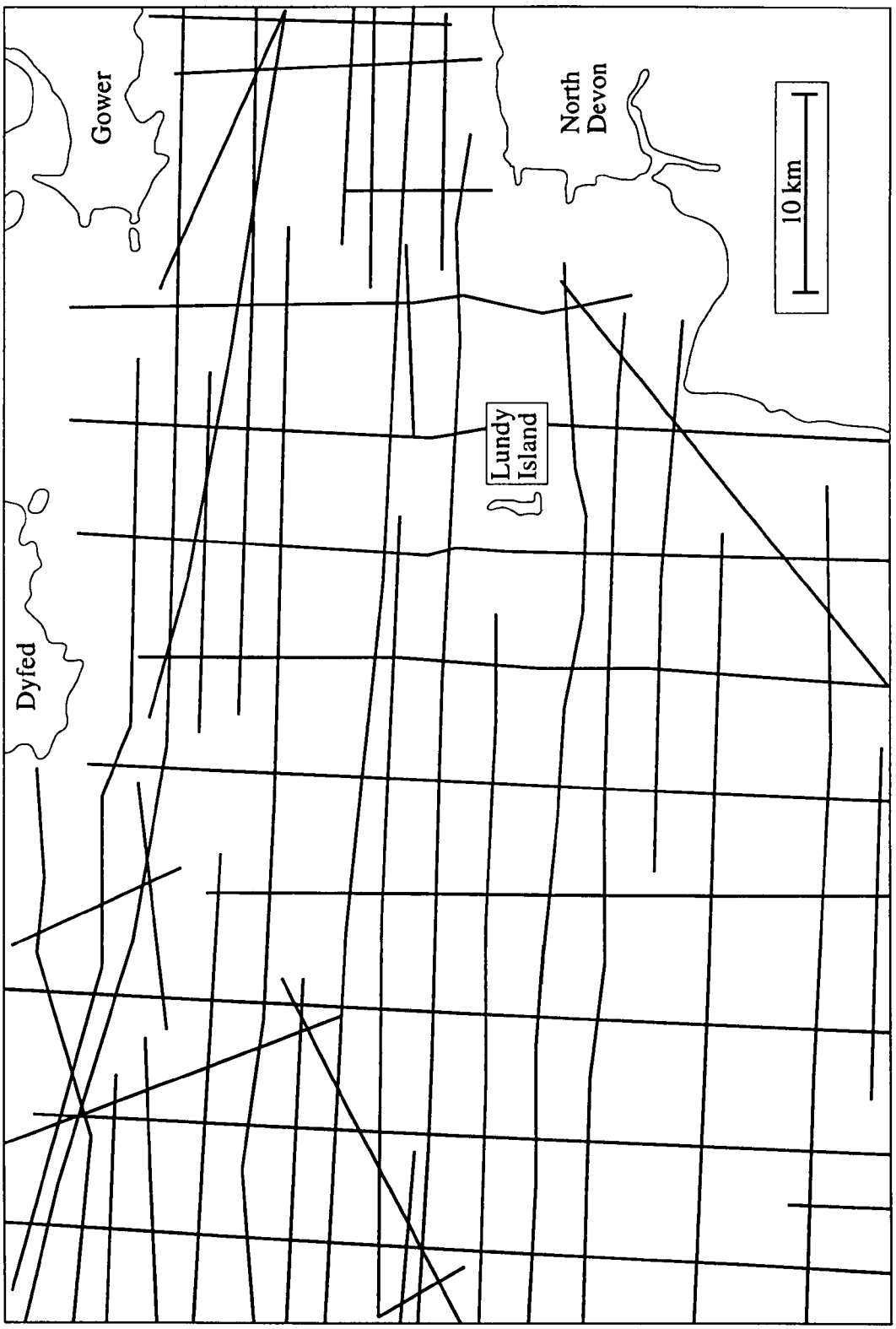

Figure 2.5: Marine gravity sample lines in the Outer Bristol Channel.
After Davey (1970) and Brooks and Thompson (1973).

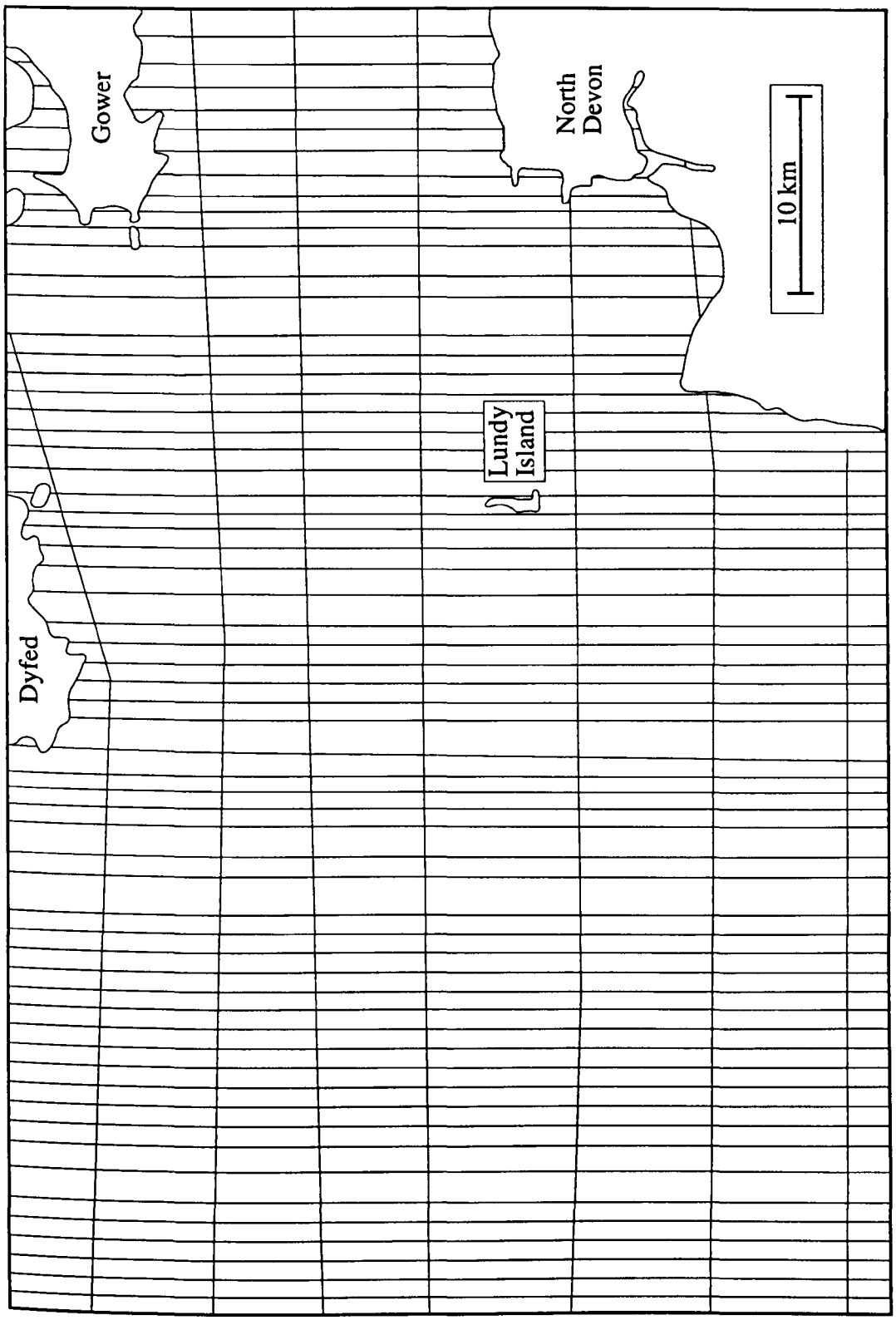

Figure 2.6: Flight lines for the aeromagnetic survey of the Outer Bristol Channel. North-south flight lines were spaced approximately 2 km apart and provided the main data set. East-west flight lines were used as tie-lines to monitor drift. Total number of sample points = 4512.

The theory for gravity calculations is taken from Ramussen and Pedersen (1979). Forward modelling and optimization allows adjustment and modification of the model until a close fit is obtained between observed and calculated fields. The quality of the fit was determined using residual anomalies; a 5% maximum error between observed and calculated fields was arbitrarily chosen as being satisfactory in areas of medium to high relief and 1% in areas of low relief. However, polygonal bodies and their physical properties needed to be restricted to reasonable geological probabilities, rather than mathematical models, even though these may provide good apparent fits.

Rock densities have been given for stratigraphical sequences in the study area by Cook and Thirlaway (1952), Bott *et al.* (1958), Brooks and Thompson (1973) and Brooks *et al.* (1977), detailed in Tables 5.1 and 5.2. In addition to these, density measurements were made on 16 granite samples, 42 basic samples, 17 intermediate samples and 21 Upper Devonian sedimentary rocks from Lundy Island.

The method used was to weigh the samples in water, based on Archimedes' principle. For this, rock samples were first weighed in air and then suspended in water. To ensure that all pores were water saturated, samples were soaked for at least 48 hours in water. The addition of a small amount of detergent to the water decreased surface tension and allowed more complete saturation without significantly changing the density of the water. From Archimedes' principle, the volume of the rock sample, V_r (cm^3), when immersed in water is -

$$V_r = m_a - m_w \text{ (masses in g)} \qquad \text{equation 2.13}$$

where, m_a = mass of water saturated sample in air

m_w = mass of sample in water

It thus follows that the density of the rock sample, ρ_r, is given by

$$\rho_r = \frac{m_a}{(m_a - m_w)} \text{ g cm}^{-3} \qquad \text{equation 2.14}$$

2.3.3 MODELLING OF MAGNETIC DATA

Gravmag was also used for computer modelling of magnetic data, using similar procedures to those described in section 2.3.2. The magnetic anomaly contour map derived with UNIMAP contained higher relief features than the Bouguer anomaly map, allowing smaller areas of interest to be modelled to a higher degree of sensitivity. This not only reflected the greater numerical range in anomalous magnetic values in the area, but was also because the magnetic survey lines were closer together than the gravity survey lines, i.e. 2 km separation for magnetics, 12 km for gravity. The theory for magnetic calculations was taken from Shuey and Pasquale (1973).

Magnetic susceptibility values used in modelling were either taken from Mussett *et al.* (1976) or averaged from those obtained from cored samples, as described in section 2.2.2. Mussett *et al.* (1976) carried out detailed palaeomagnetic work on 66 dykes from Lundy, both basic and intermediate in composition, and noted a strong correlation between magnetic susceptibility and natural remanent intensity. Transposed into SI units, they report a bimodal lognormal distribution pattern for magnetic susceptibility with peak values of 4×10^{-4} and 3×10^{-2}. These two values were taken as the starting susceptibility values during modelling procedures, the underlying assumption being that the dykes were probably derived from ancient plutonic bodies in the area and thus would be expected to have some similarities in physical properties with those bodies. To supplement these data, susceptibility values from cored samples of dykes, granite and sedimentary rocks on Lundy were also considered in the modelling. Although all cores were relatively unweathered, susceptibility values obtained are likely to be minimum values, as subaerial oxidation and alteration of magnetic minerals may not be mirrored at depth in larger igneous bodies. Magnetism in the sediments, however, is probably very weak and secondary.

The starting values for remanent magnetization were also taken from Mussett *et al.* (1976), who report main values in the range 5 to 13×10^{-4} Am^2kg^{-1}, with smaller peaks around 50×10^{-4} Am^2kg^{-1} and 0.003×10^{-4} Am^2kg^{-1}. Transposed into SI units, this gives the main range of values as 1.5 to 3.7 Am^{-1}, with smaller distributions at 4.2 Am^{-1}

and 2.3×10^{-3} Am^{-1}, assuming a mean density of 2.9 gcm^{-3} for the dykes. The declination and inclination of remanence reported by Mussett *et al.* (1976), i.e. 003.6°E, -62.7° (up) with $\alpha_{95} = 1.5°$, were the preferred parameters for the Tertiary magnetic field, as these values were determined locally and may be more appropriate for the Lundy Igneous Complex than other palaeomagnetic values from the British Tertiary Volcanic Province. During the summer of 1991, the geomagnetic field at the south end of Lundy Island had a total field value of 48041 nT, calculated from the 1991.5 geomagnetic reference field. The total field was very similar to this in 1961, when the aeromagnetic survey was flown and the magnetic anomalies first calculated (pers comm, E.Harris, Geomagnetism Group, BGS), and so this value was taken as suitable for use in modelling. The field strength (H) used in all modelling procedures was taken as 39.0557 Am^{-1}, derived from the relationship

$$H = \frac{B}{\mu_0} \text{ Am}^{-1} \qquad \text{equation 2.15}$$

where B= background magnetic induction (T) and μ_0= magnetic permeability of free space, ($4\pi \times 10^{-7}$ Hm^{-1}).

2.4 LABORATORY BASED GEOCHEMISTRY TECHNIQUES

In North Devon, igneous rock samples were collected from Lee Bay, Fremington and the Horse-Shoe Rocks (Figure 2.7) and from thirteen localities around Lundy Island (Figure 2.8). The thirteen localities on Lundy Island were different to the five published dolerite analyses out of 28 dykes sampled by Thorpe and Tindle (1992) and were chosen specifically to supplement their data set whilst at the same time increasing the geographic range of sample localities for the Lundy Dyke Swarm. Analyses by Thorpe and Tindle (1992) were collected from XRF apparatus at Southampton University and an old EDXRF system at the Open University. New data presented in Chapter 3 were collected from an ARL wavelength XRF at the Open University and so all data from Thorpe and Tindle (1992) have been re-calibrated to reduce inter-laboratory errors and allow a more meaningful comparison of the results.

Figure 2.7: XRF sample localities in North Devon.

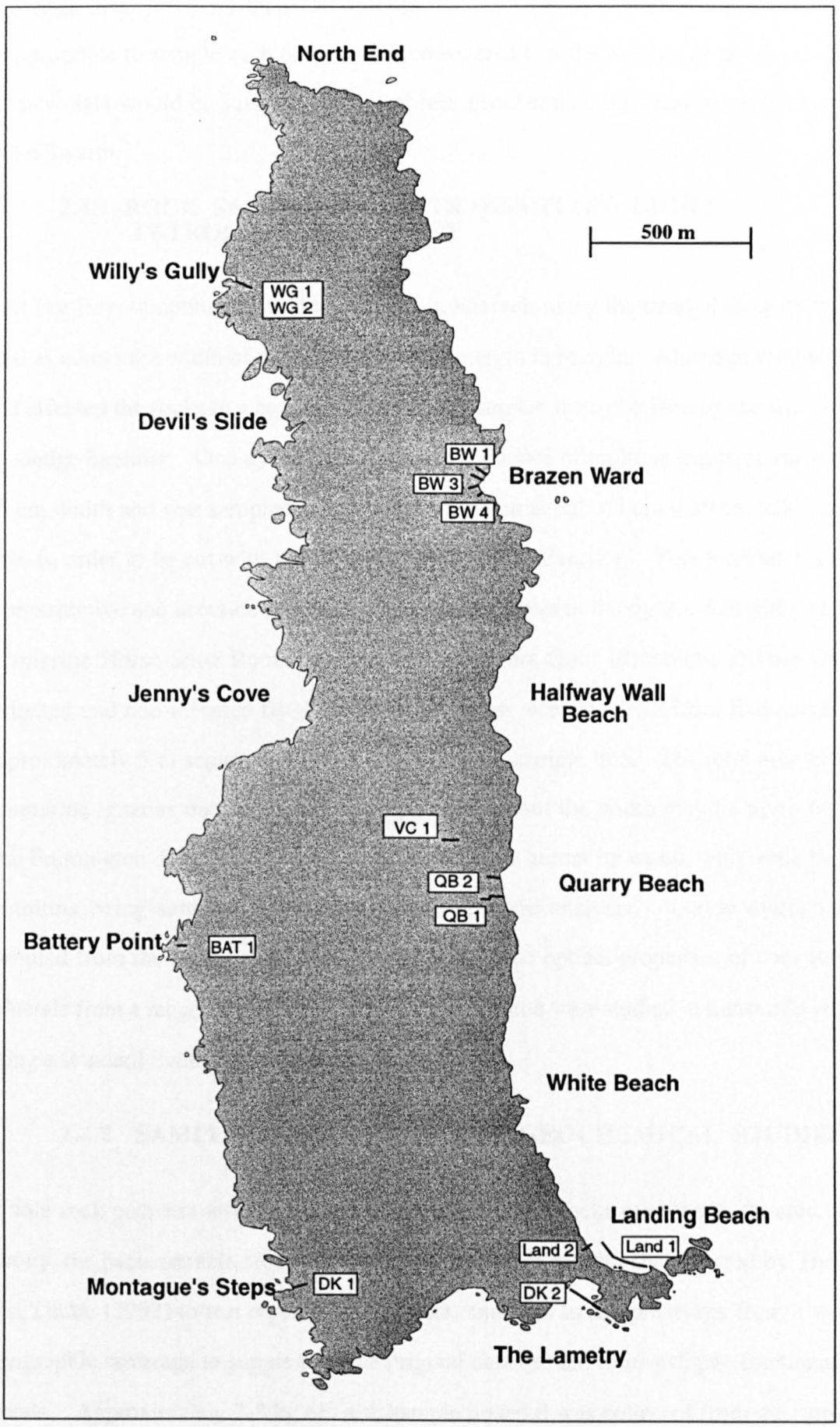

Figure 2.8: Positions of dykes on Lundy that were analysed by XRF.

Although there are more than 150 dolerite dykes on Lundy Island, it was statistically inappropriate to sample each one. It was considered that the number of dykes sampled for new data would be sufficient to reveal new geochemical information on the Lundy Dyke Swarm.

2.4.1 ROCK SAMPLING AND TRANSMITTED LIGHT PETROGRAPHIC SURVEY

At Lee Bay, sampling was undertaken at 5 m intervals along the trend of three dykes as well as across the width of the dykes, i.e. from margin to margin. Although weathering had affected the rocks to a certain degree, fresh samples were obtained by the use of a 5 kg sledge hammer. One dyke (CK30) showed evidence of multiple injection across its 45 cm width and was sampled as one large specimen about 45 cm x 30 cm x 30 cm in size, in order to be cut with a rock saw at the Open University. This facilitated more representative and accurate sampling of individual layers in the dyke. Sampling of the submarine Horse-Shoe Rocks was assisted by divers from Ilfracombe Diving Club. Oriented and non-oriented fist-sized hand specimen were obtained from five points of approximately 5 m separation, giving a 20 m linear sample line. The total area of the submarine igneous outcrop is not fully appreciated, but the width may be up to 60 m. The Fremington dyke was sampled at 20 cm intervals across its width, with some larger xenoliths being sampled at random for petrographic analysis. Lundy dykes were sampled from the centre as well as the margins. The optical properties of constituent minerals from a range of rock types within the study area were studied in transmitted light using a standard Swift petrological microscope.

2.4.2 SAMPLE PREPARATION FOR GEOCHEMICAL STUDIES

Whole rock powders were prepared from selected basic rocks over the study area. On Lundy, the basis for selection was to sample two dykes previously analyzed by Thorpe and Tindle (1992) to test repeatability of data, and then to sample dykes from a wider geographic coverage to supplement the original data set and to investigate fractionation trends. Approximately 2-3 kg of fresh sample material was collected from outcrops in the field using a 5 kg sledge hammer. Samples were then divided into smaller 3 cm

cubes by a hydraulic rock splitter and retained as material suitable for either sample preparation, thin sectioning or archiving. Material displaying evidence of oxidation of Fe-Mg minerals along cracks or erosive surfaces was disgarded. Suitable cubes were crushed in to chips < 5mm using a hardened steel jaw crusher, a fraction of this crushate then being powdered in an agate tema for 10-12 minutes. For some rocks, sieving produced grains in the size range 0.250-0.500 mm and 0.500-1.0 mm. Individual fresh feldspar grains were then hand picked from these fractions using a binocular microscope and a dental probe. Crystals were then rinsed twice with distilled water in an ultrasonic bath to remove superficial impurities. About 3 mg of feldspar material from dolerites with the correct grain size was utilized for Ar-Ar dating procedures.

2.4.3 X-RAY FLUORESCENCE (XRF) ANALYSIS

XRF procedures were carried out using the methods described by Potts *et al.* (1984), Ramsey *et al.* (1995) and Watson (1996) at the Open University.

2.4.3.1 Sample Preparation

(i) Major elements: glass discs (36 mm diameter) are produced by a 20 minute fusion of 1 part rock powder (dried at 110 °C) with 5 parts of dried lithium metaborate/tetraborate flux (Johnson Matthey Spectroflux 100B) in Pt/5% Au crucibles at 1100 °C. The melt is swirled repeatedly to ensure complete dissolution and homogenisation, then poured into a mould and pressed onto a hot plate to form a thin (1.5mm thickness) disc.

(ii) Loss on Ignition (LOI) determination: dried rock powder is ignited in silica crucibles at 1000 °C and the percentage weight loss is obtained. This is an essential part of major element analysis, accounting for the main constituents (e.g. H_2O, CO_2) that cannot be measured directly by XRF procedures.

(iii) Trace Elements: powder pellets (35 mm diameter) are produced by mixing thoroughly rock powder (ca. 9 gm) and 0.7 cc of ploy vinylpyrollidone (PVP)-methyl cellulose binder. The moist powder is pressed at 9 ton per square inch to a minimum thickness of 3.5 mm and dried overnight at 105 °C.

2.4.3.2 Instrumentation

All analyses were completed at the Open University in two sessions using an ARL 8420+ dual goniometer wavelength dispersive XRF spectrometer, equipped with a 3 kW Rh anode end-window X-ray tube with flow proportional and scintillation counters (fully collimated). The diffracting crystals used in the XRF apparatus are AX06 (multilayer), PET (penta-erythrytol), Ge111, LiF200 and LiF220. Dr. Peter Webb calibrated and supervised the sample runs using standard procedures developed in the Department of Earth Sciences (Ramsey *et al.*, 1995).

2.4.4 $^{40}Ar/^{39}Ar$ DATING METHODS

Plagioclase samples for dating from Lee Bay and the Horse-Shoe Rocks were irradiated in the Ford nuclear reactor (Michigan, U.S.A.), where they received approximately 10^{18} fast neutrons cm^{-1}. Hornblende flux monitors MMhb-1 and Hb3gr (Turner *et al.*, 1971; Alexander *et al.*, 1978) were used during radiation to calculate J values (the irradiation parameter). These were 0.00467 ± 0.00002 for the Fremington dyke and 0.00575 ± 0.00002 for the Lee Bay dykes and the Horse-Shoe Rocks. The methodology for argon extraction is given by McDougall and Harrison (1988) and Kelley (1995). All samples were analysed at the Open University, where argon was released from individual plagioclases by firing short pulses of a Nd YAG (yttrium, aluminium and garnet) laser beam (TEMoo and wavelength 1064 nm). The beam was focused to a spot size of around 25 μm with up to powers of 17 W and with pulse lengths of 100-150 ms. Longer times were not needed to release argon, as they produced excessive melting over larger areas than required in some test samples. This resulted in some regions of impurity within the crystal being analysed and could be a potential source of error.

The argon was purified using a SAES GP10 getter at about 380 °C for 5-8 minutes and isotope analyses were undertaken using a Mass Analyser Products 215 mass spectrometer with an electron multiplier detector. The seven atomic masses analysed were 35, 36, 37, 38, 39, 40 and 41. Mass 41 was measured as control on the level of hydrocarbons in the gas sample. Levels above about 1.5% could indicate the presence of excess argon.

Similarly, mass 35 was measured to monitor the amount of Cl in the sample, a potential source of ^{36}Ar from β-decay. At the end of each analysis, peaks were regressed to the inlet time and a blank run was completed after each sample to avoid contamination in the following analysis and to monitor the ambient background.

Average background levels during the isotopic analysis were 7.59×10^{-12}, 6.48×10^{-12}, 0.42×10^{-12}, 1.77×10^{-12} and 0.81×10^{-12} cm^3 STP for ^{40}Ar, ^{39}Ar, ^{38}Ar, ^{37}Ar and ^{36}Ar respectively. Data were corrected for the interfering interaction of neutrons with isotopes of calcium and potassium, which produce small amounts of argon isotopes during the irradiation process to give incorrect ratios. Correction factors used were $(^{40}Ar/^{39}Ar)_K = 0.031 \pm 0.008$, $(^{39}Ar/^{37}Ar)_{Ca} = 0.000781 \pm 0.000053$ and $(^{36}Ar/^{37}Ar)_{Ca} = 0.000205 \pm 0.000022$. Also, corrections were applied to counter mass spectrometer fractionation and ^{37}Ar decay since the time of irradiation. For the latter, time delay between irradiation and analysis was less than 1 month, resulting in almost insignificant corrections.

CHAPTER 3

THE LUNDY DYKE SWARM

3.1 INTRODUCTION

The precise origin of the Lundy Dyke Swarm has been a matter of conjecture, partly due to the limited regional extent and availability of material for analysis. Dykes within the British Tertiary Volcanic Province commonly display a crude NW-SE outcrop pattern, although local and regional variations have been noted. However, an underlying assumption has been that as Lundy is the southernmost example of Tertiary volcanism, the origin of its dyke swarm must lie somewhere to the northwest. Brooks and Thompson (1973) interpreted a positive lunate gravity anomaly WNW of Lundy Island as representing a basic body at shallow depth, but did not link this observation to the volcanic anatomy. The NW-SE linear magnetic anomaly to the NNW of Lundy Island, interpreted by Cornwell (1971) as a dyke or dyke swarm, is tangential to the gravity anomaly and suggests that the two may not be temporally related. It thus seems possible that volcanic activity associated with the Lundy Igneous Complex was complex and may have involved more than one phase of activity.

3.2 FIELD OBSERVATIONS

Location maps of the igneous rocks in the North Devon region are shown for convenience in Figures 3.1 and 3.2, which are précis of Figures 1.4, 2.2, 2.3, 2.7 and 2.8.

3.2.1 DIP AND STRIKE OF DYKES

Basic and intermediate dykes with similar trends and presumed similar ages are exposed at Lee Bay, Fremington and on Lundy Island. At Lee Bay, four east-west striking dykes crop out with southerly dips between 75° and 80°, which is coincident with ambient Variscan cleavage trends in Devonian sediments at that locality. A single intrusion at

Figure 3.1: Location of igneous rocks in North Devon.

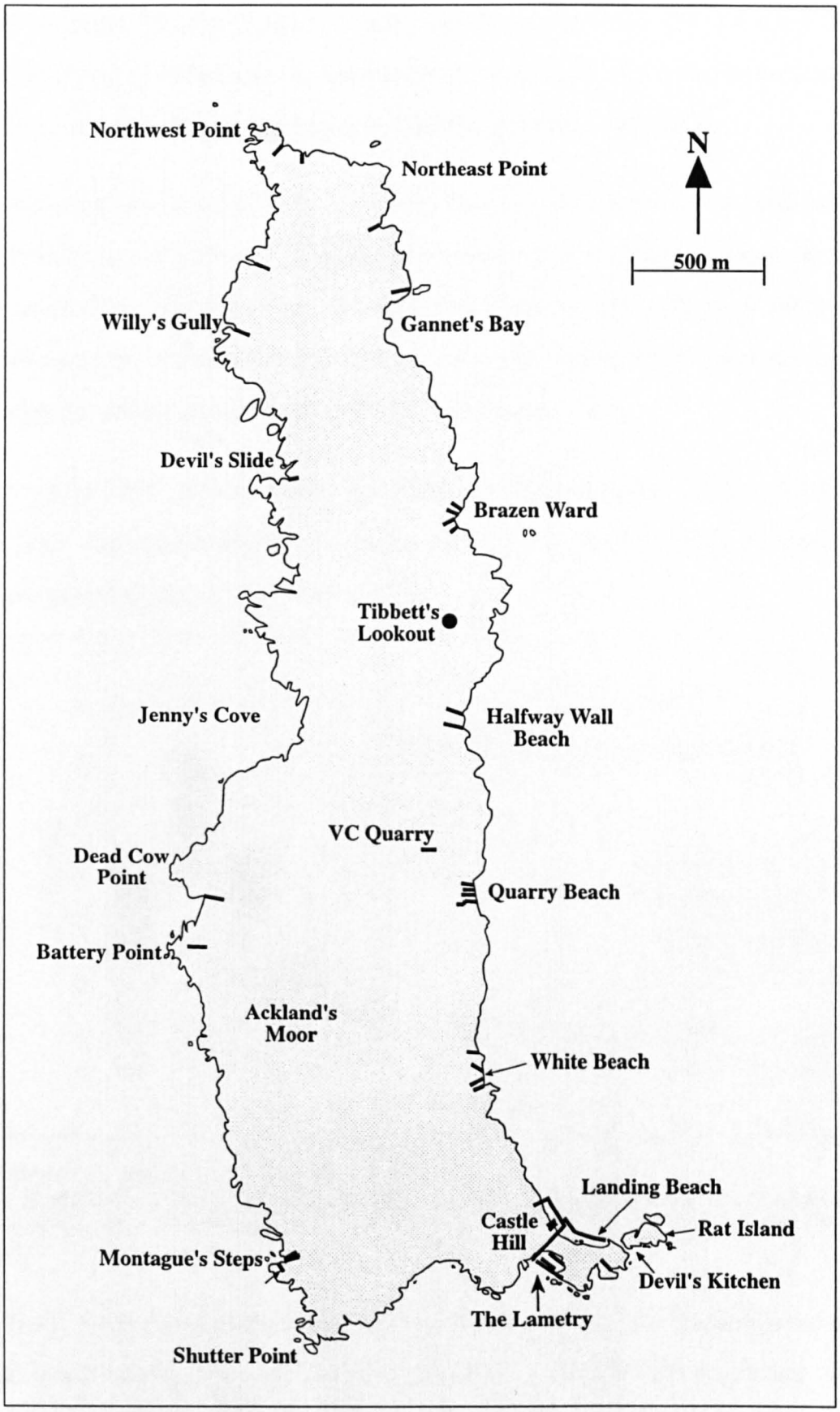

Figure 3.2: Location of reference points on Lundy Island.
Individual dyke numbers are given in Figures 2.3 and 2.8.

Fremington Pill also crops out with a southerly dip (123°/47° SW), but the main controlling trends here are the thinly bedded sequences of the Carboniferous Crackington formation, the intrusion having a very gentle cross-cutting relationship.

Although there is minimal dyke exposure over much of Lundy Island, field relations of dykes in coastal cliffs can be studied with relative ease, even though access for the most part can only be from the sea. Measurement of the dip and strike of all dykes can thus indicate precise field relations at outcrop, although underlying assumptions have to be made for interpolated trends between the east and west coasts.

A total of 164 basic and intermediate dykes were measured in the coastal cliffs around the island. The true thickness of the dykes range from 0.1 m to 6.15 m with a mathematical average thickness of 1.42 m (Figure 3.3).

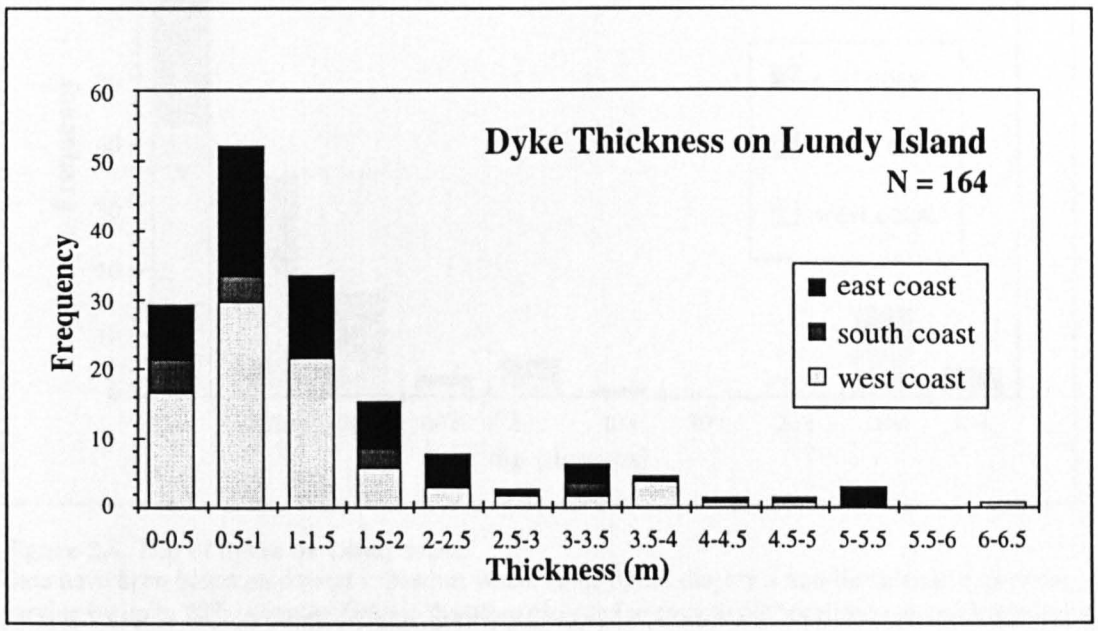

Figure 3.3: Thickness of dykes on Lundy Island.
Dyke thickness is represented by true thickness normal to dyke margins and based on outcrops around the coast of Lundy. An estimated 50-60 dykes were inaccessible for measurement and are not included in this plot.

Those dykes measuring less than 10 cm or where access was inhibited have not been included, although they may represent up to 30% of the total dyke population. Some 87 dykes were measured along the west coast (Shutter Point to North-west Point), 62 dykes along the east coast (Rat Island to North-west Point) and 14 dykes along the narrow south coast (Surf Point to Shutter Point). The increased number of dyke measurements

along the west coast is proportional to the outcrop pattern, even though not all dykes have been sampled. The narrow north coastline (trending approximately 115°) has been included in the east coast measurements.

Two distinct populations of dyke dips can be observed (Figure 3.4). The main trend varies from 40°-90° with an arithmetic average of 83.5° (N = 142) and displays a negative skew, whereas a minor trend ranges from 0°-25° with a mean value of 12.3° (N = 22), indicating normal distribution. The direction of dip is not significantly related to locality or strike direction and can be seen to vary both locally and throughout the length of the island.

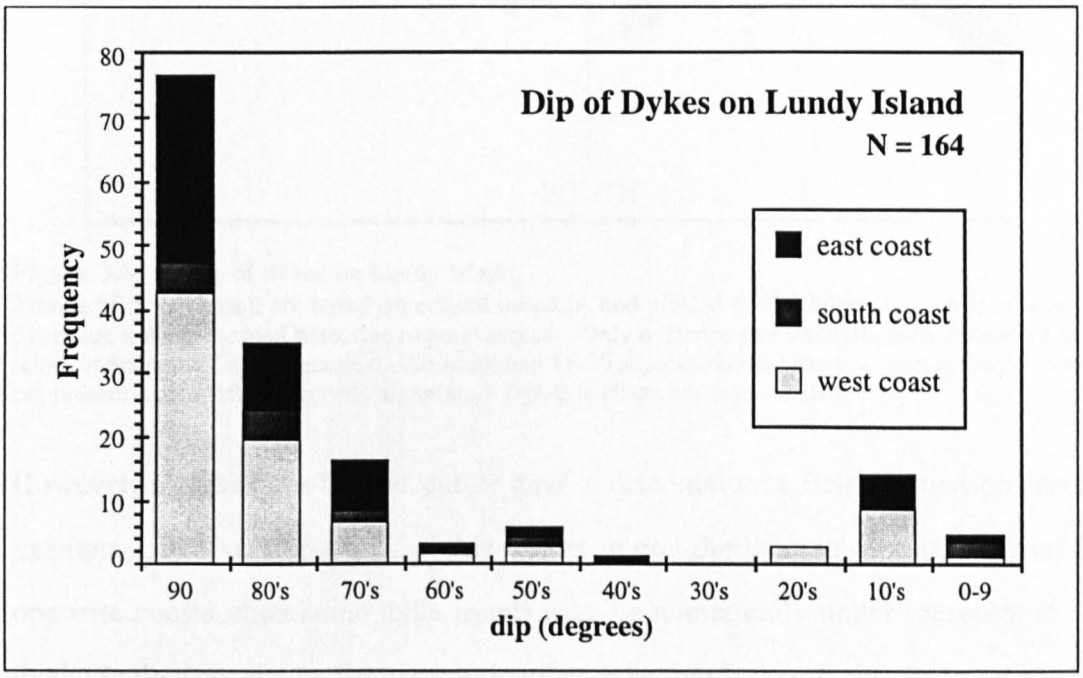

Figure 3.4: Dip of dykes on Lundy Island.
Data have been based on coastal exposures where some dykes display a non-linear field expression, dips varying by up to 20°. Average dips are therefore recorded to smooth out localized outcrop irregularities.

The strikes of the dykes range through all directions, the most numerous being between 110° and 115° (Figure 3.5), but a normal distribution cannot be supported by the sampled data. Speight *et al.* (1982) reported a close correlation between trend and dyke thickness for Tertiary dykes on Skye and indicate a Gaussian distribution for the regional linear swarm. If dykes extend through the island, some duplication of dykes along the east and west coastlines is possible, but the overall shape of the rose diagram will not be excessively distorted.

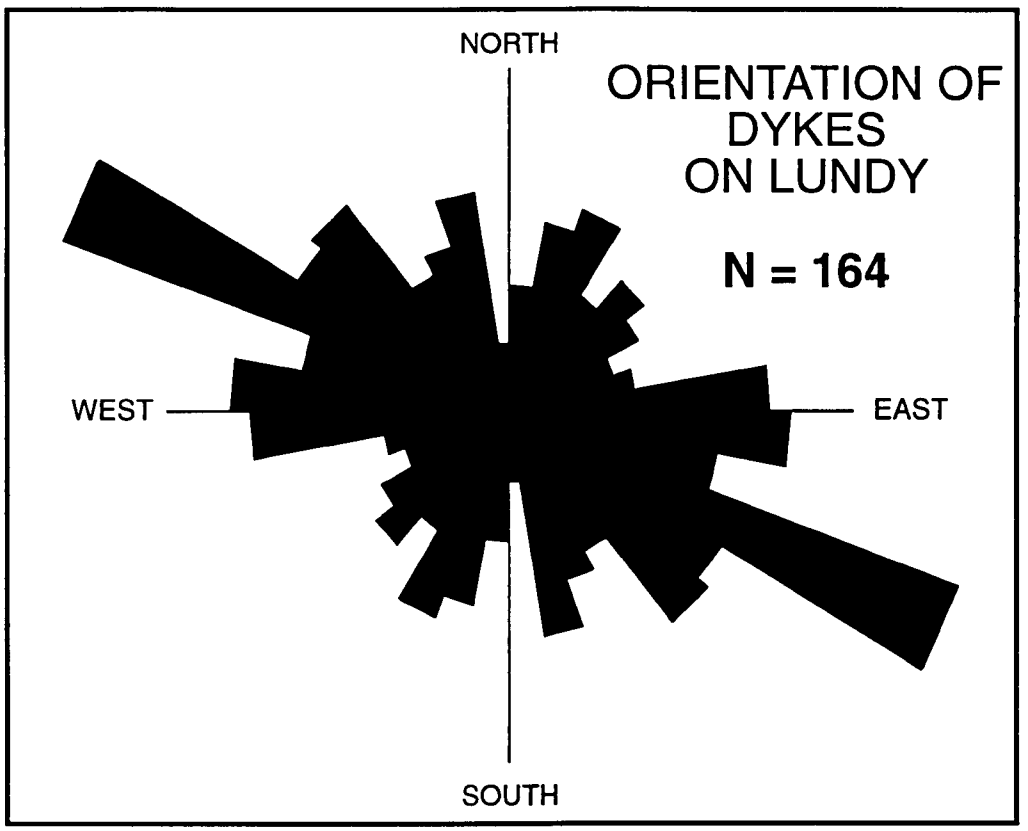

Figure 3.5: Strike of dykes on Lundy Island.
Trends of dykes based are based on coastal outcrops and plotted at 10^0 intervals. An estimated 50-60 dykes are not represented here, due to poor access. Only dolerites and trachytes were measured as these relate to magnetic field signatures. An estimated 15-20 rhyolite dykes have not been included as they do not present a recordable magnetic signature. Dykes < 10 cm are also omitted.

However, if dykes are faulted out or have a discontinuous field expression from, for example, offset or stepping, and this results in non-duplication of measurement along opposite coasts, then some dyke trends may be numerically under-represented. This method relies heavily on the assumption that dyke trends do not vary to any great extent over relatively short distances. Nevertheless, a crude radial distribution pattern of basic to intermediate dykes can be seen in the rose diagram with a slightly greater proportion of trends in the southeast quarter. A clear trend in the east-southeast to west-northwest direction is also discernible superimposed over the radial component. The Lundy Dyke swarm may thus be the product of at least two different processes - a radial component and an east-southeast to west-northwest regional component.

3.2.2 DIRECTION OF FLOW INDICATORS IN DYKES

The mechanism for dyke injection may be either active or passive. Active infilling assumes that the pressure of the magma itself wedges open a pathway for the dyke

(Anderson, 1951), presumably when the magma chamber pressure exceeds the overlying effective stress. Passive infilling usually occurs at higher crustal levels, where a fissure is formed first and later filled by invading magma, as seen in volcanoes on Hawaii and Iceland. However, in either case, magma transport could be vertical, horizontal or contain components of both. Delaney and Pollard (1981) have highlighted the phenomenon of drainback, where magma movement in a dyke has been downwards during the waning stages of an eruptive sequence. Thus, even vertical movement needs to be clarified as either up or down.

It is possible to infer localized movement of magma, where certain morphological characteristics of dykes can be measured at outcrop. Such characteristics can be internal or external, and so it is desirable to examine 3-dimensional exposures as opposed to 2-dimensional to allow accurate measurements of azimuths. The external characteristics, summarized by Rickwood (1990), include drag folds, scour marks, buds, steps and fingers. Internal characteristics include bent columns, alignment of long axes of phenocrysts, shaped vesiculation (e.g. tadpoled), ramping structures and flow lines.

At Lee Bay (Figure 3.1), all four dyke exposures display zoning and evidence of multiple intrusion, but the style and number of zonations indicate that there may only be three dykes present, at least one dyke being repeated by NW-SE faulting. In one 24 cm wide dyke (CK31), the zones are difficult to differentiate and tend to blend into one another (Photo 3.1). The average zone thickness is < 0.5 cm, but this tends to increase towards the centre, where pear-shaped filled vesicles (amygdales) < 1 mm in length occur. The tails of these amygdales point down towards the west at about 60°-70° inclination, which suggests that the original magma source may be to the west of Lee Bay. Dyke CK21 (45 cm wide) displays a more regular zonation, each zone being up to 15 mm in width, although the vesiculated centre of the dyke is about 8 cm wide.

At least 4 intrusive pulses with amygdaloidal margins can be seen (Photo 3.2), but these tend to wedge out towards the west, where the dyke terminates as a single zone in a sharp pointed tip. The field evidence for magma flow is inconclusive at outcrop, but the alignment of some plagioclase phenocrysts is probably suggestive of sub-vertical

movement. The dyke termination to the west may have resulted from passive infilling of a V-shaped void caused by a splitting effect of magma pressure from depth. Dyke CK20 (40 cm wide) displays similar characteristics to the CK21, but has suffered extensive sub-aerial erosion, so that fresh exposure is difficult to examine. However, at least 7 intrusive phases can be identified and although absolute direction indicators are unclear, lateral inpersistence of pulses suggests a vertical component to dyke injection.

The Fremington dyke has a true thickness of 82 cm and is composite in nature, with a xenolithic doleritic facies in the centre and a weathered basic exterior, indicating at least two separate episodes of magma injection. There is a 2.5 cm fine-grained chilled margin on both sides of the dyke with clear evidence of vesiculated multiple intrusion in the outer zones. The vesicles are ellipsoid and indicate sub-horizontal magma movement, whereas the centre of the dyke has few clear indicators of propagation, although some elongate xenoliths are aligned parallel or sub-parallel to dyke margins, which also indicates lateral motion. Whether magma movement was from the south-east or north-west could not be determined by the field evidence.

Thorpe and Tindle (1992) reported that there was no obvious evidence of multiple or composite intrusion from 20 dykes in their survey on Lundy Island and, for the most of the dykes on the island, this is true. However, a minority of dykes (i.e 4 trachytes and 13 dolerites out of 164 dyke measurements, although there may have been some duplication between east and west coasts) display either a composite structure or have a crude multiple injection pattern in which individual zones can be up to 20% of the dyke width. Vesiculation is more common in the trachytes than the dolerites and basalts, possibly due to the more viscous nature of the intermediate melts which trap gaseous fractions coming out of the magma due to pressure release. Three rhyolites examined were fine-grained, relatively homogenous and probably emplaced in one episode. The majority of dykes do not display any morphological expression which could be used to determine magma flow direction, but there are some notable exceptions.

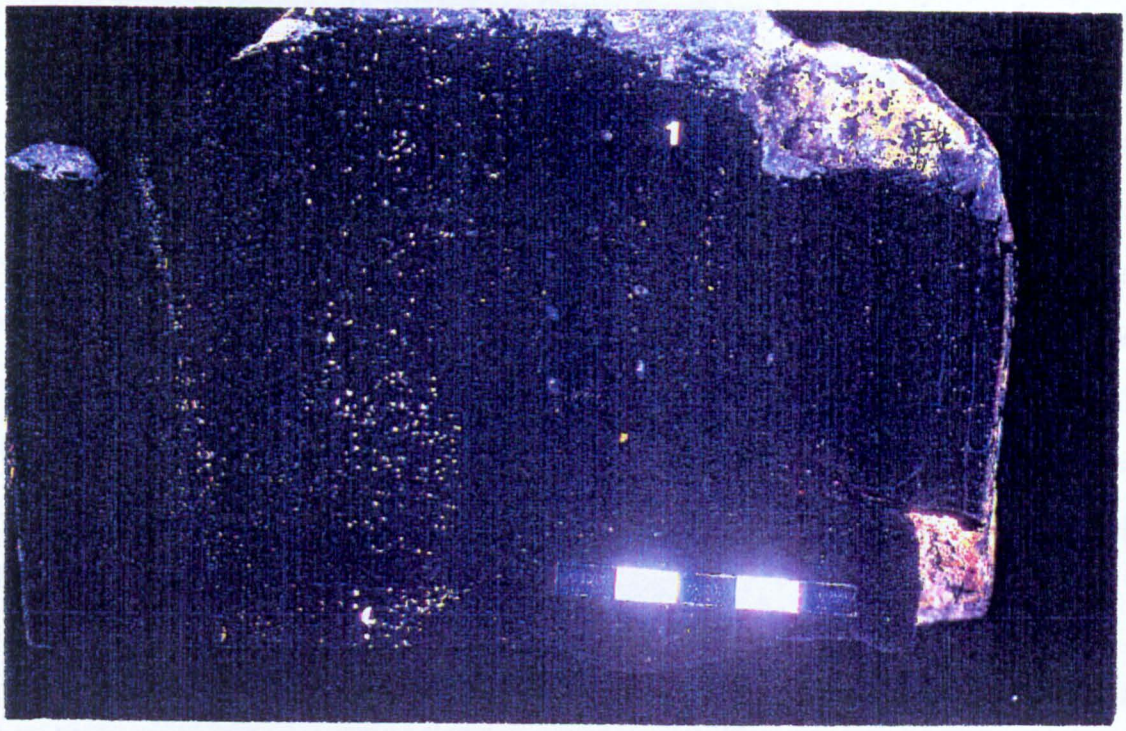

Photo 3.1: Zonation in dyke CK31 from Lee Bay

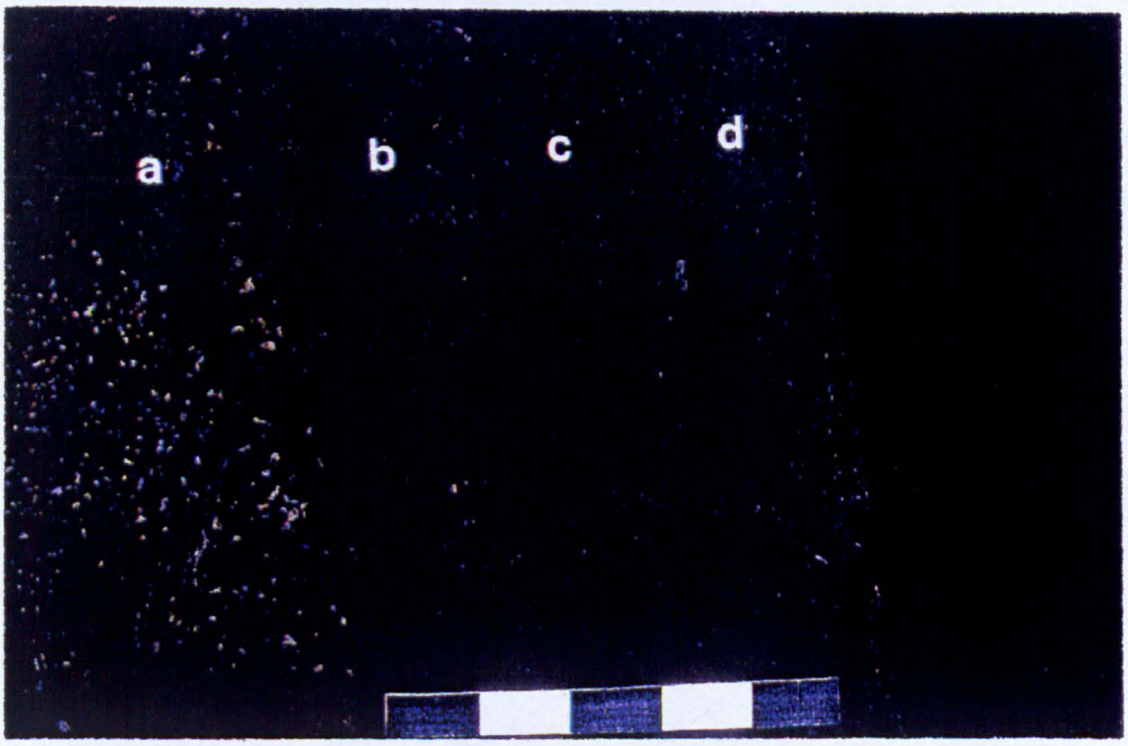

Photo 3.2: Parallel zonation in dyke CK21 from Lee Bay.
The dyke margin is to the right. Zones (a), (b), (c) and (d) correspond to different samples used in geochemical sudies (cf. appendix A4). The photograph demonstrates the zonation of pulse (a) with its feldspar phenocrysts, but does not clearly distinguish between zones (b) to (d). However, a thin border of white amygdales is located along each pulse margin. indicating vesiculation from the release of gases during emplacement. Scale bar is in cm blocks.

Granite around a trachyte (098°/86°S) on Quarry Beach has been eroded away from both margins of the dyke, revealing a 3-dimensional section of rock. The southern exterior of the dyke margin reveals vertical linear ridges and grooves (Photo 3.3) approximately 40 cm long and up to 1 cm wide. These may have been created by scouring and erosion of a cooling viscous magma at the dyke margin by relatively more fluid magma towards the dyke interior. In the same dyke, but some 10 m further up the cliff, vesicles near to the southern margin have an elliptical expression (Photo 3.4), also suggestive of vertical flow. These two features taken together indicate a possible magma origin at depth below Quarry Beach for the trachytic dyke, although they represent a local flow direction and this may not be applicable to the dyke over its entire length.

The contact zone of a large doleritic dyke (045°/90°) at Brazen Ward (BW2) displays lath-like xenocrysts of plagioclase feldspar (Photo 3.5), probably originating from the Lundy granite. The xenocrysts are widely spaced, but tend to be oblique to the dyke margin at around 10°-15°. This phenomenon was noted by Blanchard *et al.* (1979) and termed pincement. They reported that an average obliquity of 15°-20° with the acute angle always pointing towards the magma source. Using their criteria, magma flow in dyke BW2 was at intermediary angles from the north-west, i.e. a significant horizontal component to historic magma flow is present.

Other relevant features in dykes include pinch and swell structures and wall rock brecciation, although the latter is affected by erosion and not obvious in many places. The field evidence taken as a whole is suggestive of a magma origin either to the west of Lundy Island or with a component at depth beneath the island. Dykes can be seen to take abrupt 90° directional change in Lametry Beach (Photo 3.6), which cautions against using strike directions to determine magma origins. However, dyke LAM 3 (103°/46°NE) in Lametry Beach can be seen to terminate against a large trachyte (023°/85°SE) below Castle Hill (Photo 3.6). Three other similarly disposed dykes also terminating abruptly or are turned to run parallel with the larger dyke. This is highly suggestive of a magmatic origin for these dykes from the south-east, with lateral motion towards the north-west.

Photo 3.3: Vertical fingers in QB2 from Quarry Beach, Lundy Island.
Such features are created by scouring of semi-molten magma by solid coarse-grained granite and are good indicators of magma flow directions. The lens cap has diameter = 5 cm.

Photo 3.4: Elliptical vesicles in QB2 (trachyte) from Quarry Beach, Lundy Island.
Vesicles are best seen in the pale yellow fresh surface in the centre of the photograph. The two round holes are new core sites for AMS studies. The lens cap has diameter = 5 cm.

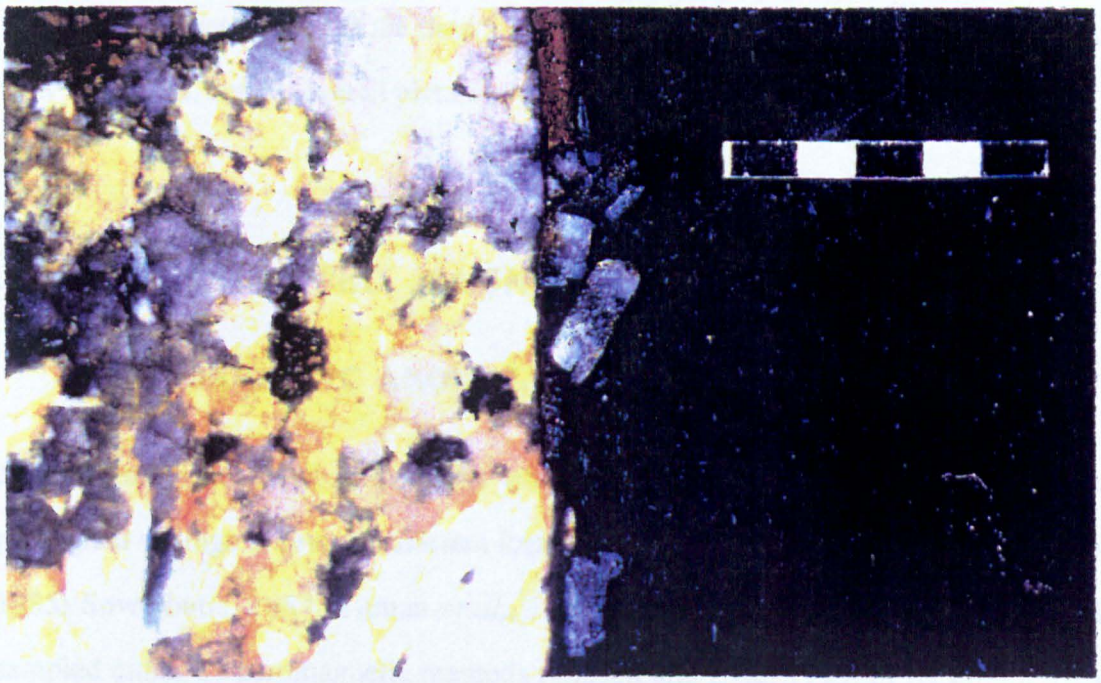

Photo 3.5: Foreign xenocryst in chilled margin of BW2 (dolerite) from Brazen Ward, Lundy Island. The coarse rock to the left is Lundy granite and the dark rock to the right is the chilled margin of BW2. Rectangular xenocrysts are contained within the outer contact of the dolerite. Scale bar = 5 cm.

Photo 3.6: Abrupt bend in dolerite dyke from Lametry Beach, Lundy Island. Host rocks are Devonian sediments and the normal thickness of the dyke is about 40 cm.

It is, therefore, not desirable (or possible) to determine either magma flow directions or assign locations to magmatic origins for dykes on Lundy Island based purely on measurements determined in the field. There is some localized supportive evidence from flow indicators, but the overall picture is unclear.

3.3 FIELD-RELATED MAGNETIC OBSERVATIONS

3.3.1 MAGNETIC ANOMALY PROFILES ON LUNDY ISLAND

Magnetometry has been successfully employed to study Tertiary dykes in different geological settings at several different localities (e.g. Robson, 1964; Ofoegbu and Bott, 1985; Sowerbutts, 1987; Titman *et al.*, 1989; Gibson and Lyle, 1993). Data can be sampled either by aeromagnetic methods (Gibson and Lyle, 1993) or by ground-based proton magnetometry (Titman *et al.*, 1989). Aeromagnetic methods are disadvantaged in many prospecting applications by missing smaller magnetic structures due to the relatively large distance between object and magnetometer, although magnetic bodies > 500 m are better detected by such methods. By definition, ground methods are more sensitive to smaller shallow structures, due to their proximity to the object. An aeromagnetic map of Lundy Island (Burley, 1979) shows an anomalous gradient of +20 nT at the south end of the island to about -50 nT at the north end. This is probably a reflection of the deep geological structure rather than being influenced by individual dykes. However, McCaffrey *et al.* (1993) concluded that a circular positive anomaly centred over the south-eastern part of the island could be ascribed to superficial magnetic metasediments.

The topography of Lundy is broadly that of a flat, planed island surface with encompassing vertical cliffs, a coastal bevel of around 30° separating the two. Although dykes can be seen to crop out along all coastlines, vegetation and superficial deposits cover most of them over the top of the island. The trend of dykes over most of Lundy island cannot therefore be directly measured. It is also unclear whether dykes cropping out in the western cliffs extend through the island to crop out along the eastern coast, and in this respect, how much actual repetition has occurred in the measurement of dip and

strike of the dykes around the coast. The amount and effect of NW-SE Tertiary faulting on Lundy is also not known.

At the south end of the island, background values are taken as 48041 nT, calculated from the 1991.5 reference field and based on monitoring procedures at Hartland Observatory. This increases by 2.1 nT per km northwards, but as the north-south distance on Lundy is only 5 km, the background field is still only likely to be around 48050 nT at the north end. Also, this geophysical monitoring station is only 25 km to the south-southeast of Lundy, so the geomagnetic field on Lundy is well constrained.

The results of an initial background reconnaissance survey are shown (Figure 3.6), for which the regional magnetic gradient has been removed and data corrected for the effects of diurnal drift. Deviations along some traverses away from a north-south orientation were necessary to avoid locations where man-made artefacts, such as walls and fences, might have caused interference to magnetic readings. The survey shows a number of positive-negative paired anomaly profiles, with wavelengths between 50 and 90 m and amplitudes up to 600 nT, superimposed over a relatively flat background.

Both granite and sediments are magnetically quiet with corrected differentials of ± 10 nT and ± 15 nT respectively. There is only a minimal legacy from human activity over the survey lines and hand auguring through 1 to 3 m of soil cover at peak magnetic amplitudes along profiles for a representative sample of areas revealed basic rocks. The maximum amplitudes of some paired anomaly profiles also coincide with dark brown soil horizons in small linear depressions, characteristic of the morphological expression of weathered dykes over the island. These can only be traced for short distances to facilitate mapping. Readings towards the centre of the island are slightly reduced in amplitude, due to a greater depth to the top of the dykes, as there is thicker soil and peat cover in this area, whereas readings at the south and particularly north ends are more sharp, because the soil cover is either very thin or virtually absent. All anomalies are interpreted as reflecting geological features rather than human artefacts.

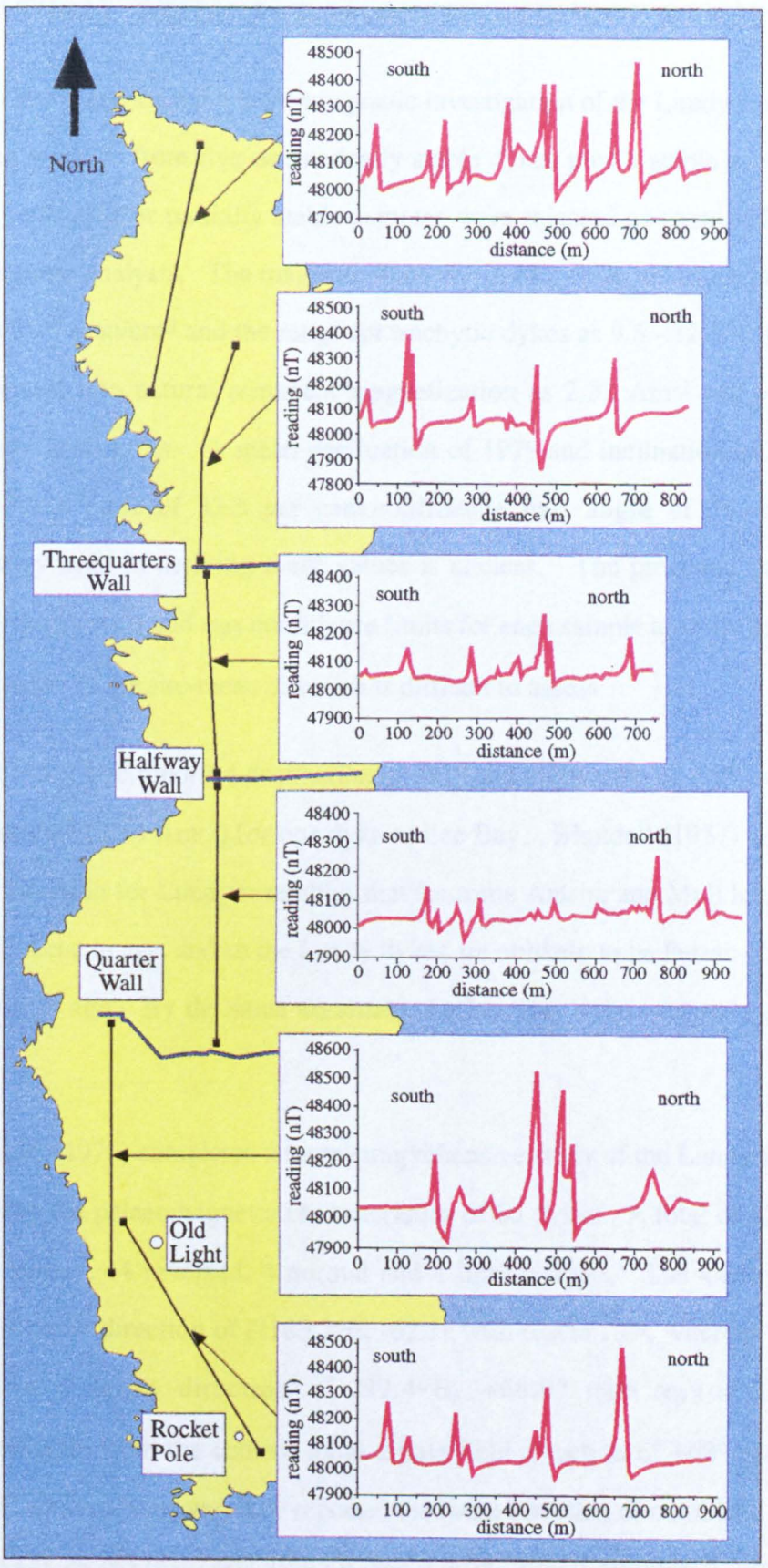

Figure 3.6: Reconnaissance magnetic survey on Lundy Island.
Red plots indicate total magnetic flux after correction for diurnal drift.

3.3.2 NATURAL REMANENT MAGNETIZATION OF DYKES

Blundell (1957) carried out a palaeomagnetic investigation of the Lundy Dyke Swarm by examining samples from five magnetically stable dykes plus 3 stable contact zones. A further 11 unstable or partially stable samples were rejected as unsuitable for reliable palaeomagnetic analysis. The magnetic intensity, *J*, of 2 fresh dolerite dykes was given as 2370×10^{-6} emu/cm^3 and the range for trachytic dykes as $9.5 - 12.5 \times 10^{-6}$ emu/cm^3, which convert into natural remanent magnetization as 2.37 Am^{-1} and ≈ 0.001 Am^{-1} respectively in SI units. A mean declination of 197° and inclination of -59° are also quoted with a cone of 33.3 per cent confidence half angle of 7°, although the methodology used in deriving these values is unclear. The precision parameter (κ), angular dispersion (s) and α_{95} confidence limits for each sample are similarly not given, thus the quality of the site-mean direction is difficult to assess.

Blundell (1957) also reports a declination of 181° and inclination of -51°, with $J = 2540 \times 10^{-6}$ emu/cm^3 (2.54 Am^{-1}) for one dyke at Lee Bay. Blundell (1957) concluded that the mean direction for Lundy resembles that for some Antrim and Mull lavas, which are probably Eocene in age, and so the Lundy dykes are unlikely to be Permo-Carboniferous, but Tertiary in age. By the same argument, the Lee Bay dyke was assigned a Tertiary age.

Mussett *et al.* (1976) completed a more comprehensive study of the Lundy Dyke Swarm, investigating the palaeomagnetic characteristics of 66 dykes. A total of 52 dykes gave stable directions: 44 reversed, 4 normal and 4 intermediate. The 44 reversed dykes produced a mean direction of N183.2°E, -62.1° with $\alpha_{95} = 1.6°$, whereas the 4 normal dykes gave a mean direction of N9.4°E, +68.9° with $\alpha_{95} = 3.5°$, almost indistinguishable from the centred axial dipole field direction of +68° expected at the latitude of Lundy. However, they reported the mean direction of combined reversed and normal dykes as N3.6°E, +62.7° with $\alpha_{95} = 1.5°$, which apparently contradicts the dominance of reversely magnetized dykes on the island. The mean was calculated by inverting reversed directions to normal polarity (P. Dagley, pers. comm.), which resolves the discrepancy in quoted values.

Blundell (1957) did not give palaeomagnetic pole positions, but Mussett *et al.* (1976) calculate a mean pole position of Lat. 82.6°, Long. 155.0° (dp = 1.8°, dm = 2.3°) from the mean direction of the 48 reversed and normal dykes. Table 3.1 provides a comparison of directions and palaeomagnetic pole positions within the British Tertiary Volcanic Province.

Table 3.1: Site-mean directions for some centres within the British Tertiary Volcanic Province. N = number of lavas or dykes used to compute directions.

N	Decl.	Incl.	α_{95}	Pole Position Lat.	Long.	Locality	Reference
24	194	-60.2	5.9	-	-	N.Ireland	Hospers + Charlesworth,1954
41	183	-64.1	6.3	-	-	N.Ireland	Wilson, 1961
25	184.7	-54.3	5.1	69.6	162.9	N.Ireland	Wilson, 1970
48	183.2	-62.1	1.6	82.6	155.0	Lundy	Mussett *et al.*, 1976
32	183.4	-58.3	2	71.5	165.2	Skye	Wilson *et al.* 1972
36	193.0	-58.8	9	71.0	141.9	Mull	Mussett *et al.* 1980
45	179.0	-65.2	10	81.7	179.8	Arran	Dagley *et al.* 1978
54	196.5	-57.9	9	68.7	136.0	Rhum	Dagley+Mussett 1981
32	180.0	-63.0	3	77.0	175.0	Ardnamurchan	Dagley *et al.* 1984
24	176.3	-63.8	3	78.4	186.9	Muck	Dagley+Mussett 1986
20	179.7	-59.3	4	73.2	174.5	Eigg	Dagley+Mussett 1986

There appears to be a significant variation in the mean pole positions for Tertiary centres and the scatter is probably outside Fisherian distribution limits, suggesting that sampling and measurement errors alone cannot explain this phenomenon. Secular variation, in which the direction of the Earth's magnetic field wanders within a cone of angle of around 20° with a period of 1 to 4,000 years (Townsend and Hailwood, 1986), could produce some variance in pole positions. However, the mean value from each locality should average out secular variation, assuming an even rate of change and an adequate sampling strategy. Given that the temporal distribution of rocks within the British Tertiary Volcanic Province may have spanned only 11 Ma (Mussett *et al.*, 1988), the tectonic setting of the British Isles in the Tertiary and associated sea-floor spreading in the North Atlantic argue against significant tectonic rotation to explain the scatter.

The reason for the scatter in mean palaeomagnetic pole positions is thus unclear. Mussett *et al.* (1988) also conclude that the preponderance of reversely magnetized dykes is only partially explained by the longer duration of reversed polarity periods, with respect to

normal polarity, and that an element of chance needs to be invoked to explain the low percentage of normally magnetized dykes within the province.

3.3.2.1 Lee Bay dykes

A total of 15 cores, of which 11 gave stable directions, were obtained from three different outcrops not previously sampled by Blundell (1957). Mean directions for each outcrop are given in Table 3.2.

Table 3.2: Results of mean palaeomagnetic directions for Lee Bay.

Outcrop	Number of samples	Decl. (°)	Incl. (°)	α_{95} (°)	Pole Position Lat. (°)	Long. (°)
CK21	4	186.7	-56.1	7.5	81.4	159.7
CK30	4	194.5	-59.6	8.9	73.8	186.9
CK4	3	016.4	+58.2	10.3	76.7	170.6

All magnetically stable cores reveal that the NRM has two main components; a high-stability characteristic component (ChRM) and a low-stability component. The high-stability component is rarely linear, but can be averaged by an anchored line fit on a Zijderveld diagram, provided that the maximum angular deviation (MAD) of the plot is $\leq 15^{\circ}$ (Butler, 1992), as shown in Figure 3.7. At Lee Bay, the ChRM has medium to high coercivity and probably represents the primary thermoremanent magnetization (TRM). The low-stability component is easily moved by partial demagnetization up to 4-6 mT and has a mean inclination (I_m) $\approx +68^{\circ}$, which is sub-parallel to the present geomagnetic field at this site. Although declination (D) values range from 295° to 345°, slightly west of north for the present north geomagnetic pole, this low coercive component probably represents a viscous remanent magnetization (VRM).

CK21 and CK30 are both reversely magnetized, whereas CK4 is normally magnetized but passes the reversal test for the site as a whole, which suggests that all three dyke outcrops are genetically related. The overall site mean directions for Lee Bay are D_m = 193.4°, I_m = -57.6° (k =32.4; s = 14.3°; α_{95} = 8.7°) when N = 11. These are shallower than the site mean direction of remanence for Lundy (Mussett *et al.*, 1976) and significantly different from the value for a dolerite dyke quoted by Blundell (1957), but

would fit comfortably into the range of palaeomagnetic directions given in Table 3.1. Direct comparison of results is difficult as Blundell does not give palaeomagnetic statistics and the same dyke (assumed by visual detection of core holes) provided unstable directions in this study. Nevertheless, comparison with other Tertiary centres (Table 3.1) implies that all dyke outcrops at Lee Bay are probably genetically related and are of Lower Tertiary age.

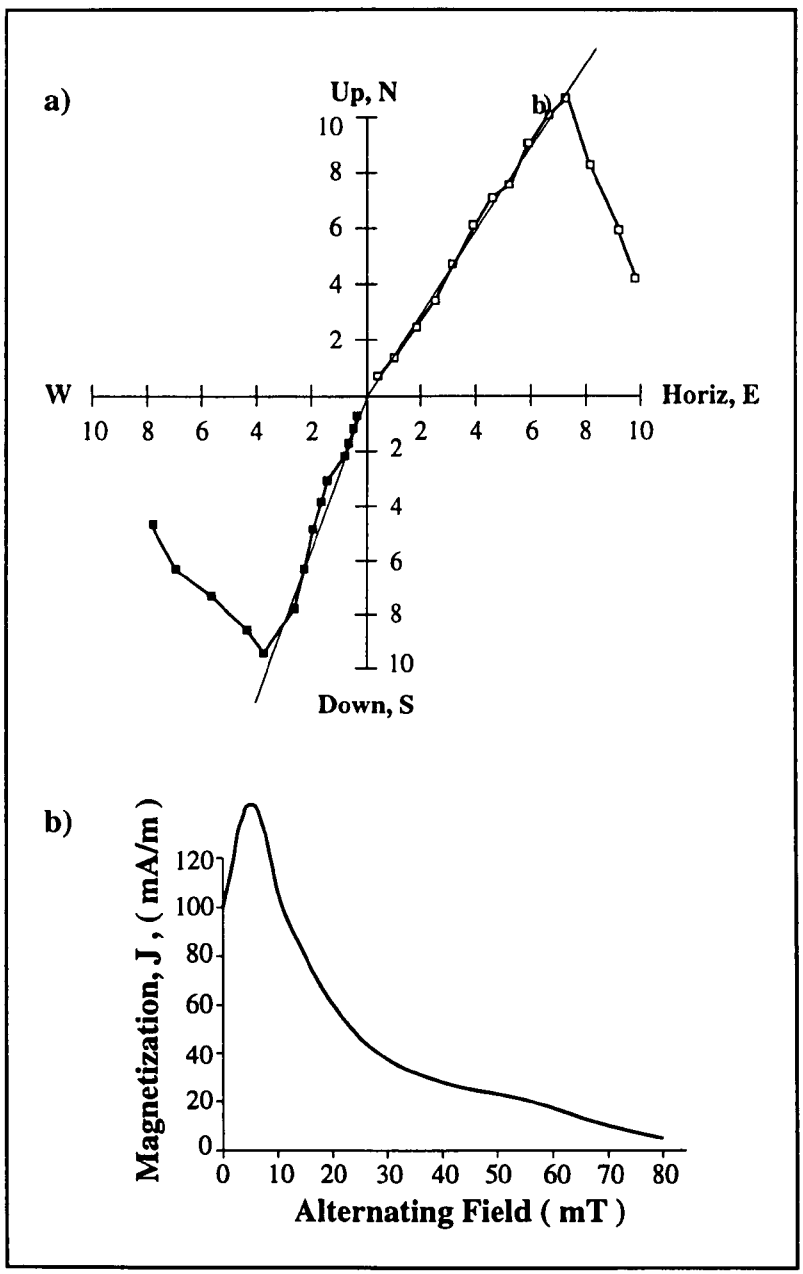

Figure 3.7: Zijderveld diagram for dyke CK21 from Lee Bay.
(a) Projection of NRM vector on a horizontal plane (open squares) and a vertical plane (filled squares). The average trend of the primary NRM (probably a TRM) is calculated from an anchored line fit passing through the origin, giving the mean inclination (I_m) and mean declination (D_m). In this case, $I_m \approx -57^o$ and $D_m \approx 190^o$. The secondary VRM has $I_m \approx +68^o$ and $D_m \approx 305^o$. Units on both the X and Y axes are $10^1 \times$ mA/m. (b) Partial demagnetization intensities for the same sample.

The normal/reversed polarity relationships may indicate that intrusion of magma straddled a period of magnetic reversal, indicating at least two temporally distinct sequences of emplacement.

3.3.2.2 Horse-Shoe Rocks

Five samples were taken from an oriented hand specimen of the submarine Horse-Shoe rocks, made up by chloritized dolerites of unknown age some 5 km northwest of Lee Bay. Palaeomagnetic directions obtained from 5 specimens are given in Table 3.3.

Table 3.3: Palaeomagnetic directions for the Horse-Shoe rocks

Specimen	Decl. (°)	Incl. (°)	α_{95} (°)	Number of Demag. steps
HSR1	154.3	-56.5	4.3	10
HSR2	136.1	-35.1	12.6	9
HSR3	161.6	-35.6	11.6	10
HSR4	192.5	-61.3	13.4	9
HSR5	112.7	-19.4	14.1	10

Vector component diagrams for all specimens display a crude three component system, most clearly defined in HSR1 (Figure 3.8). The least stable component is removed by demagnetization up to 3 mT and is probably similar to a recent VRM as seen at Lee Bay. A prominent component with high coercivity is present between 60 - 100 mT, but is only partially removed by demagnetization procedures. Such high stability is not characteristic of magnetite and may represent breakdown of magnetic minerals to haematite, which is secondary to the primary NRM. A relatively stable component is revealed between 3 and 50 mT, most clearly demonstrated in HSR1 (Figure 3.8), and this is interpreted as the primary NRM.

The circle of 95% confidence is greater than 11° in four out of five specimens, so a determination of a site-mean direction would have low precision. HSR1 and HSR4 show typical Tertiary inclinations, but HSR1 has a declination somewhat east of the Tertiary average. HSR2 and HSR3 have intermediate inclinations untypical of Tertiary rocks, although Mussett *et al.* (1980) have recorded shallower inclinations in Tertiary lavas on Mull.

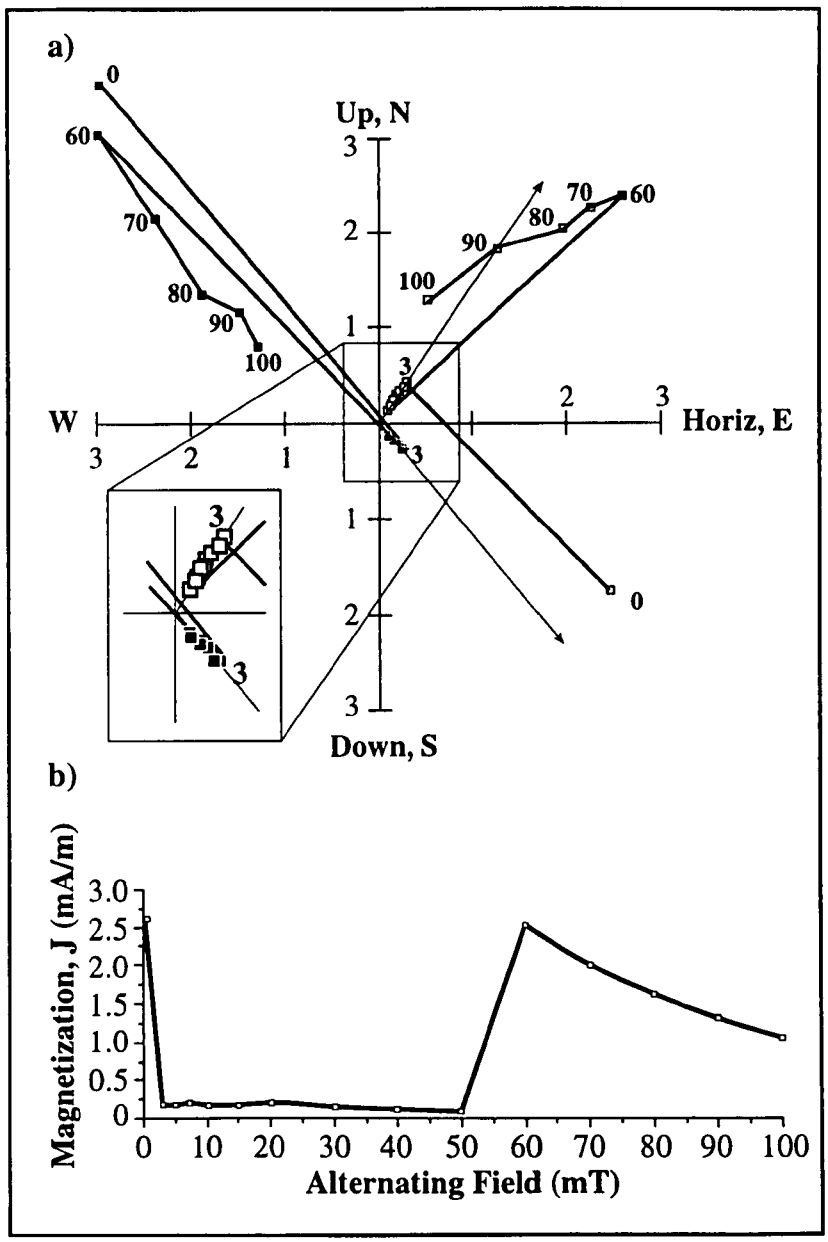

Figure 3.8: Zijderveld diagram for specimen HSR1 from the Horse-Shoe rocks.
(a) Projection of NRM vector on horizontal plane (open squares) and a vertical plane (filled squares). The inset shows an anchored line fit between 3 and 50 mT represents the primary TRM with Im = -57^{o} and Dm = 154^{o}. Between 0 and 3 mT, a modern VRM similar to that seen in Figure 3.5 is removed by partial demagnetization. Units on both the X and Y axes are 10^{1} × mA/m. (b) Partial demagnetization intensities for the same sample.

Notwithstanding the low sample and poor confidence limits, the Horse-Shoe rocks have relatively stable palaeomagnetic directions similar to the Tertiary, which implies that this submarine outcrop may be temporally related to the Lundy Igneous Complex. This evidence is not, however, conclusive and is tested later by the Ar/Ar dating procedure.

3.3.2.3 The Fremington dyke

10 sample cores were obtained from this very weathered dyke, from which only 4 specimens produced semi-stable directions over a maximum of three demagnetization steps, ranging from 10 mT to 30 mT. Although α_{95} confidence limits are between 15° and 22° for palaeomagnetic directions, which is rather large for a reliable conclusion, the inclination of all the specimens ranges from -2° to -7° for the semi-stable component. Declination is not well constrained and ranges from NW to SSE and east. Nevertheless, this poorly defined semi-stable component suggests that the palaeomagnetic direction of the Fremington dyke is too shallow for a Tertiary intrusion, being some 23 to 28 degrees less than the shallowest inclinations recorded for Tertiary rocks by Mussett *et al.* (1980). Negative shallow inclinations in the U.K. are commonly recorded in Upper Permian rocks (Tarling, 1983). The Fremington dyke is thus likely to be Permian in age and as such, too old to be related directly to the Tertiary igneous complex of Lundy. This initial conclusion is tested later by the Ar/Ar dating method.

3.3.3 THE KOENIGSBERGER RATIO AND MODELLING OF INDIVIDUAL DYKES

The ages of almost all Tertiary dykes in Great Britain and Ireland fall between 63 Ma and 52 Ma (Mussett *et al.*, 1988). This corresponds to magnetic polarity chrons 28 to 23r (Harland *et al.*, 1982) or chrons 26r to 22r according to the geomagnetic polarity scale of Berggren *et al.* (1985). Both broadly agree that this interval was marked by normal magnetic polarity for some 30% of the time, thus the Lower Tertiary geomagnetic field was dominantly reversed. This is reflected in the prevalence of reversely magnetized dykes, although the low percentage of normally magnetized dykes associated with many centres is not typical of a Gaussian distribution and suggests relatively anomalous volcanic quiescence during normal polarity at this time.

In support of the conclusions of Blundell (1957), Mussett *et al.* (1976) report dominantly reversely magnetized dykes on Lundy Island with only 4 out of 52 stable dykes demonstrating normal polarity. If this is the case, then the field signature for Tertiary

dykes on Lundy should demonstrate a negative magnetic anomaly to the south and a positive anomaly to the north, as shown in surveys of Tertiary dykes elsewhere by Robson (1964), Sowerbutts (1987), Goulty *et al.* (1984), Titman *et al.* (1989) and Gibson and Lyle (1993). However, dykes on Lundy almost universally show a paired anomaly profile with a large positive anomaly to the south and smaller negative anomaly to the north; more typical of a normally magnetized body at this latitude. Average amplitude ranges from 400 to 450 nT usually with wavelengths up 90 m, although amplitudes up to 900 nT are detected with slightly longer wavelengths, as illustrated in Figure 3.9.

The relationship between natural remanence and induced magnetization is given by the Köenigsberger ratio (Q) as

$$Q = \frac{J_r}{J_i} \qquad \text{equation 3.1}$$

where J_r = Intensity of NRM and J_i = Intensity of induced magnetization

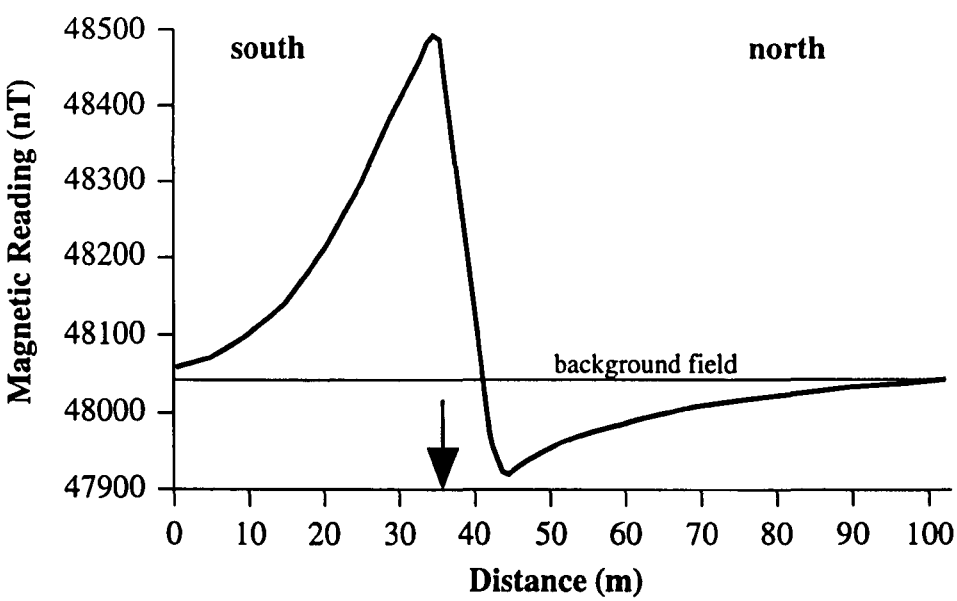

Figure 3.9: Paired anomaly profile of a dyke on Ackland's Moor, Lundy Island.
Total field readings were taken at 1 m intervals and corrected for the effects of diurnal drift. The arrow indicates the presence of weathered basic material at 36.7 m from the start of the line, confirmed by hand auguring, approximately 1.2 m below ground level.

The observed magnetic profiles on Lundy could reflect the fact that (i) the dykes are normally magnetized, (ii) NRM properties have been destroyed and replaced by a secondary characteristic component with normal polarity (e.g. modern VRM) or (iii) Q is <1, which would be the case when J_i dominates over a small J_r component. Palaeomagnetic data from Lundy (P. Dagley, pers comm) is relatively well constrained and ranges from 0.39 to 778.64 x 10^{-5} Am^2kg^{-1} (N = 227). Assuming a mean density of 2.98 g/cm^3 for basic Tertiary dykes (Olhoeft and Johnson, 1989), this converts into SI units as 0.01 to 23.20 Am^{-1} with a mean value for intensity of NRM (J_r) = 2.84 Am^{-1}. The geomagnetic field strength on Lundy is taken as 38.2298 Am^{-1}, calculated from the 1991.5 base reference field.

Mussett *et al.* (1976) report a bimodal lognormal distribution pattern for magnetic susceptibility with peak values of 4 x 10^{-4} and 3 x 10^{-2} (SI units), the latter probably representing basic dykes and the former intermediate rocks. On this evidence, the strength of induced magnetization (J_i) ranges from 0.015 to 1.147 Am^{-1} and the Koenigsberger ratio has a value between 2 and 2.5 for the basic dykes. This suggests that the magnetic field signature of the dykes is more influenced by natural remanence than by induced magnetization with the result that paired anomaly profiles detected by proton magnetometry represent normally magnetized dykes. However, this can only be partially true as both Blundell (1957) and Mussett *et al.* (1976) indicate a preponderance of reversely magnetized dykes on Lundy.

3.3.4 COMPUTER MODELLING OF INDIVIDUAL DYKES

Several factors may affect the shape and amplitude of magnetic anomalies, not least being the shape and size of the source of magnetism. Here, the source of magnetism is taken to be associated with intrusive volcanic rocks, which can be realistically modelled as vertical or inclined elongated prisms. Such polygonal prisms can be thought of as monopoles rather than dipoles within a modelling context, because the lower positive pole is too far away from the magnetometer to influence the magnetic signature (assuming the dyke is steep and has a large depth to width ratio). Dykes may thus be represented for the most part by a line of negative monopoles along strike, except where they become

sub-horizontal, in which case both poles will influence the field signature. Modelling procedures assume that magnetization is uniform within the target model and that there is a significant magnetic contrast between model and host rock.

The observed field signature (magnetic flux) is the vectoral sum of induced and remanent magnetization and can be expressed by the relationship -

$$J = J_i + J_r \qquad \text{Equation 3.2}$$

Where, J = Total Magnetization, J_i = Induced Magnetization and J_r = Natural Remanent Magnetization.

Computer modelling using 'Gravmag' software (Pedley, 1991) was undertaken to compare the theoretical response of hypothetical geologically-indicated models to the observed magnetic anomalies. As a starting point, a reasonable analysis of depth estimation can be obtained from Peters' half-slope magnetic interpretation method (Milsom, 1992). In this method, a tangent is drawn along the steepest part of the magnetic profile to give the maximum slope line. The half-maximum slope line is then geometrically constructed, as shown in Figure 3.10. Tangents parallel to the half-maximum slope line are then drawn at two points on the anomaly curve and their intersection marked. The horizontal distance (x) between these two points is a guide to the depth of the top of the source body and has been shown from many case studies to vary between a factor of 1.2 and 2.0. On average, the top of the source body is approximately 1.6x.

For a sample of dykes on Lundy Island (N = 15) with magnetic readings at 1 m intervals, the depth to the top of the dykes ranged from 0.8 to 3.4 m, with 2.5 m as the average value. Other starting values were taken from Mussett *et al.* (1976), previously defined in section 2.3.3.

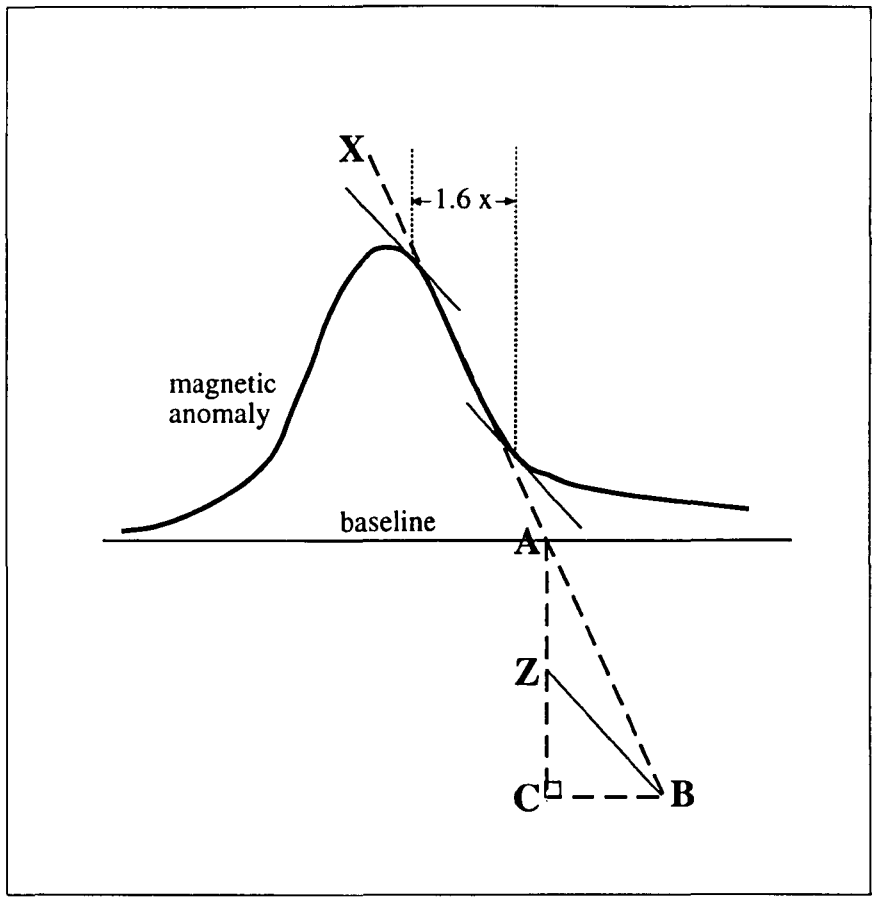

Figure 3.10: The Peters' half-slope interpretation method.
The line AB represents an extension of the maximum slope of the magnetic anomaly. In the triangle ACB, the line ZB is constructed so that AZ = ZC and ZB is the half-maximum slope line. The distance 1.6x is defined in the text.

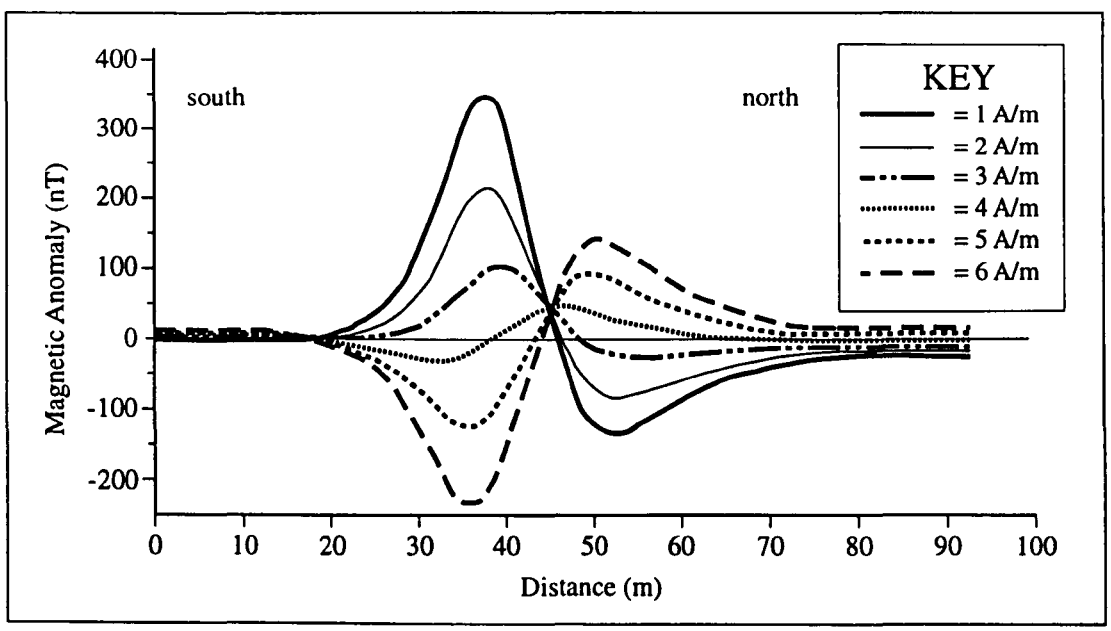

Figure 3.11: Theoretical magnetic responses.
The theoretical magnetic response to a vertical basic dyke 2 m in width and 2.5 m below ground level. Bulk susceptibility has a maximum value of 0.1 (dimensionless), with declination and inclination of remanence set at 003.6°E and -62.7° respectively, i.e. the Tertiary geomagnetic pole values (Mussett *et al.*, 1976). The present-day geomagnetic field on Lundy is 38.2298 Am^{-1}. The key shows a range of NRM values for Tertiary basalts (Carmichael, 1992).

3.3.4.1 Reversely magnetized dykes

As the field signature of dykes is a function of both susceptibility and remanence, both parameters need to be varied within the software to achieve parallelism with observed and computed anomalies. Increasing the susceptibility values generally only changes the amplitude of the anomaly, whereas variations in remanence values changes both the amplitude and shape of the paired anomaly profile (Figure 3.11).

With bulk susceptibility (χ) set at 0.1, a typical reversely magnetized dyke profile (with a negative anomaly to the south and a positive anomaly to the north) is only apparent when NRM is > 3.5 Am^{-1}. As virtually all observed paired anomaly profiles on Lundy have a negative to the south and a smaller positive anomaly to the north, it seems probable that if dykes are reversely magnetized, then their NRM cannot exceed 3.5 Am^{-1}.

3.3.4.2 Normally magnetized dykes

Mussett *et al.* (1976) reported almost 8% of stably magnetized dykes on Lundy to be normally magnetized (N = 56 from a possible maximum of about 200) and record a minority of samples as having a NRM intensity value between 14 and 22 Am^{-1}, which is considerably higher than the total sample mean value of 2.88 Am^{-1} (op. cit. section 3.3.2). At the latitude of Lundy, the magnetic profiles of normally magnetized dykes would always be characterized by a positive to the south and a smaller negative anomaly to the north, as NRM enhances induced magnetization, which is in turn a response to the present positive geomagnetic field.

However, the largest magnetic anomaly measured by proton magnetometry on Lundy Island is approximately +900 nT over the airfield in the south of the island. If NRM values between 14 and 22 Am^{-1} are attributed to normally magnetized dykes, the modelling procedure indicates that bulk susceptibility must be very low, around 0.006. The strong correlation between NRM and susceptibility described by Mussett *et al.* (1976) is contradicted and thus it seems likely that such high NRM values cannot be attributed solely to magnetized dykes detected over the island surface. With bulk susceptibility set at 0.1, a magnetic anomaly of +900 nT can be modelled with a positive

NRM value of 1.8 Am-1, which is within the distribution range described by Mussett *et al.* (1976).

The distinction between normal and reversely magnetized dykes is relatively easily determined by computer modelling, but this does not facilitate deciphering paired anomaly profiles on the ground. Whilst the probability exists that an apparent normally magnetized dyke signature, measured by proton magnetometry, is probably a reversely magnetized dyke with relatively low NRM, it is difficult to unequivocally determine such interpretations in the field. Nevertheless, computer modelling procedures are able to give theoretical ranges of both susceptibility and NRM. On Lundy Island, the following relationship is true for normally magnetized dykes; for any given susceptibility value, bulk susceptibility and NRM are described by the relationship -

$$\text{Bulk Susceptibility } (\chi) \approx L \times \text{NRM}, \qquad \text{equation 3.3}$$

where $L \approx 0.0286 \pm 0.0012$ m/A.

The Lundy magnetic parameter (L) has the unusual unit of m/A, as bulk susceptibility is dimensionless. Equation 3.3 shows that a change in value for either χ or NRM directly affects the value of the other.

3.3.5 IMPLIED FIELD RELATIONS OF DYKES ON LUNDY

Proton magnetometry on the ground indicates that paired anomaly profiles can be detected using the methods described in section 2.1.3. The underlying assumption is that paired anomaly profiles represent the surficial expression of basic or intermediate igneous intrusions within the solid geology, i.e. Tertiary granite or Devonian metasediments, as previously discussed. Detailed mapping of such magnetic anomalies therefore allows the trends of dykes to be recorded with a reasonably high degree of accuracy. Figure 3.12 demonstrates the mapping strategy over a sample area.

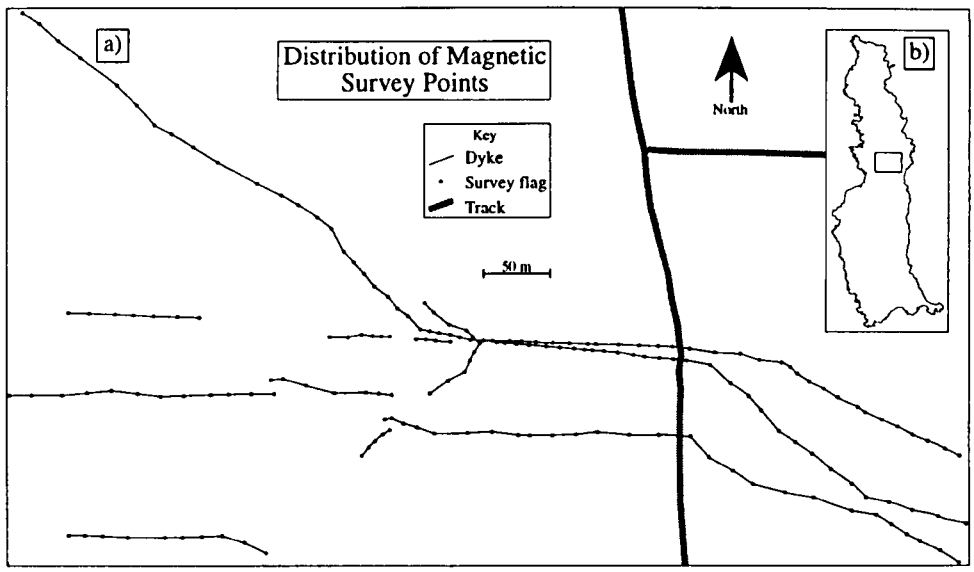

Figure 3.12: Magnetic surveying strategies on Lundy Island.
(a) A sample of the distribution of observation posts. Trends of dykes were determined by taking readings of magnetic 'highs' every 5 m and marking positions with fluorescent flags. These were placed at points of directional change or every 10 to 20 m and bearings recorded with a siting compass.
(b) Location sample area of observation posts on Lundy Island.

Where dykes converged or had cross-cutting relationships, short north-south magnetic traverses at 5 m spacings were undertaken to reveal the characteristic magnetic signature and hence indicate the position of peak readings. In some places, destructive interference of adjacent dyke signatures made it difficult to record dyke trends with unambiguous accuracy. These positions were not mapped to reduce interpretation errors. Also, anomalies lower than a maximum 100 nT amplitude, although probably overlying dykes, were inferred as being too low to be traced in the field with any degree of accuracy due to variations in magnetic induction along the strike of the dyke. However, there were not many of these instances, which suggests that the majority of detectable dykes are represented by the full magnetic survey. The results of the full magnetic survey are presented in Figure 3.13. Where possible, dyke positions were visually correlated with known outcrops in the coastal cliffs, although difficulty of access hampered definition in many instances. Nevertheless, correlation between outcrop and the magnetic termination of dykes was facilitated by observations from a boat around parts of the island. Some magnetic anomalies coincided with well developed basalt soil horizons along the sides of the island, the soils often forming in the floor of shallow gullies.

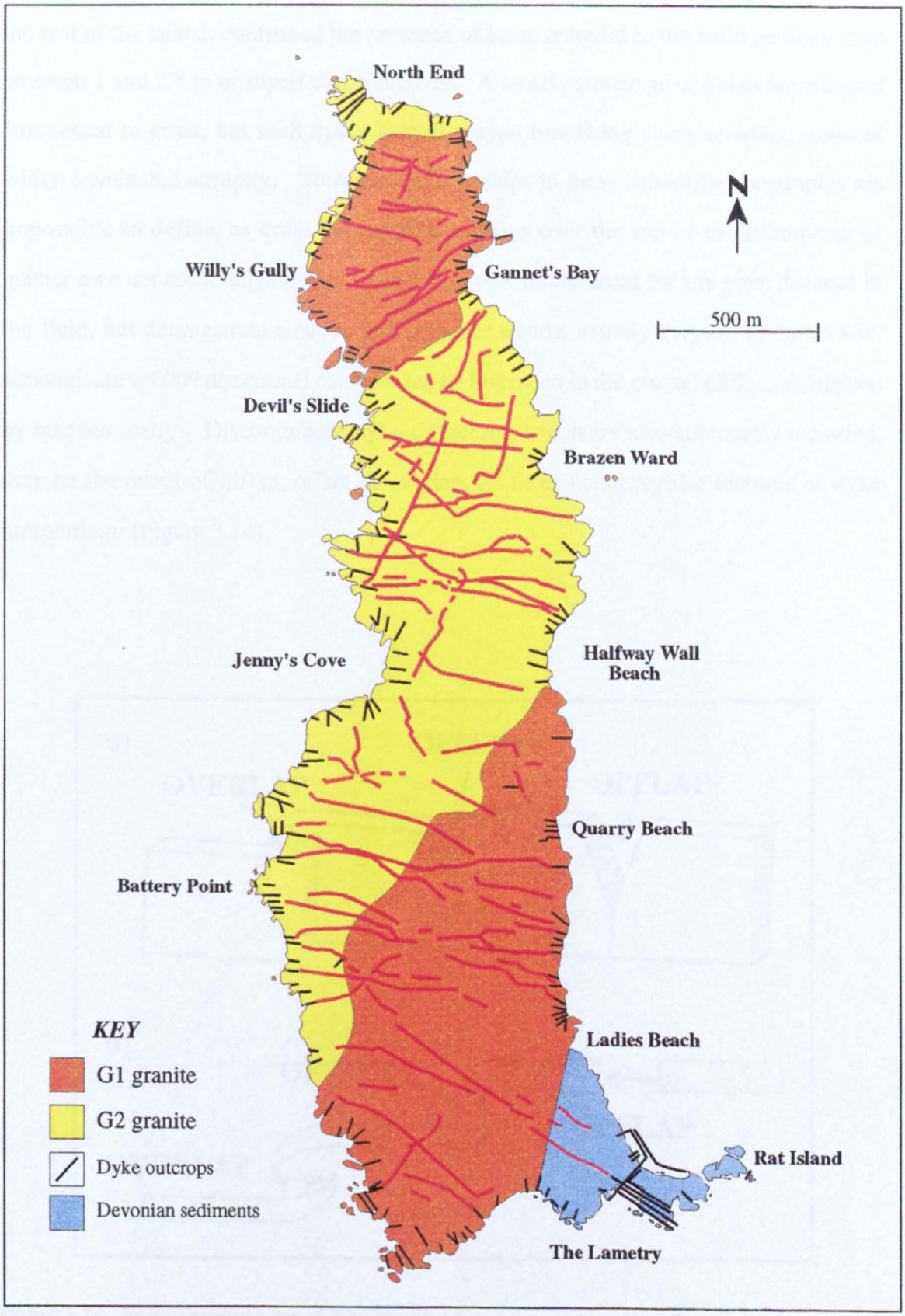

Figure 3.13: Implied Filed relations of dykes on Lundy Island.
The red lines represent dykes that were traced by proton magnetometry, as described in section 3.3.5.

Hand auguring here, as well as over a random selection of postulated dyke positions over the rest of the island, confirmed the presence of basic material in the solid geology with between 1 and 2.4 m of superficial soil cover. A small percentage of dykes were traced from coast to coast, but such dykes also displayed branching characteristics, some of which terminated abruptly. Temporal relationships in these sub-surface examples are impossible to define, as cross-cutting relationships over the top of the island can be neither seen nor accurately implied. Most dykes are rarely linear for any great distance in the field, but demonstrate sinuous and irregular trends, usually varying by up to 45°, although abrupt 90° directional changes can be both seen in the coastal cliffs and mapped by magnetometry. Discontinuous dyke signatures, which are also commonly recorded, may be the result of offlap, offset or overlap, all three being regular features of dyke morphology (Figure 3.14).

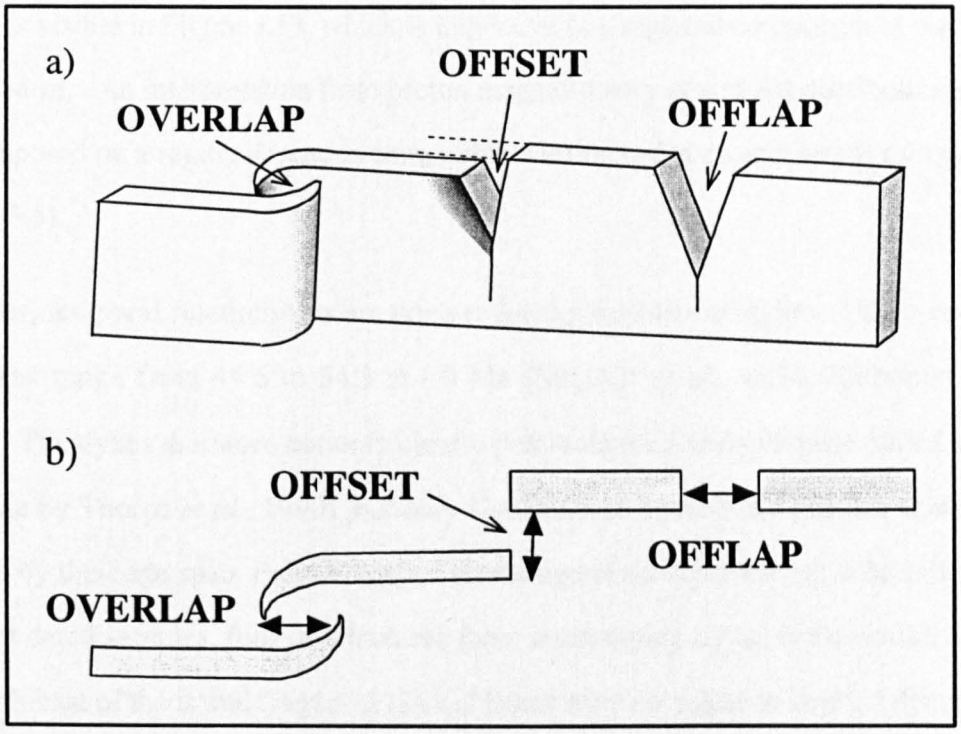

Figure 3.14: Some characteristics of dyke morphology.
Theoretical form in a) block diagram and b) plan view.

Magnetic induction varies in most dykes along strike, most commonly as a result of variations in magnetic mineralogy, which is reflected in variable susceptibility. Differences in depth below ground level to the top of the dykes may also affect magnetic induction, although variability in soil thickness alone would tend to have minimal influence. Nevertheless, it is possible to record trends of dykes, even where such variations are marked, by monitoring the magnetic profile signature over the wavelength width. Dykes are still located at positions of magnetic 'highs' along the profile.

Figure 3.13 shows that dyke trends are not purely NW-SE, as previously suggested by Hains *et al.* (1983). Towards the southern end of the island, a NW-SE trend is discernible, but in the northern quarter, a SW-NE orientation is dominant. A less obvious E-W component is also present over the central parts of the island. Such trends indicate a crude radial distribution pattern on Lundy, as suggested by Figure 3.5, and extrapolation suggests some dykes may have originated from a common focus 2-3 km west of the island. In addition, a WNW-ESE trend without apparent geographical control is visible in Figure 3.13, which is indicative of a regional component to the Lundy dyke swarm. An interpretation from proton magnetometry of a radial distribution pattern superimposed on a regional trend is compatible with recorded coastal trends of dykes (cf. Figure 3.5).

However, temporal relationships are unclear for the majority of dykes. K/Ar dates for the dykes range from 44.6 to 54.3 ± 1.0 Ma (Mussett *et al.*, 1976; Edmonds *et al.*, 1979). The dykes therefore not only clearly post-date the Lundy Granite (dated as 58.7 ± 1.6 Ma by Thorpe *et al.*, 1990), but may also indicate a relatively protracted intrusive episode by their age span. Precise control on the age of the dyke swarm is broadly based on eight dated samples, four of which are from outcropping dykes in Devonian Slate to the south-east of the island (Figure 3.12) and hence may not relate to implied dykes in the main magnetic survey. The remaining four dykes have some devitrified glass and relatively large amounts of potassium (4.13% to 6.23%), possibly due to contamination from underlying slates. As a consequence, the calculated ages of the dykes could be artificially young.

The most reliable dated sample by Mussett *et al.* (1976) has 0.555% potassium (wt.% K_2O), fresh feldspars, no glass and yields an age of 54.3 ± 1.0 Ma, which is close to the age of the granite. The apparently protracted intrusive episode (54 to 45 Ma) may thus be an artefact of the weathered nature of the samples. There are clearly insufficient data to define the precise date of intrusion of the Lundy dyke swarm, but it is feasible that most of the dykes were formed during more than one phase of volcanic activity soon after the crystallization of the granite.

3.4 PHYSICAL PROPERTIES OF DYKES AND INTRUSIONS

3.4.1 MAGNETIC GRANULOMETRY from HYSTERESIS LOOPS

Magnetic hysteresis is a property displayed by magnetic minerals when subjected to a magnetic field from a relatively large positive value to a relatively large negative value (Tarling, 1983; Banerjee, 1991). Parameters that can be determined from hysteresis loops include saturation magnetization (M_s), saturation magnetic remanence (M_{rs}), coercive force (H_c) and coercivity of remanence (H_{cr}). Saturation magnetization (M_s) is independent of grain size, but the other three parameters are inherently influenced by the domain state of the magnetic minerals (Figure 3.15). In turn, the domain states are a function of individual grain sizes, thus magnetic granulometry can be achieved by undertaking hysteresis loops on a variety of rock samples (Stacey and Banerjee, 1974). Day *et al.* (1977) devised a method to study the relationship between grain size and domain state by using a plot of M_{rs}/M_s against H_{cr}/H_c. As such a plot is normalized to M_s, which is not a function of grain size, this method is valid for both varying mixtures and concentrations of magnetic minerals and for varying values of M_s, which may be relevant when comparing haematite with magnetite.

This method is preferable in many ways to experimental observations on individual grains (Dunlop,1981,1986; Stacey and Banerjee,1974), because the net effect of interactions between assorted magnetic grains in a rock is unclear and any consequent reduction in both remanence and coercive force is unquantifiable. Also, rocks have variety in the

concentrations of magnetic minerals, thus magnetic granulometry should use a methodology that encompasses these concepts.

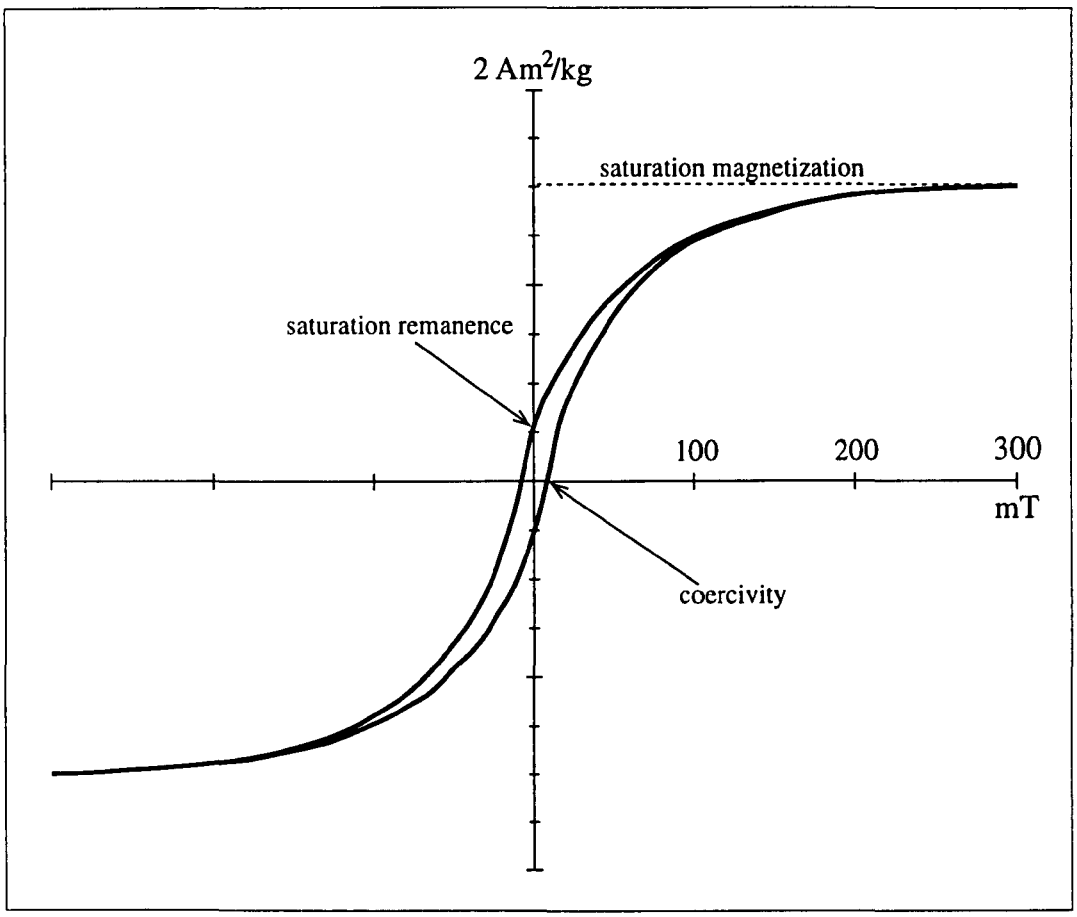

Figure 3.15: Typical hysteresis loop for basic rocks on Lundy Island.
Sample BW1 was used in this simple humming bird plot.

However, domain state is not in itself diagnostic of specific grain size or magnetic mineralogy. For example, single domain (SD) magnetite has a critical grain size diameter of about 1 μm, which leads to two or more domains when exceeded (Butler and Banerjee, 1975). Similarly, multidomain (MD) magnetite has grain sizes > 10 μm and pseudo-single-domain (PSD) magnetite between 1 and 10 μm. By comparison, the stable SD grain size range in haematite is large, extending from 0.05 μm to 15 μm (Butler, 1992). On this basis, identification of SD magnetic minerals can be interpreted as either magnetite or haematite of variable size, although there are other mineralogical possibilities.

3.4.1.1 Hysteresis loops of rocks from Lundy and Lee Bay

Data for the hysteresis loops obtained for rock samples from Lundy Island and Lee Bay are given in Appendix A1 and graphically presented in Figure 3.16. All four dykes at Lee bay were analysed, compared to 10 dykes from the dyke swarm on Lundy Island. The 10 dykes represent a reasonable geographic coverage of the island. The graph shows that although most of the magnetic grains are within the pseudo-single-domain (PSD) field, the results can be grouped into two distinct regions, i.e. Lundy and Lee Bay. Lundy samples have saturation magnetization (M_S) in the range 0.791 to 3.084 Am^2kg^{-1} and saturation magnetic remanence (M_{rs}) from 0.057 to 0.241 Am^2kg^{-1} (mean values being 1.601 Am^2kg^{-1} and 0.141 Am^2kg^{-1} respectively) with coercive force (H_c) in the range 3.93 to 7.93 mT (mean = 5.79 mT) and coercivity of remanence (H_{cr}) in the range 13.18 to 25.09 mT (mean = 19.89 mT). Conversely, Lee Bay has M_S values in the range 0.498 to 1.088 Am^2kg^{-1} (mean = 0.723 Am^2kg^{-1}) and M_{rs} values from 0.132 to 0.234 Am^2kg^{-1} (mean = 0.173 Am^2kg^{-1}), with H_c from 6.67 to 12.08 mT (mean = 9.66 mT) and H_{cr} in the range 12.06 to 22.38 mT (mean = 17.27 mT). The M_{rs}/M_S ratio for Lundy is in the range 0.065 to 0.115 (mean = 0.089) and from 0.221 to 0.302 (mean = 0.259) for Lee Bay. The H_{cr}/H_c ratio for Lundy is in the range 2.62 to 4.75 (mean = 3.51) and from 1.73 to 1.85 (mean = 1.79) for Lee Bay.

Although M_{rs} and H_{cr} are similar in both areas, M_S on Lundy differs by a factor of 2 compared to Lee Bay and this significantly lowers the M_{rs}/M_S ratio, so that Lundy basalts and dolerites are magnetically characterized by a constant ratio in plots as a function of their H_{cr}/H_c ratio. By comparison, the lower H_{cr}/H_c ratio of samples from Lee Bay is due to H_c values almost twice those of Lundy, whereas H_{cr} values are similar in both regions. Lee Bay values plot in a vertically prolate area close to the SD/PSD boundary and are a function of variable M_{rs}/M_S ratio.

Day (1977) reported that the J_{rs}/J_S ratio in multidomain grains is proportional to H_c, but this does not hold true for these samples, perhaps because most of the samples are PSD grains. Also, the appearance of two distinct fields in Figure 3.16 suggests that there may be a difference in mineralogy between the two areas. If the graph were to be interpreted

in terms of grain size only, there should be a crude linear relationship with a negative slope between both x and y axes (Dunlop, 1990). The two sets of data are clearly not linked by a linear relationship, thus a direct comparison of the two fields is not justified and a variance in magnetic mineralogy may be indicated.

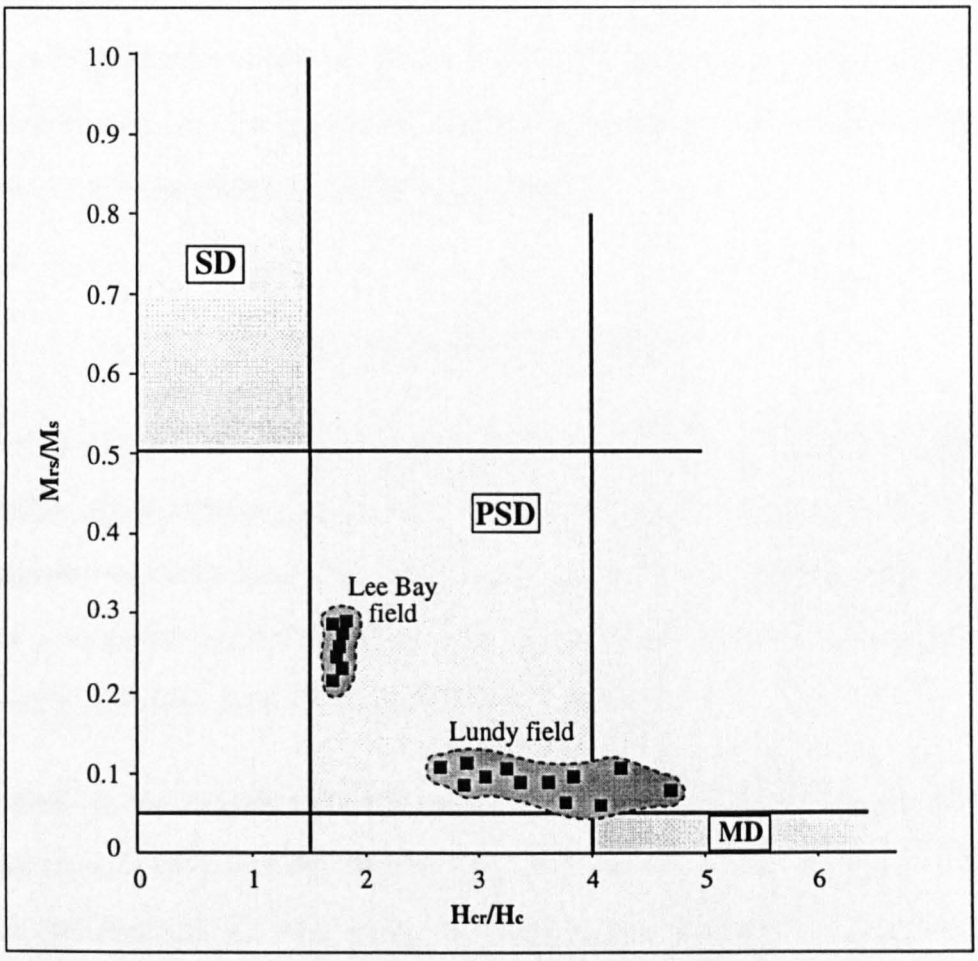

Figure 3.16: Domain state diagram for rocks from Lee Bay and Lundy Island. Methodology for plotting the data is from Day (1977). The fields for single domain (SD) , pseudo-single-domain (PSD) and multidomain (MD) particles have been shaded for clarity. Data fields for Lundy (N = 12) and Lee Bay (N = 8) are superimposed. Each plot represents a different sample.

3.4.2 CURIE TEMPERATURE DETERMINATIONS AND CONCENTRATIONS OF MAGNETIC MINERALS

One possible method of determining the magnetic mineralogy of specific rock samples is to study their thermo-magnetic curves in which the magnetization of a sample, acquired by exposure to a strong magnetic field of ≥ 100 mT, is monitored whilst the temperature is increased from that at ambient room conditions up to 700 °C. This technique is particularly useful in rock samples where the dominant grain size of magnetic minerals is mostly below the optimum resolution for microscopic examination. Samples in which magnetization is mostly carried by ferromagnetic grains, as opposed to paramagnetic and/or diamagnetic grains, the measured strong-field magnetization approximates J_S, saturation magnetization (Butler, 1992). Curie temperatures (T_C) are estimated from major decreases in J_S with significant changes in the slope of the measured thermo-magnetic curve, most clearly seen as inflection points.

3.4.2.1 The Lee Bay dyke assemblage

The thermo-magnetic curves for 6 samples from the four basic dykes at Lee Bay were very similar and are considered to be representative of the same magnetic mineral. As the ferromagnetic concentration in the rock samples was sufficiently high to allow accurate analysis, a magnetic concentrate from crushed rock was not required. A representative thermo-magnetic curve for the samples is given in Figure 3.17.

The heating leg shows an initial Curie temperature (T_C) of 280 to 290 °C, followed by a small increase in magnetization which peaks at around 400 °C. A second T_C occurs between 490 and 500 °C, after which there is minimal magnetization variation with increasing temperature. The first T_C ranged from 277 to 317 °C ($T_{C(mean)}$ = 286 °C) and the second from 488 to 508 °C ($T_{C(mean)}$ = 497 °C). An inversion of this type between 300 to 400 °C is typical of titanomaghemite (O'Reilly, 1984), which is a non-stoichiometric metastable single-phase mineral with a spinel crystal structure. In the case of titanomaghemite, inversion is independent of heating in air or a vacuum (Wasilewski, 1968; Ozima and Larson, 1970) and the magnitude of the magnetization shoulder at

inversion is directly related to the oxidation parameter (z) and composition parameter (x) (Özdemir, 1987; Readman and O'Reilly, 1970). In this case, the magnitude of the inversion shoulder indicates z = 0.20 to 0.25 and x = 0.35 to 0.40.

The cooling leg shows inflection points at 570 to 580 °C, 450 to 465 °C and 180 to 200 °C, which suggests three inversion products from the heating process. A T_c of 570 to 580 °C is indicative of virtually stoichiometric magnetite, whilst a T_c of 450 to 465 °C probably represents a titanomagnetite with x = 0.15 to 0.20 (Nagata, 1964). The lowest T_c dominates the cooling leg and may represent titanohaematite with x = 0.50 to 0.55 (Butler, 1992). Nagata (1964) found that titanomaghemite inverts irreversibly to hematite on heating, but Özdemir (1987) reports spinel inversion products of near stoichiometric titanomagnetite and a rhombohedral phase of near ilmenite composition. As the cooling leg demonstrates almost 100% increase in magnetization, titanomaghemite has probably inverted to ilmenite (x = 0.5), with some titanomagnetite (x = 0.2) and magnetite.

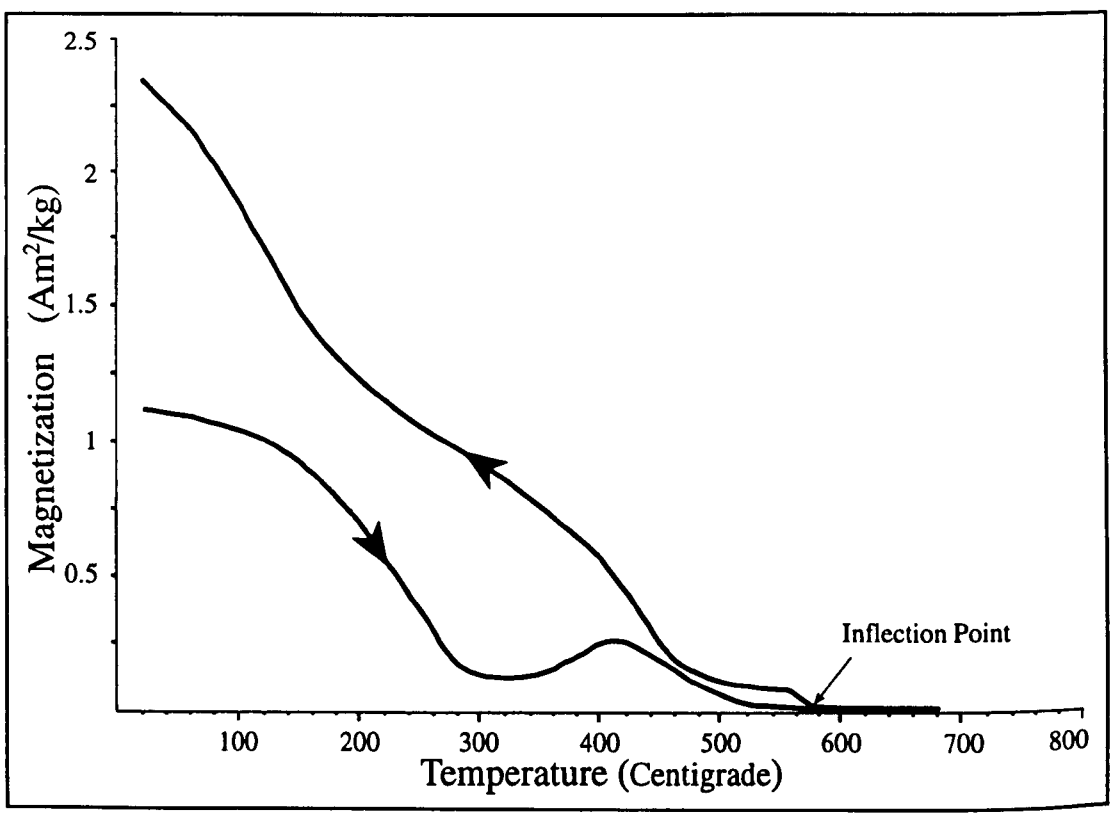

Figure 3.17: Thermo-magnetic curve for dyke CK21 from Lee Bay.
This response to heating is typical of all four dykes at Lee Bay and suggests a common history.

3.4.2.2 The Lundy dyke association

Thermo-magnetic experiments were also carried out on 10 samples from Lundy Island to investigate magnetic mineralogy and to compare thermo-magnetic curves from Lee Bay. Sample sites on Lundy were distributed over a wide geographic area, so that the probability of sampling the same dyke more than once was remote and so the suite of results obtained provides a reasonable model for the Lundy Dyke Swarm. Apart from one rock sample, Curie temperature determinations from all dyke samples displayed similar characteristics and have consequently been represented by a single thermo-magnetic curve in Figure 3.18.

The first thermo-magnetic curve (Figure 3.18a) is for sample VC1 - a moderately weathered basalt. The heating curve shows two significant inflection points at 500 °C and between 570 and 580 °C, indicating two Curie temperatures (T_c). The second T_c between 570 and 580 °C suggests near stoichiometric magnetite, but the first T_c could indicate titanomagnetite (x = 0.1) or titanohaematite with x = 0.25 to 0.30 (Nagata,1964; Butler, 1992). To differentiate between the presence of more than one magnetic mineral or oxidation/exsolution effects during heating, a second run was performed on the same sample, i.e. after its initial heating (Figure 3.18b). This shows a virtually reversible curve with a T_c around 570 °C, indicating magnetite. Therefore, it is unlikely that the heating curve in Figure 3.18a is a response to two magnetic minerals, but rather the second T_c is an artefact of oxidation and there is probably only one magnetic mineral in the sample.

However, precise identification is still ambiguous between titanomagnetite and titanohaematite, although magnetization of the sample at room temperature was considerably lower before the experiment than it was afterwards. Stacey and Banerjee (1974) summarize the canted antiferromagnetic coupling effect in titanohaematites with $x < 0.45$ and report a consequent reduction in saturation magnetization relative to the ferrimagnetic coupling observed when $0.45 < x < 1.0$. Also, Nathans *et al.* (1964) observed that secondary contributions to magnetization in haematite may arise from defects or impurities preferentially occupying one sub-lattice or another, even if canted

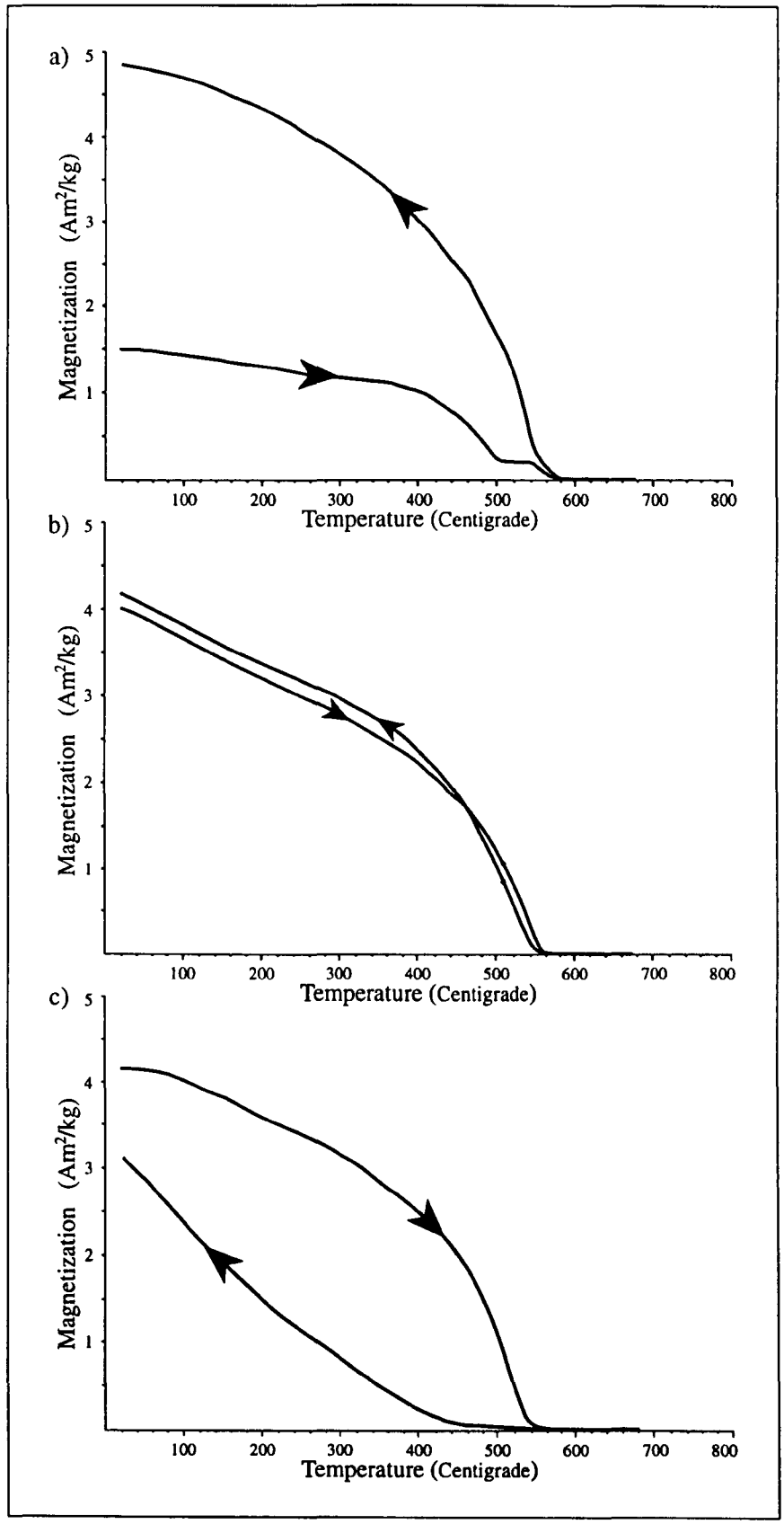

Figure 3.18: Thermo-magnetic curves for basic dykes from Lundy Island.
a) Sample VC1 - curve shows two inflection points, indicating two magnetic minerals.
b) Second run on VC1 - reversible curve indicating titanomagnetite. c) Sample BW4 - the shape of the curve is representative of all other dykes sampled on Lundy and is markedly different from Lee Bay samples (cf. Figure 3.17).

antiferromagnetism occurs. It thus follows that in view of the relatively low level of magnetization, the heating leg in Figure 3.18a is more diagnostic of titanohaematite rather than titanomagnetite. Titanohaematite is a primary FeTi oxide in basic igneous rocks (Gribble and Hall, 1988), but confirmation is required by optical microscopy to eliminate a secondary mode of formation.

3.4.3 ANISOTROPY OF MAGNETIC SUSCEPTIBILITY (AMS)

The property of magnetic anisotropy is often used as an indicator for petrofabric and structural analyses in rocks (Owens and Bamford, 1976; Hrouda, 1982; Ellwood, 1978,1982; Knight and Walker, 1988; Jackson and Tauxe, 1991; Ernst and Baragar, 1992). The principle of anisotropy of magnetic susceptibility (AMS) is basically simple and has been reviewed by Rochette *et al.* (1992) and Tarling and Hrouda (1993). Susceptibility is a function of the overall ferro-, para- and diamagnetic mineral assemblage in rocks and can be defined by the relationship

$$\mathbf{M} = k \times \mathbf{H} \qquad \text{equation 3.3}$$

where **M** = induced magnetization, **H** = inducing magnetic field and k = volume or bulk susceptibility. For a small number of rocks, the induced magnetization in a symmetrical specimen has a constant strength, unrelated to the direction in which a weak magnetic field is applied. In such instances, the rocks are magnetically isotropic. However in most cases, induced magnetization is partly influenced by the orientation of the sample relative to that of the constant inducing field and such rocks are magnetically anisotropic. The change in susceptibility values with respect to orientation is mathematically described by a second-rank tensor (cf. 2.2.1) or graphically depicted by a susceptibility ellipsoid (Figure 3.19).

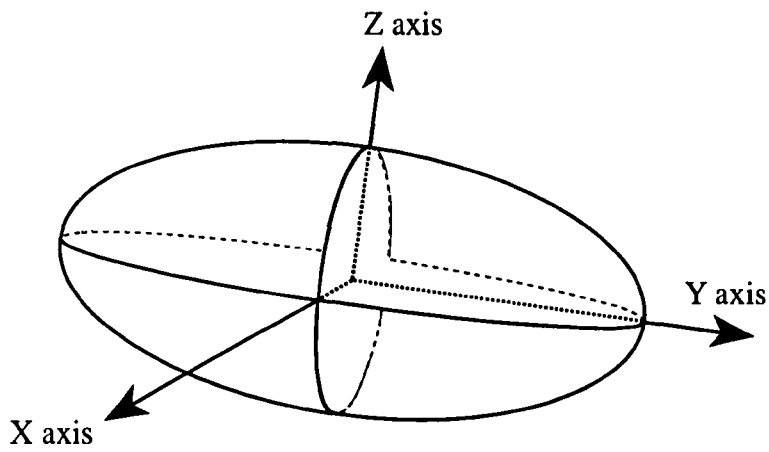

Figure 3.19: The susceptibility ellipsoid.
The tensor is described by three orthogonal axes that correspond to maximum (K1), intermediate (K2) and minimum (K3) principal susceptibility axes, where the length of the axis is proportional to the susceptibility value. In this example the y-axis = K1, z-axis = K2 and x-axis = K3, together giving a prolate shape. Oblate shapes occur when K1 = K2 > K3.

Anisotropy of magnetic susceptibility (AMS) in individual grains is governed by two main criteria - shape and crystalline anisotropy. Shape anisotropy is due to induced magnetization being preferentially directed along the long axis of a grain so that the internal magnetostatic forces, which create north and south poles at diametrically opposite positions on the surface of the grain, are significantly reduced. These internal forces are greatest when the poles are close together, but are reduced in non-symmetrical grains when the poles are furthest apart (Tarling and Hrouda, 1993). Shape anisotropy usually dominates over crystalline anisotropy in most basic igneous rocks, since most basic rocks contain magnetite grains with irregular and non-uniform shapes (Ellwood and Fisk, 1977; Knight and Walker, 1988). Magnetite that is almost entirely shape dominated by cubic structures has fairly symmetric crystalline anisotropy. Crystalline anisotropy develops when magnetization is acquired most readily along an easy axis within a crystal lattice with respect to hard axes, along which magnetization is poorly manifested and is particularly associated with haematite.

Magnetite is characterized by weak crystalline anisotropy and strong shape anisotropy, whereas the converse is true of haematite. However, the size of the magnetite grains are also important. For instance, multidomain (MD) magnetite particles have a 'normal' AMS, in which the maximum low-field susceptibility is parallel to their long axes and

minimum susceptibility is aligned with their short axes. Single domain (SD) magnetite particles display an 'inverse' AMS, in which the maximum low-field susceptibility is normal to their long axes (Jackson, 1991). This SD effect arises because the applied field does not increase the overall magnetization, as SD grains are already magnetically saturated, but causes a rotation about the long axis (Potter and Stephenson, 1988). It is however rare to encounter rock types that contain entirely single domain particles, as most rocks contain a mixture of many different magnetic grain sizes. The response of pseudo-single-domain (PSD) grains is uncertain, but in terms of energy conservation, they may mimic SD behaviour when the grain size is close to the SD zone and MD behaviour as grains approach the PSD/MD boundary.

3.4.3.1 Magnetic anisotropy in volcanic rocks

AMS techniques have been used for many years to study flow directions and strain relationships in both intrusive and extrusive volcanic rocks. Khan (1962) demonstrated that the physical orientation of the long, intermediate and short axes of magnetite grains in some volcanic dykes and sills corresponded very closely to the principal AMS ellipsoid axes, whilst developing a dominant foliation within the flow plane of the intrusive body. Khan (1962) also notes a magnetic lineation perpendicular to the flow direction in a lava flow, but does not define which magnetic minerals are responsible.

Kolofíková (1976) and Hrouda (1982) described the orientation of principal susceptibilities from a closely mapped basaltic lava flow in Northern Moravia and concluded that magnetic lineations from magnetite grains are near to the mean direction of the lava flow body. In this case, therefore, magnetic lineation was parallel to the flow direction. Differences may be due to grain size and/or mineralogical variance or the type of magma flow, e.g. aa or pahoehoe. Rochette *et al.* (1992) defined the 'normal' magnetic fabric of 61 basaltic dykes from the Oman ophiolite as having maximum susceptibility axes (K1) in the same plane as dyke bodies, with minimum susceptibility axes (K3) perpendicular to dyke margins, but they noted that this only occurs in about 50% of all dykes. Variations from this fabric are due to multi-mineral combinations and mineralogical variance, which may be difficult to decipher accurately without

corroborative evidence from other techniques or without reliable morphological features of flow patterns.

Rochette *et al.* (1992) also noted that interactions are possible between AMS and NRM with the result that structural interpretations should be viewed with some degree of caution. This is particularly relevant for rocks with a potentially large NRM and relatively low anisotropy, e.g. basalts and dolerites. Following the work of Rees (1968), who noted that particles should rotate under inertial depositional conditions to ensure resultant forces of collision act parallel to the principal axes, Knight and Walker (1988) showed K1 axes in the same sense as magma movement with additional evidence of magnetic imbrication in prolate ellipsoid magnetite grains at both dyke margins, the imbrication angle being between 10 and 30°. Ernst and Baragar (1992) noted lateral emplacement of magma in the Mackenzie dyke swarm, Canada from AMS studies and used such data to infer the position of the parent magma source.

3.4.3.2 AMS results for the Lundy Dyke Swarm

Macroscopic surface lineations are a relatively common features of intrusive rocks (Rickwood, 1990; Parker *et al.*, 1990), which indicate the sense of movement rather than absolute flow directions, but not all dykes on Lundy show lineations (loc. cit. 3.2.2). The exposed disposition of dykes in coastal outcrops also makes it difficult to reveal such lineations. Surface lineations are artefacts of an initial magma pulse and so if the dyke is zoned or multi-phased, movement of the main magma body may differ from those features at the margins. In any case, it is often difficult to differentiate between surface lineations and slickenside-type grooves and scours, even in historic dykes. AMS techniques are thus more useful than field observations to investigate flow directions in dykes, particularly the Lundy Dyke Swarm. A comparison of flow directions in different trending dykes also allows comparison between flow directions in the hypothetical radial distribution and that of the postulated linear regional dyke patterns on Lundy. Data for AMS experiments are presented in Appendices A2.1 and A2.2.

A total of 38 dykes on Lundy Island, 3 dykes at Lee Bay and the Fremington dyke were examined for anisotropy of magnetic susceptibility (AMS) using the methodology outlined in section 2.2.1. AMS samples 7, 31, 40 and 42 (cf. Figure 2.3) from Lundy Island were excessively weathered and were hence neglected for examination. However, reliable AMS measurements were obtained from 34 Lundy dykes and two dykes (AMS samples 18 and 16) showed measurable surface lineations to give some control on absolute magma movements. Agreement between field observations and theoretically calculated AMS directions was good (within $\pm 9^{o)}$ and so some confidence can be placed on the results, although more corroborative evidence is required to significantly improve the confidence limits. Conversely, samples 34, 35 and 36 from Lee Bay produced random orientations of AMS axes, despite good field evidence of lateral emplacement. Similalry, the Fremington dyke did not reveal an ordered arrangement of AMS axes. Both data sets were therefore not used to add information to magma flow directions.

Flinn (1978) introduced a graphical representation of a three dimensional strain ellipsoid and this has been adapted by palaeomagnetists to give an appreciation of the amount of lineation and foliation in a set of data by plotting the ratio of K_1/K_2 against the ratio of K_2/K_3 (Tarling and Hrouda, 1993). Lineation (characterized by prolate ellipsoids) is defined when $K_1/K_2 > K_2/K_3$ and foliation (typically oblate ellipsoids) is described by $K_2/K_3 > K_1/K_2$, whereas neutral ellipsoids are indicated when $K_1/K_2 = K_2/K_3$. A "Flinn" type plot is given in Figure 3.20 for Lundy data, but such ratios do not reflect either the lognormal distribution of susceptibility or the magnitude of anisotropy. Although commonly used to define ellipsoid shapes, this type of plot could distort the true proportions of ellipsoid shapes (Hrouda, 1982).

Jelinek (1981) introduced the shape parameter (T) and corrected anisotropy degree (P_J) to incorporate not only logarithmic properties of susceptibility, but also to include values for all three principal axes rather than simple ratios alone. This approach was considered by Hrouda (1982) to be mathematically more meaningful and was recommended by Tarling and Hrouda (1993) as the preferred method of graphical representation for the form of magnetic ellipsoids.

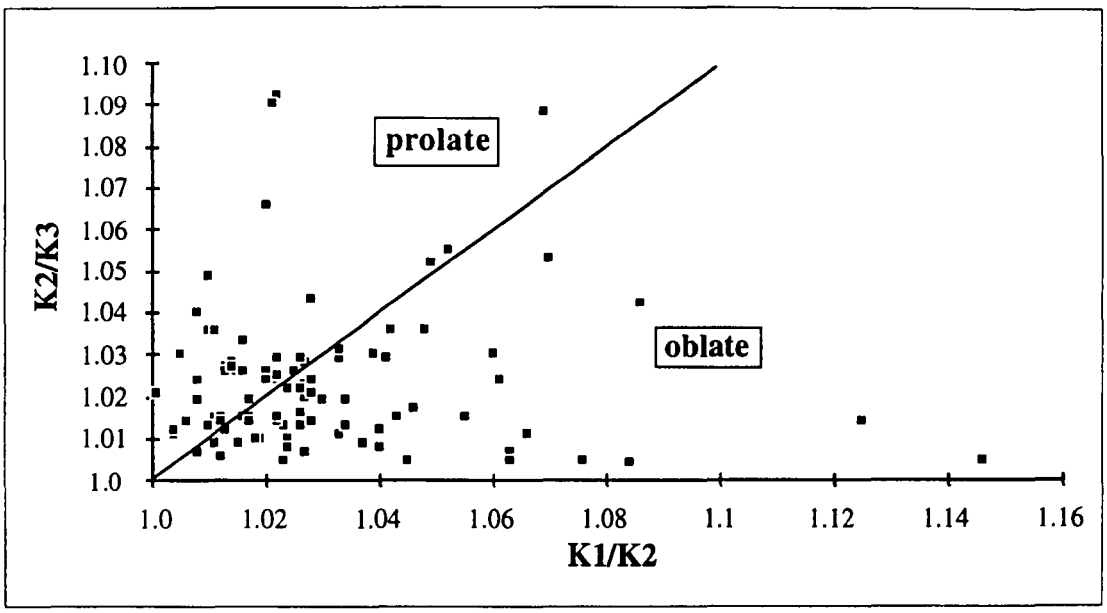

Figure 3.20: AMS plot for Lundy Dyke Swarm.
Shapes derived from magnetic properties can be equated with actual grain shapes. Here 56% of the plots are within the oblate field, 30% within the prolate field and 14% have a neutral (i.e. spherical) form. Samples 7, 31, 40 and 42 have been omitted due to excess weathering. (N = 124 from 34 dykes).

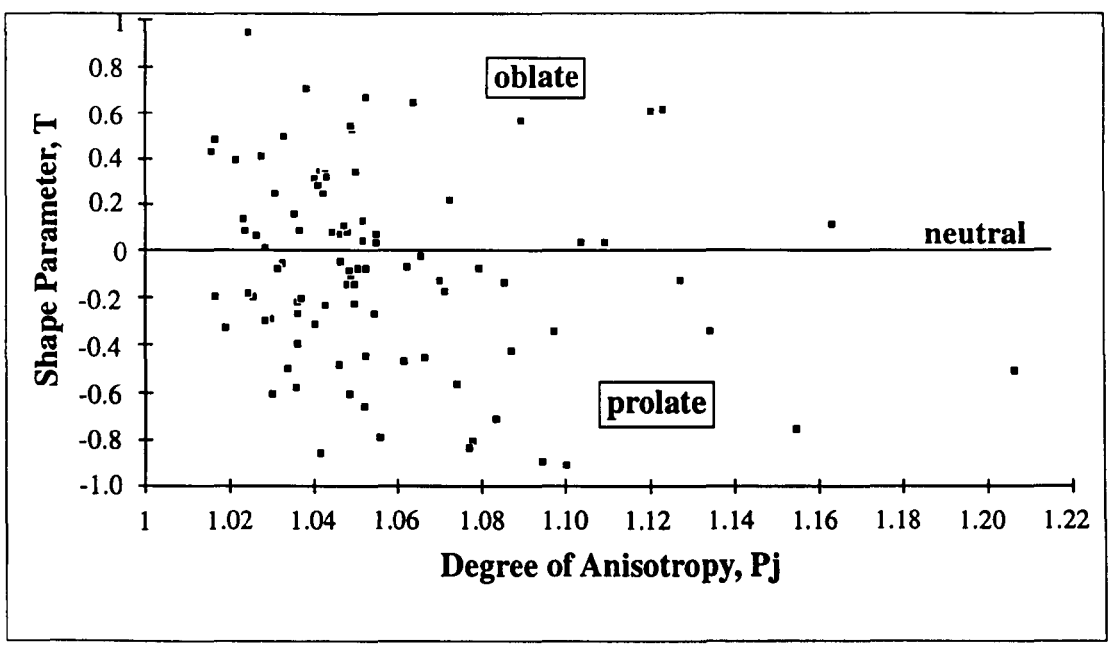

Figure 3.21: Alternative AMS plot for the Lundy Dyke Swarm.
Data from Figure 3.20 has been recalculated and plotted using the methodology of Jelinek (1981). See text for discussion of interpretations. (N = 124 from 34 dykes).

Oblate ellipsoids are indicated when $0 < T \leq +1$ and prolate ellipsoids have $-1 \leq T < 0$, whilst neutral ellipsoids correspond to $T \approx 0$. Figure 3.21 shows data from Figure 3.20 recalculated using both T and P_J. When plotted by this method, the data show 57% of samples to be characterized by prolate ellipsoids, 37% by oblate ellipsoids and 6% to be represented by neutral ellipsoids. Prolate ellipsoids are thus dominant, reflecting the importance of a net lineation of the long axes of the grains in these dyke samples.

Directions for susceptibility magnitudes are conventionally plotted on equal-area stereographic projections to illustrate different types of AMS axial distributions. Ellwood *et al.* (1988) recommend that magnetic anisotropy data are represented by lower hemisphere plots with filled symbols; maximum susceptibility axes (K1) denoted by squares, intermediate susceptibility axes (K2) by triangles and minimum susceptibility axes by (K3) by circles. This convention is adopted here.

As the susceptibility ellipsoid is a graphical representation of the summation of individual magnetic grains, it follows that when the associated magnetic components change magnitude or orientation, then the AMS ellipsoid will also change in character. This allows an interpretation of the changing nature of the magnetic fabric of rocks. Equal-area projections for the Lundy Dyke Swarm (Figure 3.22) show four main groups (Table 3.4).

Table 3.4: Categories of AMS classifications in the Lundy Dyke Swarm (N = 34).

Dyke Category	No. of Examples	% of Sample Population
1	9	26
1a	4	12
2	5	15
2a	2	5
3	6	18
4	8	24

Category 1 dykes display good clustering of both maximum (K1) and intermediate (K2) susceptibility axes sub-parallel to the plane of the dyke with minimum susceptibility axes (K3) perpendicular to the dyke plane. Category 1a dykes display similar K1 and K2 clusters, but also have a bimodal distribution of their K3 axes.

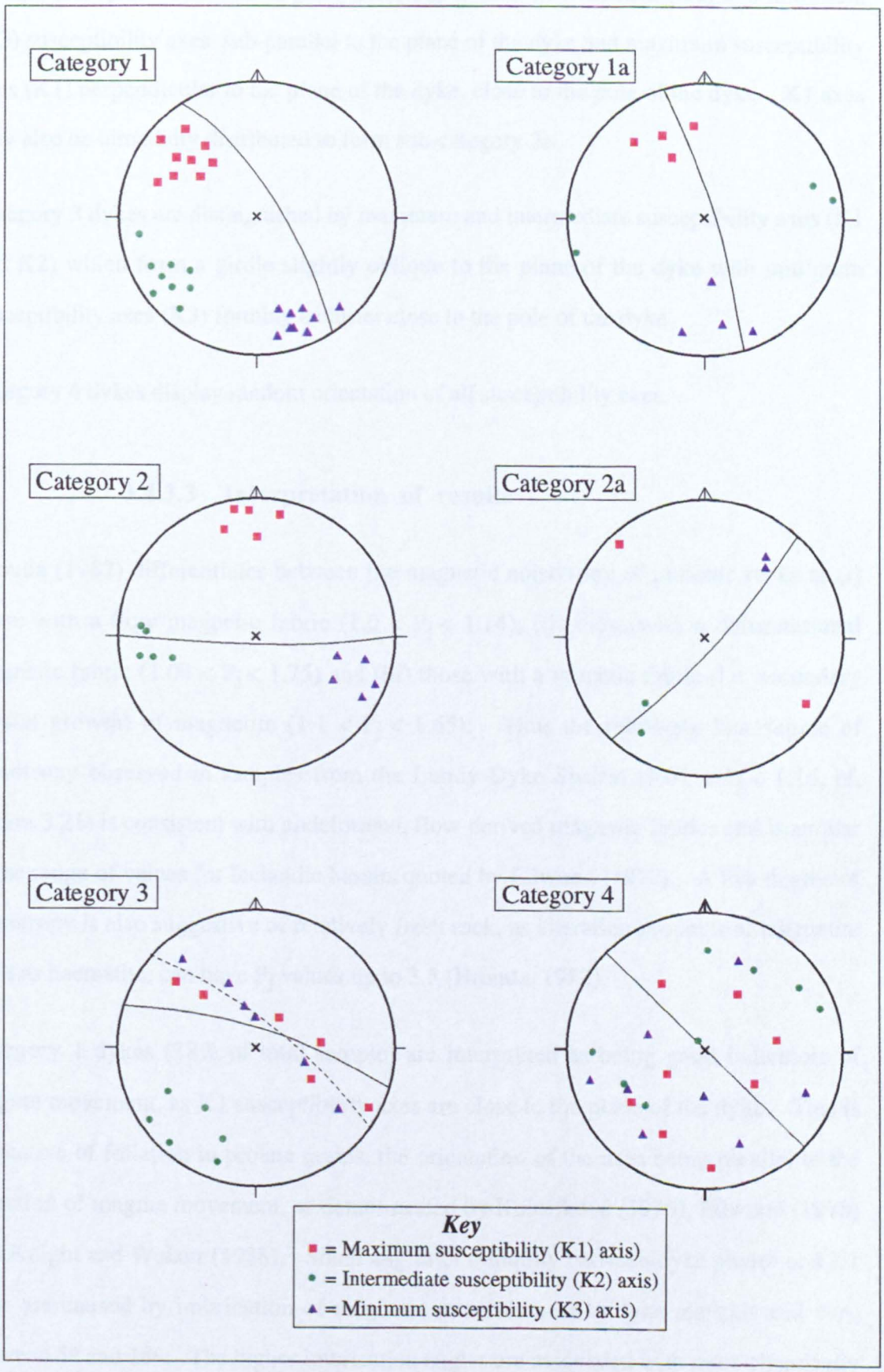

Figure 3.22: Anisotropy of Magnetic Susceptibility (AMS) results for the Lundy Dyke Swarm. Data are plotted on equal-area stereographic projections. See text for interpretations.

Category 2 dykes demonstrate good grouping of their intermediate (K2) and minimum (K3) susceptibility axes sub-parallel to the plane of the dyke and maximum susceptibility axes (K1) perpendicular to the plane of the dyke, close to the pole of the dyke. K1 axes may also be bimodally distributed to form sub-category 2a.

Category 3 dykes are distinguished by maximum and intermediate susceptibility axes (K1 and K2) which form a girdle slightly oblique to the plane of the dyke with minimum susceptibility axes (K3) forming a cluster close to the pole of the dyke.

Category 4 dykes display random orientation of all susceptibility axes.

3.4.3.3 Interpretation of results

Hrouda (1982) differentiates between the magnetic anisotropy of plutonic rocks as (i) those with a flow magnetic fabric ($1.0 < P_j < 1.14$), (ii) those with a deformational magnetic fabric ($1.09 < P_j < 1.75$) and (iii) those with a mimetic fabric (i.e. secondary crystal growth) of magnetite ($1.1 < P_j < 1.65$). Thus the relatively low degree of anisotropy observed in samples from the Lundy Dyke Swarm ($1.01 < P_j < 1.16$, cf. Figure 3.21) is consistent with undeformed, flow-derived magnetic fabrics and is similar to the range of values for Icelandic basalts quoted by Ellwood (1977). A low degree of anisotropy is also suggestive of relatively fresh rock, as alteration products of magnetite such as haematite, can have P_j values up to 3.5 (Hrouda, 1982).

Category 1 dykes (38% of total sample) are interpreted as being good indicators of magma movement, as K1 susceptibility axes are close to the plane of the dyke. This is indicative of foliation in prolate grains, the orientation of the axes being parallel to the direction of magma movement, as demonstrated by Kolofíková (1976), Ellwood (1978) and Knight and Walker (1988). Small angles of obliquity between dyke planes and K1 axes are caused by imbrication of magnetic minerals near to dyke margins and vary between 5° and 18°. The higher imbrication angles are associated with more chemically intermediate dykes, which are relatively more viscous than basic dykes and thus develop greater effects from drag resistance in the outer chilling zones. The average amount of

dip for each K1 cluster varies between 12° and 35°, although two trachytes display dips of 83° and 87°. Category 1 dykes therefore mostly demonstrate emplacement of magma by relatively simple laminar flow at shallow to intermediate angles.

Category 2 dykes display a magnetic anisotropy with K1 susceptibility axes perpendicular to dyke planes. This magnetic fabric can be caused by the dominance of single-domain (SD) ferrimagnetic particles over multidomain (MD) particles in rocks (O'Reilly, 1984; Potter and Stephenson, 1988) or by an interaction between anisotropy of magnetic remanence (AMR) and AMS (Rochette *et al.*, 1991), although contributors to AMR are less than for AMS in basic rocks and so the observed transposition of principal susceptibility axes in Category 2 dykes is unlikely to be an artefact of magnetic interaction. Although SD grains are not indicated by magnetic granulometry (cf. section 3.3.2), a mineralogical explanation for an "inverse" fabric is possible. Some pseudo-single-domain (PSD) particles may mimic SD behaviour if there are a sufficiently low number of domains in the grains, resulting in an "inverse" magnetic fabric. It could also reflect viscosity and/or flow rate differences within the magma . This group of dykes (20% of the overall sample) is thus distinguished by K3 axes being parallel to magma flow. Imbrication angles are small and emplacement dip angles are between 20° and 38°.

Category 3 dykes demonstrate foliation planes oblique to the dyke trends by girdles of K1 and K2 axes. Imbrication angles are between 8° and 20°, but it is not possible to determine dip angles of magma flow from girdle distributions. However, because both foliation and dyke planes are similar, AMS data suggest lateral magma movement of unknown flow inclination.

Category 4 dykes represent turbulent magma flow or disruption of primary AMS structures by secondary processes, e.g. hydrothermal alteration or cooling stresses in dykes. The low degree of anisotropy values ($P_j \leq 1.02$) for these dykes suggests secondary alteration, although some phenocrystic dykes did not convincingly display a preferred orientation of tabular feldspar clasts in the field. Such features would normally be typical of laminar flow and so turbulence may be indicated.

In summary, AMS data suggest that the bulk of the Lundy Dyke Swarm is the product of lateral magma movement at shallow to intermediate angles. Dykes with a NW-SE trend tend to produce shallower emplacement angles, wheres radially disposed dykes have both shallow and intermediate angles. It thus follows that the regional NW-SE dyke swarm was emplaced predominantly by lateral magma movement (possibly from a source outside of the Lundy vicinity), wheres the localized radial component was derived from relatively shallow depths to the west of Lundy Island. Reverse extrapolation of the radial distribution pattern suggests a magmatic source between 3 and 5 km to the west of the island at shallow depth.

Although many of the dykes are vesiculated and would have been reasonably buoyant when molten, a magmatic origin beneath the present day island is not indicated by the AMS evidence. However, some trachytic dykes (e.g. QB1) have steep maximum susceptibility axes, suggesting vertical motion and this is supported by the presence of lineation features on dyke margins. This may demonstrate a separate magma chamber, i.e. magmatic evolution, beneath the island or it may be an effect of turbulence in a relatively more siliceous and hence more viscous melt.

CHAPTER 4

GEOCHEMISTRY OF ROCKS FROM NORTH DEVON AND LUNDY ISLAND

4.1 INTRODUCTION

Igneous rocks in North Devon intrude Upper Devonian sediments on Lundy Island, at Lee Bay, at Fremington and around the submarine Horse-Shoe Rocks 5 km north-west of Ilfracombe (cf. sections 1.4 and 3.2). Host sediments are the Morte Slates (Edmonds *et al.*, 1979), although Thorpe *et al.* (1990) identify sediments on Lundy as Pilton Shales and the Fremington dyke may be intruded into the Lower Carboniferous Crackington Formation. Sedimentary sequences consist mostly of argillaceous rocks with varying frequencies of inter-bedded arenaceous material, the Crackington Formation having an equal distribution of both types.

The texture and mineralogy of the sediments, especially on Lundy Island, indicate low-grade regional metamorphism up to greenschist facies conditions (Hawkes, 1985), typified in North Devon by a quartz-albite-muscovite-chlorite sub-facies in pelites and probably related to late Carboniferous tectonic activity. The influence of the Lower Palaeozoic basement rocks of Southern Britain on intrusive igneous rocks is poorly defined, although it is likely to be different from that of Western Scotland and Northern Ireland, and could influence the results of geochemical analysis.

The Lundy granite is the oldest of the igneous intrusions on the island and has yielded a Rb/Sr whole rock isochron age of 58.7 ± 1.6 Ma (Thorpe *et al.*, 1990). K/Ar isotopic age determinations of 54 ± 2 Ma (Dodson and Long, 1962) and 56 ± 2 Ma (Miller and Fitch, 1962) have also been obtained from biotite crystals in the granite. Rankin (1968) provided a uraninite crystallization age of 53.9 Ma. Whole rock K/Ar dates for the dykes on Lundy range from 44.6 to 56.1 Ma (Mussett *et al.*, 1976; Edmonds *et al.*, 1979), although an Ar/Ar age of 56.4 ± 0.3 Ma reported by Mussett *et al.* (1988) from a plagioclase phenocryst is argued to have better precision than previous analyses.

This indicates that dykes on Lundy Island may have been emplaced relatively soon after emplacement of the granite. If granite cooling was protracted, which is in part a function of the depth of intrusion, there may have been some geochemical contamination and/or elemental exchange between the molten basic magma and semi-solid granitic magma. Assimilation of parts of the thick sedimentary pile in the area could also affect geochemical analyses.

Thorpe and Tindle (1992) obtained a whole rock dataset of 28 samples from the Lundy Dyke Swarm, but only published 8 results to add to the 5 whole rock analyses published by Edmonds *et al.* (1979). The ages for intrusive rocks at Lee Bay, Fremington and the Horse-shoe rocks have not been determined isotopically. This Chapter introduces new geochemical data to supplement previous studies on Lundy Island and provides new geochemical data for dykes at Lee Bay, Fremington and the submarine Horse-shoe rocks to investigate their relationship to Lundy. New Ar-Ar dates are also provided to improve temporal relationships.

4.2 PETROGRAPHY

Compositions of plagioclase feldspars have been determined optically using lamellar twinning features in the Michel-Levy Test (Gribble and Hall, 1988). This method does not allow differentiation between feldspars of composition An_{0-20} and An_{20-40}, but resolution was obtained by using the Becke Test, where An_{0-20} has a lower refractive index than Canada Balsam. Olivine compositions have been determined by optic axis figures in fresh grains.

Although both trachytes and rhyolites have been detailed on Lundy Island by Thorpe and Tindle (1992), only basic dykes have been included here. Both trachytic and rhyolitic intrusions constitute a minor part of the Lundy Dyke Swarm (< 10% by volume). Also, they cannot be geophysically differentiated from their granite host by reason of very similar magnetic and density properties between intrusion and host. As a result, only basic dykes

4.2.1 DOLERITE DYKES OF LUNDY ISLAND

The field relations and petrography of the dykes have been described by Dollar (1968), Edmonds *et al.* (1979) and Thorpe and Tindle (1992). They are mainly composed of dark grey to olive-grey/black olivine dolerites, which include both porphyritic and aphyric types. Porphyritic dykes contain phenocrysts of olivine (up to 2 mm diameter) and plagioclase (1 to 10 mm in length) or plagioclase alone set in a groundmass of varying grain size and composition containing olivine, plagioclase, pyroxene, opaque iron oxides and secondary chlorite. Plagioclase phenocrysts are normally labradorite (An_{50-70}), but groundmass crystals also contain varieties of andesine (An_{30-50}) and bytownite (An_{70-90}). Pyroxene is mostly titaniferous augite. Some olivine dolerites may be termed crinanites, as they contain analcime ($NaAlSi_2O_6.H_2O$) both in amygdales and the groundmass. Olivine-free dolerites, quartz dolerites and trachytic dykes are also present. The latter range from quartz-trachyandesites and quartz-trachytes to felsitic trachytes (Edmonds et.al., 1979).

Petrographic analyses here indicate both porphyritic and aphyric dolerites, as well as aphanitic basalts with occasional rare plagioclase phenocrysts, and trachytes. Porphyritic dolerites are almost entirely phanerocrystalline, containing unzoned as well as continuously and discontinuously zoned plagioclase phenocrysts (up to 7 mm long), which take on euhedral, subhedral and columnar habits. Some phenocrysts contain minor lineated and irregular fluid inclusions, whilst others include pyroxene chadacrysts or have been inconsistantly altered to chlorite or other clay minerals. Most phenocrysts are andesines in the range An_{38-46}, but some sections also contain labradorite phenocrysts (An_{50-60}). Such combinations imply an evolutionary history. Groundmass minerals include plagioclase (oligoclase to labradorite), olivine, clinopyroxene and equant/irregular opaque Fe-Ti oxides, all of which form intergranular and subophitic textures for the most part (Photo 4.1), although intersertal texture is also seen.

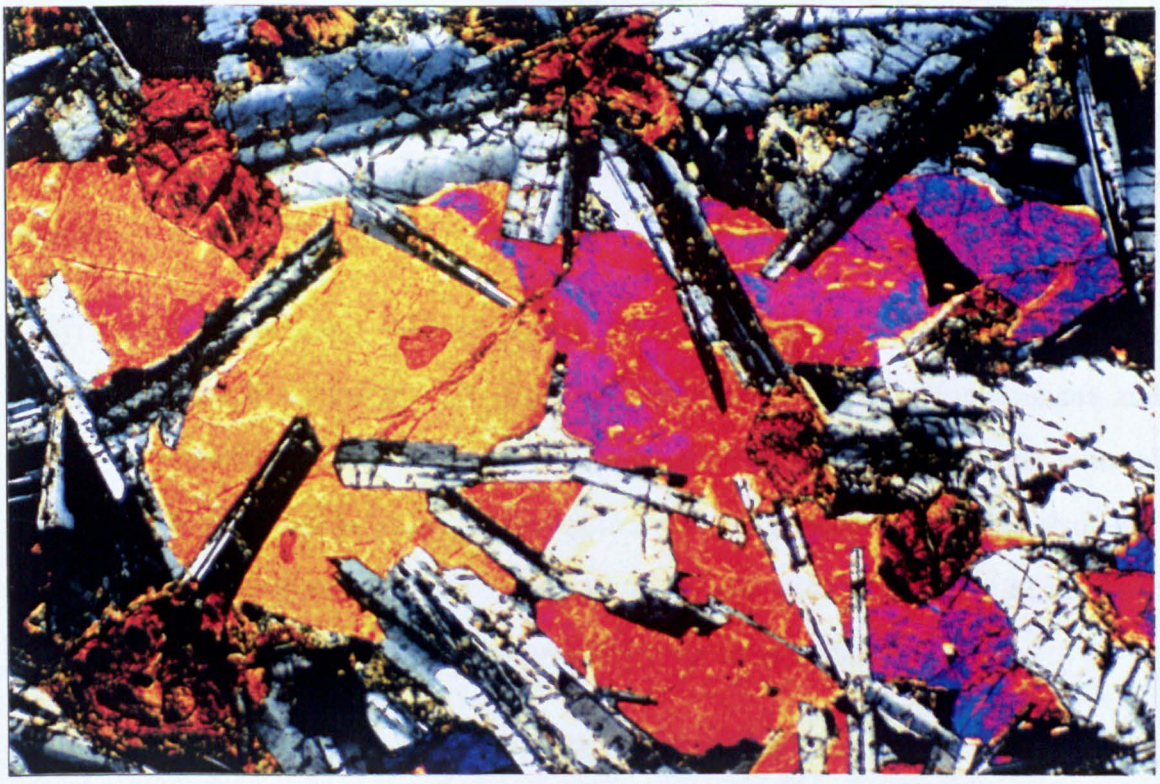

Photo 4.1: Coarse grained dolerite from Lundy Island (BW2) with subophitic texture.
Subhedral clinopyroxene is either yellow/brown and has augite composition or blue/purple, indicating more titaniferous augite. Plagioclase is in the andesine-labradorite range. XPL, FOV 3.5 mm.

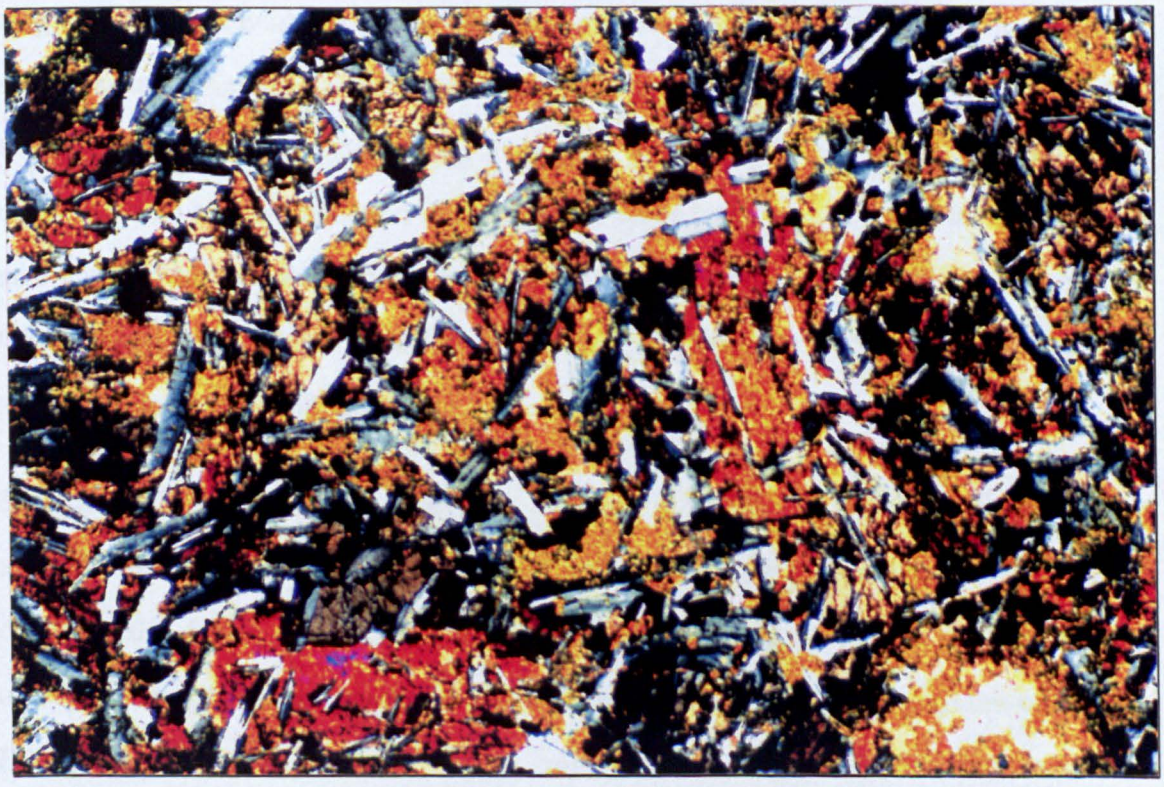

Photo 4.2: Fine grained dolerite from Lundy Island (QB1).
The dyke displays both subophitic and partial intergranular textures. Plagioclase laths have random orientation and andesine composition, whilst subhedral augite displays yellow/brown interference colours. The euhedral and subhedral anisotropic grains are probably magnetite. XPL, FOV 3.5 mm.

Seriate and subhedral granular textures are rare and contrast well to other types. Olivine in the groundmass (0.5 - 2 mm) is occasionally fresh, but otherwise partially or completely altered along cracks and around reaction coronae to serpentine, iddingsite and Mg/Al-rich chlorite.

Aphyric dolerites are mostly microcrystalline (Photo 4.2) containing prismatic or lath-like plagioclase crystals (andesine - An $_{34-48}$), olivine pseudomorphs, clinopyroxene and opaque Fe-Ti oxides with intergranular or subophitic textures and rare simple twinned labradorite phenocrysts (An $_{54-66}$). Euhedral to subhedral granular textures are also seen. Analcime, acicular apatite and rare biotite are accessory minerals. Many of the finer groundmass minerals have been badly corroded and appear as rutile or haematite.

4.2.2 THE LEE BAY MINI-DYKE ASSOCIATION

Although there are five discrete exposures of basic rocks at Lee Bay, these may only represent two or three dykes due to repetition caused by NW-SE strike slip faulting. Both display good field evidence of zonation and multiple injection, in contrast to the postulated single-event dykes on Lundy Island described by Thorpe and Tindle (1992). Sample CK21 displays at least nine discrete magma pulses within the intrusion, each pulse demonstrating a small reduction in grain size towards its margin, whereas the overall grain size varies from an aphanitic chilled margin to a fine phanerocrystalline centre. Sample CK30 shows less obvious evidence of multiple injection, but clear evidence of mineral alignment and pulsing of magma.

Sample CK21 is weakly porphyritic and has a highly vesiculated centre, mostly amygdaloidal, irregular in shape and filled with calcite and/or chlorite. Calcite normally occupies the centre of the vesicles, which are lined with a layer of fibrous chlorite, otherwise amygdales are completely filled with fibrous fans or orbicular crystals of chlorite. Filled and unfilled vesicles are present throughout the whole rock, but tend to have an increased distribution towards the margin of individual phases, indicating high level pressure release of gaseous fractions during emplacement of magma. Phenocrysts are euhedral plagioclases of either labradorite (An $_{56-60}$) or andesine (An $_{42-46}$) composition and up to 5 mm in length (Photo 4.3).

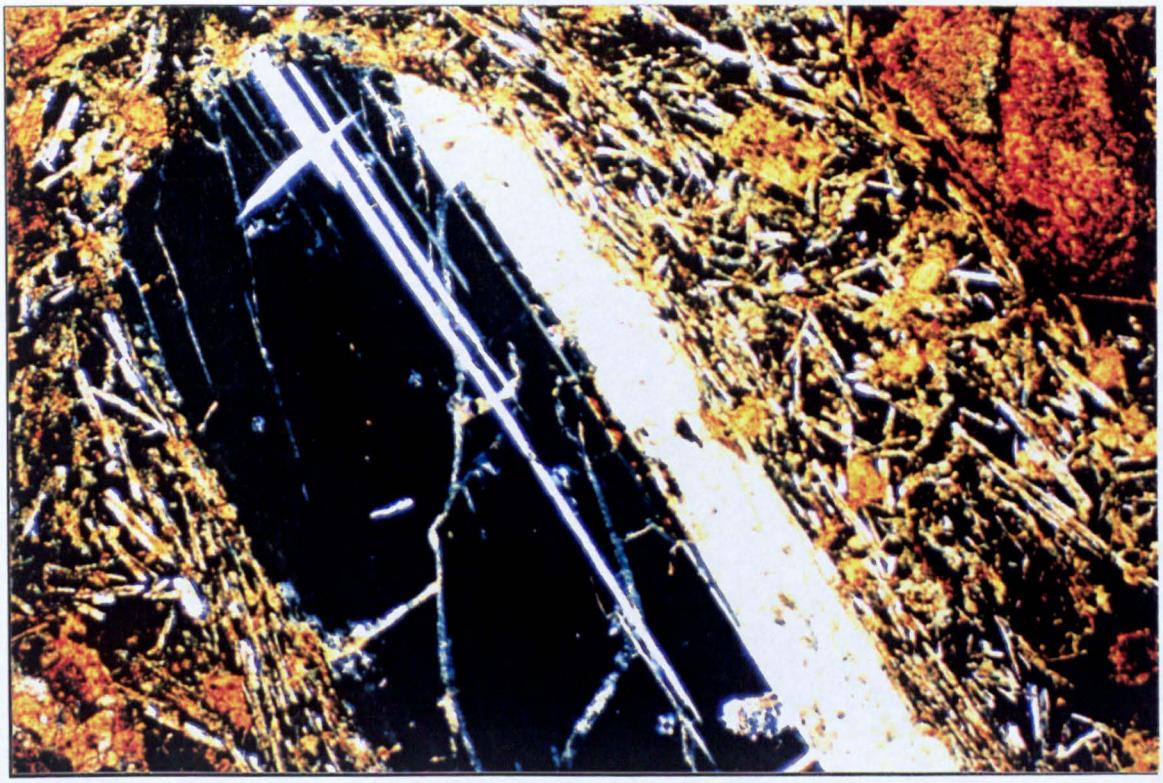

Photo 4.3: Rounded plagioclase phenocryst from CK30, Lee Bay.
The phenocryst has andesine composition (An $_{40-50}$) and is set in a fine-grained doleritic texture. Note parallelism of plagioclase laths around the larger phenocryst. The small light brown patches are corroded pyroxenes and the larger dark brown areas are filled amygdales. FOV = 3.5 mm (XPL).

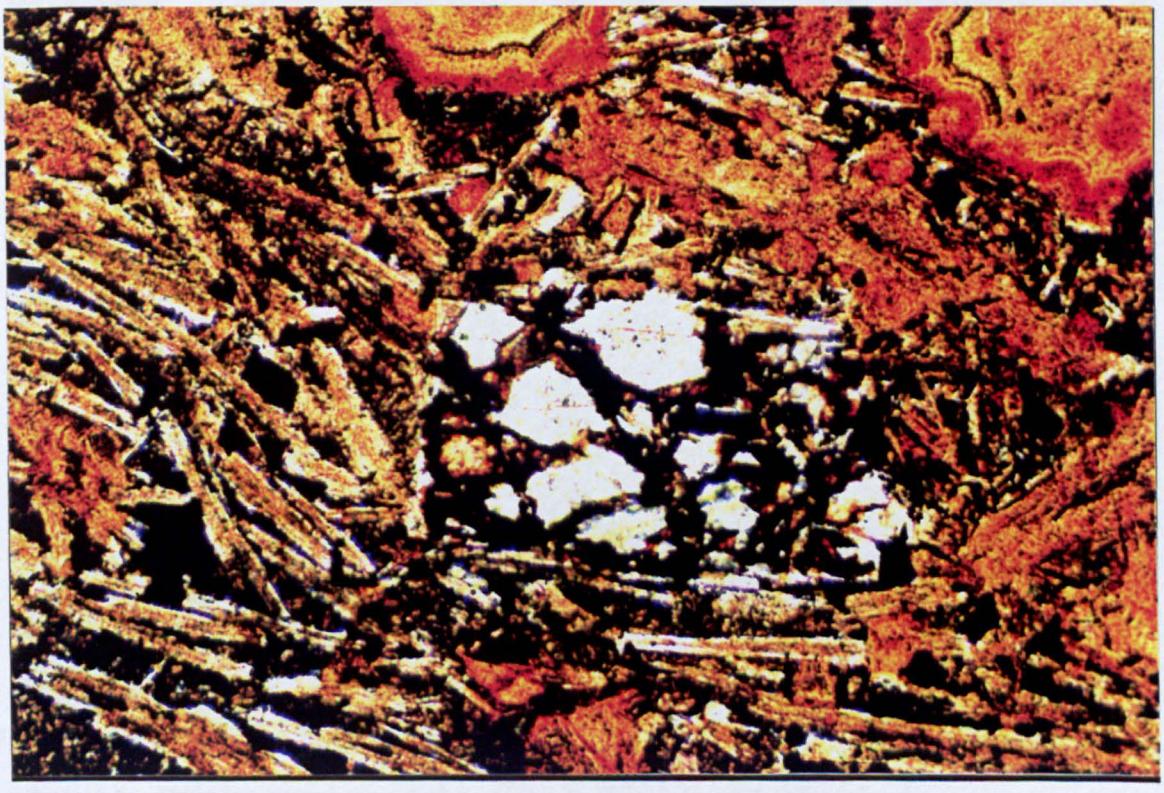

Photo 4.4: Relatively fresh Mg-rich olivine phenocryst in CK30, Lee Bay.
The phenocryst has composition Fo $_{80-85}$ (based on a 2V angle approaching 90^{o}) and was taken from the centre of CK30-C (Lee Bay). The zoned amygdales and sub-parallel plagioclase laths are the result of one phase within a multi-phase intrusion history for the dyke. FOV = 1.6 mm (PPL).

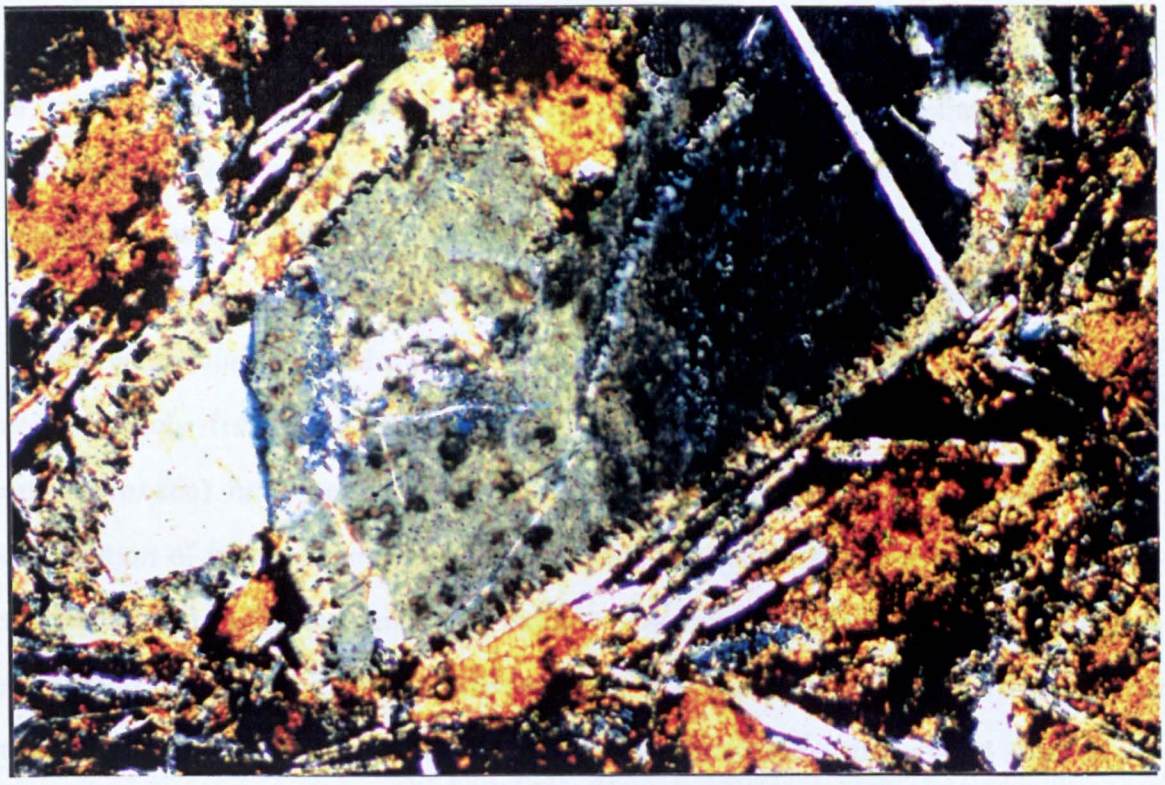

Photo 4.5: Rounded and embayed plagioclase phenocryst from CK30, Lee Bay.
In this case the phenocryst displays zonation and has an outer rim of pyroxene inclusions. The white streak in the top right hand corner is a false artefact. FOV = 1 mm (XPL).

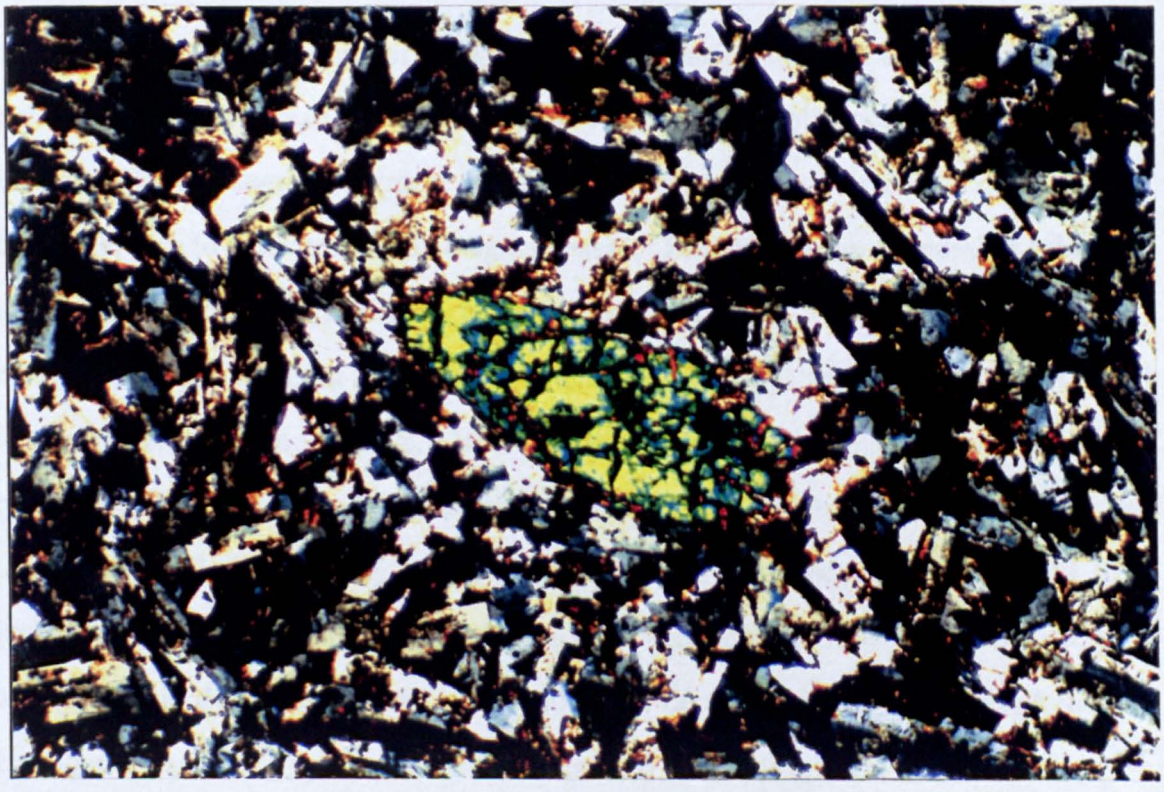

Photo 4.6: Rounded clinopyroxene phenocryst in CK30, Lee Bay.
Plagioclases are equant and tabular with a composition of andesine to labradorite and set in a matrix of plagioclase and pyroxene. Groundmass pyroxene has degraded to phyllosilicate minerals and iron oxide completes the assemblage. FOV = 3.5 mm (XPL).

Some are veined and patchily chloritized, whilst others contain minor inclusions consisting of trains of fluid inclusions or pyroxene. All exhibit polysynthetic lamellar twinning, but continuous zoning is rare. The groundmass is composed of euhedral and subhedral plagioclase laths (andesine to labradorite composition), clinopyroxene, olivine and Fe-Ti oxides. Olivine is partially or wholly pseudomorphed by chlorite, although relatively fresh crystals with iddingsite-filled cracks are seen (Photo 4.4). Some subhedral clinopyroxenes are relatively fresh, but other euhedral crystals (possibly early formed Mg-rich orthopyroxene) have been completely pseudomorphed by chlorite, accompanying degradation of high temperature olivine. Clinopyroxene contains secondary acicular, reticulated and dendritic opaque iron oxides. Overall, sample CK21 has an ophitic or subophitic texture, although intergranular features are apparent in places. Sub-parallel alignment of plagioclase laths occurs at some phase boundaries and around some of the larger plagioclase phenocrysts. An apparent variolitic texture shown by some plagioclase laths may not be a primary feature, but possibly represent a partial stellate arrangement caused by magma fluid dynamics.

Sample CK30 is also a porphyritic dolerite with aphanitic margins that demonstrates an ophitic or subophitic texture. Alignment of vesicles and/or plagioclase phenocryst laths indicate relative magma movement parallel to dyke margins, but there is no obvious grain size difference to indicate discrete magma phases. Phenocrysts are euhedral or subhedral unzoned and zoned plagioclases of oligoclase (An_{24-30}) to labradorite (An_{50-54}) composition up to 3 mm in length, some with alteration haloes and embayments. A zoned feldspar phenocryst in sample CK30 (Photo 4.5) indicates disequilibrium and at least a two-stage cooling history. The outer zone is untwinned and has a base of altered pyroxene inclusions. The main body of the phenocryst also has random pyroxene and fluid inclusions and although slightly corroded, an optic axes analysis indicates a composition of augite. This dyke thus started to crystallize at depth, possibly in a ponded magma chamber, before rising upwards to solidify nearer to ground level.

Groundmass minerals in CK30 are dominated by andesine plagioclases (An_{40-50}) with rarer labradorite laths (An_{50-70}). Chlorite and other phyllosilicates are found in the

corroded cores of most plagioclases. Pale yellow-brown anhedral to subhedral clinopyroxene crystals in the groundmass are probably made up by augite, possibly titaniferous in places. Euhedral prismatic crystals, completely pseudomorphed by Mg/Al-rich chlorite (blue interference colours to indicate relatively low Fe content), may represent an earlier pyroxene phase, similar to examples in sample CK21. Up to 8% of Fe-Ti oxides by volume complete the assemblage.

4.2.3 THE HORSE-SHOE ROCKS

Donovan *et al.* (1971) obtained dredged dolerite samples from the Horse-shoe Rocks and suggested that their sheared and slightly metamorphosed nature (comparable to a spilite) indicated an Upper Palaeozoic age, but they could not establish whether the sample represented an *in situ* outcrop or a superficial deposit. By contrast, Brooks and Thompson (1973) infered a Tertiary age, based on a low amplitude reversely magnetized signature of -50 nT with bilateral peaks of 15 nT over a wavelength of 0.5 km. They also suggested that reference to the spilitic nature of the rocks was unjustified.

All samples obtained from the Horse-Shoe rocks described in this study (HSR 1, 2, 3, 4, 12, 34, 13A, 23A, 3A and 4A) have a coarse grained phanerocrystalline and aphyric character, which suggests reasonable homogeneity throughout a slowly cooled igneous body. The main fresh primary minerals are clinopyroxene (Photo 4.7) and mainly simple twinned plagioclase of albite (An_{8-10}) to andesine (An_{30-40}) composition, although many of the feldspars show degradation to phyllosilicate minerals (Photo 4.8). Rounded chlorite pseudomorphs after olivine and subhedral/euhedral prismatic pseudomorphs (probably after pyroxene), displaying anomalous Berlin blue interference colours, are common and give the rock an overall green colour. Calcite is a rare accessory and probably represents amygdales. The grain/grain boundaries between some chlorite pseudomrphs and fresh clinopyroxene crystals are sharp and suggest selective hydrothermal alteration rather than simple sub-solidus weathering. The presence of rare subhedral pumpellyite grains and acicular prehnite crystals in sheaf-like orientations closely associated with the chlorite supports low temperature metamorphism up to 250 - 300°C (cf. section 4.2.2.2). Although both intergranular and subophitic textures are common within the sections,

poikilitic networks are also present. In places, albite is seen to have an ophitic relationship with clinopyroxene. This indicates that albite crystallized first and is a primary mineral, not a secondary product as would be expected in a true spilite (Mason, 1986). Thus, the Horse-Shoe Rocks may not have reached greenschist metamorphic grade (up to 400°C), as secondary albite, epidote and actinolite are not observed in thin section.

4.2.4 THE FREMINGTON DYKE

The Fremington dyke is a fine grained porphyritic dolerite with microphenocrysts, containing a considerable number of xenolithic inclusions from < 1 mm to > 20 mm. The matrix has an intergranular texture with Na-rich plagioclase in the albite to andesine range (Photo 4.9), although much of this is heavily chloritized or broken down to other phyllosilicates. Equant Fe-Ti oxides are evenly dispersed and make up around 5 - 10% of the matrix, but the previous presence of olivine and/or pyroxene is difficult to analyse as these minerals have been almost completely pseudomorphed by chlorite, phyllosilicate minerals and haematite.

Microphenocryst minerals up to 1mm are subhedral plagioclase prisms (An_{15-34}) and almost euhedral pyroxenes, pseudomorphed by secondary minerals. Differentiation between clinopyroxene and orthopyroxene is difficult where much of the original characteristics are altered. Chlorite crystals with or without calcite are present as amygdales in local abundance, but these are unevenly dispersed throughout the rock. Biotite is a rare accessory mineral in both subhedral tabular and acicular form, although some grain/grain boundaries suggest a secondary mode of origin rather than primary.

Pleochroic haloes occur in some of the tabular crystals, but identification of the included mineral is uncertain. Xenoliths form a large range of sizes in terms of clast and constituent grain dimensions and form a sub-seriate texture. Clast sizes range from 0.1 to 2.5 mm with compositions that are either wholly quartz, quartz and 10% albite/oligoclase or 70 - 80% albite to andesine and quartz, with calcite as a minor constituent. Quartz is often present as sub-rounded crystals, but in other cases forms a close interlocking network. There is also evidence of recrystallization within some larger grains, but the precise history of the xenoliths is hard to decipher.

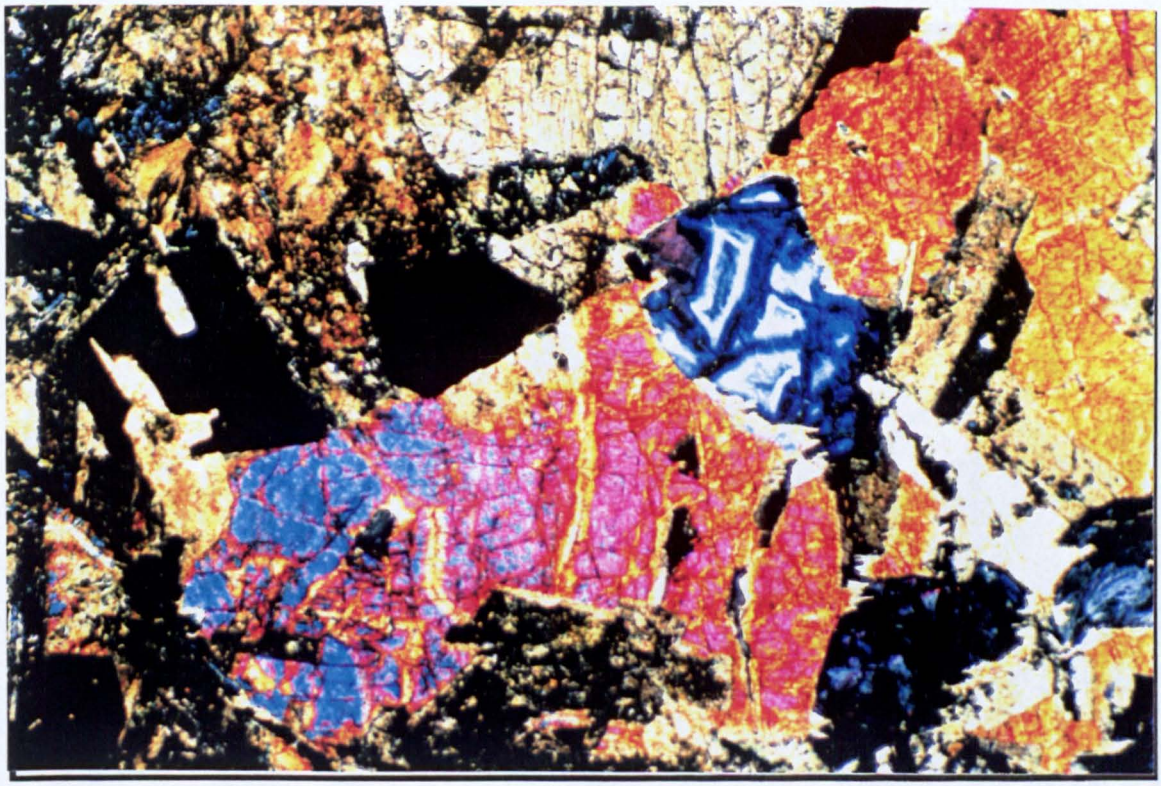

Photo 4.7: Fresh clinopyroxene in the Horse-Shoe Rocks.
Olivine is pseudomorphed by chlorite (bright blue colour) and plagioclases are badly corroded, although simple twinning is still discernible. FOV = 3.5 mm (XPL).

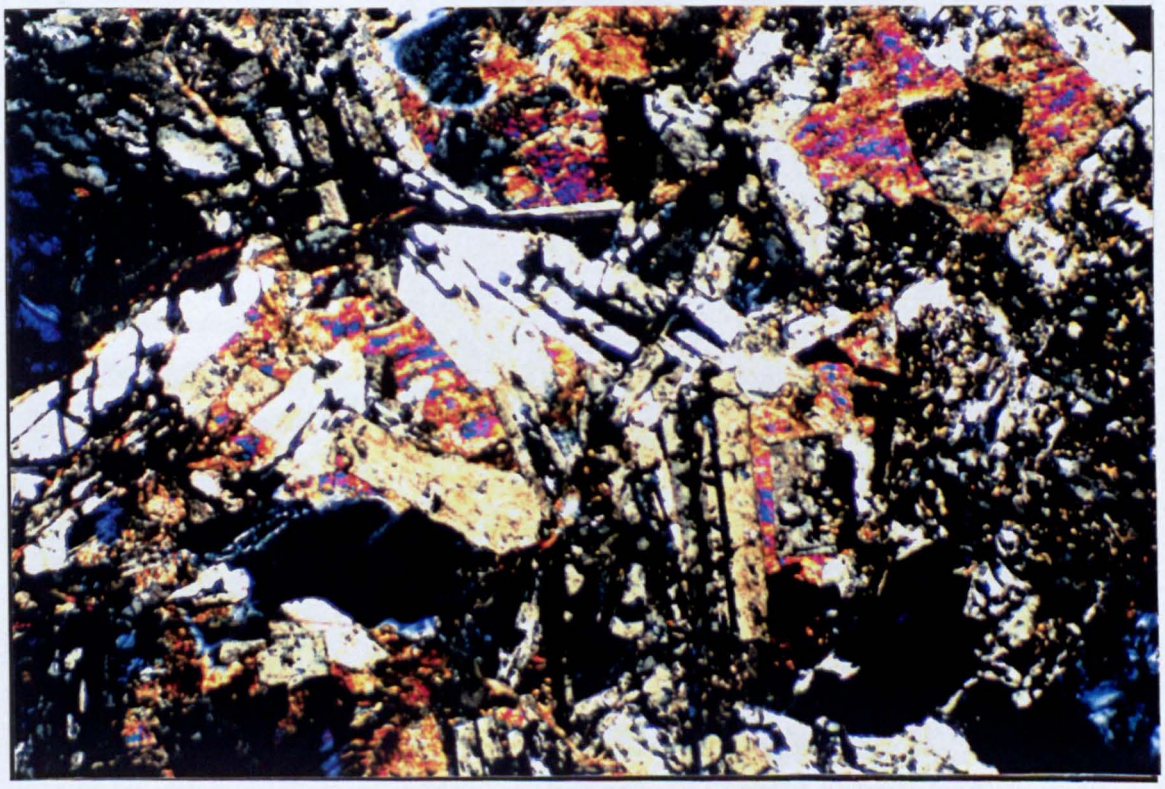

Photo 4.8: Feldspar crystals in the Horse-Shoe Rocks.
There is no preferred orientation in these relatively fresh tabular plagioclase crystals, which are mostly oligoclase in composition (An_{20-30}) FOV = 3.5 mm (XPL).

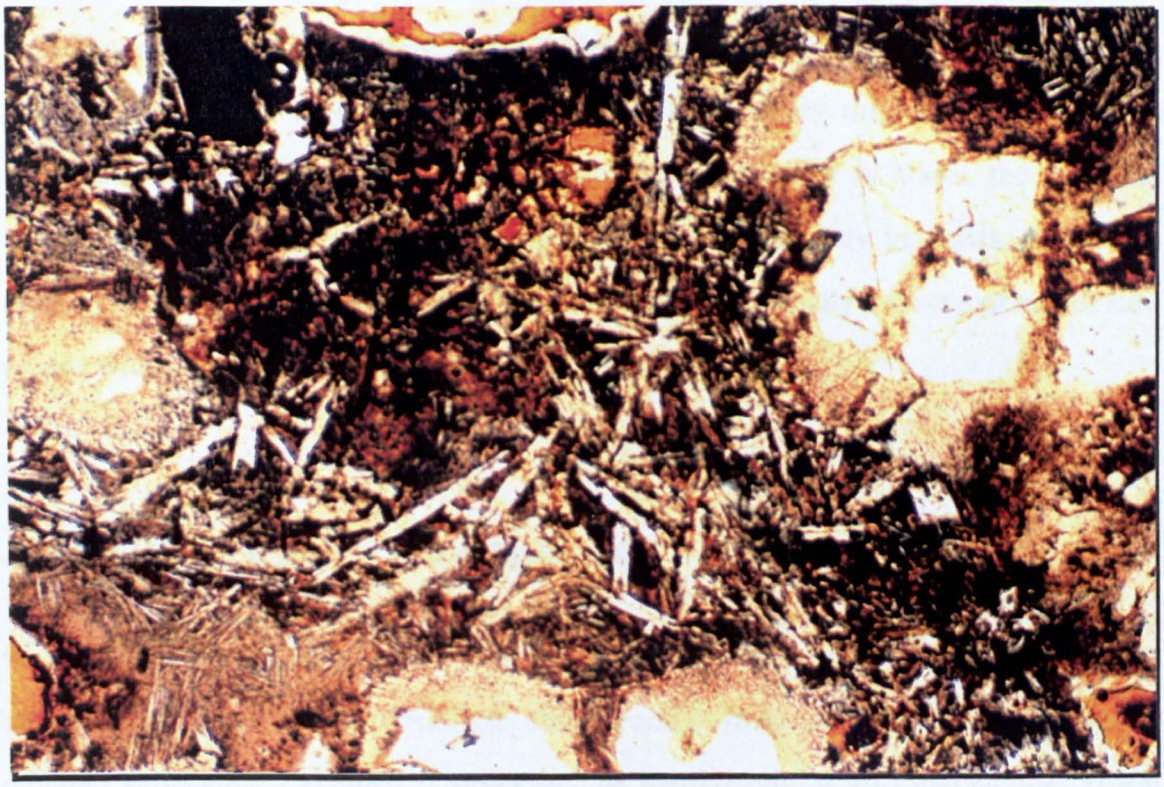

Photo 4.9: Groundmass minerals in sample Frem 2, Fremington.
Xenolithic patches of quartz and feldspars are interspersed with white lath-like oligoclase crystals with swallow tail and tuning fork morphologies, indicating rapid quenching. FOV = 1.8 mm (PPL).

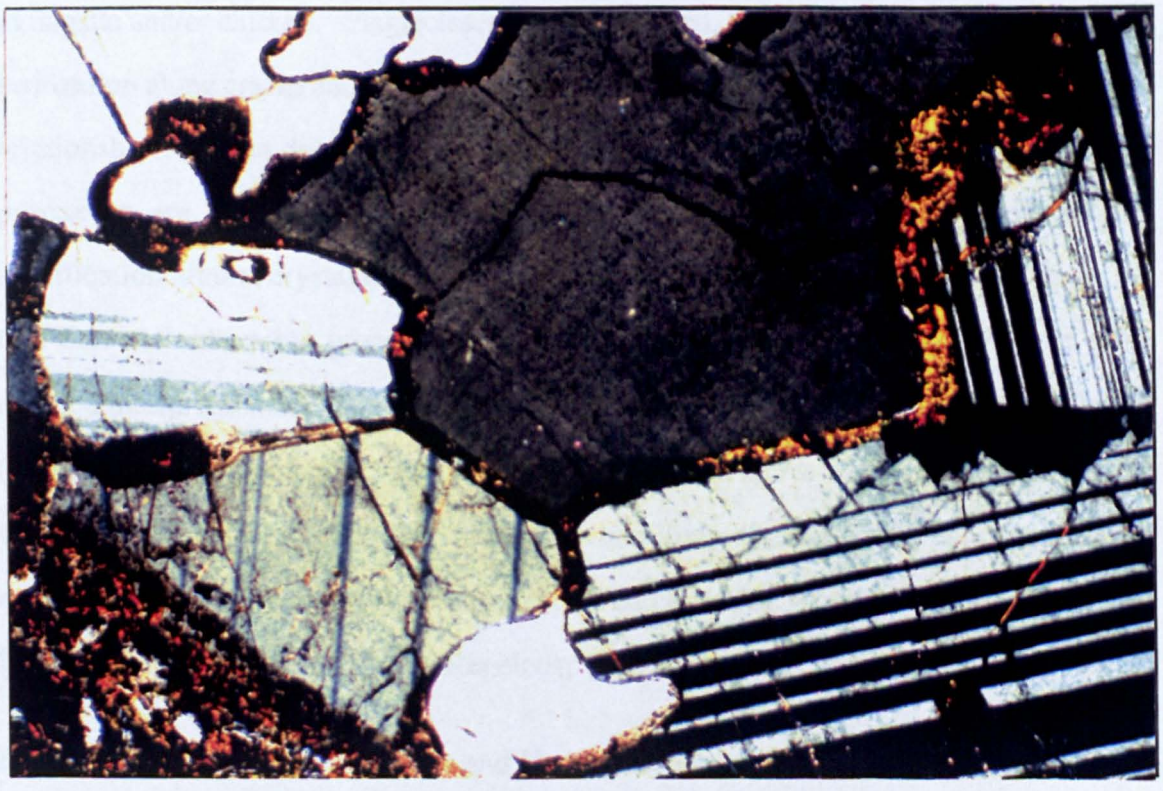

Photo 4.10: Buchite structure in xenolithic fragment in Frem 4, Fremington.
Grain/grain boundaries between quartz and albite-oligoclase crystals have been partially melted to give brown glass, which has destroyed the original crystal contact features and hence complicated the interpretation of a sedimentary or igneous origin. FOV = 3.5 mm (XPL).

Grain boundaries in some of the clasts are partially melted to give a buchite texture (Photo 4.10), which makes diagnosis of an igneous or sedimentary origin for the xenoliths complicated. However where plagioclase crystals dominate in clasts, the chemical composition has a very small range (e.g. An $_{8-10}$) and possibly indicates an igneous derivation. Other clasts are clearly sedimentary in origin, usually a quartz arenite or sub-arenite with minor amounts of argillaceous material.

4.3 THE ROLE OF WEATHERING

Most rock samples at outcrop have suffered varying degrees of weathering and subsolidus alteration, although it was possible to obtain enough fresh material from each site for detailed geochemical analysis. However, the petrography of all samples does reveal significant subsolidus alteration and Permo-Carboniferous rocks show more changes than Tertiary ones. In thin section, olivine has either been totally or partially replaced by iddingsite and/or chlorite. Plagioclases can be unaltered, but where altered take the form of seritization along cracks and throughout the cores of tabular grains. There appears to be no relationship between degree of alteration, the age or chemical composition. Although pyroxenes are freshest in the older dykes, younger Tertiary samples show limited modification around crystal edges and along some fractures. It is important to assess the role that such alteration processes have had on the geochemistry of rocks before more detailed interpretations are undertaken. Rocks from Phanerozoic continental flood basalt (CFB) provinces have been extensively studied for post-eruptive weathering and alteration, with the conclusion that these processes have had limited effect on the concentrations of most major and trace elements in the rocks (Pearce, 1976; Wood *et al.*, 1976; Cox and Hawkesworth, 1985; Peate, 1989; Regelous, 1993).

Rollinson (1993) indicated that Ca and Na are almost always mobilized in basalts under hydrothermal conditions, as opposed to the relative immobile behaviour of Ti, Al and P. Peate (1989) suggested that devitrification of glass, i.e. low-temperature hydration with ion-exchange and element mobility, could have a significant effect on dolerites that contain relatively large proportions of glass. This would modify the concentrations of the more

incompatible elements (K, Rb, and Ba), which are most probably concentrated in the late-stage glass phases. Sr concentrations would usually be concentrated in plagioclase crystals. Weathering and alteration would normally be accompanied by relatively high loss on ignition (LOI) values (Lechler and Desilets, 1987), which provide a crude measure of secondary processes. High LOI values (cf. Appendix A4) in DK2 and DK3 are not entirely caused by weathering, as these basalts also contain hydrous analcime in amygdales, which may not have been derived from the host rocks themselves.

In conclusion, although a comprehensive analysis of the geochemical consequences of subsolidus alteration has not been attempted in this study, the relative freshness and low glass concentration in thin section samples implies that weathering has had restricted effect in modifying major and trace element concentrations. It is thus justifiable to analyse the freshest material from the study area to derive geochemical information and to study possible fractionation processes.

4.4 AGES OF THE ROCKS

The dating of rocks in the British Tertiary Volcanic Province (BTVP) has been mostly completed by either the K-Ar or the Rb-Sr isochron methods, both having some analytical constarints (Mussett *et al.*, 1988). Variable argon loss can lead to spuriously high as well as low ages in K-Ar dating which, to a large extent, was improved by the use of the Rb-Sr isochron method (Brooks *et al.*, 1972). However, this latter technique is most effective on acid rocks and as the bulk of BTVP rocks are basic in composition, especially dykes, accurate ages are vulnerable to relatively large errors. Compston *et al.* (1984) introduced high precision isotope measurements on zircon fragments using an ion probe to determine rock ages, but the size of error bars on younger rocks (i.e. < 60 Ma) and the lack of acid material (in which zircon is normally found as an accessory mineral) in most of the dykes does not make this a suitable choice for Tertiary geochronology. Mussett *et al.* (1988) recommended the $^{40}Ar/^{39}Ar$ step-heating method as giving the best dating results, but also noted that only one in three samples produce acceptable plateaux and that analytical errors (1σ) range from $\pm$ 0.5-2 Ma.

They concluded that volcanic activity in the Lower Tertiary spanned the approximate interval 63-52 Ma (with a peak around 59 Ma) and that there is no discernible geographical pattern to igneous activity. To emphasize the possible errors in isotopic dating, they also noted that the rocks from various centres cannot be unambiguously assigned to the polarity time scales of either Harland *et al.* (1982) or Berggren *et al.* (1985), although there is more compatibility with the former.

4.4.1 THE Ar-Ar DATING METHOD

Conventional K-Ar dating techniques are based on the natural occurrence of the radioactive isotope of potassium (^{40}K), which decays to ^{40}Ca and ^{40}Ar with a half-life of 1250 Ma. The method involves firstly measuring the K concentration in a given sample by XRF procedures and then calculating the amount of ^{40}K from the natural $^{40}K/K$ ratio of 0.0001167 (as revised by Garner *et al.*, 1975), and then the Ar concentration by isotopic dilution using a ^{38}Ar spike. Following Ar purification, the concentration of radiogenic ^{40}Ar ($^{40}Ar^*$) is determined by a second run in a mass spectrometer. The concentrations of ^{40}K and $^{40}Ar^*$ combined with the known decay of ^{40}K to $^{40}Ar^*$ enables an age to be calculated with a precision of better than 1%, providing that the proportion of 40Ar* in the sample is > ~10% (Cox and Dalrymple, 1967; Dalrymple and Lanphere, 1971).

The ^{40}Ar-^{39}Ar dating method, first described by Merrihue and Turner (1966), was fully expounded in McDougall and Harrison (1988) and has been reviewed by Kelley (1995). In this method, the sample to be dated is first irradiated in a nuclear reactor to produce ^{39}Ar from ^{39}K through the reaction -

$$^{39}_{19}K(n,p) = {}^{39}_{18}Ar \qquad \text{equation 4.1}$$

Following fusion of the sample in a vacuum, argon is extracted and purified before being analysed isotopically in a mass spectrometer (cf. section 2.4.4). The $^{40}Ar^*/^{39}Ar_K$ ratio, where $^{39}Ar_K$ is the amount of ^{39}Ar produced from ^{39}K during irradiation, is then calculated from the measured $^{40}Ar/^{39}Ar$ ratio after correcting for Ar isotope concentrations attributable to various interferences in the irradiation process (McDougall and Harrison, 1988).

The age of the sample (t) is related to its $^{40}Ar^*/^{39}Ar$ ratio by the standard age equation -

$$t = \frac{1}{\lambda} \ln \left(1 + J \frac{^{40}Ar^*}{^{39}Ar}\right) \qquad \text{equation 4.2}$$

where λ is the decay constant for ^{40}K ($5.543 \pm 0.010 \times 10^{-10}a^{-1}$) and J is a dimensionless irradiation parameter, which has a value of 0.00575 ± 0.00002 for all data given here. Errors for age determinations (σ_t) were determined by Dalrymple *et al.* (1981) and given by the relationship -

$$\sigma_t^2 = \frac{J^2\sigma_R^2 + R^2\sigma_J^2}{\lambda^2(1 + RJ)^2} \qquad \text{equation 4.3}$$

where R is the $^{40}Ar^*/^{39}Ar$ ratio, σ_R is the error on R and σ_J is the error on the J value.

There are five basic assumptions that must be fulfilled before meaningful geological conclusions can be drawn from calculated ages (McDougall and Harrison, 1988):

1) The radioactive decay of ^{40}K is independent of pressure and temperature. This major assumption has been tested by Frielander *et al.* (1981), who confirmed its validity.

2) The $^{40}K/K$ ratio in nature is constant. Whilst this is broadly true, differences up to 3% have been noted by McDougall and Harrison (1988).

3) Radiogenic argon measured in a sample is the product of *in situ* decay of ^{40}K since the last crystallization event in that sample. This premise has been shown to be false in some studies of sea-floor basalts, where extraneous ^{40}Ar may be the result of incomplete outgassing of older $^{40}Ar^*$ or by contamination of a magma by older material (e.g. Dalrymple and Moore, 1968; Dymond, 1970)

4) Non-radiogenic ^{40}Ar present in a rock is atmospheric in composition with the $^{40}Ar/^{36}Ar$ ratio of 295.5 (Steiger and Jäger, 1977). Although this is usually true, important exceptions have been noted (McDougall and Harrison, 1988).

5) The sample must have remained a closed system since crystallization, i.e. there should have been no loss or gain of K or $^{40}Ar^*$ other than by radioactive decay of ^{40}K. This assumption is often not fully vindicated, as non-interference of samples is geologically uncommon in many areas.

An important advantage of the Ar-Ar technique is that daughter:parent isotope ratios can be measured in a single stage in a mass spectrometer. This overcomes the problem of a second analysis to determine the K concentration, which may not be valid for inhomogenous samples or where small changes in macroscopic mineralogy are suspected. Consequently, a more reliable age can be determined from measured isotope ratios than by the separate measurement of K and Ar.

Turner (1971) developed the inverse isochron technique to obtain a best age estimate for a range of samples from a single site (Figure 4.1). This approach has the advantage of using ^{40}Ar, the most abundant and hence easily measured, as the reference isotope and has been successfully utilized in age determination studies (e.g. McDougall, 1985; Kelley *et al.*, 1986; Heizler and Harrison, 1988). The initial trapped argon is incorporated into an igneous rock at the time of its crystallization or at a later thermal event, e.g. during reheating or hydrothermal alteration. Cadogan and Turner (1977) noted that the isotopic composition of atmospheric argon has not significantly changed during the Phanerozoic and so the $^{40}Ar/^{36}Ar$ ratio of 295.5 (Steiger and Jäger, 1977) may be well constrained. Trapped argon may thus consist of pure atmospheric argon with or without radiogenic contamination of ^{40}Ar from host and basement rocks.

The radiogenic component ($^{40}Ar^*$) is made up by *in situ* decay of ^{40}K and ^{39}Ar, which is produced during the irradiation process. Assuming that the sample effectively represents a closed system since formation, the $^{40}Ar/^{39}Ar$ radiogenic component (which is proportional to the age of the sample when the $^{40}Ar/^{36}Ar$ ratio is zero) can be determined by linear regression using the least squares method (York, 1968).

4.4.2 NEW Ar-Ar DATA

Crushed rock samples for dating were prepared and analysed at the Open University by the methods described in section 2.4.3. The data were corrected for interfering nuclear reactions involving Ca and K, mass spectrometer fractionation, ^{37}Ar decay since the time of irradiation and background levels of Ar (monitored from the analysis of blanks). All processed argon data are presented in Appendix A3.

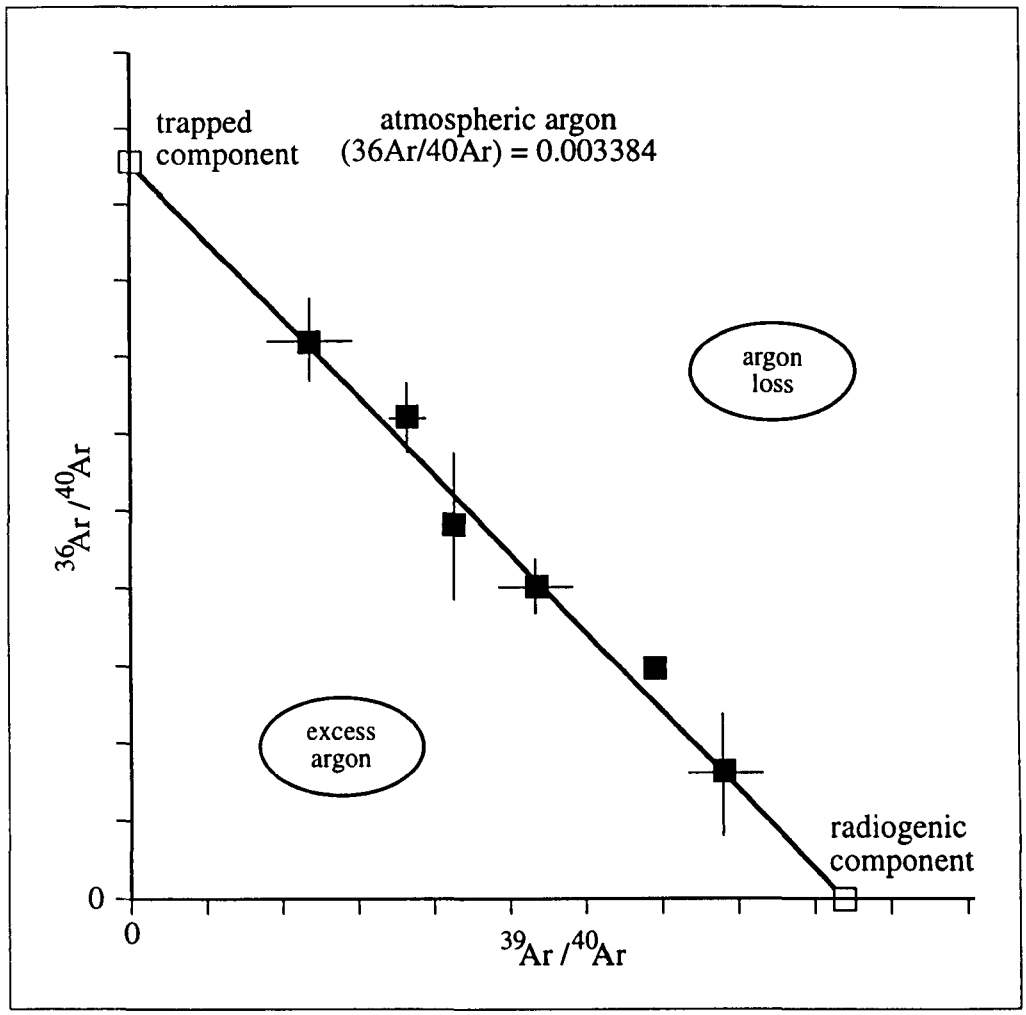

Figure 4.1: The inverse isochron analysis (Turner, 1971).
Assuming that the sample has remained a closed unit with respect to Ar since crystallization, data lies upon a basic two-component linear mixing series. At the Y-axis intercept, atmospheric argon has a $^{36}Ar/^{40}Ar$ ratio of 0.003384 and represents the trapped component. The X-axis intercept represents the radiogenic component, the origin of the graph being pure radiogenic ^{40}Ar. Loss of radiogenic ^{40}Ar displaces data above the line and a gain pushes data below the line. The best-fit mixing line is derived from linear regression using the methodology of York (1968).

4.4.2.1 Age of dykes at Lee Bay

Fresh plagioclase feldspar phenocrysts were hand picked from crushed rock for Ar-Ar analysis from dykes CK21 and CK30. Although whole rock fragments do contain K, their small grain size makes assessment of freshness difficult and secondary matrix minerals, which produce spurious element concentrations, are common from breakdown processes. However, plagioclase phenocrysts can be optically evaluated for alteration with relative ease and small amounts of K are usually present within the crystal lattice.

Dyke CK30 presented fine-grained aphyric chilled margins with plagioclase phenocrysts located towards the dyke centre, which implies limited temporal distribution and similar mineralogy. Dyke CK21 displayed plagioclase phenocrysts within several of its zonations, although the outer margins were too fine-grained to allow individual mineral separation. This may imply relative temporal diversity and hence slightly changing mineralogy. Large analcime and zeolite amygdales were noted in both dykes, but not sampled due to their probable low K concentrations (<0.1% in Tertiary basalts; Deer, Howie and Zussman, 1992). Conversely, plagioclases may contain up to 1% K within their structure. None of the samples displayed significant subsolidus alteration, which could produce a loss or gain of $^{40}Ar^*$. Figure 4.2 shows the spread of analysed ratios. Most ratios are contained within a small group, apart from three anomalously distributed analyses from CK21, which were obtained from two different plagioclase grains. Here, the $^{39}Ar/^{40}Ar$ ratios > 0.2 indicate Ar loss and the $^{36}Ar/^{40}Ar$ ratio of < 0.001 a significant gain in $^{40}Ar^*$, but otherwise the low scatter about the mixing line suggests reasonable closure to argon since formation.

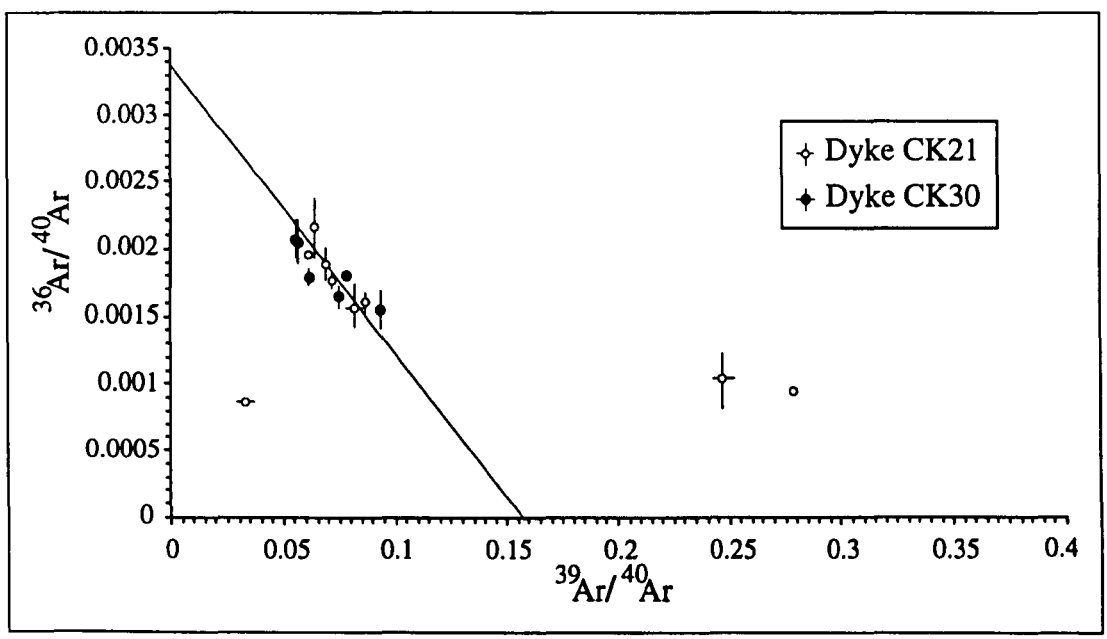

Figure 4.2: Total argon isotope composition for dykes at Lee Bay.
The average trend for the majority of samples, represented by a simple line, is determined by linear regression and indicates a common association of the two dykes.

A best fit mixing array for CK21 is shown in Figure 4.3. Although this dyke has between ~ 0.55 and 0.6 % K_2O (see Figure 4.11), which is lower than the average for both Tertiary alkalic and tholeiitic rocks (1.4 and 0.7% respectively), much of this is likely to be incorporated into plagioclase rather than groundmass minerals such as titanaugite, augite and glass. Therefore, the plagioclases may have a relatively low Ar content. The Ar released from the plagioclases by fusion has a trapped $^{40}Ar/^{36}Ar$ ratio of 303.9 ± 6.5, close to atmospheric composition but indicating a small ^{40}Ar gain, possibly by contamination from host sediments. The $^{40}Ar/^{39}Ar$ ratio of the radiogenic component (5.974 ± 0.103) corresponds to an age of 60.9 ± 0.6 Ma (MSWD = 1.364), where MSWD is the Mean Standard Weighted Deviation.

McDougall and Harrison (1988) noted that MSWD values > 2.5 may indicate that a simple isochron model is inappropriate for a given data set. The spread of the Lee Bay data is poor and determinations are relatively depleted in the radiogenic end member compared to other Tertiary basalts (Mussett *et al.*, 1976). Nevertheless, the age obtained has a small error and the best fit mixing line has a trapped component close to the ratio for atmospheric argon, i.e. $^{40}Ar/^{36}Ar$ = 295.5 (Steiger and Jäger, 1977). The initial conclusion from this set of data is that dyke CK21 is older than the Lundy granite (58.7 ± 1.6 Ma; Thorpe *et al.*, 1990) and hence pre-dates the basic and intermediate dykes on Lundy Island that cut both granite and host sediments.

The best least squares fit for dyke CK30 (Figure 4.4) gives an apparent radiometric age of 45.3 ± 2.4 Ma (MSWD = 1.16), but the $^{40}Ar/^{36}Ar$ ratio (408.3 ±12.3) is considerably higher than atmospheric composition. This suggests excess $^{40}Ar^*$ (possibly incorporated from basement rocks as magma moved through them) and is indicative of an abnormally young age which does not represent the crystallization age of the dyke. If the best line fit is anchored to atmospheric composition for the trapped component (Steiger and Jäger, 1977), an apparent age of 63.1 ±1.7 Ma (MSWD = 2.386) is obtained from the radiogenic Ar end-member.

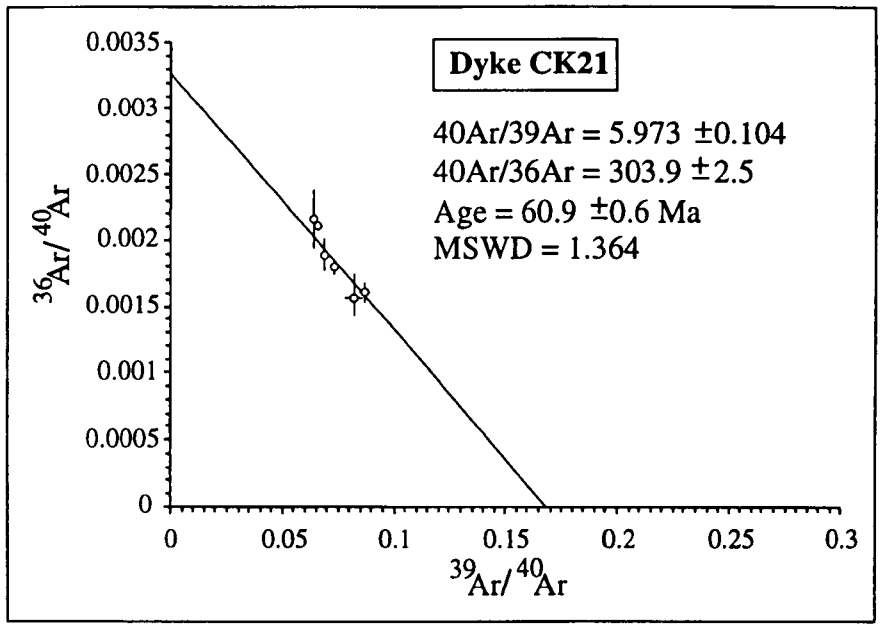

Figure 4.3: Argon isotope composition and age of three plagioclase separates from Dyke CK21. Two plagioclases that gave anomalous isotope composition (Figure 4.2) and have been excluded.

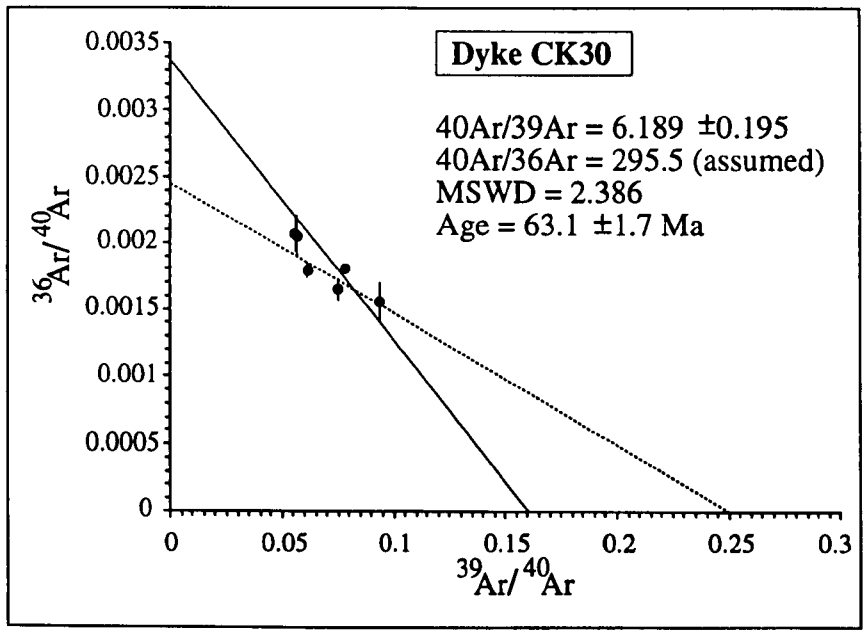

Figure 4.4: Argon isotope composition and age of three plagioclase separates from Dyke CK30. The solid line represents a best-fit isochron with lowest MSWD when the trapped component is anchored at 295.5. The dashed line represents the best-fit isochron with lowest overall MSWD (1.16). Note that trapped argon on the dashed line does not have atmospheric composition has thus been disgarded for age analysis (see text for discussion).

The five data points are somewhat bunched around the midpoint of the best fit line with a small lateral spread, so more samples from a variety of minerals may better define the true age. This is the oldest age obtained from Tertiary rocks in southwest England and is just within the reliability criterion set by McDougall and Harrison (1988) of MSWD < 2.5. It also compares with the oldest rocks associated with the BTVP from Muck (63.3 ±1.8 Ma; Dagley and Mussett, 1986). If this radiometric age is correct, it not only implies protracted igneous activity at Lee Bay (around 3Ma) but also that the Lee Bay dykes pre-date the entire Lundy Igneous Complex. CK21 and CK30 may thus represent the oldest, but not necessarily most primitive, magma associated with Tertiary magmatic activity in Southwest England.

4.4.2.2 Date of the Horse-Shoe Rocks

Although the Horse-Shoe Rocks have been chloritized and have a low K content of ~0.4% (section 4.4), relatively fresh crystal fragments of plagioclase were obtained for laser fusion. A best fit line to the data (Figure 4.5) yielded an age of 339.6 ±7.4 Ma (MSWD = 1.664) with a $^{40}Ar/^{36}Ar$ ratio of 319.6 ±7.3, which is slightly higher than atmospheric argon composition and indicates that the crystals contain small but significant amounts of excess radiogenic argon, possibly from underlying sources.

At first sight, the rocks appear to be Upper Carboniferous in age, but this contradicts the palaeomagnetic signature, which suggests Lower Tertiary (cf. section 3.3.2.2). Anomalously old values have been recognized in plagioclases from both igneous and metamorphic rocks due to low K content and incorporation of excess argon (Damon *et al.*, 1967; Dalyrymple *et al.*, 1975; McDougall and Harrison, 1988). If the Horse-Shoe rocks are indeed Lower Tertiary, secondary processes must have considerably modified their argon content. Lower Tertiary basalts would normally be expected to have a $^{40}Ar/^{39}Ar$ ratio of around 5.8 - 6.6 for the radiogenic component, which is considerably lower than the Permo-Carboniferous range (30 - 36), because older rocks would develop higher concentrations of naturally occurring $^{40}Ar^{*}$ from radiogenic decay.

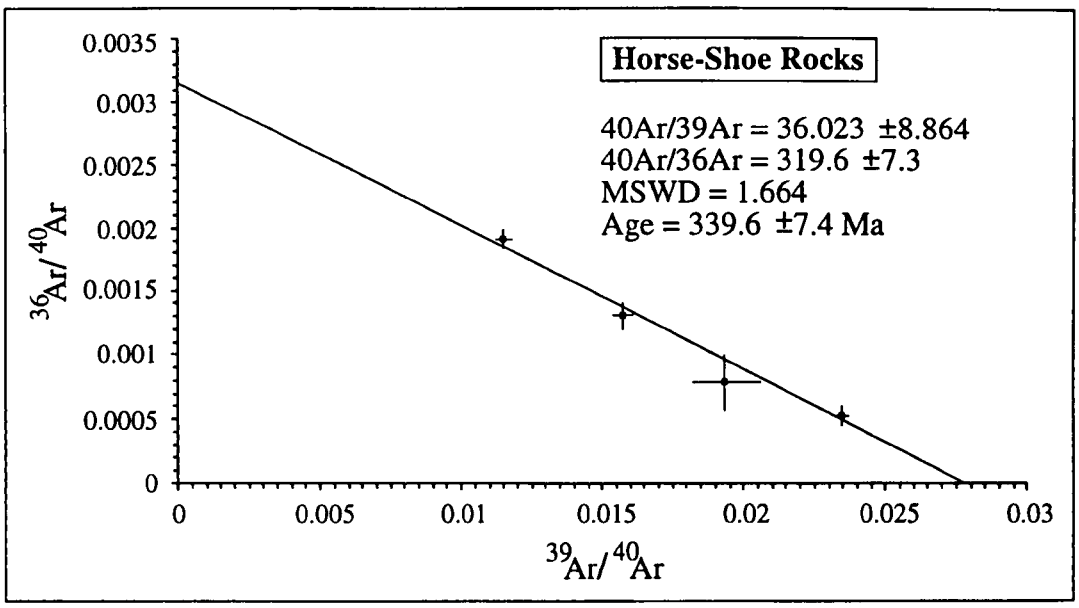

Figure 4.5: Argon isotope composition and isochron age of two plagioclases from Horse-Shoe Rocks.

However, excess ^{40}Ar and $^{40}Ar^{*}$ could be locally derived from other sources such as hydrothermal circulation, where fluids may be saturated with respect to argon. McDougall and Harrison (1988) define the blocking temperature of plagioclase as 200 - 250°C, which is within the prehnite-pumpellyite metamorphic facies range (Mason, 1986). As the Horse-Shoe rocks contain prehnite, pumpellyite, chlorite and actinolite (section 4.2), approaching greenschist facies grade, they could have been re-heated to between 250° and 400°C. If plagioclases have not remained closed to argon since crystallization, argon loss and/or gain could therefore have taken place to give an anomalous age (Figure 4.6).

It is unusual for the Ar-Ar isochron line in Figure 4.5 to demonstrate relatively low scatter about the mixing line if extensive hydrothermal activity has occurred. Also, Ar-saturated perculating fluids are likely to have considerable effect on the overall Ar ratios in the Horse-Shoe rocks, deviating the trapped component of an isochron away from normal atmospheric concentration. An isotopically re-set Tertiary age thus seems improbable.

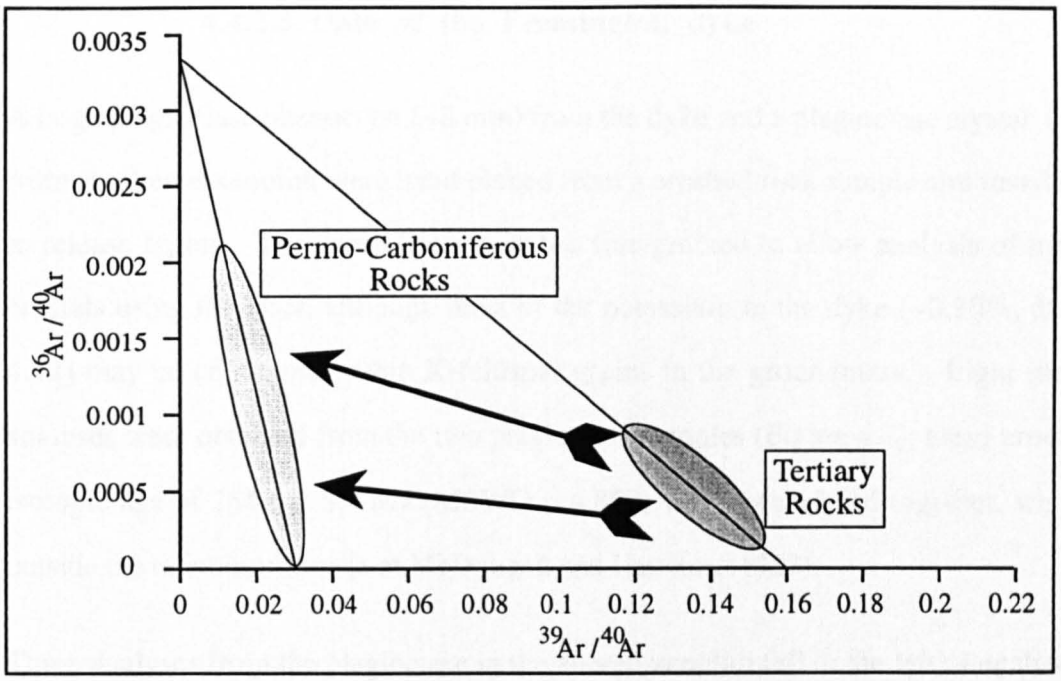

Figure 4.6: Theoretical isotope composition diagram for hydrothermally altered Tertiary rocks. In this case the rocks have become relatively enriched in ^{40}Ar by circulating hydrothermal fluids, moving the best-fit mixing line to the left. Arrows indicate the direction of enrichment. Note that the altered rocks have a wider spread of isotopic compositions, indicating a greater participation of atmospheric argon. Both mixing arrays have been anchored to atmospheric composition for the trapped argon content.

Alternatively, the calculated isochron age could be a true estimate and the rocks pre-date the Tertiary by some 275 - 285 Ma. If this is so, then the Horse-Shoe rocks must have been re-heated above 300-350°C (the magnetic blocking temperature of magnetite) in the Lower Tertiary for magnetite to be re-set into a Tertiary palaeomagnetic signature. A primary remanence is unlikely to have been acquired at temperatures lower than 300°C and in any case, this would be easily removed by demagnetizaton procedures - not observed during palaeomagnetic investigations of the Horse-Shoe rocks (cf. Figure 3.6). As there is evidence for metamorphic minerals up to greenschist facies in the rocks (Mason, 1986), it seems likely the rocks have been re-heated within the Lower Tertiary.

The Horse-Shoe rocks are therefore remnants of a phase of igneous activity in North Devon within the Middle Carboniferous, contemporaneous with Variscan granites in Britanny and Normandy, but significantly pre-dating Cornubian rocks (300-270 Ma; Floyd *et al.*, 1993). There is no direct evidence for a common link, but a more detailed sampling and dating strategy would improve the data base.

4.4.2.3 Date of the Fremington dyke

A large plagioclase phenocryst (~8 mm) from the dyke and a plagioclase crystal (~2 mm) from an altered xenolith were hand picked from a crushed rock sample and fused by laser to release argon. The groundmass was too fine-grained to allow analysis of individual crystals using the laser, although most of the potassium in the dyke (~0.30%; cf. Figure 4.12) may be contained within K-feldspar grains in the groundmass. Eight individual analyses were obtained from the two plagioclase samples (Figure 4.7); these produced an isotopic age of 254.6 ± 8.4 Ma (MSWD = 4.808) when considered together, which falls outside the reliability criteria of McDougall and Harrison (1988).

Three analyses from the plagioclase in the altered xenolith fall to the left of analyses from the plagioclase phenocryst (Figure 4.7), indicating a net gain of argon (relative to the other five analyses) within the crystal, even though optically it appeared relatively fresh with minimal breakdown products. The reasons for this are unclear, but may be related to the source of the xenolithic material or associated with the process of magmatic intrusion. In contrast, the plagioclase phenocryst itself has suffered little sericitization and is thus relatively unaltered. Accordingly, analyses from the altered xenolith have introduced a substantial error into the isotopic composition of the best-fit isochron mixing line of both plagioclases and have thus been disregarded for age determinations of crystallization in the Fremington dyke.

A best-fit isochron mixing line for the plagioclase phenocryst from the dyke revealed a $^{40}Ar/^{39}Ar$ ratio for the radiogenic end-member of 37.679 ± 0.209 (Figure 4.7), which corresponds to an isotopic age of 353.8 ± 4.3 Ma (MSWD = 1.642). Even though the low MSWD indicates a good statistical fit for the isochron line, a $^{40}Ar/^{36}Ar$ ratio of 231.4 ± 6.4 for the trapped component is significantly lower than atmospheric composition and suggests some loss of argon by either sub-solidus weathering or exposure to temperatures above 250°C (the plagioclase blocking temperature; McDougall and Harrison, 1988) after crystallization of the dyke. Whether such apparent argon loss is real or a function of statistical linear regression is unclear, but the determined age of 353 Ma by this isochron is artificially old.

Although the trapped component should have a theoretical $^{40}Ar/^{36}Ar$ ratio of 295.5, it is not possible to achieve a satisfactory isochron fit (MSWD <2.5) for the phenocryst analyses by anchoring the trapped component end of the line to this atmospheric ratio. The most acceptable MSWD value, when the $^{40}Ar/^{36}Ar$ ratio is closest to atmospheric composition, is achieved when $^{40}Ar/^{36}Ar$ = 284.4 ± 6.4 (MSWD =2.364), giving a $^{40}Ar/^{39}Ar$ ratio of 30.581 ± 0.371. This corresponds to a isotopic age determination of 292.4 ± 1.7 Ma. Whilst there is a reasonable spread of data points about the mixing line, the MSWD could be further improved statistically by increasing the number of analyses from fresh plagioclase feldspars and by analysing more gas during laser ablation during each sample run, which would reduce error bars on those samples where the volume of collected gas was low (cf. Appendix A3)

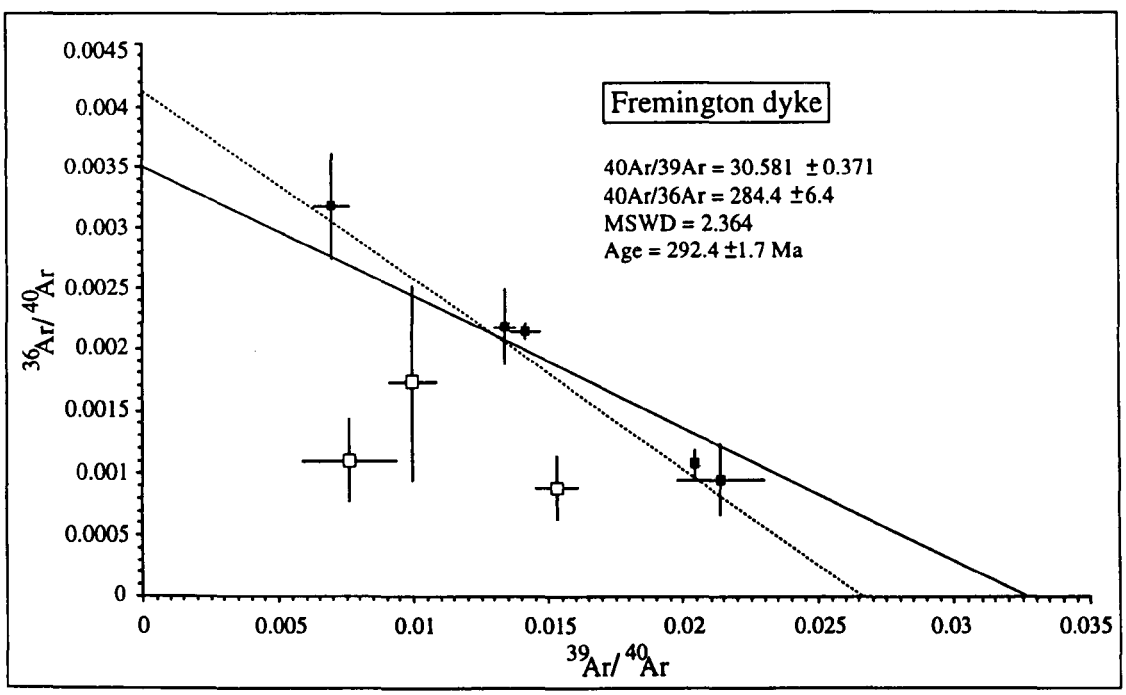

Figure 4.7: Age determination for the Fremington dyke.
Argon isotope composition and isochron age of two plagioclases from the Fremington dyke. Filled squares represent a plagioclase phenocryst, whilst unfilled squares symbolize a plagioclase crystal from a xenolith within the dyke. The dashed line represents a best-fit isochron age of 353.8 ±4.3 Ma (MSWD = 1.642), but with a $^{40}Ar/^{36}Ar$ ratio of 231.4 ±6.4 (see text for discussion). The solid line represents an isochron age of 292.4 ±1.7 Ma. Note that both age determinations are derived using the plagioclase phenocryst. The best-fit isochron for all eight analyses has low precision (MSWD = 4.808) and has been omitted for clarity.

The apparent Lower Permian age for the samples is in broad agreement with palaeomagnetic evidence. The Fremington dyke considerably pre-dates the Lundy Igneous Complex and is not directly related to Tertiary volcanism. However, its apparent age of 292 ± 1.7 Ma is coeval with basic lava flows, dykes (291 ± 6 Ma, Miller *et al.*, 1962; Thorpe *et al.*, 1986) and lamprophyres (average 291 Ma; Hawkes, 1982) of the Exeter Volcanic 'Series' in South and mid-Devon (ages determined by whole rock K/Ar analyses). In addition, microgranular enclaves with igneous textures and mineralogies aged 275 to 290 Ma (Chen *et al.*, 1993) included within Cornubian granites have been interpreted by Stimac *et al.* (1995) as the product of magma-mixing in an array between biotite granite and an unobserved end-member of mafic composition - a lamprophyric parent being discounted on evidence from REE data and overlapping of fields in discrimination plots.

Stimac *et al.* (1995) indicated that although basalts in the Exeter Volcanics (EV) are relatively common in southern Devon, a definite link between EV basalts and biotite granite in the mixing array cannot be established. The nature and composition of the mafic end-member is thus unknown. The Fremington dyke is more basic (cf. Figure 4.12: MgO up to 7.24 dry wt. %, Cr ~375 ppm, Ni ~230 ppm) than the EV basalts and as such may be closest to the geochemical characteristics of the mafic end-member than other basic options. In this context, mixing between basic and granitic magma could produce enclaves of the appropriate composition. The mechanism by which this could occur in southwest England is unclear.

Thorpe *et al.* (1986) and Leat *et al.* (1987) imply subduction related magmatism for potassic lavas within the EV Series, connecting volcanism to the lithospheric mantle as source material. In any case, the mantle heat required to generate the EV rocks (and the Fremington dyke) must have also been a major factor in melting the pelitic crust to generate large volumes of granitic magma (290 - 270 Ma; Floyd *et al.*, 1993) in Devon and Cornwall. A more detailed study of the Fremington dyke is required to test this initial hypothesis. A summary of Ar/Ar dating procedures in this study is placed within the framework of other data on ages in Table 4.1.

Table 4.1 Summary of geochronological relationships of igneous rocks in North Devon

Location	Petrographic Characteristics	Weathering and Alteration Products	Palaeomagnetic Age	Isotopic Age	References
Lundy Island					
a)	crinanites, dolerites and trachytes	unaltered	Tertiary $D_m = 197^o$, $I_m = -59^o$	-	Blundell (1957)
b)	basalts with devitrified glass	rel. fresh with minor seritization of plag.	Lower Tertiary N 3.6° E, $I_m = +62.7^o$	44.6 ±1 Ma to 54.3 ±1 Ma (K/Ar)	Mussett et al. (1976)
c)	dolerites and trachytes	olivine → serpentine pyroxene → chlorite	-	51.9 ±3 Ma to 56.1 ±4 Ma (K/Ar)	Edmonds et al. (1979)
d)	basalt	unpublished	Tertiary	56.4 ±0.3 Ma (Ar/Ar)	Mussett et al. (1988)
e)	coarse-grained megacrystic granite	fresh rock, some turbid feldspars	-	58.7±1.6 Ma (Rb/Sr)	Thorpe et al. (1990)
Lee Bay					
a)	dolerite (N.B.- may equal CK31 in this study)	unaltered	Tertiary $D_m = 181^o$, $I_m = -51^o$	-	Blundell (1957)
b)	phenocrystic and amygdaloidal basalts (multi-phased)	mostly fresh with some seritization of plagioclase in places	Lower Tertiary $D_m = 193.4^o$, $I_m = -57.6^o$	60.9 ± 0.6 Ma to 63.1 ± 0.7 Ma (Ar/Ar)	this study
Horse-Shoe Rocks	aphyric coarse dolerites	heavily chloritized with plagioclase → phyllosilicates	Tertiary (over-print) $D_m = 154^o$, $I_m = -57^o$	339.6 ± 7.4 Ma (Ar/Ar)	this study
Fremington Dyke	multi-xenolithic dolerite	devitrified glass and moderate sub-solidus weathering	Permo-Carboniferous $I = -2^o$ to -7^o (semi-stable TRM)	292.4 ± 1.7 Ma (Ar/Ar)	this study

4.5 WHOLE ROCK MAJOR ELEMENT GEOCHEMISTRY

4.5.1 LUNDY ISLAND

The basic to intermediate dykes of Lundy Island sampled here can be classified according to Le Maitre (1989) as forming a series of basalts to basaltic andesites or basaltic trachyandesites with some trachybasalt and basanite exceptions (Figure 4.8a), although there is a relatively large compositional divide between 49 and 52 % SiO_2 that may preclude assuming a common link. Whether this can be attributed to incomplete/discrete sampling or a 'Daly Gap' (Wilson, 1993) is uncertain, but could be resolved by the modelling of fractionation trends. All geochemical data are presented in Appendix A4.

The basalts can also be considered as transitional basalts according to the criteria of Middlemost (1975) and Wilson (1993), in which K_2O values plot against SiO_2 in the sub-alkaline basalt field, whereas Na_2O values plot in the alkalic basalt field. One evolved sample (DK2; SiO_2 = 53.96 dry wt.%) is alkalic (Figure 4.9). Data from Thorpe and Tindle (1992) are generally lower in total alkalis than the new data presented here (Figure 4.8a), which could be a function of Na and K mobility from weathering processes (Pearce, 1976). More probably, it represents differences in fractionation trends and/or degrees of partial melting.

Higher-Na basalts may respond by having relatively more oligoclase in groundmass plagioclase than the lower-Na counterparts, which usually have more labradorite to bytownite grains, i.e. more Ca-rich. CIPW normative compositions, calculated assuming that 20% of the total Fe is in the Fe^{3+} state as recommended by Middlemost (1989), show the basic to intermediate dykes of Lundy to be either Si-saturated quartz tholeiites or Si-undersaturated alkaline-olivine basalts (Figure 4.10), the latter being up 9.4% Ne-normative. This implies at least two discrete populations of magma.

Major element variation trends within Lundy basic to intermediate dykes are non-linear for the most part (Figure 4.11) with MgO concentrations between 2.07 and 8.19% and SiO_2 between 44.92 and 56.13%. At least two main rock groups can be identified from the data, a high-Ti/high-Fe group and a low-Ti/low-Fe group.

a)

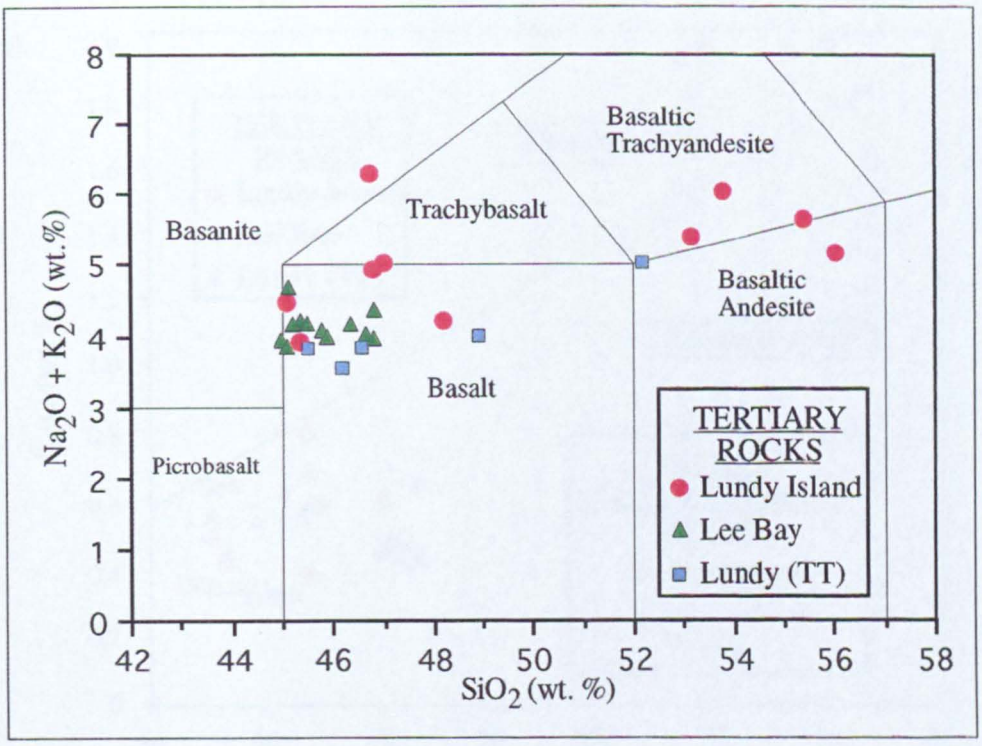

b)

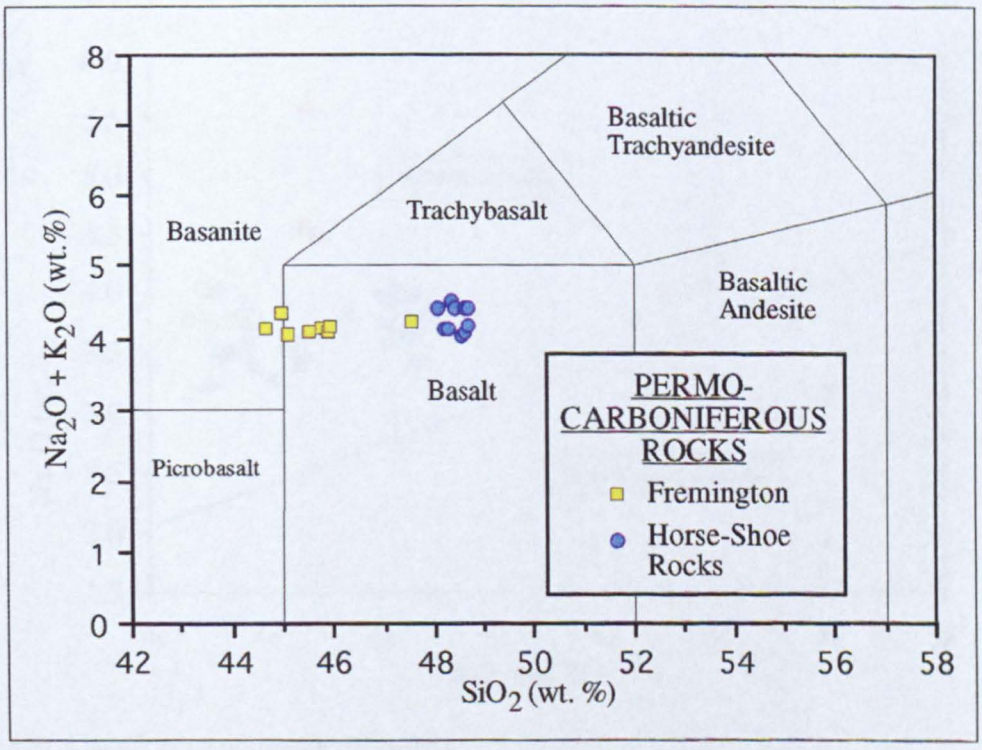

Figure 4.8: Chemical classification of a)Tertiary and b) Permo-Carboniferous rocks.
Data have been plotted in the style of the total alkalis versus silica diagram (TAS) of Le Maitre *et al.* (1989). Lundy (TT) data are taken from Thorpe and Tindle (1992). Rhyolites have not been sampled for geochemical analysis, as they did not present a magnetic field signature. A comparison of geophysical and geochemical interpretation is therefore inappropriate. All data have been normalized water free.

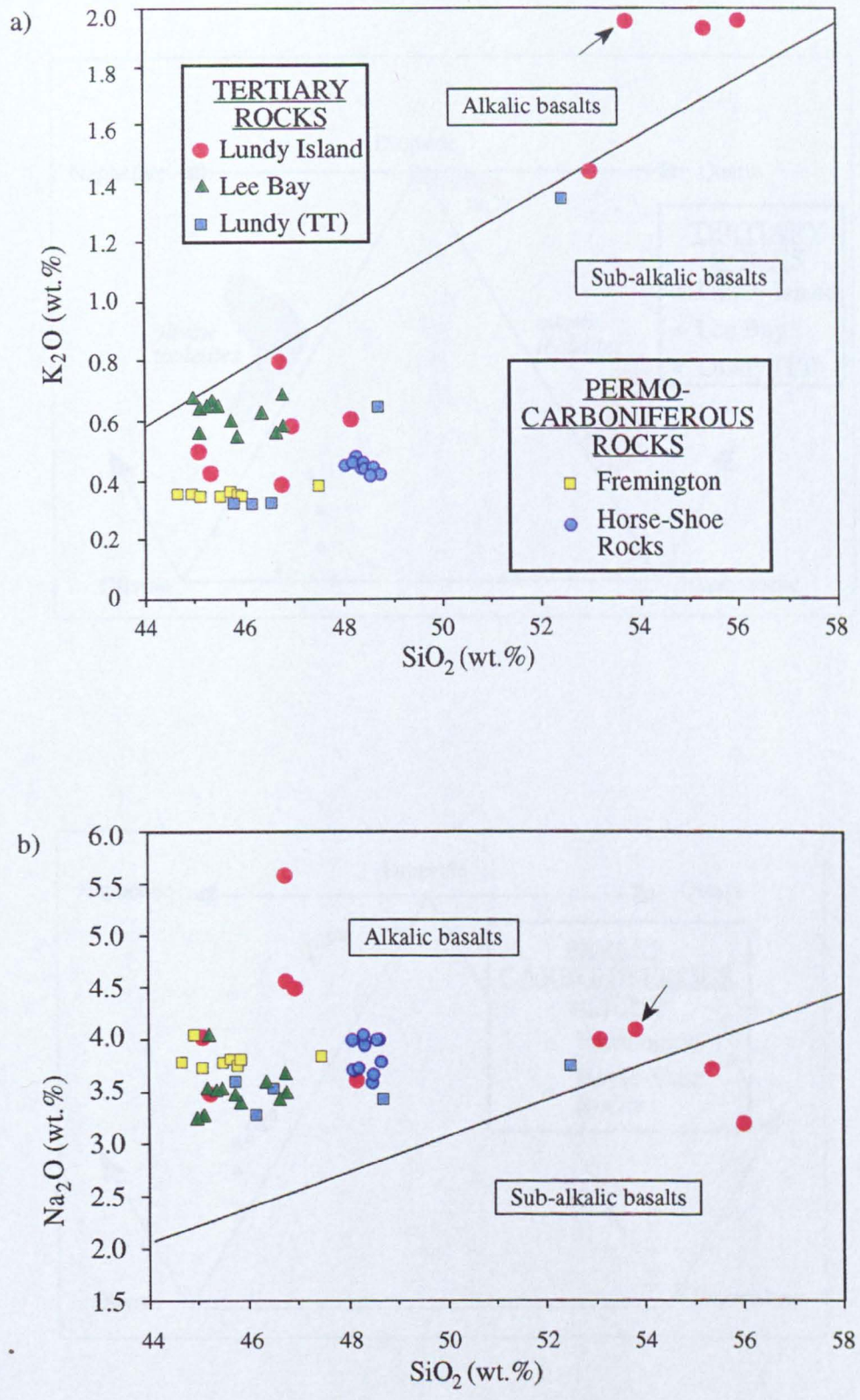

Figure 4.9: Classification of transitional basalts.
Data is plotted using the conventions of Middlemost (1975) and Wilson (1993). The arrow highlights sample DK2 from Lundy Island as an alkali basalt. Corrected for hydrous phases and including 'TT' data from Thorpe and Tindle (1992).

a)

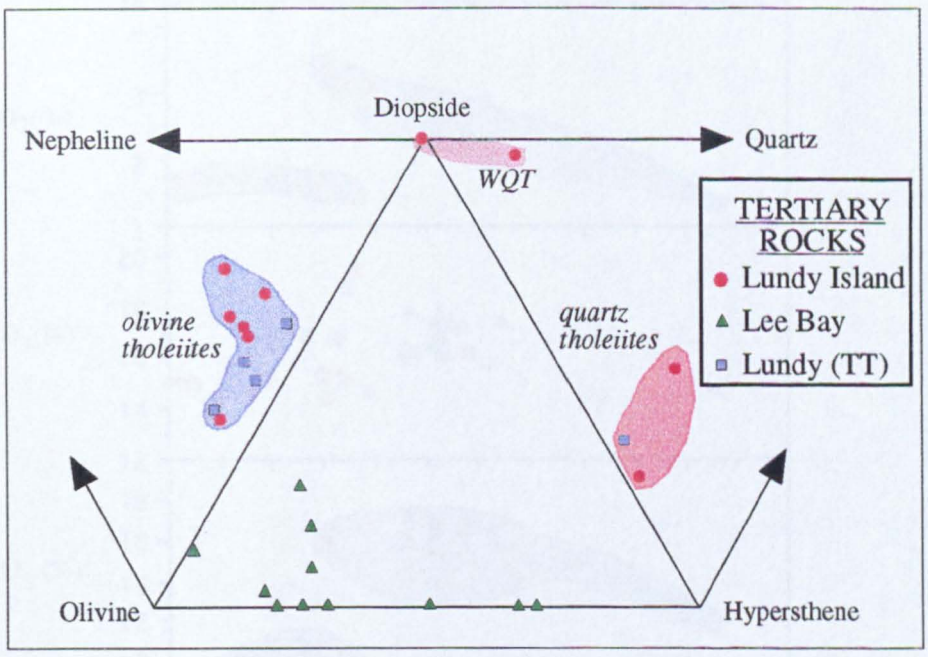

b)

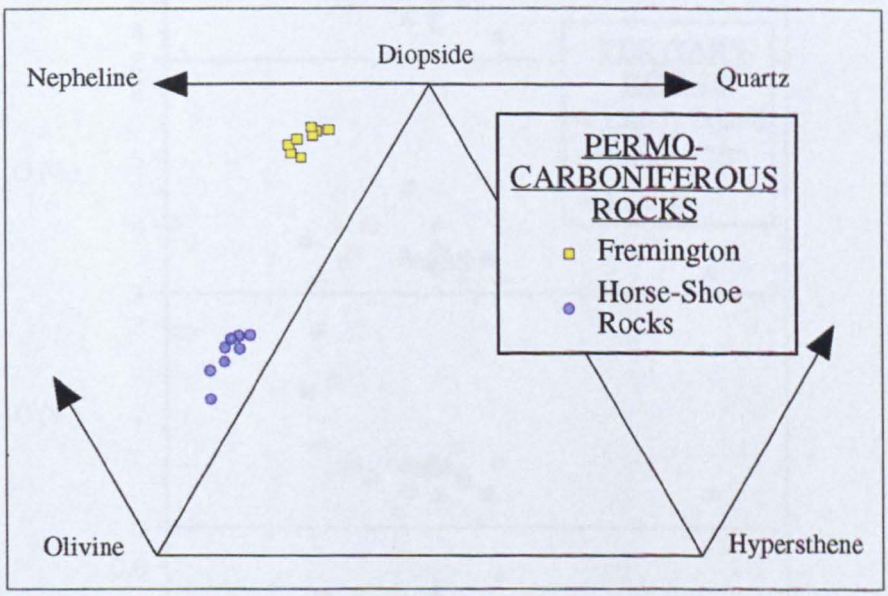

Figure 4.10: CIPW classification of rocks from North Devon.
Normative plot (CIPW, weight %) of olivine, diopside, hypersthene and nepheline or quartz for a) Tertiary rocks and b) Permo-Carboniferous rocks from North Devon. Calculations were completed using the computer program CIPWNorm 3.1 (Mason, 1990), based on Cross et al. (1903). WQT represents the field of weathered quartz tholeiites.

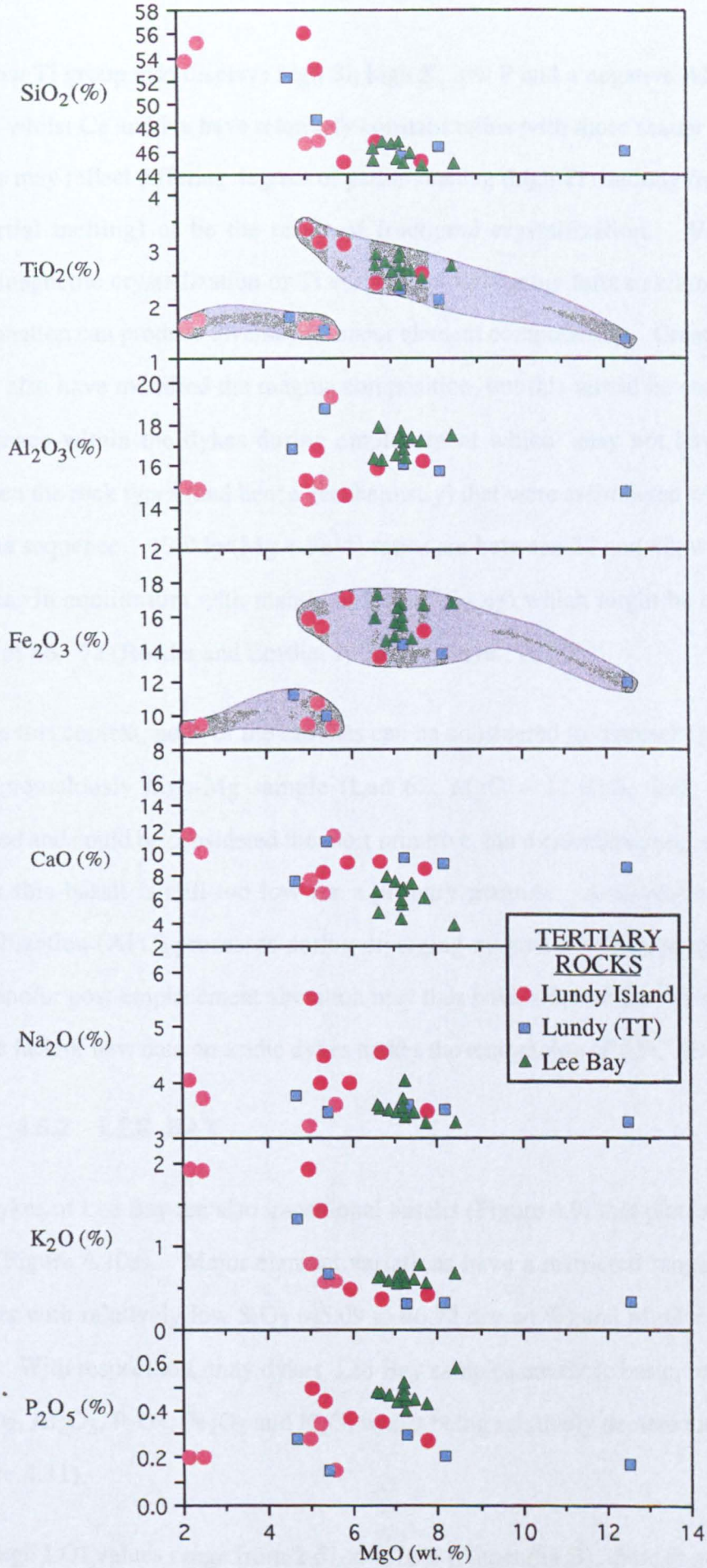

Figure 4.11: Major Element variation within Tertiary rocks from Lundy and Lee Bay. Lundy (TT) information is taken from Thorpe and Tindle (1992). The shaded red plots indicate values for the two groupings highlighted in the Ti and Fe fields. Only dolerites and trachytes are plotted here as anhydrous values. Rhyolites are excluded from these analyses as they have not been sampled.

The low Ti group also displays high Si, high K, low P and a negative Al correlation with MgO, whilst Ca and Na have relatively constant ratios with more scatter in Na. The two groups may reflect differing degrees of partial melting (high Ti resulting from small degrees of partial melting) or be the result of fractional crystallization. Varying levels of titanomagnetite crystallization or Ti enrichment with more ferroan clinopyroxene during fractionation can produce diversity in major element compositions. Crustal contamination might also have modified the magma composition, but this would be controlled more by turbulence within the dykes during emplacement which may not have discriminated between the rock types (and hence geochemistry) that were assimilated within the evolved magma sequence. $100Mg/(Mg + Fe^{2+})$ ratios are between 22 and 42, well below that of magmas in equilibrium with mantle olivine (Fo_{86-92}) which might be expected to have ratios of 66 - 72 (Roeder and Emslie, 1970; Frey *et al.*, 1978).

Within this context, none of the samples can be considered to represent primary magmas. One anomalously high-Mg sample (Lun 62; MgO = 12.02%, SiO_2 = 44.38%) was sampled and could be considered the most primitive, but a calculated magnesium number of 56 for this basalt is still too low for a primary magma. Assimilation and fractional crystallization (AFC) processes during diverging magma routes through the continental crust and/or post-emplacement alteration may thus have affected the overall compositions, but the lack of new data on acidic dykes makes the recognition of AFC processes difficult.

4.5.2 LEE BAY

The dykes of Lee Bay are also transitional basalts (Figure 4.9) that plot in the Si-saturated field (Figure 4.10a). Major element variations have a restricted range and show good clusters with relatively low SiO_2 (45.09 to 46.72 dry wt.%) and MgO = 6.39 to 8.05 dry wt.%. With respect to Lundy dykes, Lee Bay samples are more basic, relatively enriched in TiO_2, Al_2O_3, P_2O_5, Fe_2O_3 and K_2O, whilst being relatively depleted in CaO and Na_2O (Figure 4.11).

Although LOI values range from 2.67 to 4.76% (Appendix B), there is no significant loss in MgO content, which implies that weathering has not overly modified major element concentrations. Individual dykes show a small degree of Si enrichment from margin to

centre, which indicates some degree of fractionation within each outcrop or perhaps by small.amounts of sediment assimilation at the margins of the dykes.

CIPW normative calculations show the Lee Bay rocks to be olivine tholeiites (Figure 4.10a), as suggested by Thompson *et al.* (1983). The spread of data points for Lee Bay in this ternary plot is excessively broad and indicates some degree of element mobility, suggesting that the samples may not be true tholeiites. Several samples lack normative diopside, due to an excess of Al_2O_3 over CaO after the formation of normative apatite, resulting in the appearance of normative corundum and the reduction of normative anorthite at the expense of wollastonite (and hence diopside) formation (Cross *et al.*, 1903).

As corundum has never been recorded in basic igneous rocks (Thorpe, 1981), its presence indicates an Al_2O_3-rich phase not included amongst minerals used in normative calculations. This could either be caused by Ca depletion from sub-solidus weathering or suggests the occurrence of phyllosilicate minerals in the original rock sample such as biotite, sericite or siderophyllite. Such peraluminous characteristics may thus be artificial and not diagnostic of original magma composition. Magnesium numbers for the Lee Bay dykes range from 32 to 38 and although MgO concentrations are comparable to or higher than their Lundy counterparts, the Mg/Fe ratio reflects the relatively high Fe_2O_3 content (11.27 to 13.59 %). This is also unlikely to represent a primary magma.

4.5.3 THE HORSE-SHOE ROCKS

Major element distribution in the Horse-Shoe Rocks shows tight clustering (Figure 4.12) and restricted ranges of values with relatively low TiO_2, CaO and P_2O_5 and relatively high Al_2O_3 and Na_2O. This cannot be entirely due to a limited, spatial sampling strategy, as the data are derived from 5 discrete localities over the sub-marine outcrop. The rocks themselves are derived from a transitional alkaline-olivine basalt melt (Figures 4.8b, 4.9 and 4.10b) that plot near to the trend of a fertile anhydrous mantle source between ~10 and 30 kbar, postulated by Thompson *et al.* (1983).

However this may be misleading, as the MgO content of melts generated at such pressures should be in the order of up to 20 - 25%, whereas the MgO major element content in the

Horse-Shoe Rocks is clustered around 9% (Figure 4.12). The observed spread of the data may be a function of Ca mobility caused by weathering and/or hydrothermal alteration in the chloritized rocks, where lower diopside concentrations correspond to relative depletion of CaO. A small fractionation trend parallel to the diopside-olivine axis might also be responsible for the distribution, but the clustering seen in Figure 4.12 argues against significant magma evolution.

Nevertheless, the Horse-Shoe Rocks plot close to the Mg-rich basalt 66018, which is an experimental anhydrous liquidus equilibrium with olivine, orthopyroxene and clinopyroxene at 16.5 kbar (Thompson, 1974). If the Horse-Shoe Rocks were generated at such depths, there may have been considerable potential for crustal contamination as the magma ascended.

Magnesium numbers for the Horse-Shoe Rocks are between 50 and 53, despite subsequent chloritization, and are similar to values of Tertiary flood basalts elsewhere such as the Columbia River Province (Basaltic Volcanism Study Project, 1981), which are though to represent primitive magmas and where the maximum 100Mg/(Mg+Fe) ratio is 60. The Horse-Shoe Rocks may thus be more primitive than all the Tertiary igneous rocks in North Devon, although the precise tectonic setting of magmatism in the Lower Carboniferous (~340 Ma; cf. Figure 4.5) is unclear (Floyd *et al.*, 1993) and hence a direct comparison may be more complicated.

4.5.4 THE FREMINGTON DYKE

The Permo-Carboniferous Fremington dyke (~290 Ma; cf. Figure 4.7) has relatively unvarying major element compositions that show good clusters (Figure 4.12), where CaO, TiO_2, Fe_2O_3 and P_2O_5 are enriched and Al_2O_3 and SiO_2 depleted with respect to the Lower Carboniferous Horse-Shoe Rocks. The rock is a Ne-normative alkaline-olivine basalt, but relatively low in normative olivine (Figure 4.10). This may be an artefact of subsequent weathering and/or alteration, because normative diopside is preferentially high due to an excess of CaO (as a result of secondary calcite in amygdales and veins) over Al_2O_3, which favours the assignment of normative wollastonite (and hence diopside). Relatively high normative apatite also indicates high CaO levels.

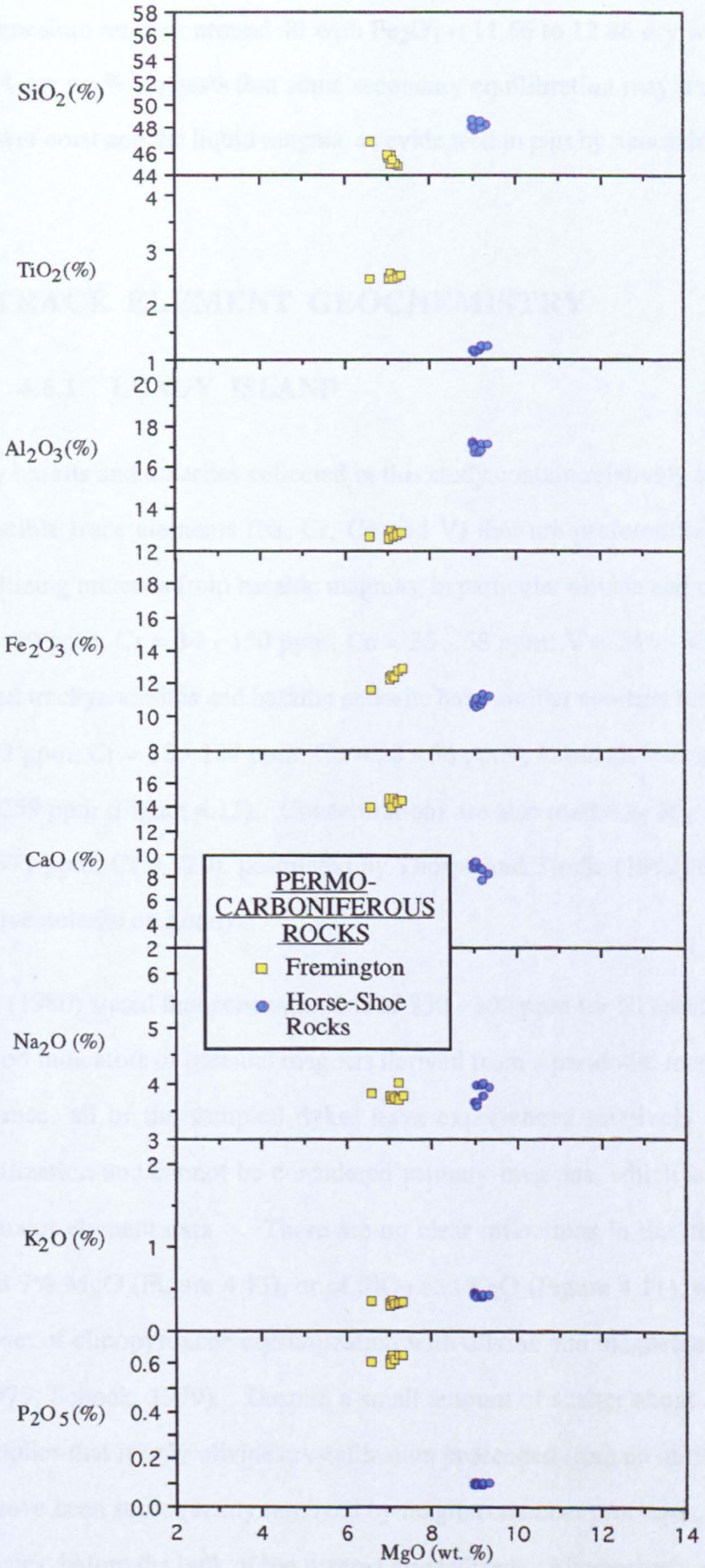

Figure 4.12: Major element variation within Permo-Carboniferous rocks from North Devon. Corrected for hydrous phases.

A magnesium number around 40 with Fe_2O_3 = 11.66 to 12.86 dry wt.% and MgO = 6.52 to 7.24 dry wt.% suggests that some secondary equilibration may have occurred between the lower crust and the liquid magma, as evidenced in part by xenolithic inclusions.

4.6 TRACE ELEMENT GEOCHEMISTRY

4.6.1 LUNDY ISLAND

Lundy basalts and dolerites collected in this study contain relatively low concentrations of compatible trace elements (Ni, Cr, Co and V) that are preferentially concentrated into crystallizing minerals from basaltic magmas, in particular olivine and clinopyroxene (i.e. Ni = 21 - 89 ppm; Cr = 34 - 150 ppm; Co = 35 - 58 ppm; V = 245 - 438 ppm). The more evolved trachyandesites and basaltic andesite have similar contents for Ni, Cr and Co (Ni = 46 - 92 ppm; Cr = 32 - 134 ppm; Co = 28 - 56 ppm), although V is significantly lower at 147 - 259 ppm (Figure 4.13). Concentrations are also markedly low relative to LUN 62 (Ni = 371 ppm; Cr = 720), postulated by Thorpe and Tindle (1992) to represent the most primitive dolerite on Lundy.

Green (1980) stated that concentrations of 250 - 300 ppm for Ni and 500 - 600 ppm for Cr are good indicators of parental magmas derived from a peridotite mantle source and so, in that sense, all of the sampled dykes have experienced relatively extensive fractional crystallization and cannot be considered primary magmas, which is in broad agreement with major element data. There are no clear inflections in the trends of Ni and Cr at around 7% MgO (Figure 4.13), or of SiO_2 and K_2O (Figure 4.11), which would indicate the onset of clinopyroxene crystallization with olivine and magnetite (Arth, 1976; Cox *et al.*, 1979; Schock, 1979). Despite a small amount of scatter about a linear relationship, this implies that if only olivine crystallization proceeded from an initial melt, most crystals must have been subsequently removed by magma chamber processes, e.g. the formation of cumulates, before the bulk of the magma crystallized. Alternatively, olivine may not have been a major phase of crystallization in the magma and as such, has not influenced the evolutionary trend of trace elements.

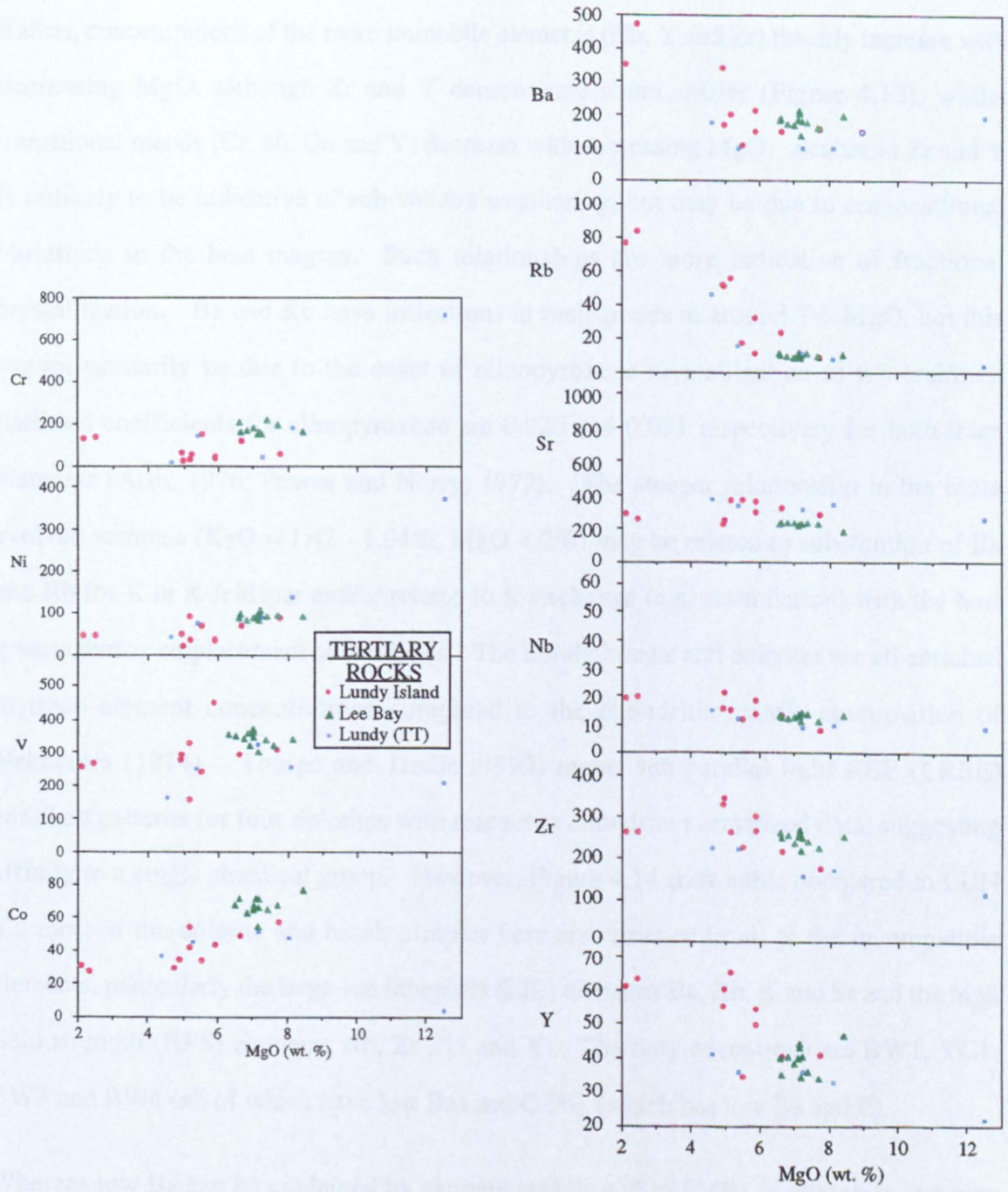

Figure 4.13: Trace element geochemistry in Tertiary dolerites from Lundy Island and North Devon. MgO concentration is given as dry wt.% and Lundy (TT) data are taken from Thorpe and Tindle (1992).

Overall, trace element geochemistry does not adequately demonstrate the two data population sets suggested by major element variation in Ti and Fe (section 4.5.1). Rather, concentrations of the more immobile elements (Nb, Y and Zr) linearly increase with decreasing MgO, although Zr and Y demonstrate some scatter (Figure 4.13), whilst transitional metals (Cr, Ni, Co and V) decrease with decreasing MgO. Scatter in Zr and Y is unlikely to be indicative of sub-solidus weathering, but may be due to compositional variations in the host magma. Such relationships are more indicative of fractional crystallization. Ba and Rb have inflections in their trends at around 7% MgO, but this cannot primarily be due to the onset of clinopyroxene crystallization as mineral/melt partition coefficients for clinopyroxene are 0.026 and 0.031 respectively for both trace elements (Arth, 1976; Pearce and Norry, 1979). The steeper relationship in the more evolved samples (K_2O = 1.42 - 1.94%; MgO < 7%) may be related to substitution of Ba and Rb for K in K-feldspar and/or related to K-exchange (e.g. assimilation) with the host granite during emplacement of the dykes. The Lundy basalts and dolerites are all enriched in trace element concentrations compared to the chondritic-mantle composition of Nakamura (1974). Thorpe and Tindle (1992) report sub-parallel light REE (LREE) enriched patterns for four dolerites with respect to chondrite normalized data, suggesting affinity to a single chemical group. However, Figure 4.14 shows that compared to LUN 62, most of the dolerite and basalt samples here are enriched in all of the incompatible elements, particularly the large-ion lithophile (LIL) elements Ba, Rb, K and Sr and the high field strength (HFS) elements Nb, Zr , Ti and Y. The only exceptions are BW1, VC1, BW3 and BW4 (all of which have low Ba) and C-001 (which has low Ba and P).

Whereas low Ba can be explained by element mobility, P in C-001 is immobile and may suggest a different evolution from LUN 62. Figure 4.14 demonstrates that individual dykes display divergent spidergram patterns, although there is a general negative slope from left to right in order of increasing compatibility in a small fraction melt of the mantle (Rollinson, 1993).

The Lundy plots can be subdivided into three distinct groups (Figure 4.15). The first group is characterized by Zr peaks and Ti troughs accompanied by high values for Ba, Rb and K (Figure 4.15a), although C-001 has depressed LIL values with a K trough.

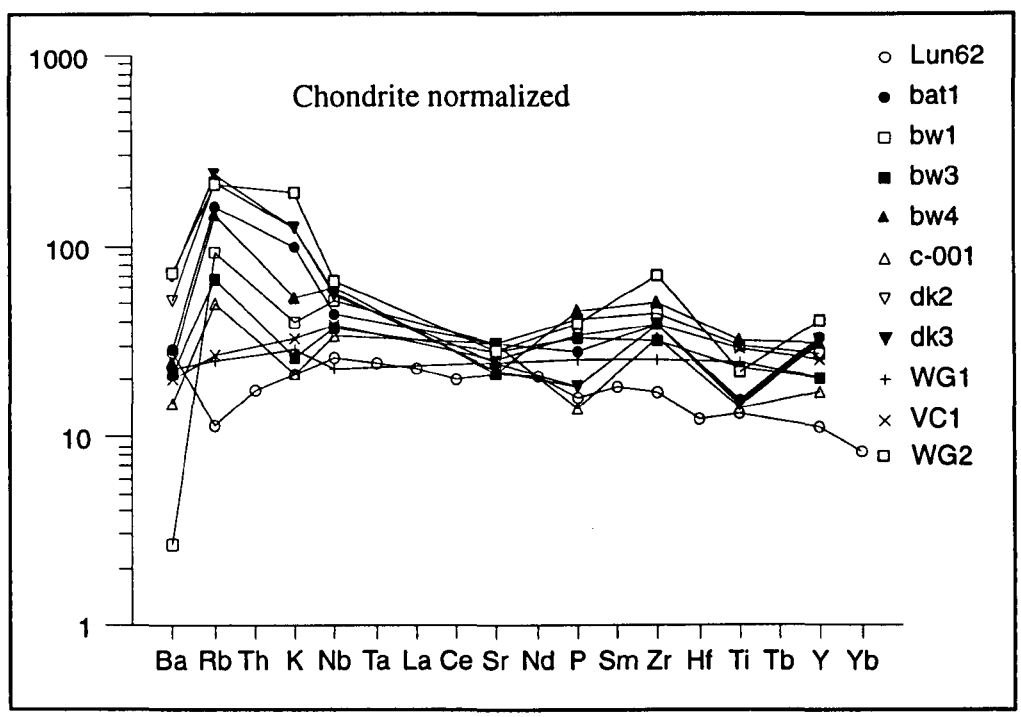

Figure 4.14: Trace element composition of dolerite dykes from Lundy Island.
Values for Lun 62 aretaken from Thorpe and Tindle (1992) and represent their most primitive basalt. All dyke plots are normalized to the chondritic model of Thompson (1982), although Rb, K and P are from the chondrite and undepleted mantle data of Sun (1980). The order of elements is that recommended by Thompson (1982) and is indicative of increasing compatibility from left to right.

a)

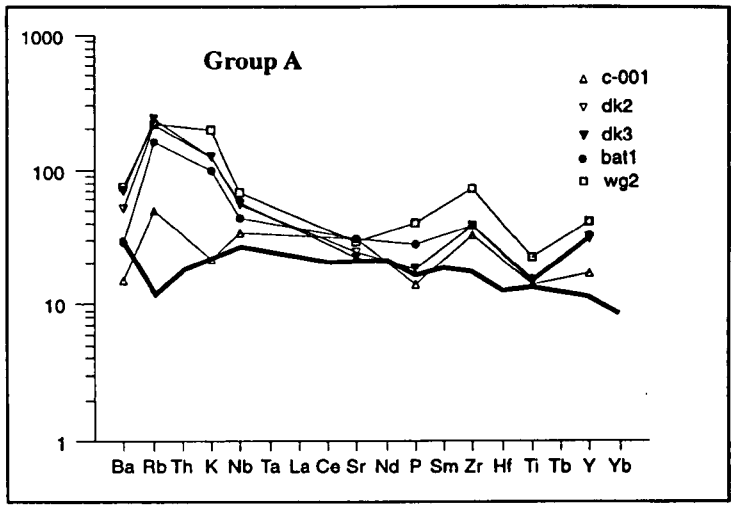

b)

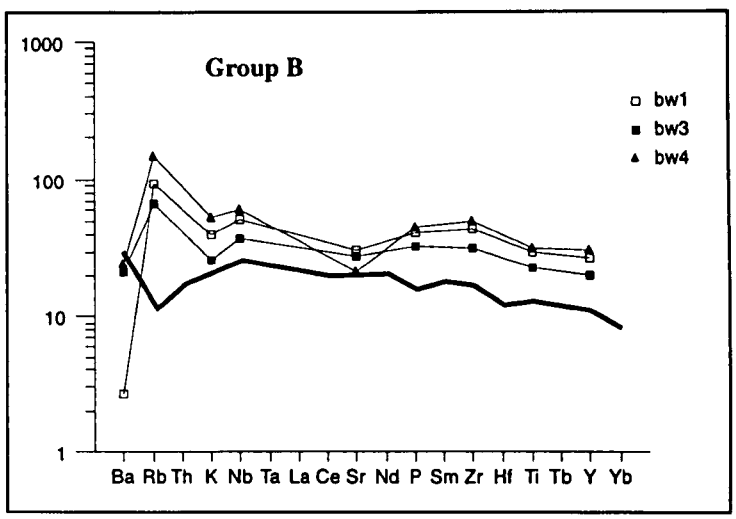

c)

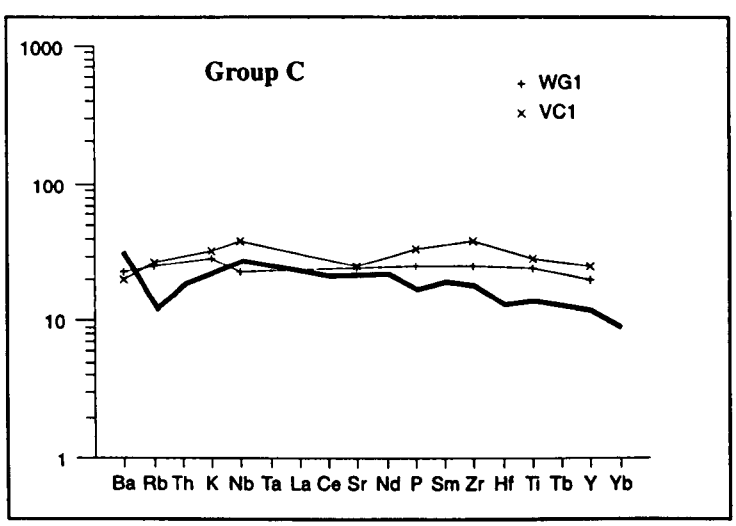

Figure 4.15: Spidergram plots of three sub-groups of dolerite dykes from Lundy Island. Data used in this diagram are taken from Figure 4.14 and chondrite normalized (Thompson, 1982). The solid black line in each sub-group represents the geochemical signature of LUN 62 (Thorpe and Tindle, 1992)

The second group has a gently negative sloping trend with K and Sr troughs and one low Ba value in BW1 (Figure 4.15b). The third group shows a relatively flat trend (Figure 4.15c), although only two samples fit this signature. The overall appearance of the spidergrams is hampered by the lack of REE data, but the variance between enriched patterns suggests possible divergence in chemical affinities for the Lundy dykes (e.g. high-TiO_2 and low-TiO_2 series, as seen in Figure 4.11). This pattern of trace element signatures is typical of within-plate tholeiites in continental flood basalt provinces (Basaltic Volcanism Study Project, 1981; Thompson *et al.*, 1983). However, Wilson (1993) argued caution against interpreting petrogenetic features where element mobility is uncertain. Cox and Hawkesworth (1985) also noted the importance of crustal contamination in modifying trace element signatures in derived basalts. It thus seems likely that most basic dyke compositions on Lundy have been modified by some degree of crustal contamination, crystal fractionation and weathering processes.

4.6.2 LEE BAY

The Lee Bay dolerites are typified by Figure 4.16, where spidergram plots define a trend similar to the third group on Lundy Island, but with significant Sr troughs and depletion of HREE and the HFS elements Zr, Ti and Y. A minor Sm trough is also distinctive. Although these rocks are more basic than their Lundy counterparts, they demonstrate enriched patterns relative to LUN 62 (Figure 4.17), the most primitive dyke on Lundy (Thorpe and Tindle, 1992).

Lee Bay dykes cannot, therefore, have been directly fractionated from the primitive Lundy magma, assuming that Lun 62 is close to the parental composition of that magma. The marked Sr trough is probably due to low pressure fractionation and preferential removal of plagioclase. Low Ba (relative to Lun 62, cf. Figure 4.17) probably reflects some mobility of low field strength elements in these moderately altered rocks. All samples from Lee Bay have similar trending spidergram patterns and so are genetically related to each other, but distinct from most of the Lundy dolerites.

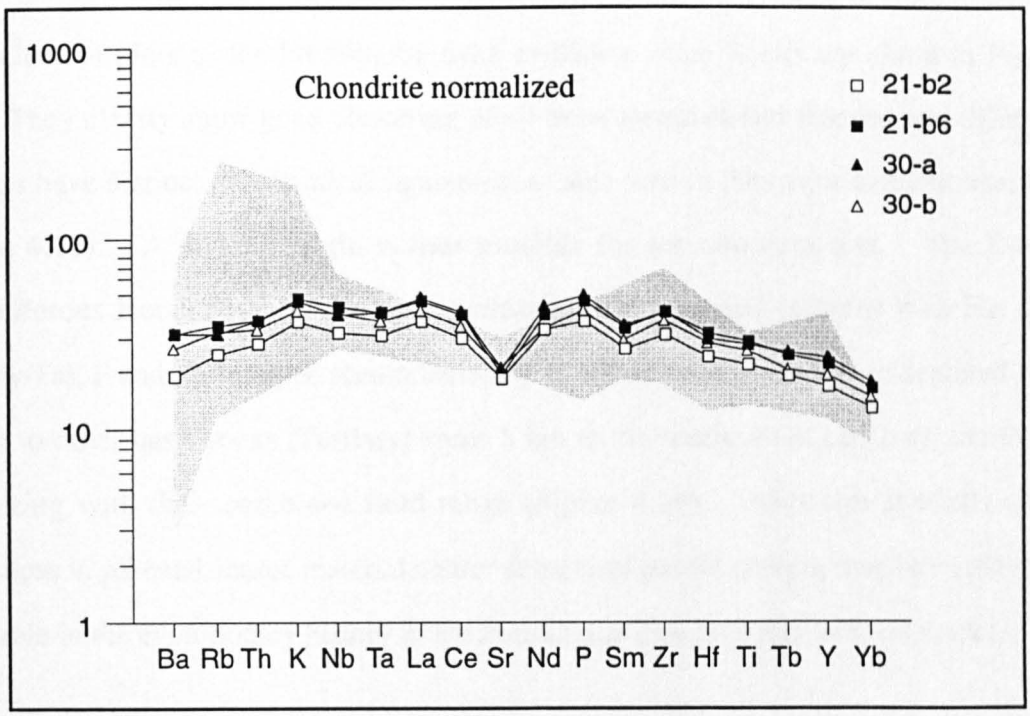

Figure 4.16: Trace element geochemistry of the Lee Bay doleritic dykes.
The shaded area represents the range of compositions from Lundy Island as shown in Figure 4.14. All data have been normalized to the chondritic model of Thompson (1982) and Sun (1980).

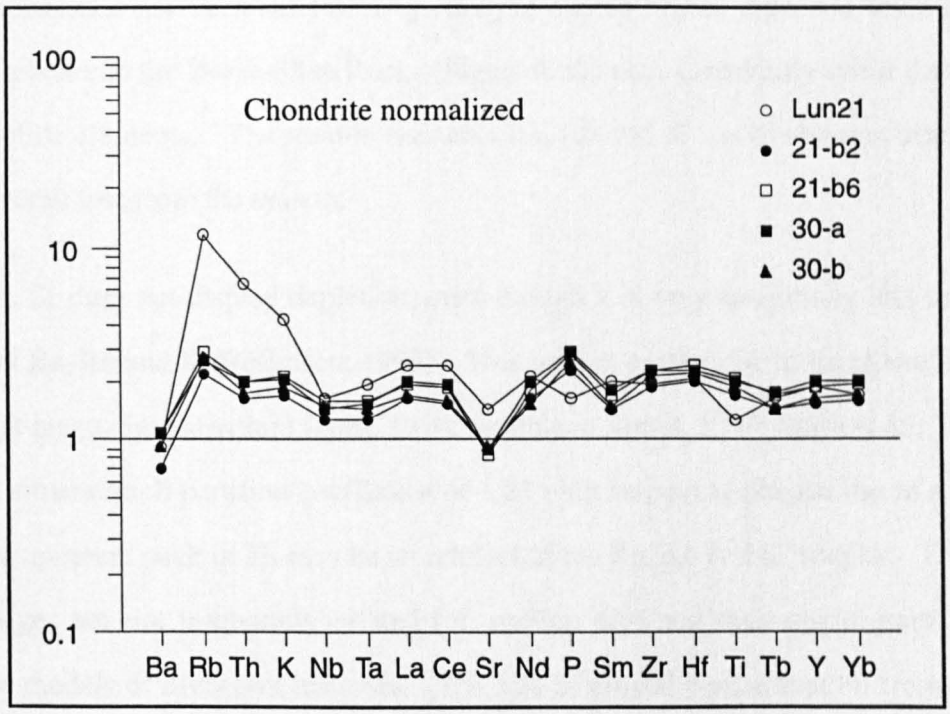

Figure 4.17: Data from Figure 4.16 normalized to Lun 62.
The composition of Lun 62 was postulated by Thorpe and Tindle (1992) as the most primitive dyke on Lundy Island. Lun 21 is the most evolved of the basic dykes sampled by Thorpe and Tindle (1992) and is included todemonstrate the range of dyke compositions on Lundy. All data normalized to Thompson (1982).

4.6.3 PERMO-CARBONIFEROUS ROCKS

Trace element plots of the Fremington dyke andHorse-Shoe Rocks are given in Figure 4.18. They clearly show good clustering of all trace elements and that the two different outcrops have distinct geochemical signatures, as also seen in the major element analyses (Figure 4.12). A diverse origin is thus possible for the two data sets. The Lower Carboniferous Horse-Shoe Rocks have decreasing trace element patterns with Nb (and possibly Ta), P and Th troughs, accompanied by K and Sr peaks. These are depleted with respect to other basic rocks (Tertiary) some 5 km to the southeast at Lee Bay, markedly contrasting with their combined field range (Figure 4.19). Although spatially near, differences in parental source material and/or degrees of partial melting may have played a major role in the evolutionary history of the Fremington dyke and Horse-Shoe Rocks.

Alternatively, the data could indicate different degrees of fractionation from a common parent. The total data set may be too small to be more precise here. There is no overall depletion of the more mobile elements (Ba, Rb, K and Sr) and so weathering and alteration may have proceeded in a relatively closed system. By contrast, the Upper Carboniferous/Lower Permian Fremington dyke shows highly enriched trace element patterns relative to the Horse-Shoe Rocks (Figure 4.20) with a markedly linear decrease in the immobile elements. The mobile elements Ba, Rb and K have obvious troughs and reflect overall loss from the system.

However, Sr does not display depletion, even though it is only marginally less mobile in water that Ba, Rb and K (Rollinson, 1993). This may in part be due to incorporation of Sr within the plagioclase structure (Arth, 1976; Smith and Smith, 1976; Stille *et al.*, 1983), as Sr has a mineral/melt partition coefficient of 1.83 with respect to plagioclase in a basaltic melt. An apparent peak in Th may be an artefact of the Ba, Rb and K troughs. These two assemblages are not temporally related (cf. section 4.3) and their spidergram patterns reinforce models of divergent histories. The role of crustal contamination from the vast array of partially melted xenolithic inclusions in the Fremington dyke is unclear, but this is more likely to have more effect on the incompatible elements rather than the compatible mineral assemblage.

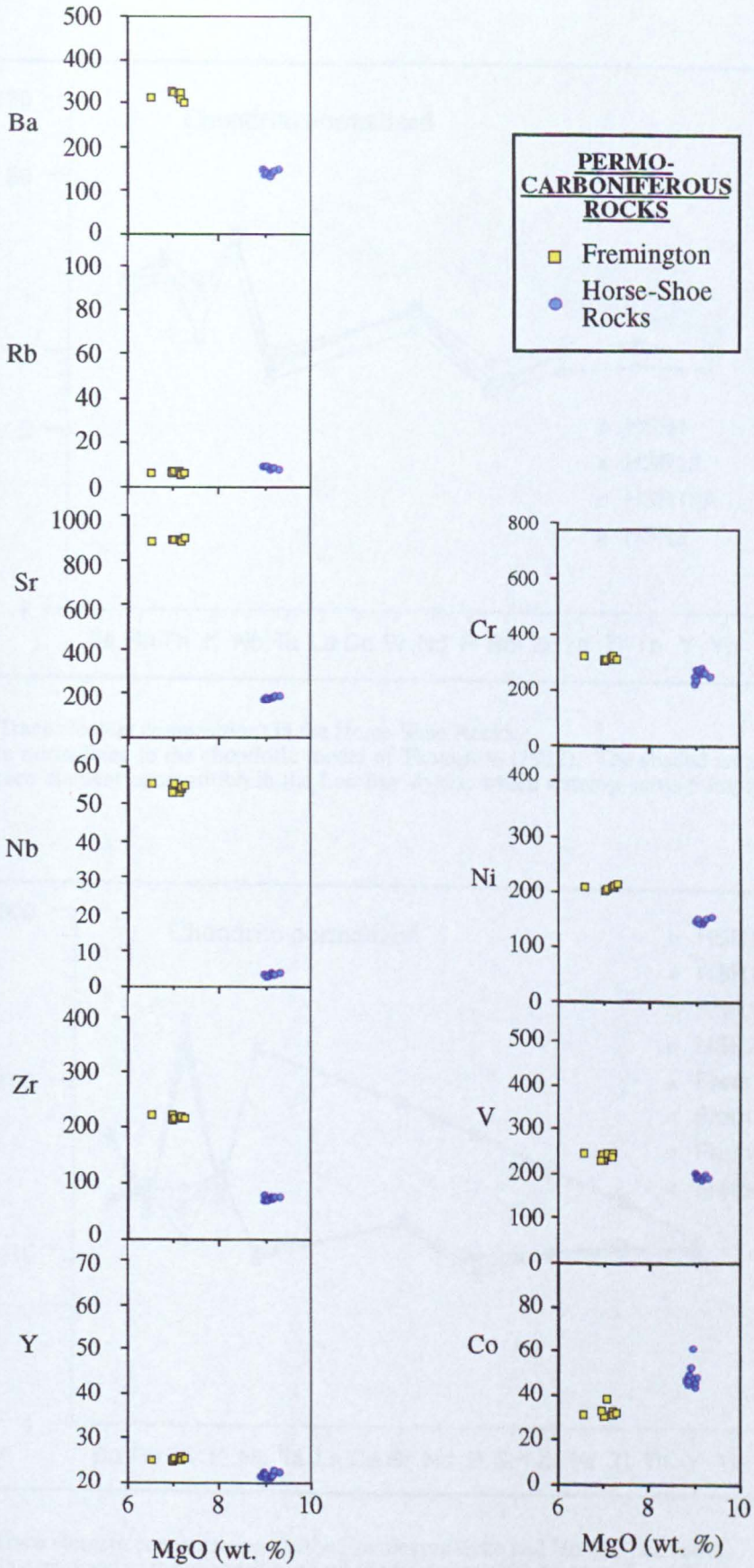

Figure 4.18: Trace element geochemistry in the Horse-Shoe Rocks and Fremington dyke. Petrogenetic relationships for these two data sets are not relevant in the context of this thesis, as the rocks are Permo-Carboniferous and hence not related to Tertiary magmatism (see sections 4.2.2.2 and 4.2.2.3). MgO content presented as dry wt.%.

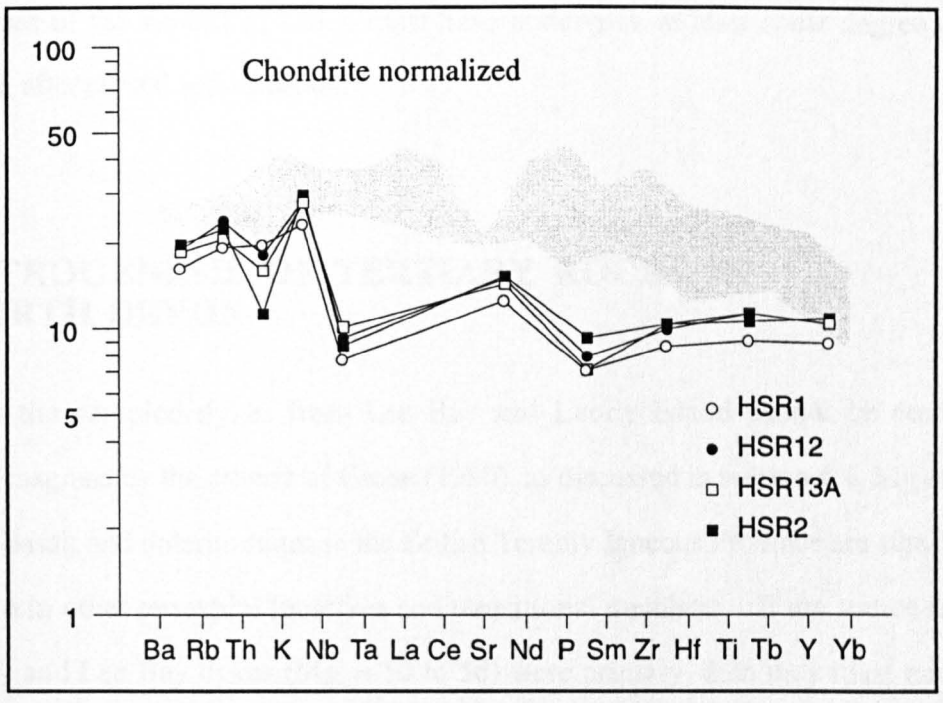

Figure 4.19: Trace element compositions in the Horse-Shoe Rocks.
Data have been normalized to the chondritic model of Thompson (1982). The shaded area represents the range of trace element composition in the Lee Bay dykes, which outcrop some 5 km towards the south-east.

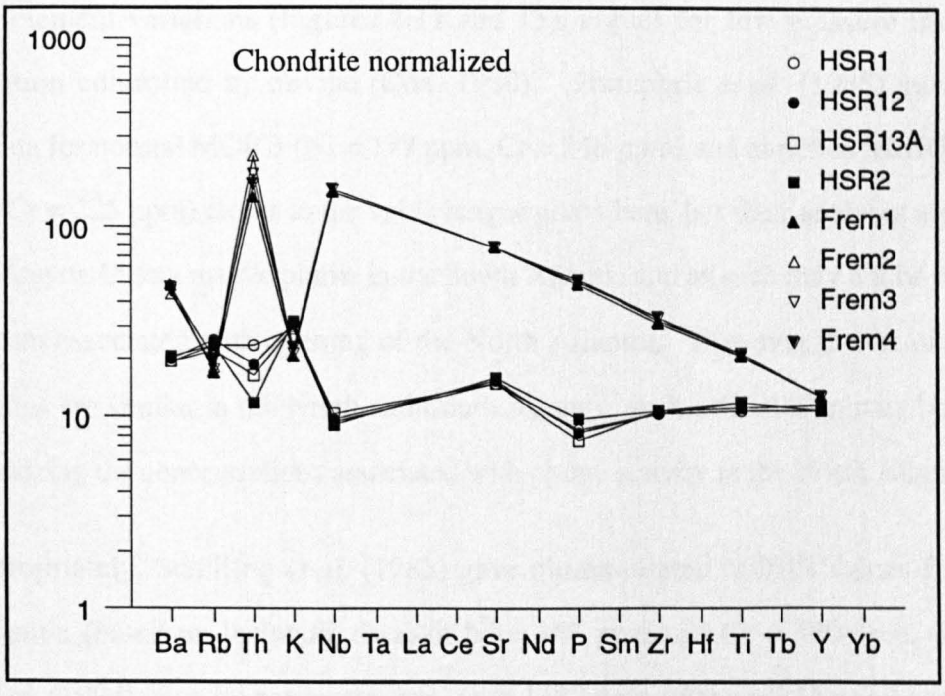

Figure 4.20: Trace element concentrations in the Fremington dyke and Horse-Shoe rocks.
Data have been normalized to the chondritic model of Thompson (1982). Note the difference in scale of the Y-axis compared to Figure 4.19

The evidence for this conclusion comes from the observation of partially melted buchites in the matrices of the xenoliths, which must have undergone at least some degree of fluid interaction after crystal solidification.

4.6 PETROGENESIS OF TERTIARY ROCKS IN NORTH DEVON

Although the sampled dykes from Lee Bay and Lundy Island cannot be considered primitive magmas by the criteria of Green (1980), as discussed in section 4.4, Mg numbers (Mg') for basalt and dolerite suites in the British Tertiary Igneous Province are significantly lower than in other terrestrial tholeiites and transitional members. If the source magmas for Lundy and Lee Bay dykes (Mg' = 30 to 56) were primary, then they must have been generated from mantle material more Fe-rich than normal MORB/OIB source regions (Cox, 1980; Basaltic Volcanism Study Project, 1981). The low range of Ni and Cr values (21-106 ppm and 34-216 ppm respectively), combined with linear relationships in both major and trace element variations (Figures 4.11 and 13), argues for low pressure fractional crystallization controlled by olivine (Cox, 1980). Humphris *et al.* (1985) gave trace element data for normal MORB (Ni = 177 ppm, Cr = 346 ppm) and enriched MORB (Ni = 132 ppm, Cr = 225 ppm) closer to the value ranges given here, but their analyses are based on the Tristan da Cuhna mantle plume in the South Atlantic and as such may not be relevant to volcanism associated with opening of the North Atlantic. However if overall mantle compositions are similar in the North and South Atlantic, such information may be useful in hypothesizing the concentrations associated with plume activity in the North Atlantic.

More appropriately, Schilling *et al.* (1983) gave plume-related MORB values from the North Atlantic (based on Icelandic data) of Ni = 143 ppm and Cr = 330 ppm, whereas Larsen *et al.* (1994) gave Ni concentrations up to 1487 ppm (mean = 246 ppm) and Cr up to 1694 ppm (mean = 665 ppm) from site 917 (ODP leg 152) situated between Greenland and Iceland. The major question, then, in terms of geochemistry is the relative contribution of the lithospheric mantle and asthenosphere to Lundy Volcano (with or without crustal contamination processes).

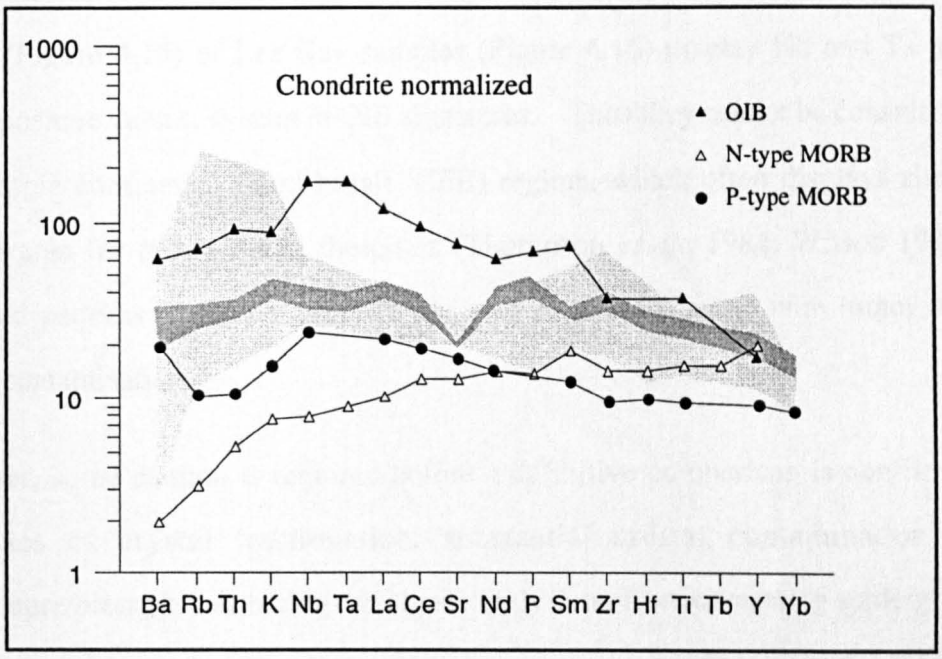

Figure 4.21: Comparative spidergram plot for different tectonic settings.
Average trace element concentrations in OIB are from Sun (1980), in N-type MORB from Saunders and Tarney (1984) and in P-type MORB from Schilling *et al.* (1983). The dark shaded area represents the range of values from Lee Bay, whereas the light shaded area represents the range of trace element concentrations from Lundy Island.

The absence of xenoliths from the continental lithospheric mantle within host rocks on Lundy is problematical in that the precise nature and chemical composition of the base of the lithosphere is uncertain within the outer Bristol Channel area, and indeed thoughout most of Southern Britain.

The Tertiary suite of rocks analysed here are situated between typical OIB and P-type MORB signatures (Figure 4.21), contrasting noticeably with N-type MORB patterns (Sun, 1980; Wilson, 1993). None of the spidergram patterns for the three dyke groups from Lundy (Figure 4.15) or Lee Bay samples (Figure 4.16) display Nb and Ta peaks and HREE positive values, as seen in OIB signatures. Thus they cannot be considered as part of a simple continental flood basalt (CFB) regime, which often displays similarity to spidergrams for ocean-island tholeiites (Thompson *et al.*, 1984; Wilson 1993). The observed patterns fit most closely to plume-related magmatism with minor degrees of crustal contamination.

However, some caution is required before a definitive comparison is confirmed. The processes of crystal fractionation, substantial crustal contamination and low temperature/pressure weathering can significantly deter from comparing spidergram trends, when one trend may be altered enough to be make a comparison invalid. It follows that LUN 62, the most primitive dolerite sampled by Thorpe and Tindle (1992), might be closest to a primary composition but it is still inconclusive whether this would support or disprove a plume-related magmatism model.

Nevertheless, further evidence for plume-driven magmatism is given by Zr/Nb ratios of ~ 15, K/Rb = 180-400, K/Ba = 27-37, La/Sm = 2.2 and La/Ce = 0.46 (Figures 4.22 and 4.23). Additionally, Schilling *et al.* (1983) define La/Sm ratios > 1.0 as indicating P-type MORB volcanism from data along the Mid-Atlantic Ridge between Lat. 25°N and 75°N. Both Humphris and Thompson (1983) and Schilling *et al.* (1983) deduce coherent La/Ce ratios of 0.43 from different data sets in the North Atlantic and hypothesize that this reflects a MORB mantle composition. Tertiary volcanism in North Devon thus appears to be more closely aligned with plume-related magmatism as opposed to conventional mid-ocean ridge activity.

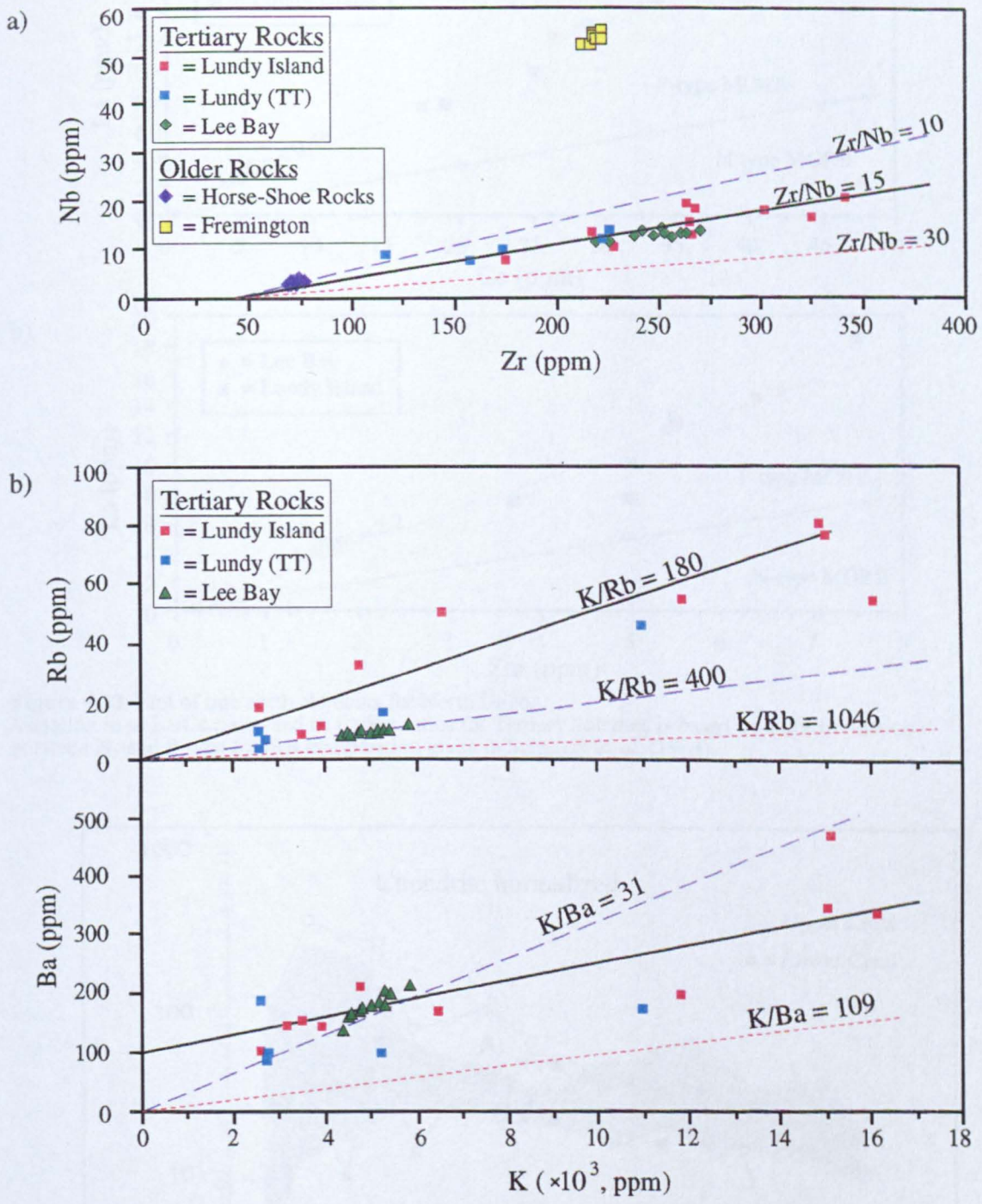

Figure 4.22: MORB discrimination diagrams for trace element data.
The dashed blue lines represent average P-type MORB composition, whereas the dashed red lines indicate typical N-type MORB composition (after Rollinson, 1993). Rhyolites and granites are not included in in these diagrams. a) Data are plotted following the style of Woods *et al.* (1979). Both Lundy and Lee Bay basic dykes have Zr/Nb ratios around 15. b) Data are plotted following recommendations of the Basaltic Volcanism Study Project (1981). Here, Lundy dolerites have K/Rb and Ba/K ratios around 180 and 80 respectively, whereas Lee Bay dolerites have K/Rb and K/Ba ratios around 400 and 30.

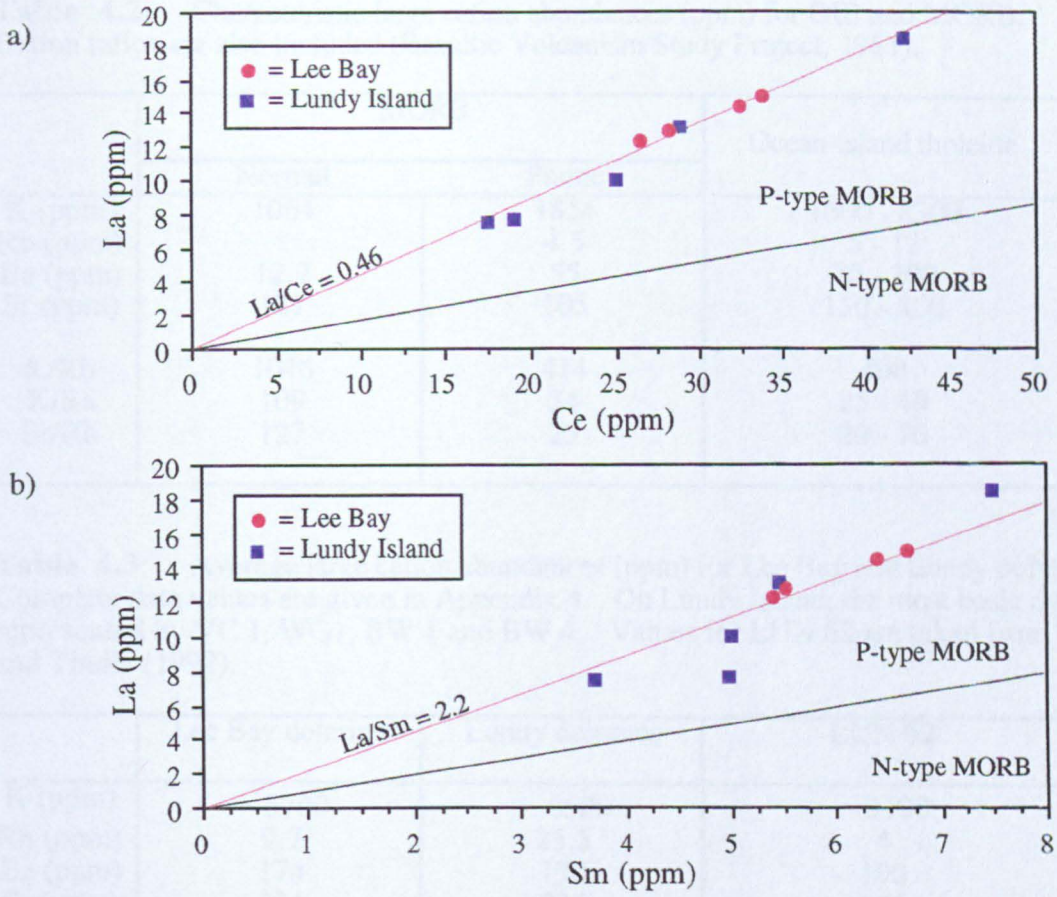

Figure 4.23: Plot of rare earth elements for North Devon.
Variaiton in a) La/Ce ratios and b) La/Sm ratios for Tertiary dolerites is based on a discrimination between N- and P-type MORB composition given in Schilling *et al.* (1983).

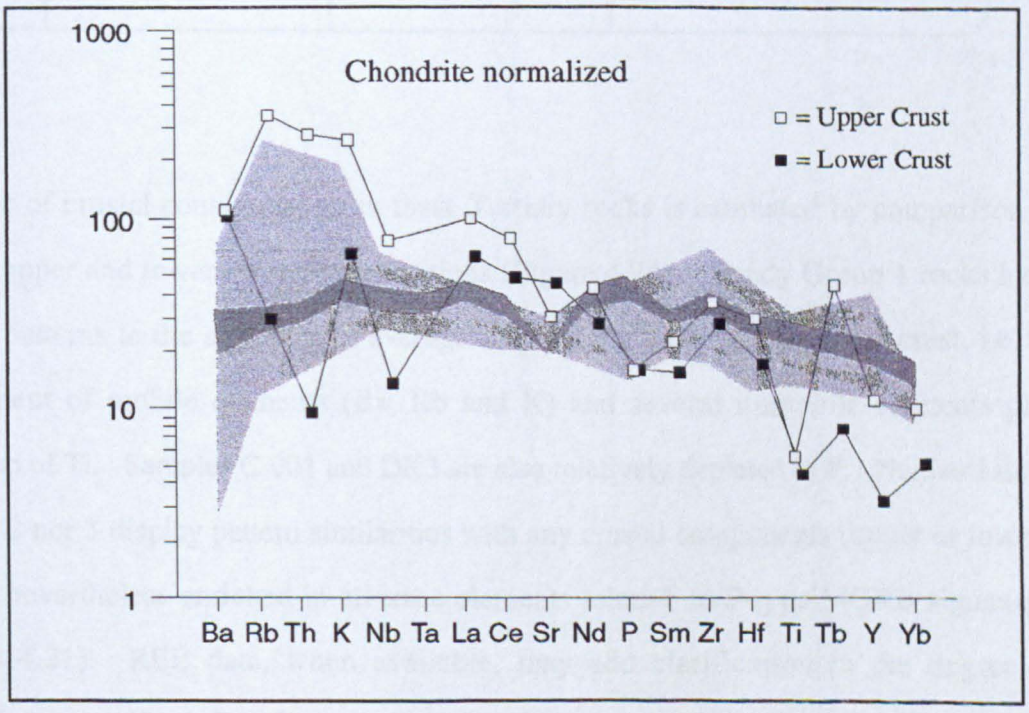

Figure 4.24: Continental crustal composition.
Trace element compositions for the upper continental crust from Taylor and McLennan (1981) and lower continental crust from Weaver and Tarney (1984). The dark shaded area represents Lec Bay dykes, whereas the light shaded area represents Lundy dolerites.

Table 4.2: Characteristic large cation abundances (ppm) for OIB and MORB. Cation ratios are also included (Basaltic Volcanism Study Project, 1981).

	MORB		Ocean-island tholeiite
	Normal	Plume	
K (ppm)	1064	1854	1600 - 8300
Rb (ppm)	1	4.5	5 - 12
Ba (ppm)	12.2	55	70 - 200
Sr (ppm)	127	105	150 - 400
K/Rb	1046	414	400
K/Ba	109	34	25 - 40
Sr/Rb	127	23	20 - 70

Table 4.3: Average large cation abundances (ppm) for Lee Bay and Lundy dolerites. Complete data values are given in Appendix 4. On Lundy Island, the most basic dykes are represented by VC 1, WG1, BW 1 and BW 4. Values for LUN 62 are taken from Thorpe and Tindle (1992).

	Lee Bay dolerites	Lundy dolerites	LUN 62
K (ppm)	~ 5700	~ 4500	~ 3100
Rb (ppm)	9.7	25.5	4
Ba (ppm)	174	170	190
Sr (ppm)	221	286	256
K/Rb	590	186	775
K/Ba	33	27	12
Sr/Rb	23	12	64

The role of crustal contamination in these Tertiary rocks is estimated by comparison to typical upper and lower crustal compositions (Figure 4.24). Lundy Group 1 rocks have similar patterns to the signature of average amphibolite facies of the upper crust, i.e. an enrichment of mobile elements (Ba, Rb and K) and several immobile elements plus depletion of Ti. Samples C-001 and DK3 are also relatively depleted in P. Neither Lundy Groups 2 nor 3 display pattern similarities with any crustal components (upper or lower), but are nevertheless enriched in all trace elements relative to P-type MORB signatures (Figure 4.21). REE data, when available, may add clarification to the degree of contamination. A puzzling feature of all three Groups is the lack of a significant Nb (and Ta) trough, which is a distinctive signature for all primitive basaltic magmas contaminated by crustal rocks (Thompson *et al.*, 1983; Wilson, 1993). This may simply be a function

of low Nb and Ta concentrations in basement rocks within the study area or low percentages (< 2%) of assimilation by the scavenging magmas.

This indicates that either magmas have not been modified by bulk assimilation (or have low degrees of contamination) or that the lower crust in the Lundy area is not typically granulite facies composition. In the former case, parent magmas must be slightly enriched relative to average P-type MORB compositions, which could imply enrichment of the mantle beneath Lundy. The near flat profiles of Groups 2 and 3 are more akin to primary magma signatures (Figure 4.21) than crustal components (Figure 4.24), which argues against significant crustal contamination in these dykes. Low Ba can be explained by element mobility and low Sr by crystal fractionation. In the latter case, there is scant geochemical data on deep rocks from the outer Bristol Channel.

Meissner *et al.* (1986) indicate that the thickness of the crust in the Lundy - Lee Bay area is between 27 and 30 km, although the precise composition and nature of the crystalline basement is uncertain. Nevertheless, granulite and amphibolite facies are probably appropriate as bulk models for the lower and upper crust in the vicinity of Lundy, even though detailed trace element composition may vary from that proposed from crustal averages (Taylor and McLennan, 1981; Weaver and Tarney, 1984). The relevance of these two contrasting facies to the geochemical analyses presented here is that the presence of a recognized spidergram pattern (Figure 4.24) in such analyses might signify the presence of either granulite or amphibolite facies at depth beneath the Bristol Channel. However, geochemical data presented here does not categorically signify an influence from either facies.

Lee Bay rocks most obviously display a close genetic relationship to Lundy Group 3 composition. The absence of a Nb-Ta trough is again indicative of minimal crustal contamination and suggests that fractional crystallization has proceeded without associated assimilation. Indicators of laminar flow within the narrow dykes and the presence of multiple injection phases are also corroborative evidence against excessive contamination. A dominant Sr trough probably indicates fractionation of plagioclase, as discussed earlier. Geochemical modelling would help to put constraints on amount of contamination

involved, but there is insufficient data here to provide accurate estimates.

The variations in bulk geochemical composition, possible degrees of contamination and trace element signatures is indicative of discrete and distinct magma storage bodies (from a common source) at different levels below the surface of the postulated Lundy Volcano, rather than indicating separate sources. For example, the Si-oversaturated and Si-undersaturated rocks on Lundy were probably not derived from each other, but crystallized separately in different magma chambers. Some of the magmas chambers may have equilibrated at shallow depths in the upper crust before dyke injection, whereas some magmas were more likely to have been generated at great depth and to have moved quickly upwards through the crust without significant contamination. Huppert and Sparks (1985) suggest that intrusions < 3 m in width are emplaced by laminar flow and have minimal wall-rock interaction, as opposed to the significant wall-rock interaction of dykes > 3 m thickness, emplaced during turbulent flow.

Higher level magma chambers were probably long-lived and underwent AFC processes, because they display more crustal contamination than the other two groups, e.g. those associated with Group 1 dykes on Lundy. Deeper storage bodies may have been less mature and more mobile, resulting in less modification as they ascended through the crust (e.g. Group 3 dykes on Lundy, cf. section 4.6.1). It is possible that some magmas were stored at more than one depth in the crust before emplacement at shallow depths. The variation in geochemical composition is more typical of Rayleigh melting in the upper mantle than of simple batch melting.

The form and morphology of Lundy volcano cannot be modelled on geochemical evidence alone. If Lundy was a central or composite volcano (Thorpe and Tindle, 1992) with either fissure or pipe eruptions, the remnants of a large magma chamber may still be present below the sea floor. On the other hand, if Lundy was more part of a complex of volcanoes (Walker, 1993), where several separate edifices and cone structures were supplied by feeder dykes, there may be evidence of more than one magma chamber in the region. Such models can be determined by the geophysical modelling of regional gravity and magnetic data and this will be the function of Chapter 5.

CHAPTER 5

MODELLING OF REGIONAL GEOPHYSICAL DATA

5.1 INTRODUCTION

Potential field data in the form of ASCII data files of regional aeromagnetic and gravity surveys were made available for processing by BGS, as described in section 2.3.1. Although there have been previous attempts at qualitative and semi-quantitative interpretations of derived anomaly maps, detailed interpretation of the deep geological structure remains difficult to establish, due in part to the lack of definitive borehole control or Precambrian and Lower Palaeozoic outcrop development south of the Pembrokeshire coastline.

Whilst earlier researchers have considered some of the geophysical evidence with specific reference to Tertiary magmatism (Brooks and Thompson, 1973), no attempt has previously been made to explain and correlate aeromagnetic and gravity information together into a coherent model of Tertiary magmatic activity. Although no new original regional survey work was completed as part of this study, this chapter assesses the strength of published geophysical contour maps and presents new models of sub-surface geology based on computer modelling of geophysical information.

5.2 REGIONAL MAGNETIC DATA

Aeromagnetic surveys have the advantage of being able to sample both relatively deep and shallow features, but the limiting depth of penetration is determined by distance between magnetic source and aeroplane as well as flight line separation. As a result, deeper sources of magnetism tend to have relatively low amplitudes and longer wavelengths than shallow sources, and vice versa. Spector and Grant (1970) introduced a technique whereby the

log-power spectrum of a magnetic anomaly is computed and the depth to the source determined mathematically from an assumed linear gradient.

Although such examples of spectral analysis can provide rapid depth estimates of anomalies (Kearey and Brooks, 1993), original data sets should ideally be regularly gridded and the magnetic source should similarly possess relatively high susceptibility values so that concealed anomalies can be reasonably extracted from within a given waveform. Such a technique is not always appropriate or unambiguous, but is useful in certain circumstances. This section assesses the confidence limits and accuracy of both supplied aeromagnetic data and published contour maps and finally introduces new, detailed magnetic anomaly contour maps for the Morte Point and Lundy areas to supplement existing contour maps published by Burley (1979) and Brown (1980a).

5.2.1 DATA REDUCTION

Corrections for diurnal drift have been estimated relative to absolute observations performed at Hartland Observatory on the mainland, approximately 20 km south-southwest of Lundy Island, throughout the survey period (pers. comm. David Barraclough, BGS). As these were applied during the period of the original flight-lines, no further corrections for drift were required. Magnetic anomaly values were calculated after the application of a geomagnetic correction based on a linear reference field for the British Isles, derived from the International Geomagnetic Reference Field (IGRF) and interpreted as an increase in total force of 2.17 nT km^{-1} northwards and 0.26 nT km^{-1} westwards.

The IGRF is a mathematical representation of the Earth's main magnetic field due to sources in the core, so a fundamental assumption of geomagnetic modelling maintains that the IGRF is accurately described by the core field. Over large distances (greater than 500 km) the reference field is non-linear, but broadly linear over smaller distances (Peddie, 1983) and so the applied geomagnetic correction is assumed to be accurate. Similarly, secular variation in the main field has not had any significant effect in derivation of magnetic anomalies. The base datum used was that of the British National Grid origin, which had an absolute value of 47 903 nT in 1961 (Burley, 1979) and all magnetic data have been reduced relative to that position.

An unquantified potential source of error in airborne magnetic surveys is the field of the aeroplane itself producing unwanted noise. The standard procedure is to obtain passive compensation by using 3-axis coil systems to correct for the induced and permanent fields of the aircraft. The accuracy of such methods is variable and some erratic error may be smoothed by subsequent software processing (Dobrin and Savit, 1988). The extent to which this was a factor during the data gathering stage in the original survey is uncertain, but was estimated by monitoring values along tie lines (pers. comm. David Barraclough, BGS) with the conclusion that the aeroplane did not have any significantly distorting effect on measured aeromagnetic anomalies.

Breiner (1973) described a simple method of profile smoothing, the three points weighted running average, to minimize spurious magnetic anomalies of very short wavelength, which are not related to geological artefacts. In this, the value at a given station (B) is first multiplied by 2, and then the values of the two adjacent stations (A and C) are added to give a localized sum total, which is divided by 4 to give the weighted mean of the original station (B). All regional magnetic data were re-processed using the three points weighted mean method to compensate for uncorrected noise from the aeroplane and for any possible short wavelength near-surface magnetic artefacts that could complicate sub-surface magnetic bodies.

After this method was applied, the difference between the original data set processed by BGS and magnetic data re-processed here was found to be < 1 nT for most of the surveyed area. Some areas of high magnetic relief, however, were found to have magnetic anomaly values up to 3 nT less than in the original data set. Despite this, both data sets were very similar and so a high degree of confidence can be given to the amplitude of derived magnetic anomalies, which are probably related to the sub-surface macro-geology rather than to artificial sources or very small geological bodies, e.g. 3 m wide basic dykes. The results of contoured data are presented in section 5.2.2.

5.2.2 AEROMAGNETIC ANOMALY MAP OF OUTER BRISTOL CHANNEL

Processed magnetic data were contoured using UNIRAS graphic software, in particular UNIMAP 2000, to produce an aeromagnetic anomaly map as seen in Figure 5.1. Interpolation using the maximum number of grid cells in the software package (200 along both X and Y axes) allowed detailed interpretation of the data set, whilst at the same time keeping artificial products of the modelling procedure to a minimum. A contour interval of 10 nT was chosen not only to produce enough relief to allow accurate definition of magnetic contours where magnetic relief was low, but also to prevent confusion of closely spaced magnetic contours in areas of high magnetic relief. A comparison with a simplified geological map of the region is also provided in Figure 5.1 to facilitate interpretation. Figures 5.2 and 5.3 give more detailed definition of magnetic anomalies at more closely spaced contour intervals.

The main feature of Figure 5.1 is that of a relatively gentle regional magnetic field with more intense magnetic anomalies to the west of Morte Point (Figure 5.2) and to the northwest of and near to Lundy Island (Figure 5.3). The background varies from around -20 to -30 nT along the northern margin of the Outer Bristol Channel to around -60 nT along a crude east-west trend passing through the North Devon coast at Hartland Point. Magnetic intensity in the Bristol Channel itself decreases from -30 nT in the mouth of the Channel in Bridgwater Bay ~ 130 km east of Lundy Island (Aeromagnetic Map, 1965) to below -150 nT north-west of Lundy Island and increasing back up to -100 nT further to the west near to the Western Approaches. Widely spaced contours within the Bristol Channel area could be the result of a sparse data set, but are more probably reflective of a relatively low level of magnetic interest within the bulk of the sub-surface geology where the Upper Palaeozoic and Mesozoic sedimentary pile is between 4 and 8 km in thickness. Higher levels of magnetic intensity are seen over land areas to the north-east on the Gower peninsula (peak +120 nT) and to the north in South Pembrokeshire/Carmarthenshire (peaks over +200 nT), but are not so well developed to the south-east over North Devon, where magnetic levels are between -60 and -100 nT.

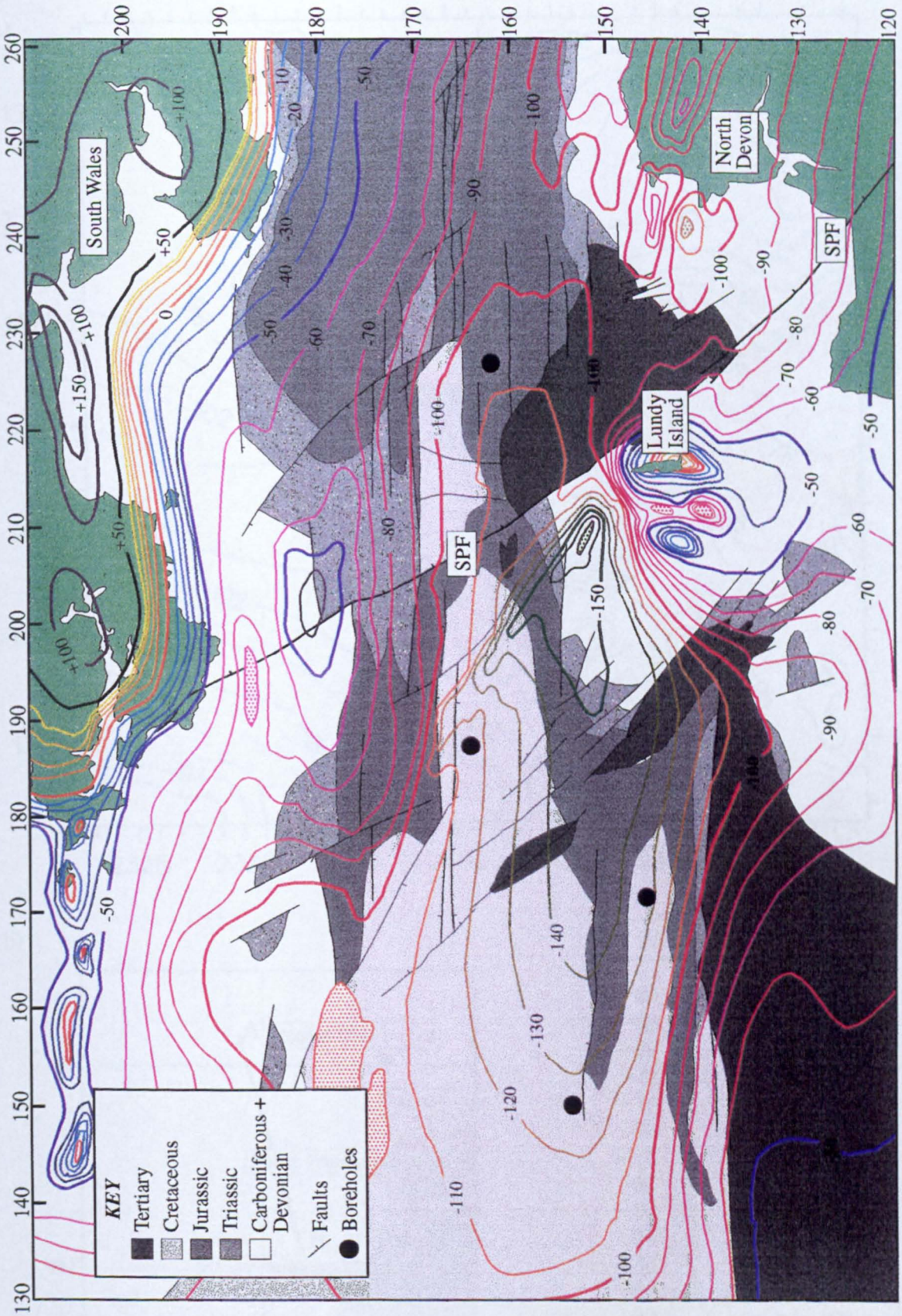

Figure 5.1: Magnetic anomaly map for the Outer Bristol Channel.
Contour units are nanoteslas. and units along the X and Y axes are km from the British National Grid (BNG). Land areas in North Devon and South Wales are represented by filled green areas. Stippled areas represent magnetic lows. SPF represents the Sticklepath Fault. Only representative boreholes given by Kammerling (1979) are included to avoid obscuring underlying geology.

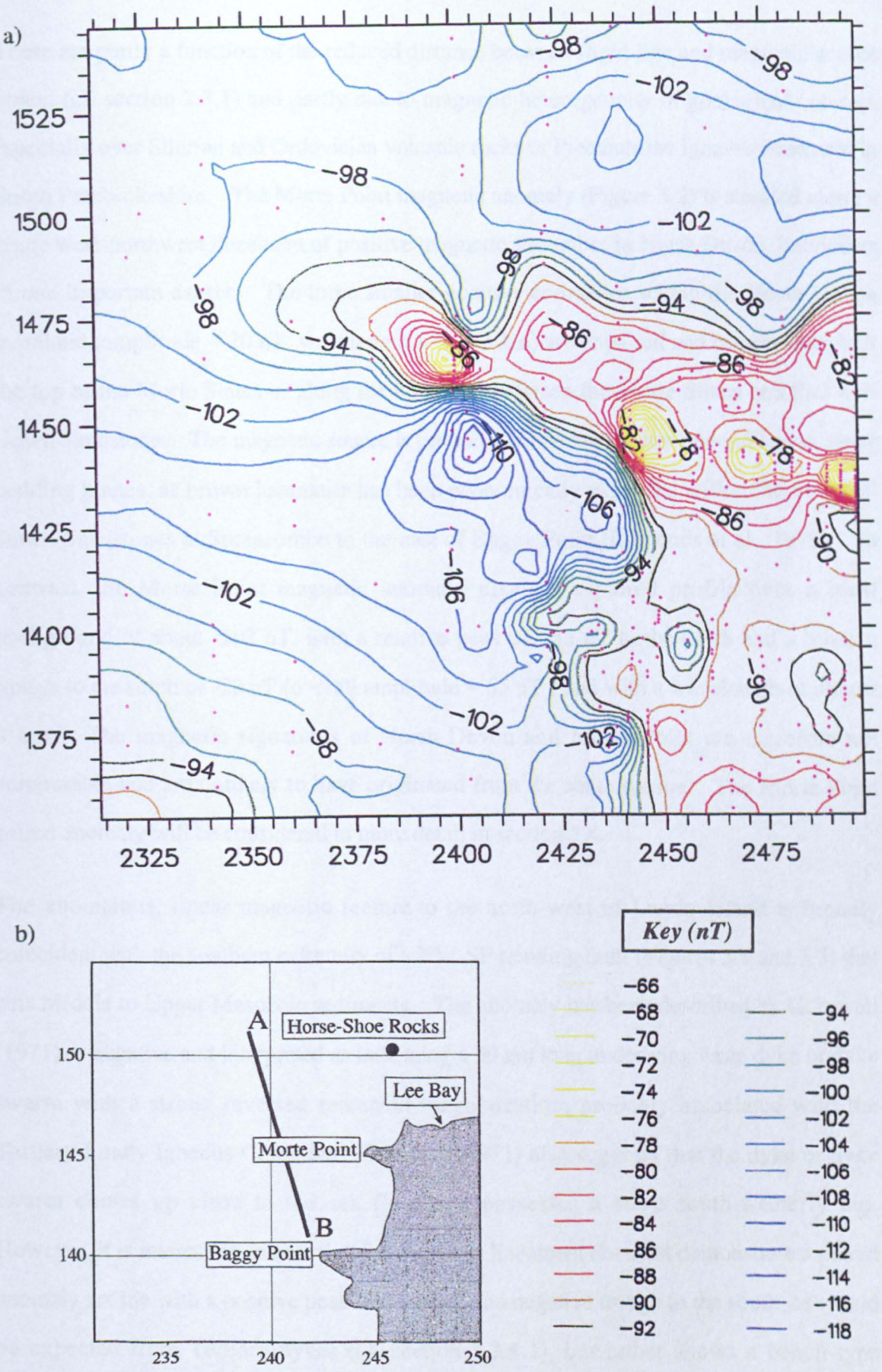

Figure 5.2: Magnetic anomaly map for the Morte Point area.
a) Notation along both axes indicates BNG references (x 10^2m) and original sample localities are given by dots. b) A location map is presented to aid the location of magnetic features. Anomaly units are in nanoteslas. The line AB is used for modelling procedures in section 5.4.1.1.

These are partly a function of the reduced distance between flight line and magnetic source object (cf. section 2.3.1) and partly due to magnetic heterogeneity in geological outcrop, especially over Silurian and Ordovician volcanic rocks or Precambrian igneous basement in South Pembrokeshire. The Morte Point magnetic anomaly (Figure 5.2) is situated along a crude west-northwest lineament of positive magnetic anomalies in North Devon, but differs in one important aspect. The three smaller positive anomalies within the North Devon mainland (amplitude ~ 20 nT; wavelength ~ 2 to 3 km) are unpaired and occur either near the top of the Morte Slates or along the boundary between the Morte Slates and Pickwell Down Sandstones. The magnetic source is probably connected to iron mineralisation along bedding planes, as brown haematite has been economically exploited within the Pickwell Down Sandstones at Spreacombe to the east of Baggy Point (Edmonds et al., 1979). In contrast, the Morte Point magnetic anomaly displays a paired profile over a local background of about -102 nT, with a relative peak of +35 nT to the north and a relative trough to the south of -20 nT (overall amplitude ≈ 55 nT;) and with a wavelength of almost 8 km. The magnetic signatures of North Devon and Morte Point are therefore not comparable and are unlikely to have originated from the same source. The Morte Point paired anomaly will be considered in more detail in section 5.4.

The anomalous, linear magnetic feature to the north-west of Lundy Island is broadly coincident with the southern extremity of a NW-SE trending fault (Figures 5.1 and 5.3) that cuts Middle to Upper Mesozoic sediments. The anomaly has been described by Cornwell (1971) as negative and interpreted as indicating a 30 km long underlying basic dyke or dyke swarm with a strong reversed remanent magnetization, probably associated with the Tertiary Lundy Igneous Complex. Cornwell (1971) also suggests that the dyke or dyke swarm comes up close to the sea floor and possesses a steep south-westerly dip. However, it is interesting to note that the magnetic lineament does not demonstrate a paired anomaly profile with a positive peak to the north and negative trough to the south, as would be expected from Tertiary dykes (cf. section 3.3.4.1), but rather shows a bench-type morphology (Figure 5.4) with a magnetic plateau to the north and magnetic floor to the south.

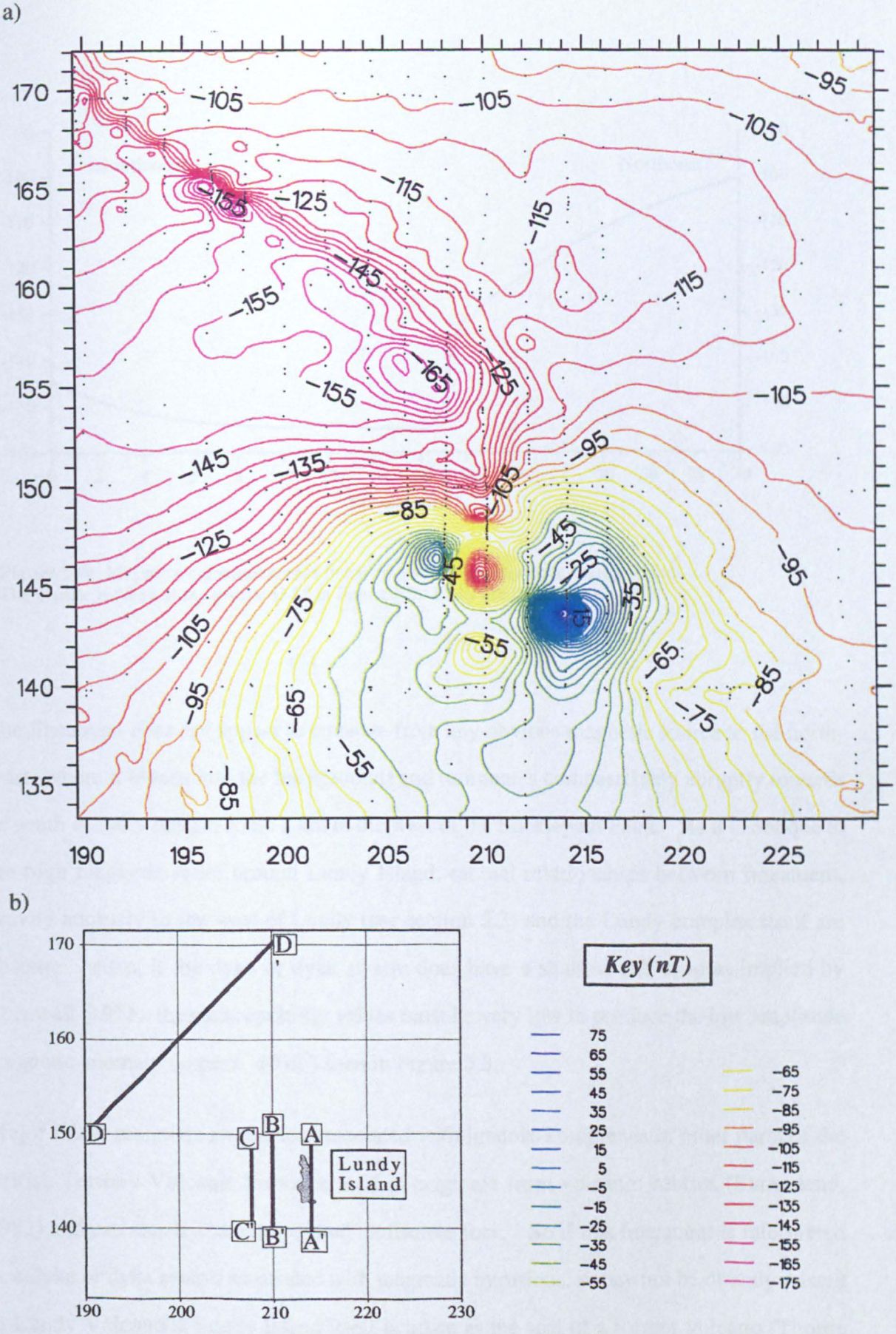

Figure 5.3: Magnetic anomaly map for the Lundy area.
a) Notation along both axes indicates BNG references (x 10^3m) and original sample localities are given by dots. b) A location map is presented to aid the location of magnetic features. Anomaly units are in nanoteslas. The lines A-A', B-B', C-C' and D-D' are for modelling procedures in section 5.4.1.2.

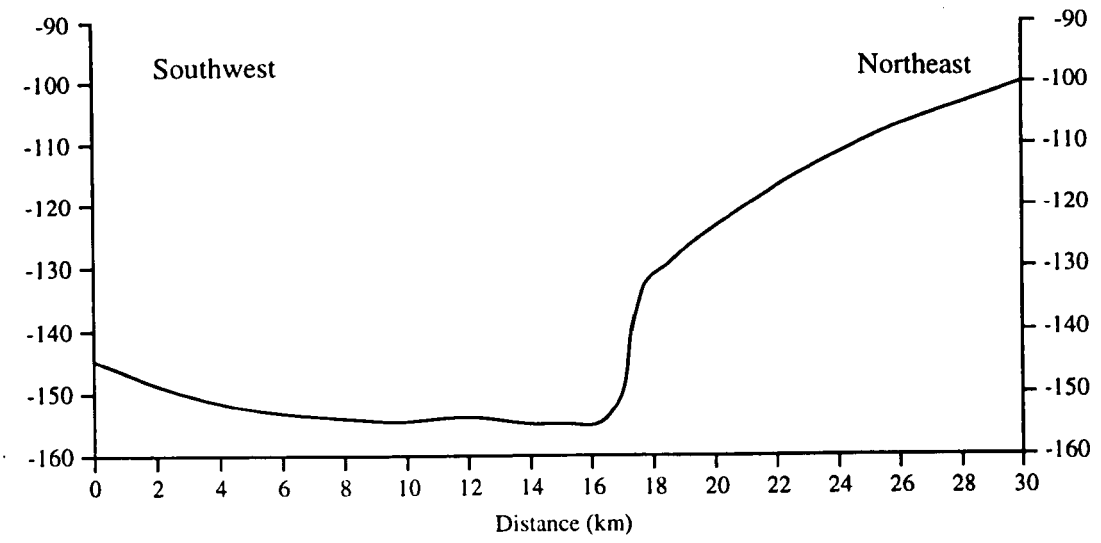

Figure 5.4: Magnetic signature across linear magnetic anomaly near Lundy Island. The profile is taken along profile D-D' in Figure 5.3. Units are in nanoteslas (nT).

The lineament does not appear to emanate from any obvious magnetic source to the north-west (where it blends into the background) and terminates comparatively abruptly towards its south-easterly margin some 3 km to the west of the Sticklepath Fault. As it is oblique to the high magnetic relief around Lundy Island, mutual relationships between lineament, gravity anomaly to the west of Lundy (see section 5.3) and the Lundy complex itself are obscure. Also, if the dyke or dyke swarm does have a shallow sub-crop as implied by Cornwell (1971), then susceptibility values must be very low to produce the low amplitude magnetic anomaly (approx. 40 nT) seen in Figure 5.3.

Major linear magnetic anomalies associated with igneous complexes in other parts of the British Tertiary Volcanic Province tend to originate from volcanic centres (Sutherland, 1982) and can usually be extrapolated to discrete foci. So if this lineament is interpreted as a dyke or dyke swarm associated with magmatic intrusions, it may not be directly related to Lundy Volcano if Lundy Island itself is taken as the seat of a former volcano (Thorpe and Tindle, 1992). The magnetic anomaly could alternatively be interpreted as the magnetic expression of a relatively deep normal fault within Palaeozoic and/or basement stratigraphy, downthrowing to the south and masked by overlying Mesozoic sediments.

These two hypotheses will be tested in section 5.4.

Circular magnetic anomalies to the west of and over the south-east corner of Lundy Island (Figure 5.3) have two types of anomaly patterns. Positive peaks of 95 nT (G.R. 2142 1439) and 4 nT (G.R. 2079 1465) occur over the south-east of the island and ~ 5 km to the west of the island respectively. As these are superimposed over a local background of approximately -55 nT, the relative amplitude of the peaks are 160 nT and 60 nT. A linear trend of 3 negative anomalies lies along easting grid line 210, approximately 2 - 3 km to the west of the island. Amplitudes relative to background are -32 nT, -90nT and -20nT.

Figure 5.5 displays the magnetic relief in contoured 2.5D format. Although indicating magnetic heterogeneity in the sub-surface geology, the precise form of the circular anomalies is influenced by both the method of drawing contours within UNIMAP 2000 and by the 2 km width of data collection lines. Thus, although the interpreted anomalies indicate a relative high degree of magnetic relief, more closely spaced data collection points will be required to define the precise shape of the anomalies more accurately. Nevertheless, section 5.4 will utilize these circular anomalies to model sub-surface geological features.

5.3 REGIONAL GRAVITY DATA

Although processed regional gravity data were made available by BGS (cf. section 2.3) with a Bouguer reduction density of 2.67 Mg m^{-3} used for marine gravity data, the raw data were re-processed to compare derived values in the original data set and determine possible sources of errors in the supplied gravity data. Errors in the regional compilation of published gravity data from individual surveys may result in variable errors, which in turn are a function of variability in data processing and/or the data gathering stage. The manipulation of uncorrected gravity station values provides an opportunity to reduce possible processing errors by disparate manipulation methodologies. A direct comparison between published Bouguer anomaly maps and the contoured results of re-processed data presented here can then be made.

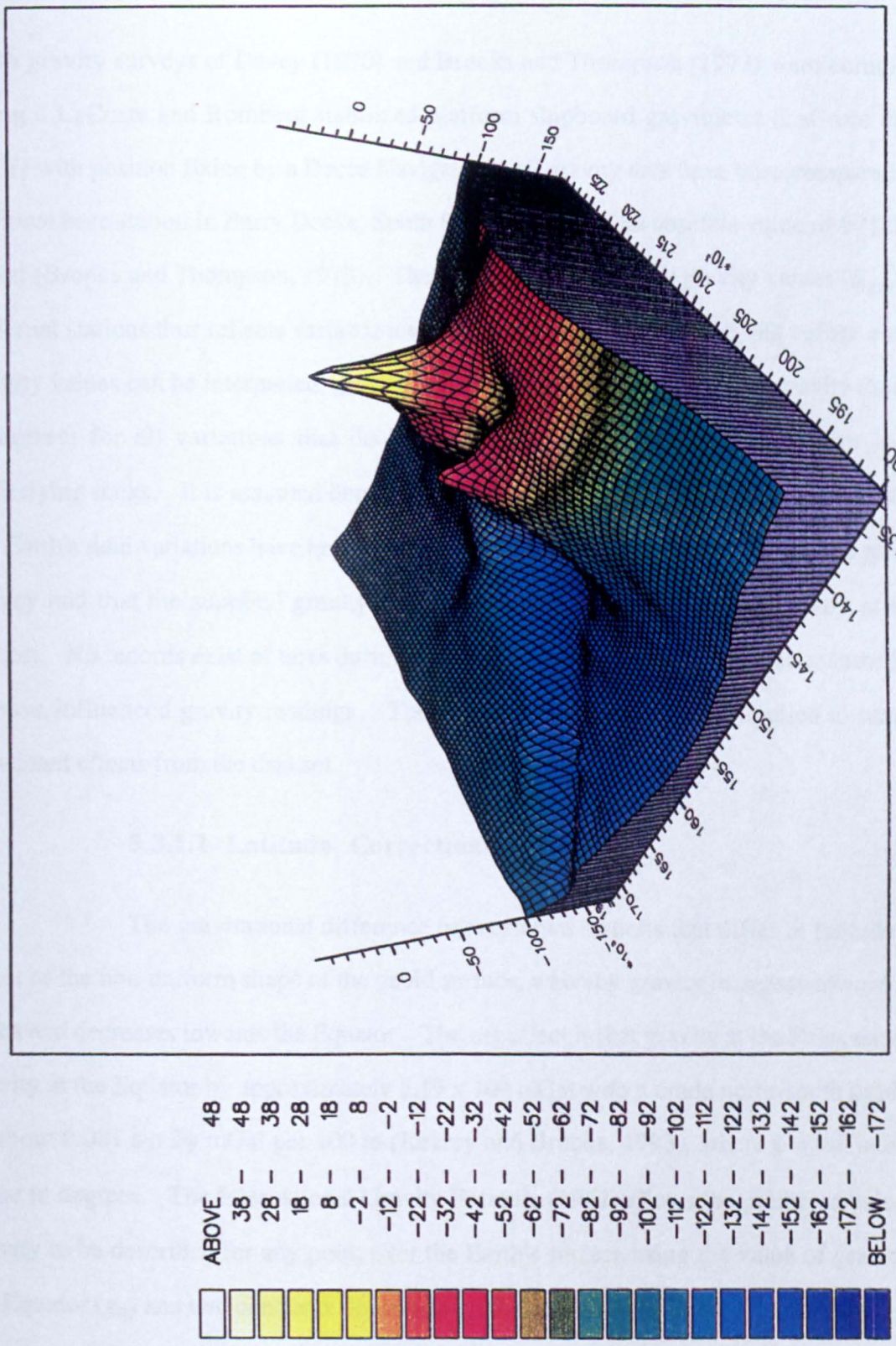

Figure 5.5: Magnetic anomalies in the Lundy area viewed towards the northeast.
Units along the base are BNG coordinates and the vertical axis indicates anomaly values in nanoteslas. The magnetic plateau in the Lundy horst with associated highs and lows can be seen to the south, whereas the bench-like form of the magnetic lineament (cf. Figure 5.4) extends to the northwest.

5.3.1 REDUCTION OF DATA

Both gravity surveys of Davey (1970) and Brooks and Thompson (1973) were completed using a LaCoste and Romberg stabilized platform shipboard gravimeter (LaCoste et al., 1967) with position fixing by a Decca Navigator. All gravity data have been compared to a regional base station in Barry Docks, South Glamorgan with an absolute value of 981202.3 mGal (Brooks and Thompson, 1973). The difference in observed gravity values (Δ_{grav}) at different stations thus reflects variance away from the base station value, but before overall gravity values can be interpreted, gravity reductions must be applied to the gravity data set to correct for all variations that do not originate from differences of density in the underlying rocks. It is assumed here that corrections for instrumental drift and effects of the Earth's tidal variations have been considered and remedied as part of the original gravity survey and that the supplied gravity data represent changes in observed gravity at each station. No records exist of tares during gravity surveying, but these are also assumed not to have influenced gravity readings. The following corrections were applied to remove unwanted effects from the data set.

5.3.1.1 Latitude Corrections

The gravitational difference between two stations that differ in latitude is a result of the non-uniform shape of the geoid surface, whereby gravity increases towards the Poles and decreases towards the Equator. The net effect is that gravity at the Poles exceeds gravity at the Equator by approximately 5.19 x 10^3 mGal with a crude north-south gradient of about 0.081 sin 2ϕ mGal per 100 m (Kearey and Brooks, 1993), where ϕ = the latitude value in degrees. The International Gravity Formula (1967) allows the predicted value of gravity to be described for any point over the Earth's surface using the value of gravity at the Equator (g_o) and two constants dependent on the speed and rotation of the Earth (k_1 and k_2), expressed as the relationship

$$g_\phi = g_o (1 + k_1 \sin^2\phi - k_2 \sin^2 2\phi) \qquad \text{equation 5.1}$$

where g_ϕ is the predicted gravity at latitude ϕ, g_o = 978 031.8 mGal (the value of gravity at the Equator), k_1 = 0.0053024 and k_2 = 0.0000059 (IAG, 1971). Mittermayer (1969)

proposed a modification to the constants of this formula to minimize errors from the truncation of pre-1967 gravity data sets, but Kearey and Brooks (1993) argued that this approach was contradicted if some data had been processed using the 1967 Gravity Formula. Latitude corrections have thus been calculated using equation 5.1.

The Outer Bristol Channel lies between latitudes 51° 00'N and 51° 35'N, which corresponds to possible latitude corrections of 0.07923 mGal per 100m to the south of the area and 0.07887 mGal per 100m to the north. Point location is accurate to ± 10 m and so there could be errors up to about ± 0.001 mGal in the corrected value of gravity at sea level for the whole study area when using equation 5.1.

5.3.1.2 Free-air Corrections

In the context of this thesis, the free-air correction (FAC) allows for a decrease in gravity with increasing height above sea level due to the increased distance to the centre of the Earth, as determined by Newtonian physics. To correct gravity values to a mean sea level datum, for observations taken at height h (in metres) above sea level

$$FAC = 0.3086h \text{ mGal} \qquad \text{equation 5.2}$$

As all observations were made by a ship-borne gravimeter by definition at sea level, the magnitude of the FAC should be constant over the whole survey area. The height of the gravimeter within the survey ship was an estimated 3 m above sea level and so the FAC was nominally calculated as 0.9258 mGal. Although this should be a standard value for the survey area, some variance would have been noted in the original survey as the relationship between sea level at the time of measurement and mean sea level is governed in part by the time and date of measurement, i.e. by the magnitude and effects of tides. This in turn would change the absolute height of the sea relative to sea bottom.

As such corrections are time dependent, the original FAC values supplied by BGS were used in re-calculating gravity data. The FAC has been calculated and applied at each station to give average errors in observed gravity of ± 0.03 mGal over the study area, assuming a possible 30 cm error in determination of height of the measurement platform

relative to mean sea level.

5.3.1.3 Bouguer Corrections

The Bouguer Correction (BC) is applied to remove the gravitational effect of material between the observation station and datum by approximating a rock layer (for cases above sea level) beneath each station to an unbounded horizontal slab with an assumed density of 2.70 Mg m^{-3} and thickness equal to the height of the station above sea level. However for marine gravity surveys, the BC compensates for the lack of rock between sea bottom and the datum by a replacement of the water layer by a given rock density, conventionally 2.67 Mg m^{-3} for marine surveys in which the correction will be positive and described by the relationship

$$BC = 0.2\pi G\,(\rho_r - \rho_w)z \ \text{mGal} \qquad \text{equation 5.3}$$

where G is the Gravitational Constant (6.67 x 10^{-11} m^3 kg^{-1} s^{-2}), ρ_r = 2.67 Mg m^{-3}, ρ_w is the density of sea water (approx. 1.03 Mg m^{-3}) and z = water depth (in metres). This translates to a correction of + 0.0432 mGal per metre depth. Errors in calculating the BC value could be derived from variance in sea water density and depth estimation (cf. 5.3.1.2), but are likely to be small, i.e. in the order of ± 0.006 mGal over most of the survey area.

5.3.1.4 Terrain Corrections

The Terrain Correction (TC) is always positive and normally applied to reduce the effects of topographic relief within the proximity of the gravimeter in terrestrial surveys because the BC makes an overall assumption that the terrain is flat, which is usually not the case over most areas of land. The sea surface is inherently flat under normal conditions in marine surveys and as such suggests that the TC need not be applied to marine surveys. The survey vessel itself will introduce a small terrain effect but as this is the same for each reading, it can be ignored. Similarly, as surveys were carried out under calm weather conditions, any possible terrain effect caused by marine swell can also be ignored. Variations in the sea bottom topography are more relevant in terms of possible effects on measured gravity readings. Although depth of water varies between about 25

and 95 m depth over the survey area, the method of calculating the BC has already considered depth of water (and hence sea bottom topography) and so terrain corrections have not been applied to gravity data here.

5.3.1.5 Eötvös Correction

The Eötvös Correction (EC) compensates for the centripetal acceleration generated by movement of the boat and this can either bolster or oppose gravity. The EC can be defined by the relationship

$$EC = 7.503V \sin\alpha \cos\phi + 0.04154\ V^2 \text{ mGal} \qquad \text{equation 5.4}$$

where V is the speed of the boat in knots, α is the heading of the boat in degrees and ϕ is the latitude of the observation station. Kearey and Brooks (1993) assert that at mid-latitudes, the EC is about + 7.5 mGal for each knot of east to west motion, thus the heading and absolute speed of the boat must be known to a high degree of precision. The Outer Bristol Channel is subject to considerable variations in strong tidal currents that effect both heading and speed measurements. Uncertainty in the EC is therefore difficult to quantify, but is likely to be the biggest source of error in determining gravity anomalies. As details of the speed and detailed heading of the survey vessel were not available for processing, it was not possible to recalculate the EC values. Nevertheless, the supplied BGS data set did contain EC values for each station and these have been adopted here. Dr. I. Smith (BGS, pers. comm.) estimates a possible error in gravity at each station due solely to the EC as ± 0.4 mGal.

5.3.2 BOUGUER ANOMALY MAP

Once all relevant corrections had been considered, the Bouguer Anomaly (BA) for each gravity station was determined from the relationship

$$BA = g_{obs} - g_{\phi} + FAC \pm BC + TC \pm EC \qquad \text{equation 5.5}$$

where g_{obs} is the measured gravity at the observation station. The survey area contained 5456 gravity stations (cf. section 2.3.1) which controlled the overall number of BA values available for contouring. The results from the data processing procedures indicated

minimal difference (< 0.5 mGal) between re-calculated gravity data presented here (Figure 5.6) and the original supplied gravity data from BGS (Figure 5.7). A great deal of confidence can consequently be attributed to the calculated BA values corrected to a mean sea level datum. A re-evaluation of the raw data was nevertheless justified to test the position of any gravity highs and to ascertain whether inferred positive anomalies were not simple artefacts of processing.

BA values were contoured at 2 mGal intervals to allow easy visual inspection using the UNIMAP 2000 software drawing package, as outlined in section 2.3.1. Figure 5.6 shows the results of contouring without any modification of re-processed data. The main features of the map are relatively high anomaly values to the south of the study area with lower anomaly east-west trending basins towards the east in the Middle Bristol Channel and west of Lundy Island in the Outer Bristol Channel. The gradient of both basins increases towards Lundy from about 0 to 22 mGal, where a north-south gravity ridge up to 26 mGal separates the two. A crudely circular gravity high (>34 mGal amplitude) about 35-40 km in diameter occurs to the west-southwest of Pembrokeshire with an embayed low on its southeastern flank.

The highest anomaly values in the study area occur to the southwest of Lundy Island, where a Ω–shaped gravity anomaly pattern closely mimics the geology boundary of undivided Carboniferous-Devonian sediments. The gravity anomaly itself is superimposed on a background of about 18 mGal and peaks at 48.5 mGal some 20 km southwest of Lundy, i.e. a residual anomaly of around 30 mGal. A kidney-shaped incursion into the contours over Lundy Island prevents an otherwise localized congruency with the Sticklepath Fault. The position of the gravity high contrasts with the conclusions of Brooks and Thompson (1973), who indicated a similar amplitude residual gravity high of about 23 mGal, but approximately 10 km ***northwest*** of the island. This latter feature has been echoed by Brown (1982) and McDonald and Lee (1989), who both essentially describe kidney-shaped anomaly patterns with highs to the northwest of the island rather than towards the southwest. There is no obvious explanation why data originally processed by BGS should give a different positions of the gravity high to the west of Lundy than the same raw data re-processed here, but this will be discussed in Chapter 6.

Figure 5.6: Bouguer gravity anomaly map for the Outer Bristol Channel. Contours are in mGal. Profiles 1 and 2 are used in modelling procedures and further defined in section 5.4.2.1. Land areas in Lundy, South Wales and North Devon are shown in green. Boreholes are from Kammerling (1979). NLFZ and WLFZ represent the North Lundy and West Lundy Fault Zones.

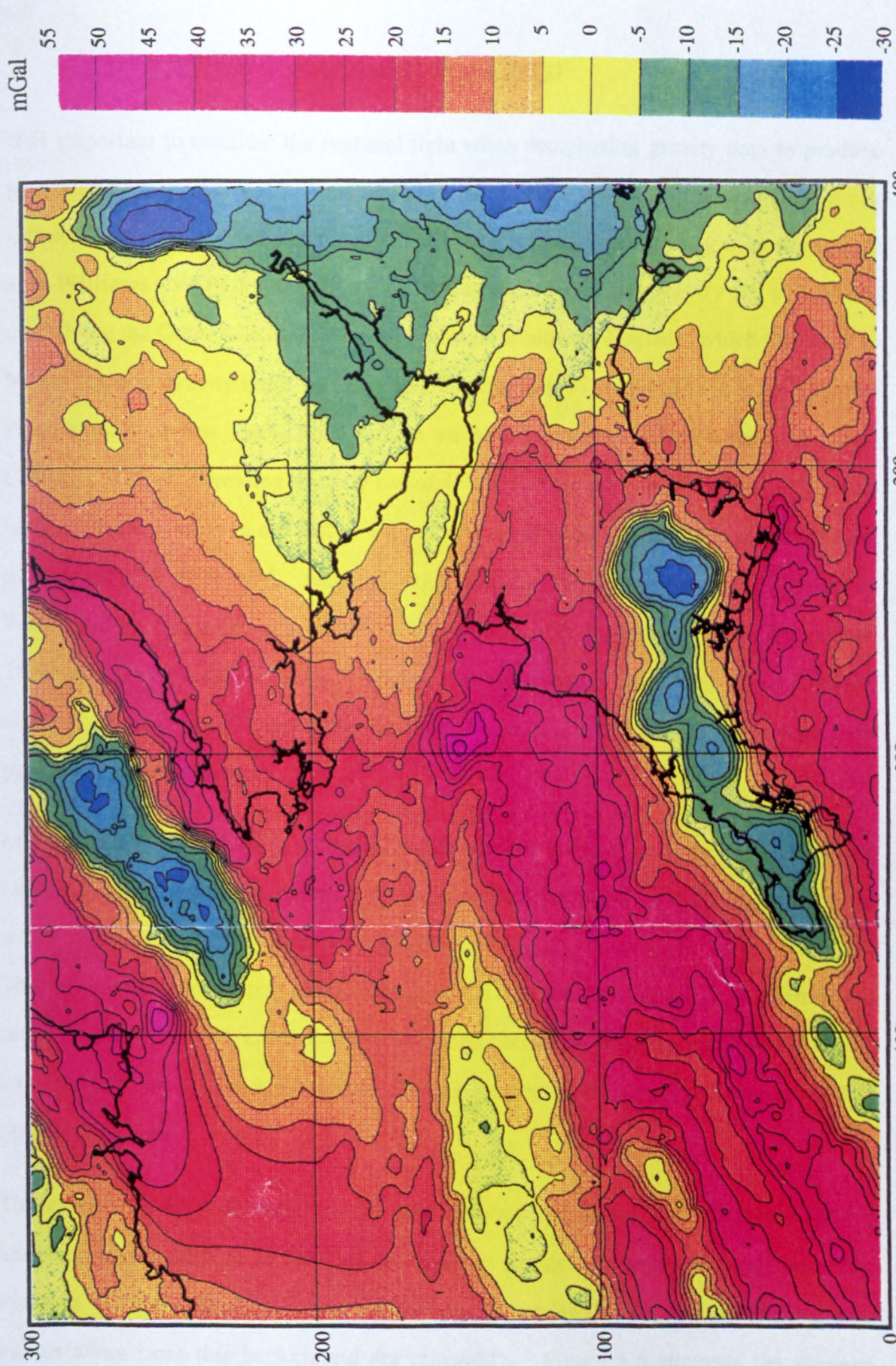

Figure 5.7: Regional Bouguer anomaly map for Southwest England, South Wales and Southeast Ireland. Data are reproduced from McDonald and Lee (1989). Notation along the axes represent British National Grid references and indicates km away from the origin. The key gives gravity anomaly values in mGal. See text for further discussion.

5.3.3 THE REGIONAL GRAVITY FIELD

It is important to consider the regional field when deciphering gravity data to produce geological interpretations, as characterizing the amplitude of the background field can influence the relative position and amplitude of any superimposed gravity anomalies. Day and Williams (1970) hypothesized a circular region of high gravity ($\geq$ +25 mGal) underlying the Outer Bristol Channel and most of Southwest England, which they took to be the regional gravity field. Brooks and Thompson (1973) identified a linear regional field, based on a first degree trend surface whilst omitting high values around the Lundy Complex, with an increasing westerly rise of 45 mGal along the axis of the Bristol Channel ranging from -5 mGal in the east to +40 mGal west of Lundy Island to give a horizontal gradient of 0.38 mGal km^{-1}. Although suggesting that variations in regional gradients in Wales and the Celtic Sea argued against a deep origin for the regional field, Brooks and Thompson (1973) conclude that a 1^{o} regional dip on the base of the crust or a lateral density contrast of 0.02 g cm^{-3} (assuming a crustal thickness of 35 km) would produce their postulated gravity gradient.

McDonald and Lee (1989) produced a Bouguer gravity anomaly map for the whole of the United Kingdom and Eire (using a Bouguer reduction density of 2.70 Mg m^{-3}), from which an extract covering Southwest England and South Wales is shown in Figure 5.7. This reveals some interesting characteristics of the regional field, which can be partitioned into two gradients. A crude S-shaped sinuous boundary, trending north-south with a value of +15 mGal, separates a gently dipping gradient to the east from a relatively flat gradient to the west.

The eastern gradient decreases to the east at about 0.15 mGal km^{-1} to give a neutral anomaly near the mouth of the Channel, whereas the western gradient is relatively flat between +15 and +20 mGal for much of the area (assuming that the positive and negative values away from this background are removed). Figure 5.6 suggests the western background component is close to 18 mGal.

This change in the slope of the regional gravity gradient is in part reflected by Meissner et al. (1989), who defined variations in crustal depth under Great Britain from seismic

evidence, shown in Figure 5.8. The crustal thickness in the vicinity of the Middle and Outer Bristol Channel is relatively level between 25 and 30 km, but steepens eastwards towards the mouth of the estuary where the depth to the Moho is > 35 km. The regional background gravity field in Southwest England is thus probably controlled in the main by depth to igneous and/or metamorphic basement rocks, with lower gravity values to the east reflecting greater depth to basement and hence a thicker sedimentary pile. A southwest-northeast ridge of relatively high gravity encompasses most of the southwest coastline and marginal marine areas. This could indicate variable thickness in the basement rocks or possibly changes in the deep structure. The net effect of the regional gravity field is to reduce the overall residual amplitude of gravity anomalies around Lundy Island. The next section will consider geological relationships to observed anomaly patterns.

5.4 COMPUTER MODELLING OF GEOPHYSICAL DATA

Computer modelling using "GRAVMAG" software allows observed magnetic and gravity profiles to be matched with a variety of theoretical polygonal bodies and the computed response to such bodies calculated. The principal objective of modelling procedures is to obtain reasonable fits between computed and observed profiles. However, some caution is required to ensure that theoretical models are firmly rooted in geological possibilities rather than in unlikely scenarios. The lack of definitive borehole control for most of the study area is not totally contradicted as supplementary geophysical evidence, especially from seismic refraction and reflection studies, as to the nature and depth of major geological boundaries is strong. Good borehole control has been established to the west and northwest during oil exploration surveys (Kamerling, 1979) with the result that thicknesses of Mesozoic strata are well defined for most of the Bristol Channel, but the nature and structure of deeper units (especially igneous and metamorphic) are not so well characterized. The positions of deep boreholes sunk as part of an oil exploration programme are shown in Figure 5.1, but noticeably fall outside the Lundy horst block.

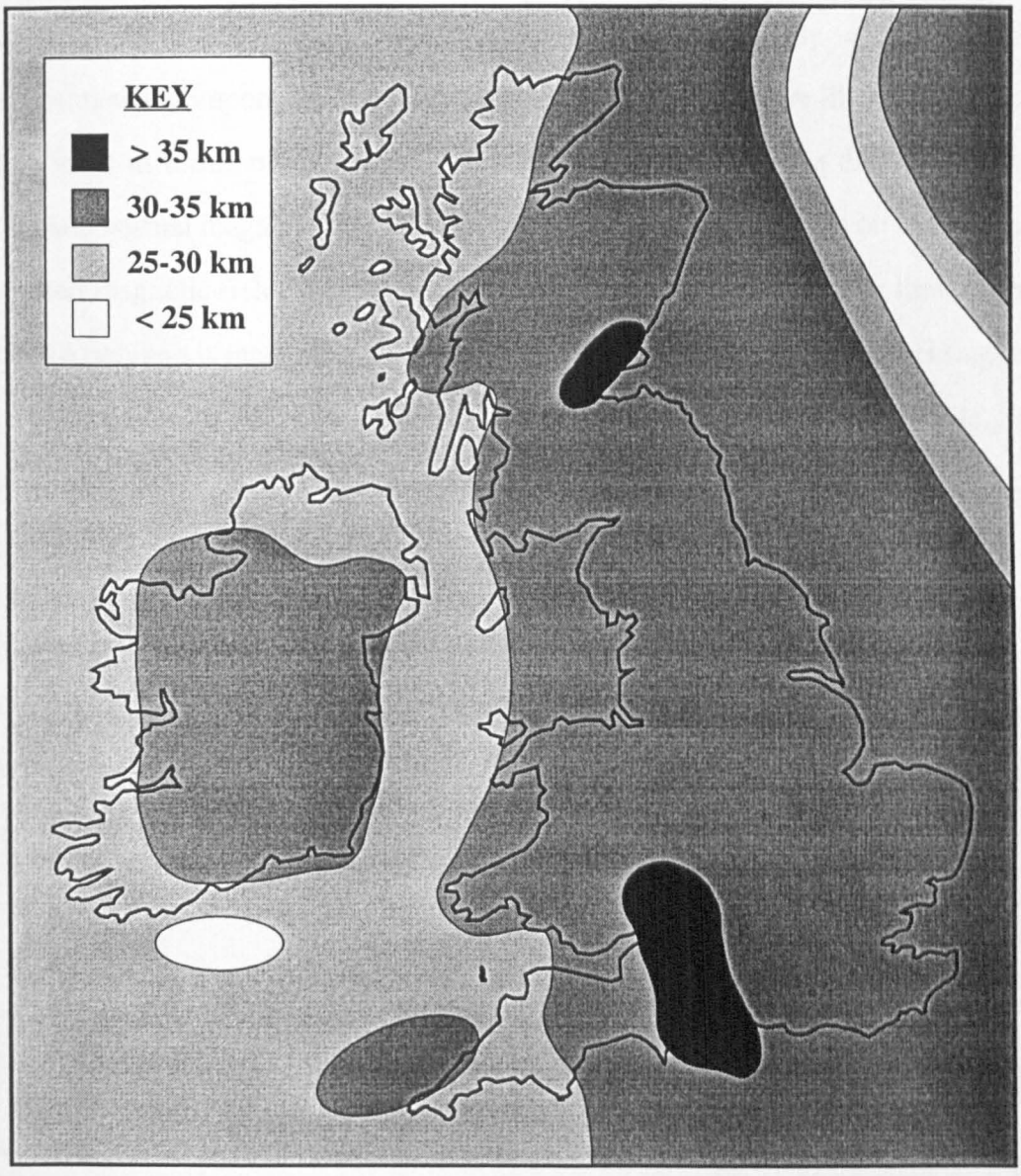

Figure 5.8: Crustal thickness in and around Great Britain.
Contour intervals of 5 km indicate depth of Moho from seismic evidence collated by the British Institutions Reflection Profiling Syndicate (BIRPS). After Meissner *et al.* (1989).

5.4.1 THEORETICAL RESPONSES TO MAGNETIC MODELS

It is assumed here that Tertiary remanence has declination and inclination values of the order of 184°; -62.7° if intrusions are reversely magnetized and 004°; +62.7° if normally magnetized (Blundell, 1959; Mussett et al., 1976). Although these directions may not be accurate in detail for every Tertiary body within the study area possessing a thermoremanent component, deviations away from these values are likely to be small and insignificant in terms of modelling procedures. Conversely, the distinction between reverse and normal magnetization is important and has profound effects on derived models. Computed magnetic fields for hypothetical bodies indicate that the lower limit of the half strike of a polygon is more meaningful than its upper limit. Indefinitely increasing the half strike value beyond a set amount does not influence a north-south magnetic profile, because the magnetic flux of components away from the profile is absent or negligible compared to the induced magnetization along the profile line itself.

However, decreasing the half strike has the effect of reducing the local magnetic flux of the intrusive body, which in turn reduces the amplitude of the computed signature, but not the overall sense of the anomaly. Half strike values between 50 and 300 m were used in different settings, the geometry of each polygon being the driving parameter in choice of half strike value.

5.4.1.1 The Morte Point Anomaly

The Morte Point anomaly (Figure 5.2) is set against a local magnetic background of about -102 nT and has an apparent reversely magnetized signature with a positive to the north and negative to the south, as outlined in section 5.2.2. In terms of the actual body causing the anomaly, the observed magnetic field signature can be influenced by depth of the body below the observation plane, level of magnetic susceptibility and strength of natural remanence. The depth of the body can be approximated from Peters' method (see Figure 3.8) by using the steepest gradient of the observed profile. In this case, the top of the Morte Point anomaly is calculated to be about 650 m ± 100 m below sea level datum. Figure 5.9 shows the result of modelling procedures.

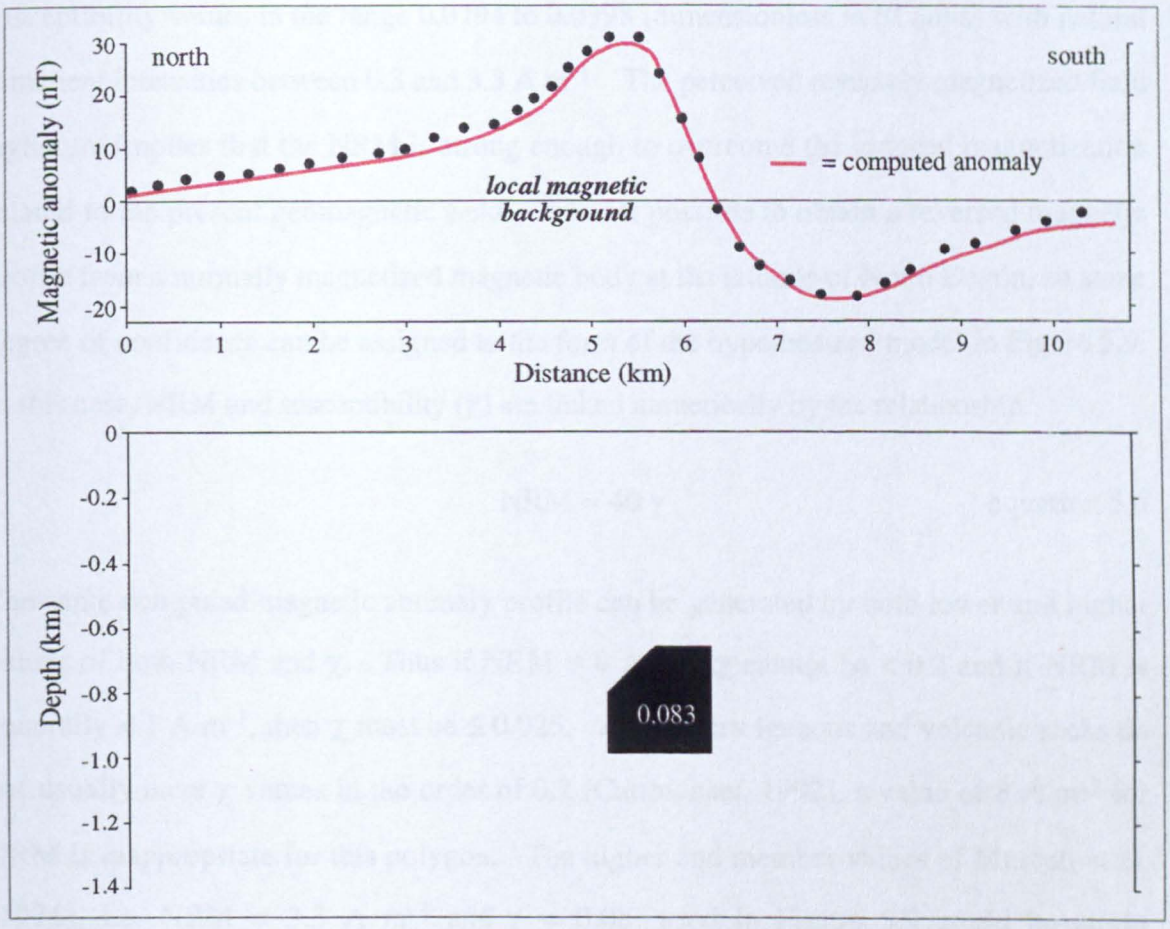

Figure 5.9: Theoretical model for the magnetic anomaly at Morte Point.
Black circles represent data sample points derived from the magnetic anomaly map for the Morte Point area (cf. Figure 5.2), from which the local background magnetic field has been estimated at -102 nT. Susceptibility (χ) in the host Morte Slates Series is in the order of 1×10^{-5}, whereas the theoretical body has $\chi = 0.083$ and is reversely magnetized with remanence set at 3.3 A m^{-1}. Declination and inclination are set at 184°; -62.7° as given in section 5.4.1. Half strike is set at 500 m.

The shape of the polygon is broadly constrained by the wavelength of the anomalous profile, in that a vertical or inclined body would lengthen the wavelength beyond observed limits. The shape of a simple cube or spherical body at 650 m depth produced a shorter wavelength response than either a vertical or inclined body at Morte Point. Mussett et al. (1976) indicated that the bulk of measured magnetic dykes from Lundy Island had susceptibility values in the range 0.0794 to 0.0398 (dimensionless in SI units) with natural remanent intensities between 0.3 and 3.3 A m^{-1} The perceived reversely magnetized field signature implies that the NRM is strong enough to overcome the induced magnetization related to the present geomagnetic field. It is not possible to obtain a reversed magnetic profile from a normally magnetized magnetic body at the latitude of North Devon, so some degree of confidence can be assigned to the form of the hypothesized model in Figure 5.9. In this case, NRM and susceptibility (χ) are linked numerically by the relationship

$$NRM \approx 40\,\chi \qquad \text{equation 5.6}$$

The same computed magnetic anomaly profile can be generated by both lower and higher values of both NRM and χ. Thus if NRM is 8 A m^{-1}, χ cannot be < 0.2 and if NRM is generally < 1 A m^{-1}, then χ must be ≤ 0.025. As Tertiary igneous and volcanic rocks do not usually have χ values in the order of 0.2 (Carmichael, 1992), a value of 8 A m^{-1} for NRM is inappropriate for this polygon. The higher end member values of Mussett et al. (1976), i.e. NRM = 3.3 A m^{-1} and χ = 0.08, used in Figure 5.9 could be slight overestimates but indicate the maximum probable magnetic parameters for the Morte Point anomaly. It is also improbable that the computed model indicates a Permo-Carboniferous body, because the associated magnetic inclination of similar aged rocks usually manifests itself as a relatively flat vector around -2° (Tarling, 1980). Such an inclination would not oppose the present-day induced magnetization field to give a reversed signature, but would have the effect of either slightly increasing or decreasing the length of a normal signature, dependent on the sign of inclination, with a positive value to the south. This is not observed on the anomaly map (Figure 5.2) and so the Morte Point anomaly is interpreted in terms of a relatively small and shallow basic body, Tertiary in age and hence related in time to the Lundy Igneous Complex. Possible relationships with the Lee Bay dykes will be discussed in Chapter 6.

5.4.1.2 Magnetic Anomalies near to Lundy Island

Figure 5.3 highlighted several small magnetic anomalies to the west of Lundy Island as well as over the southern end of the island itself. As magnetic relief in this area is high and consequently produces closely spaced magnetic anomaly contours, the original processed data values with detailed grid references of sample points were used in modelling. Observed magnetic profiles are thus accurate representations of anomaly positions and not distorted by the contouring process.

Profile A-A' (Figure 5.10) is taken along easting 214, which runs up the east shoreline of the island. The magnetic anomaly is unpaired and peaks at +95 nT over the southeast corner of the island where sediments crop out and is set against an inclined local background of about -40 nT to the south and around -75 nT to the north. The gradient of the anomaly is steeper to the north at about 0.16 nT m^{-1} relative to the south, where it approaches 0.06 nT m^{-1}. Using Peters' method as before, the principal magnetic anomaly accords with a body at around 600 m depth. At this depth, the observed magnetic gradients are best matched by a vertical column rather than by a cube or spherical shape, which would produce a steeper gradient from the south towards a maximum. A relatively large positive anomaly is indicative of a normally magnetized body, but such a mass should also produce a small negative anomaly on its northern flank. As a small negative anomaly does not coexist with the larger peak, the observed profile is probably the result of at least two discrete bodies. Figure 5.10 shows one possible solution to the observed profile.

In this case, the large polygonal body at the datum corresponds to the Lundy granite. Although essentially of low magnetization, the Lundy granite does contain trace amounts of pyrrhotite, which (Dollar, 1941) concluded was the total cause of the magnetic residue. Susceptibility for 16 Lundy samples gave a mean value 3.5×10^{-5} and remanence was estimated at 1.5×10^{-3} A m^{-1}. These two values were used for modelling polygon 1. The other two polygons correspond to basic intrusions, but two different magnetic polarities are hypothesized with the implication that the observed profile is the product of two distinct and separate magmatic events. Polygon 2 has remanence set at 2 A m^{-1} with $\chi = 0.05$, whereas polygon 3 has a remanent value of 0.5 A m^{-1} and $\chi = 0.01$.

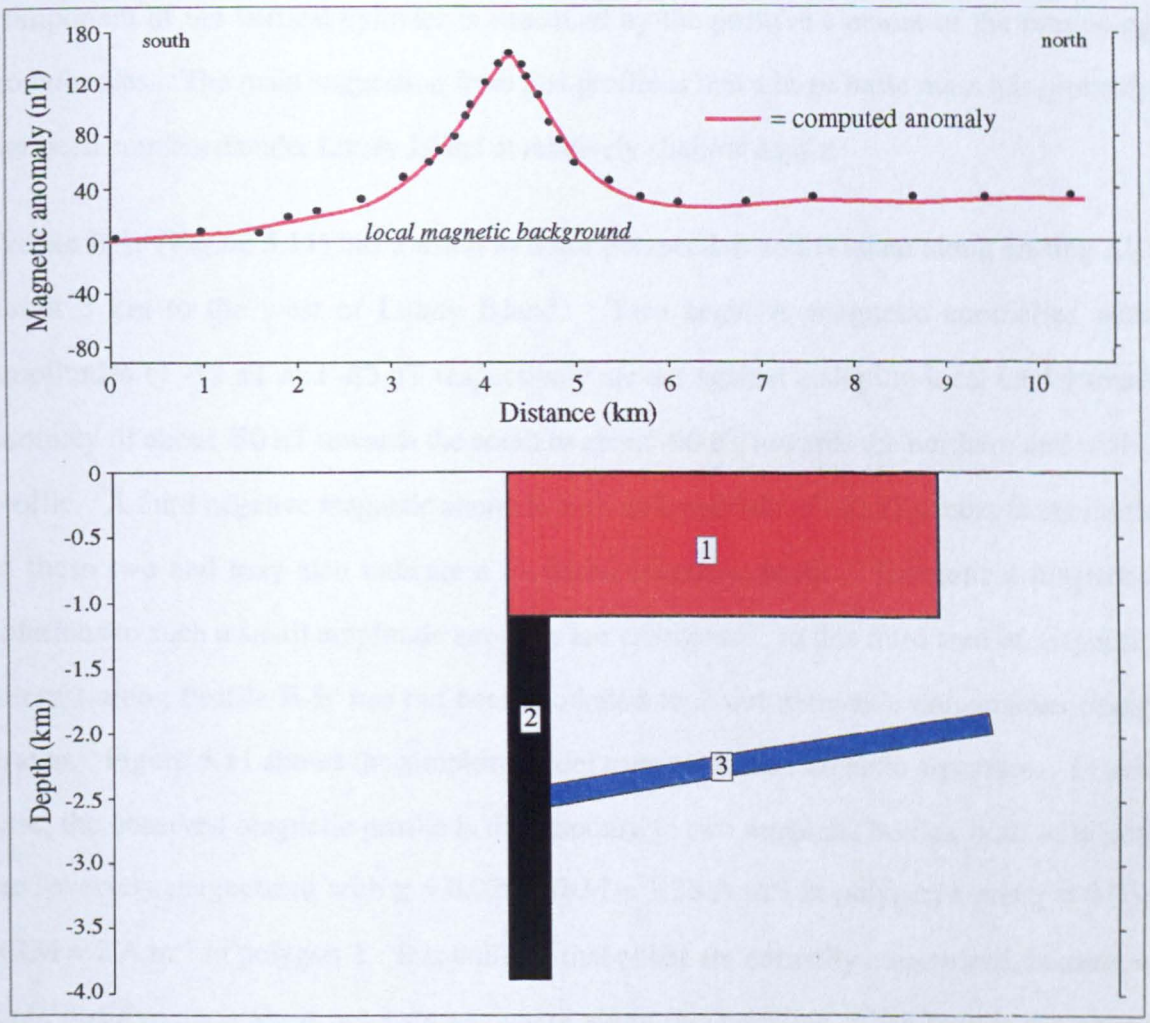

Figure 5.10: Theoretical magnetic model along grid line 214 through Lundy Island. Grid line 214 corresponds to profile A-A' in Figure 5.3. The local magnetic background slopes from -40 nT at the southern end of the profile to -75 nT at the northern end and black circles indicate data sample stations. Susceptibility (χ) of host sediments is around 1 x 10^{-5}. Bodies 1 and 2 are normally magnetized, whilst body 3 is reversely magnetized. Body 1 corresponds to the Lundy granite and has a half strike of 2 km. Body 2 has a half strike of 300 m, whilst body 3 has a half strike of 1 km. See text for details of magnetic properties.

An inclined sheet-like intrusion projecting under Lundy Island may represent a sill or an elongated storage body. Whilst the vertical column is reasonably restricted in shape by the observed magnetic signature, the inclined sheet could be replaced by one or two smaller storage bodies in close proximity. The net effect of either solution is that the negative component of the vertical cylinder is cancelled by the positive element of the remaining body/bodies. The main suggestion from this profile is that a large basic mass has probably not been emplaced under Lundy Island at relatively shallow depths.

Profile B-B' (Figure 5.11) has a south to north perspective and is taken along easting 210 about 3 km to the west of Lundy Island. Two negative magnetic anomalies with amplitudes of -32 nT and -82 nT respectively are set against a sloping local background anomaly of about -50 nT towards the south to about -90 nT towards the northern end of the profile. A third negative magnetic anomaly with an amplitude of -20 nT occurs to the north of these two and may also indicate a localized magnetic body. Theoretical magnetic solutions to such a small amplitude anomaly are ambiguous, so this third area of magnetic interest along Profile B-B' has not been modelled to avoid untenable conclusions being drawn. Figure 5.11 shows the simplest model to explain the magnetic signature. In this case, the observed magnetic profile is the response to two magnetic bodies, both of which are reversely magnetized with $\chi = 0.025$; NRM = 1.25 A m^{-1} in polygon 1 and $\chi = 0.05$; NRM = 2 A m^{-1} in polygon 2. It is unlikely that either are normally magnetized, because a large positive anomaly is not seen anywhere along this grid line. Not only is the larger amplitude negative anomaly to the north is caused by a larger polygonal body relative to the southern one, but it is also unrealistic to obtain the same amplitude field signature using a smaller polygon. The simple computed model is therefore probably the most rational of a number of possibilities.

Profile C-C' (Figure 5.12) is a south-north line taken along easting grid 208 approximately 5 km west of Lundy Island. In this profile, an anomaly of ~ +80 nT with a wavelength of about 8 km is also set against a northerly dipping background with values between -50 nT and -90 nT. In this case, it was not possible to obtain a reliable fit between computed and observed response using any one particular polygonal body, despite toggling both susceptibility and NRM directions.

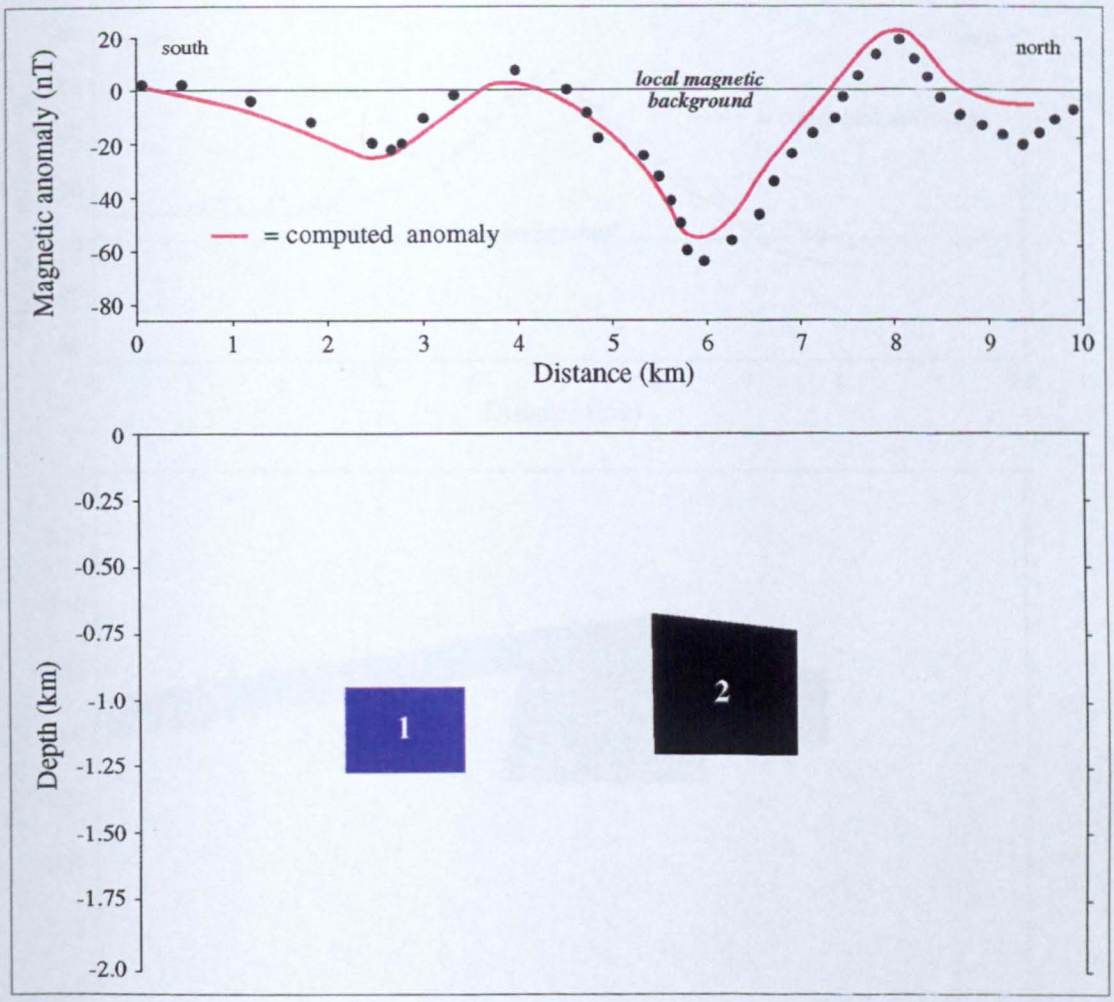

Figure 5.11: Theoretical magnetic model along grid line 210
Grid line 210 ccorresponds to profile B-B' in Figure 5.3. The local background slopes from around -50 nT at the southern end to about -105 nT at the northern end. Black circles indicate data sample points and susceptibility of host sediments is around 1 x 10^{-5}. Both polygons are reversely magnetized. Polygon 1 has a half strike of 1 km, whilst polygon 2 has a half strike of 1.5 km. See text for details for magnetic properties.

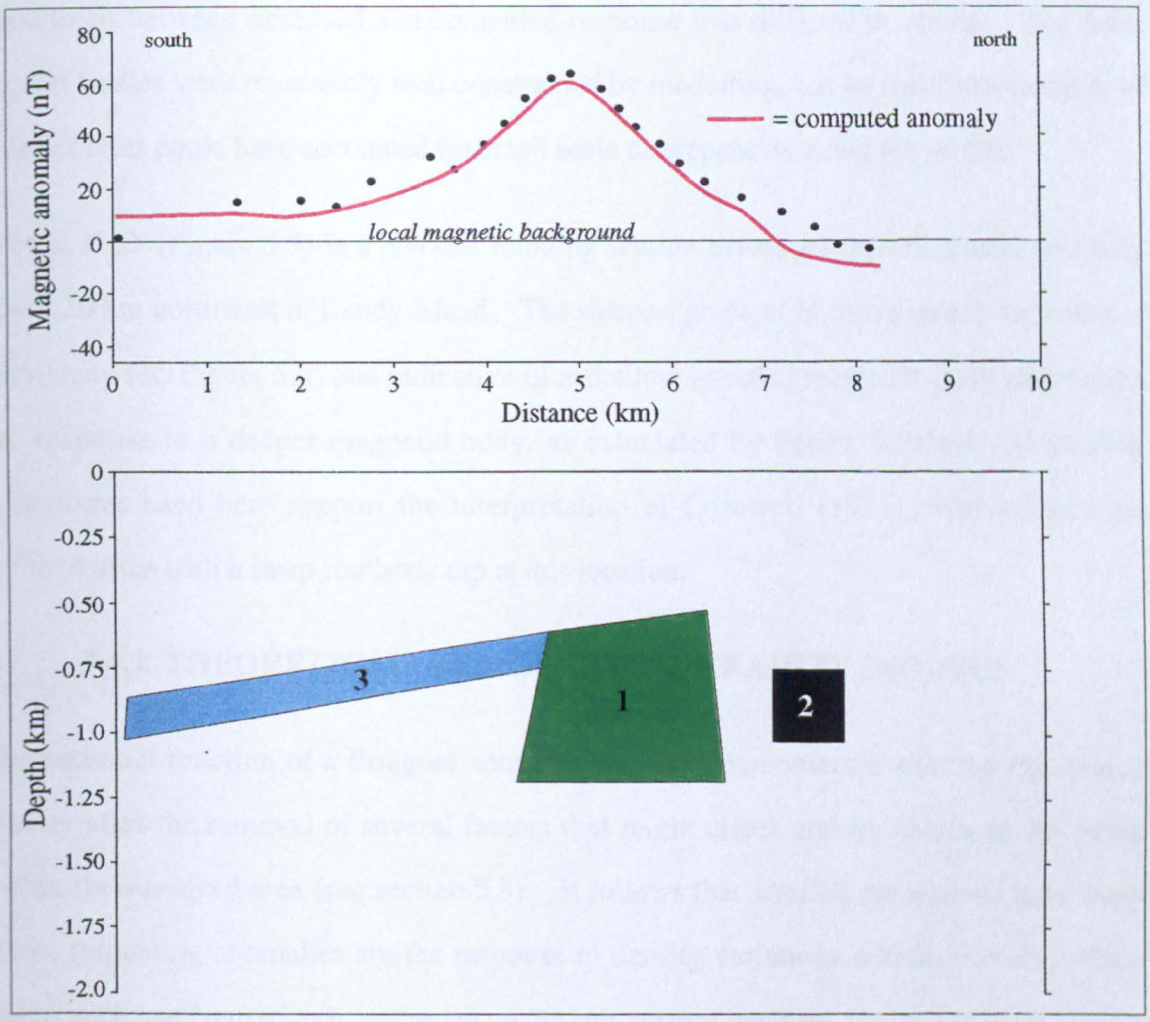

Figure 5.12: Theoretical magnetic model along grid line 206
Grid line 206 corresponds to profile C-C' in Figure 5.3. The local magnetic background slopes from -50 nT at the southern end of the profile to an estimated -75 nT at the northern end and black circles indicate data sample stations. Susceptibility (χ) of host sediments is around 1 x 10^{-5}. Bodies 2 and 3 are normally magnetized, whereas the larger body 1 is reversely magnetized. Body 1 has a half strike of 1.5 km, body 2 has a half strike of 200 m and body 3 has a half strike of 2 km. See text for details of magnetic properties.

The observed anomaly is thus the response to more than one polygon, but it proved difficult to quantify the precise number of bodies required to produce this signature. Figure 5.12 gives the simplest solution to modelling. Here, at least three bodies of reversed and normal polarity combine together to match the observed signature, although a precise fit between observed and computed response was difficult to obtain. The three largest bodies were reasonably well constrained by modelling, but an indefinite number of smaller units could have accounted for small scale discrepancies along the profile.

Profile D-D' (Figure 5.3) is a NW-SE trending section across a linear magnetic anomaly about 20 km northwest of Lundy Island. The steepest gradient of the magnetic signature is very steep (cf. Figure 5.4) and indicative of a shallow intruded magnetic body rather than the response to a deeper magnetic body, as calculated by Peters' Method. Modelling procedures used here support the interpretation of Cornwell (1971), who inferred an inclined dyke with a steep southerly dip at this location.

5.4.2 THEORETICAL RESPONSES TO GRAVITY MODELS

The essential function of a Bouguer anomaly map is to demonstrate areas of anomalous gravity after the removal of several factors that might affect gravity values at any point within the surveyed area (see section 5.3). It follows that after all corrections have been made, remaining anomalies are the response to density variations within the sub-surface and as such can be used to hypothesize on the sub-surface geology.

It should be borne in mind that different geological lithologies can have identical density values and so in that sense, gravity anomalies by themselves cannot be diagnostic of specific sub-surface units. Ground truthing is therefore very important to define density values from known geological units to help distinguish between different hypothetical models. Also, models should be tied to borehole information where possible to avoid the danger of unjustifiable conclusions being drawn. Previous relevant density values that have been published are shown in Table 5.1.

Table 5.1: Density Values in Southwest England and the Bristol Channel

Geological Unit	Density, g cm^{-3}	Reference
Cretaceous Chalk	2.23 - 2.31	Olhoeft + Johnson (1989)
Upper Jurassic	2.46 - 2.50	Brooks + Thompson (1973)
Middle Jurassic	2.55 - 2.58	Brooks + Thompson (1973)
Lower Jurassic	2.45 - 2.60	Brooks + Thompson (1973); Brooks, Bayerly + Llewellyn (1977)
Triassic Sandstones	2.35	Kearey + Brooks (1994)
Permian/Triassic	2.45 - 2.50	Brooks + Thompson (1973); Brooks, Bayerly + Llewellyn (1977)
Upper Carboniferous	2.61 - 2.69	Cook + Thirlaway (1952); Bott et al. (1958)
Middle Carboniferous	2.62 - 2.66	Thomas + Brooks (1973) Bott et al. (1958)
Lower Carboniferous	2.65 - 2.70	Bott et al. (1958) Thomas + Brooks (1973)
Upper Devonian	2.62 - 2.73	Bott et al. (1958) Brooks, Bayerly + Llewellyn (1977)
Lower Devonian	2.67 - 2.70	Bott et al. (1958)
Upper Palaeozoic Average	2.65	Brooks + Thompson (1973)
Lower Palaeozoic Average	2.70	Brooks, Bayerly + Llewellyn (1977)
Lower Palaeozoic and Precambrian Average	2.73	Llewellyn (1981)
Tertiary Granite (Lundy)	2.58	Bott et al. (1958)
Basalt	2.87 ± 0.11	Olhoeft + Johnson (1989)
Dolerite	2.90 ± 0.12	Olhoeft + Johnson (1989)

These published density values were supplemented by a second density data set from Lundy Island. In particular, the igneous rocks on Lundy were argued to be more representative of density values for in situ igneous bodies in the vicinity simply because of their close spatial relationships. Table 5.2 shows the results of density determinations carried out on a representative sample of rocks from the island using the methodology described in section 2.3.2.

Table 5.2: Densities of rocks from Lundy Island

Number of Samples	Lithology	Density (g cm^{-3})
Tertiary		
16	Granite	2.55 ± 0.03
30	Dolerite	2.83 ± 0.07
12	Basalt	2.85 ± 0.06
17	Trachyte	2.62 ± 0.08
Devonian		
21	Fine sandstone/siltstone	2.68 ± 0.02

The spread of values for the dolerites, basalts and trachytes may be related to the degree of vesicularity and/or weathering. As only fresh samples were chosen for density measurements, the amount of unfilled vesicles in the rocks is the most likely cause of variation, i.e. vesiculation and density are inversely related. Where vesicles were filled with zeolites such as analcime to give amygdales, density was also slightly reduced due to a grain density in such minerals around 2.26 g cm^{-3} (Olhoeft and Johnson, 1989). If these values are representative of other similar lithological units, then it is interesting to note that the maximum density values of basic rocks is in the order of 2.90 g cm^{-3}, which is towards the lower end of the density range for basic rocks given by Milsom (1992), i.e. 2.82 to 3.13 g cm^{-3}.

5.4.2.1 Modelling around the Lundy Horst

Borehole control within the Lundy Horst itself is poor with little known about the nature of deep rocks in the area. For the purpose of modelling, it is assumed that information on depth to Precambrian crystalline basement is similar to that proposed by Mechie (1980) and Mechie and Brooks (1984) from seismic refraction studies to the east of the Sticklepath Fault. If this information is true for the area around the Lundy Horst, the crystalline Precambrian basement interface could be located between about 6 and 8 km depth. The presence of Lower Palaeozoic rocks in the horst structure is not proven, but is nevertheless inferred here as both Ordovician and Silurian volcanic and igneous rocks crop out to the north in Pembrokeshire and Camarthenshire. Cambrian sediments also crop out in Pembrokeshire, but do not exceed 1 km in thickness. Evidence from the Devon and Cornwall mainland for Cambrian units is poor, thus Lower Palaeozoic rocks are modelled here as a generic sequence without reference to specific detail.

Figure 5.13 shows the best fitting model along Profile 1 (cf. Figure 5.6) to explain the gravity profile based on geological information in the channel by Tappin (1983) and models of the deep structure by Mechie and Brooks (1984). In this model, strata to the south under the Lundy horst dip with a gentle southerly dip, but younger sediments north of the Lundy horst either dip to the north or are broadly horizontal.

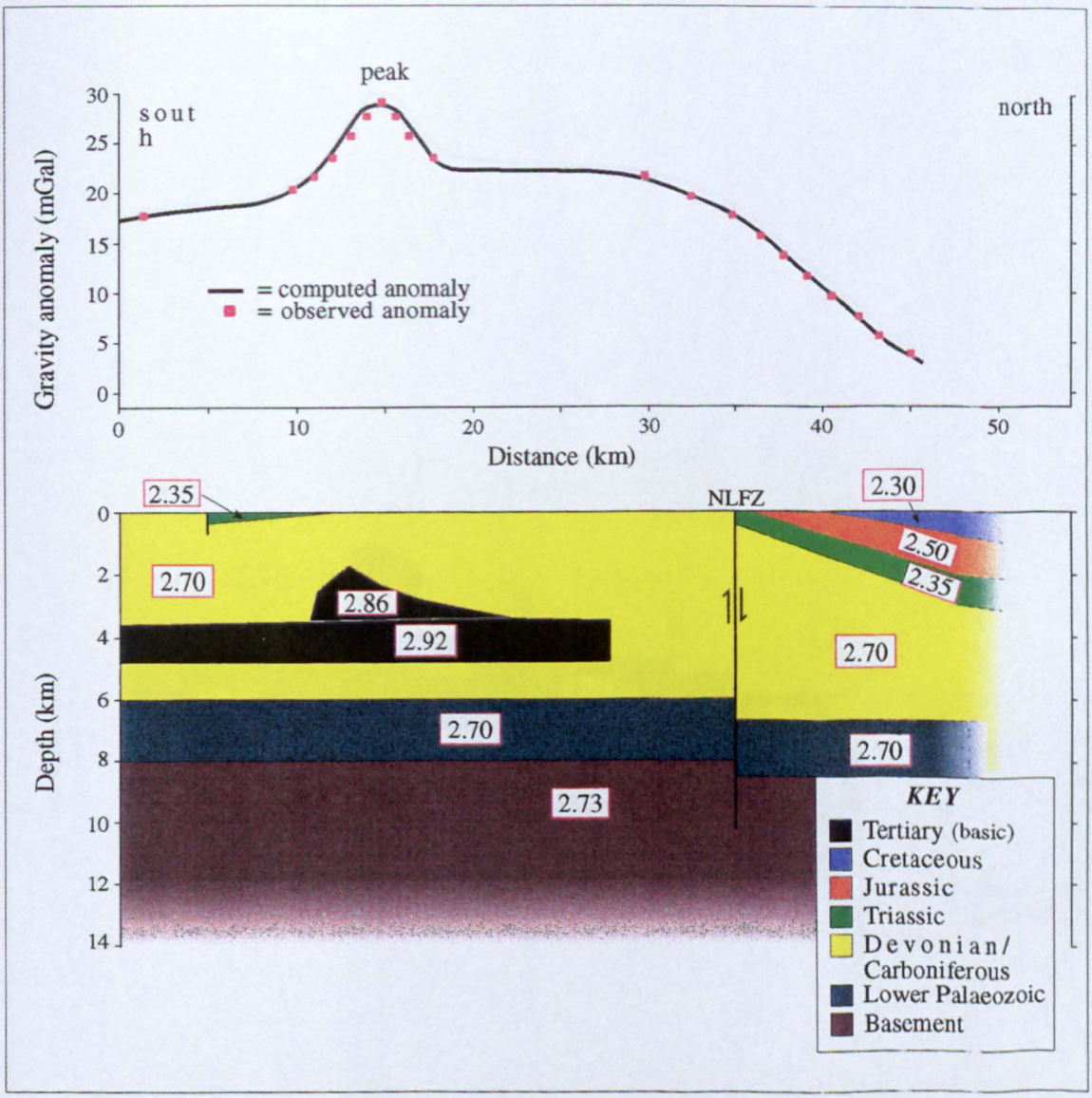

Figure 5.13: Model for residual gravity anomalies along Profile 1 in the Lundy horst. The regional background field is estimated at +18 mGal and density values (g cm^{-3}) are taken from Table 5.1. Tertiary rocks are represented here by basic rocks (black) with an average range of density. Deeper units have a slightly higher density than more superficial equivalents, as might be expected from igneous intrusive complexes. Half strike values are set at 10 km for all rocks apart from the two Tertiary bodies, which have a half strike of 5 km. See text for further discussion. NLFZ represents the North Lundy Fault Zone. The model also includes 50 m of sea water with a density of 1 g cm^{-3}, but is too small to be shown on this scale. See Figure 5.6 for the location of Profile 1.

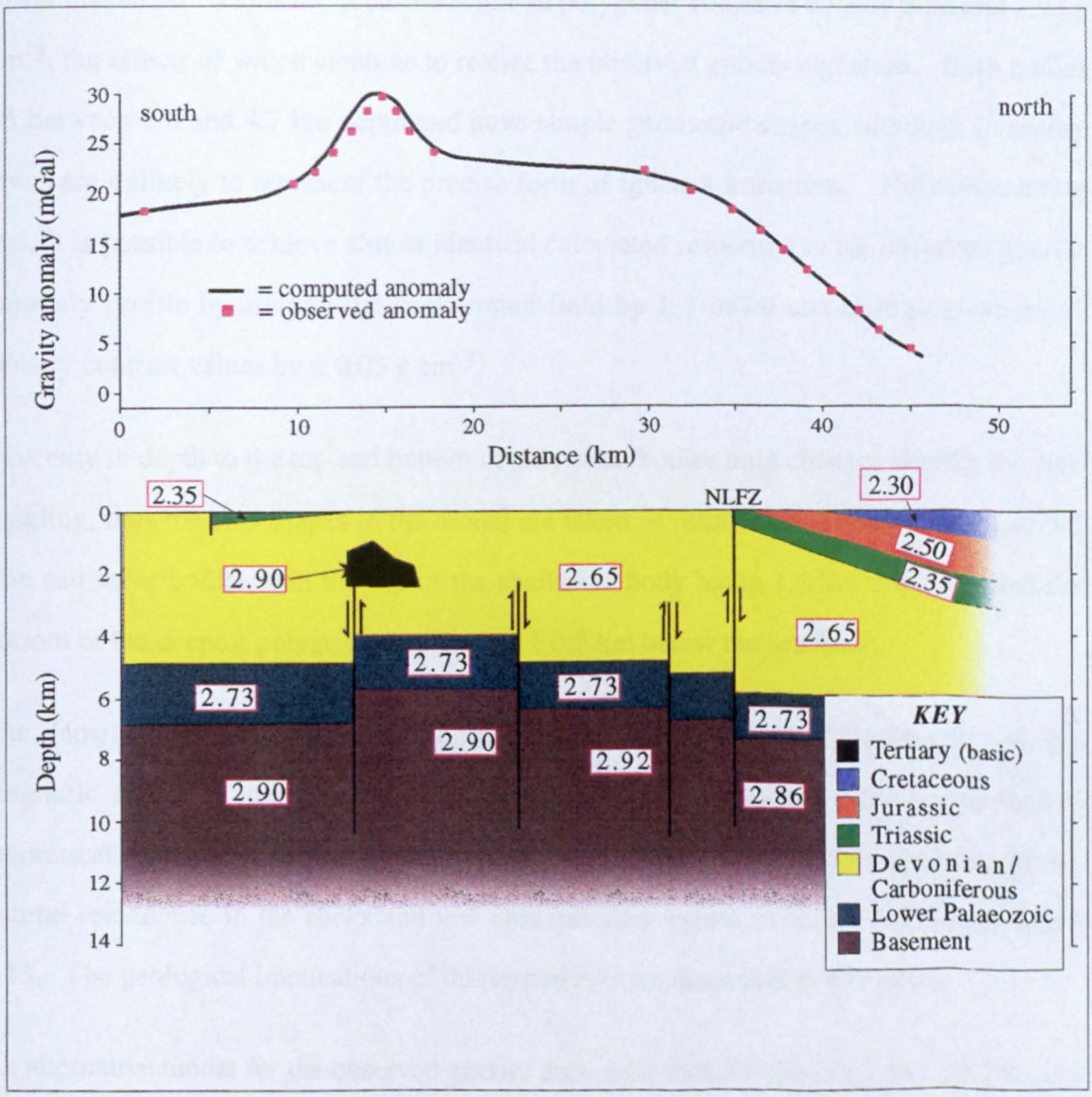

Figure 5.14: Alternative model for residual gravity anomalies in the Lundy horst. The regional background field is estimated at +18 mGal and density values (g cm^{-3}) are taken from Table 5.1. The postulated value for basement rocks is taken from Rudnick and Fountain (1995) relative to an upper crustal average density of 2.70 Mg m^{-3}. Half strike values for all rocks is set at 10 km apart from the Tertiary body, which has a half strike of 3 km. Sea water has been omitted, as explained in Figure 5.13. See text for further discussion.

A zone of east-west faulting within Mesozoic strata in mid-Channel is shown, but it is unclear whether such faults extend into the underlying Palaeozoic sequences. The main feature of interest in terms of gravity (assuming a general background of +18 mGal from lower crustal sources) is the occurrence of two polygonal bodies of density 2.86 and 2.93 g cm^{-3}, the effects of which combine to realize the observed gravity signature. Both bodies lie between 1.6 and 4.7 km depth and have simple geometric shapes, although in reality these are unlikely to represent the precise form of igneous intrusions. Notwithstanding this, it is possible to achieve almost identical calculated responses to the observed gravity anomaly profile by altering the background field by ± 1 mGal and changing estimated density contrast values by ± 0.03 g cm^{-3}.

Diversity in depth to the top and bottom of polygonal bodies only changes slightly by such toggling, thus the two shapes in the model are taken as reasonable approximations of the true causative bodies with the top of the shallower body being 1.6 km ± 0.2 km and the bottom of the deepest polygon being 4.7 km ± 0.3 km below the sea floor.

The densities of these bodies are consistent with basic rocks, but the absence of any magnetic signature at sea level is unusual for such large bodies. It is nevertheless theoretically possible to achieve relatively flat magnetic signatures by having virtually no natural remanence in the rocks and low susceptibility values as demonstrated in Figure 5.13. The geological implications of this hypothesis are discussed in Chapter 6.

An alternative model for the observed gravity data is presented in Figure 5.14. In this case background levels are still set at + 18 mGal, but the observed gravity profile is the response to relatively dense basement complex and not essentially from intrusive basic bodies. The decrease in gravity further to the north is an artefact of either relatively low density superficial sediments (average value 2.55 g cm^{-3}, cf. Table 5.1) or the presence of deeper basement faults downthrowing to the north and hence increasing the distance between observation point and causative body. A slight decrease in basement density from 2.90 g cm^{-3} to 2.86 g cm^{-3} could also add to the computed anomaly profile. In this model, a deep sub-horizontal body equated with basement rocks possesses an overall density of 2.90 g cm^{-3} with its upper margin between 6 and 8 km below sea bottom.

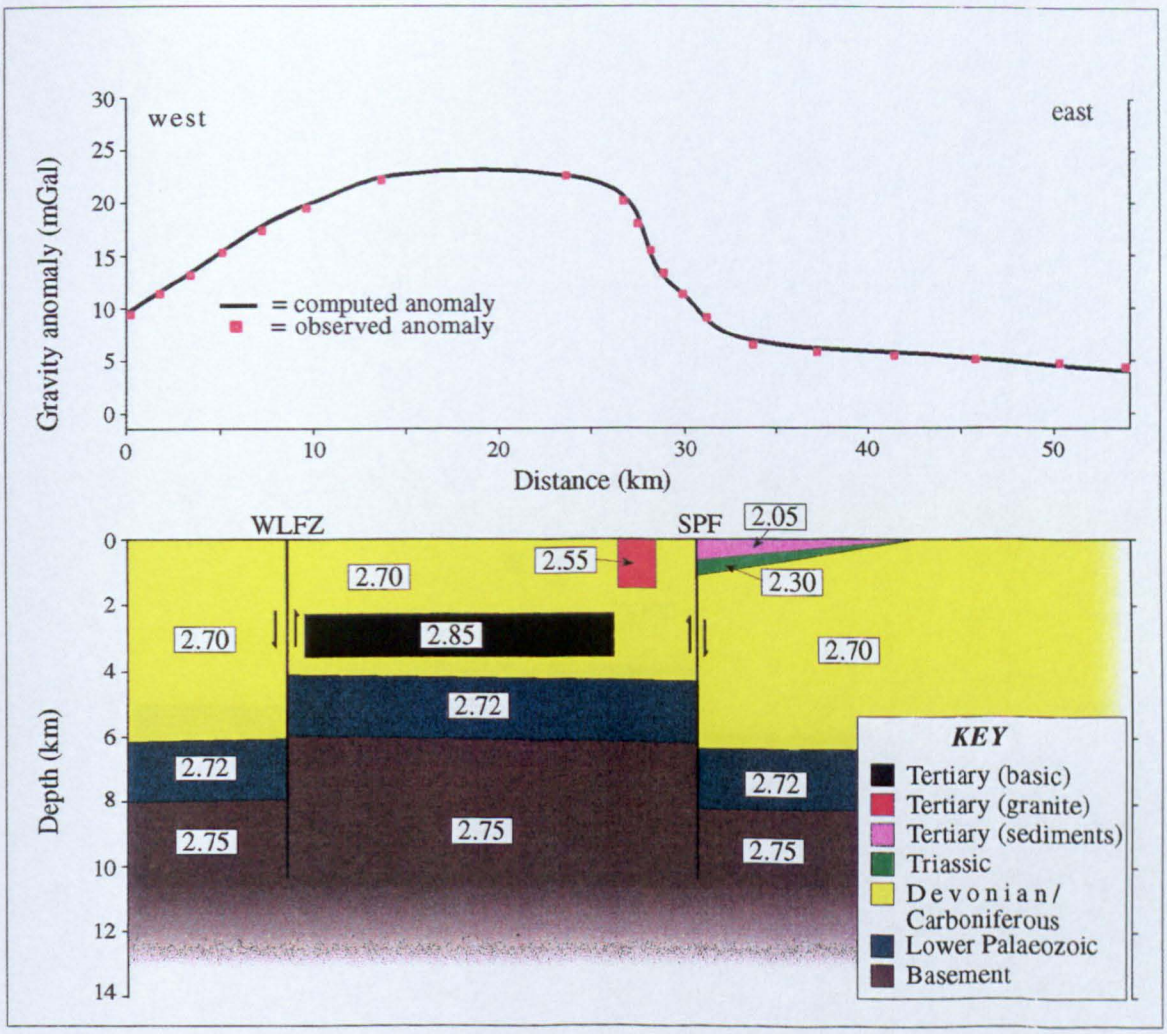

Figure 5.15: Second model for residual gravity anomalies in the Lundy horst. Regional background is estimated at 18 mGal. Density values (g cm^{-3}) are taken from Tables 5.1 and 5.2. Tertiary basic rocks have a half strike of 5 km, whilst all other rocks have a half strike of 10 km. Sea water is approximately 50 m deep and has been modelled with a density of 1 g cm^{-3}, but has been omitted from this model to aid clarity. WLFZ and SPF represent the West Lundy Fault Zone and Sticklepath Fault respectively. Both faults are thought to be vertical. Depth estimations are from Arthur (1989) and Holloway and Chadwick (1986). This traverse corresponds to Profile 2 in Figure 5.6.

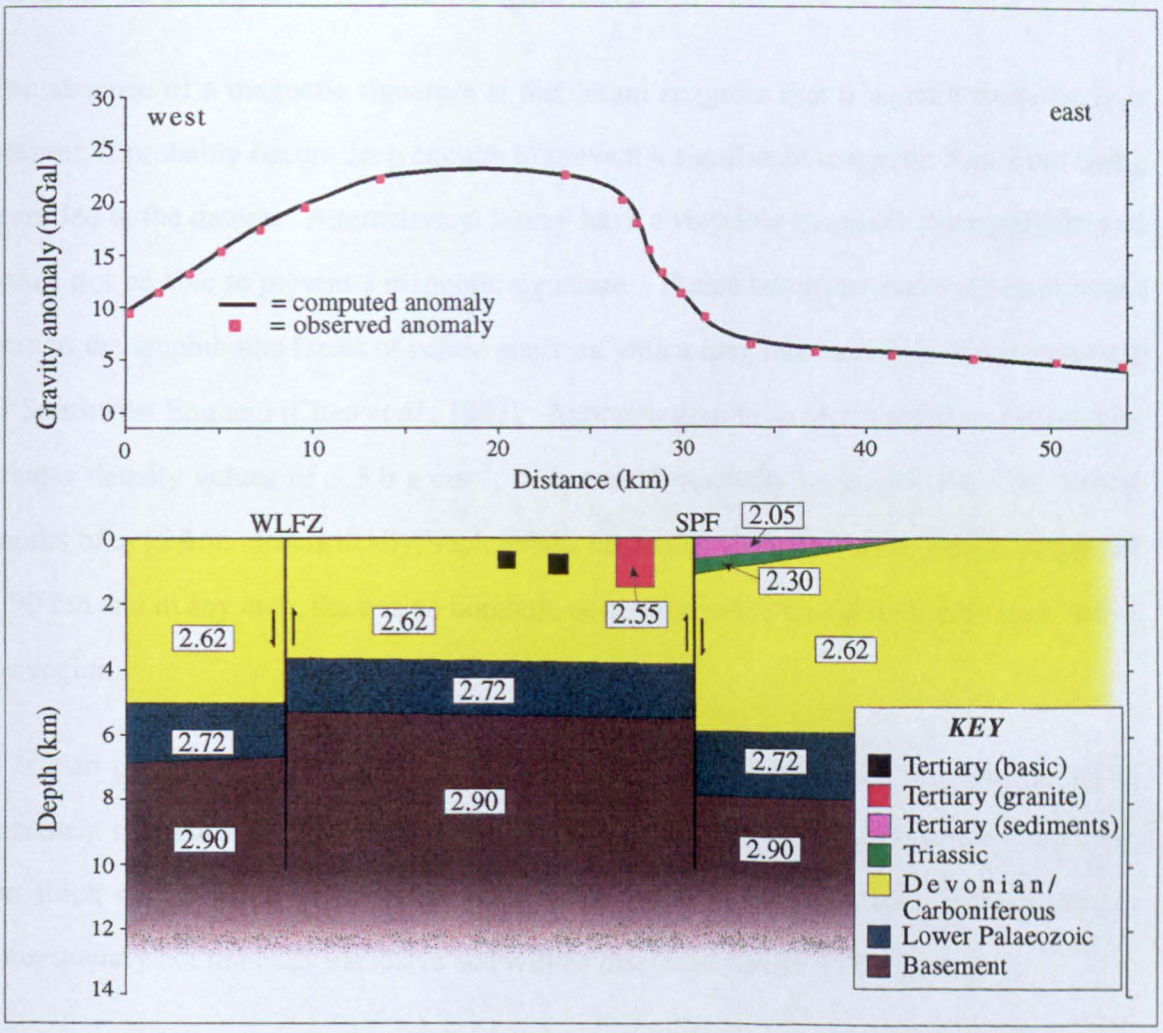

Figure 5.16: Alternative model for residual gravity anomalies in Figure 5.15.
Regional background is estimated at 18 mGal. Density values are the same as in Figure 5.13 apart from basement density values, which have been derived from Rudnick and Fountain (1995). Basic Tertiary rocks have been given a nominal density of 2.85 Mg m^{-3} and a half strike value of 2 km. WLFZ and SPF represent the West Lundy Fault Zone and Sticklepath Fault respectively.

The wavelength of the computed response to this deep basement is relatively long and by itself cannot account for the short wavelength anomaly peak to the southwest of Lundy Island. A small basic body or bodies may thus co-exist with dense basement to produce the observed gravity anomaly profile (Figure 5.14).

The absence of a magnetic signature at the datum suggests that if a small basic body is present, it probably occurs deep enough to prevent a significant magnetic flux from being recorded at the datum. Alternatively, it may have a very low magnetic susceptibility and hence not be able to present a magnetic signature. Dense basement rocks are interpreted here as the amphibolite facies of pelitic gneisses, which may represent part of the basement of Southwest England (Chen *et al.*, 1993). Although granulitic facies are characterized by greater density values of > 3.0 g cm^{-3}, they would normally be associated with crustal depths of > 15 km. Realistically, such depths cannot be modelled over profile lengths of < 90 km and in any case, there is no borehole or outcrop evidence for their existence within the region.

It is also possible to achieve the same observed gravity profile with a combination of basement rocks around 5 - 6 km depth with a lower density (around 2.78 g cm^{-3}) and a 1.5 km thick overlying layer of basic rocks (2.94 g cm^{-3}). Both sources of density are consequently not mutually exclusive and will be discussed further in Chapter 6.

Figure 5.15 shows a model for the gravity anomalies along Profile 2 (Figure 5.6). In this model, basement rocks occur about 6 km below sea bottom within the Lundy horst, but the observed gravity anomaly is essentially due to a simple sill-like basic intrusion between 2.3 and 3.7 km depth with an estimated density of 2.85 g cm^{-3}. Such a model would be consistent with the theories of Brooks and Thompson (1973). Alternatively, Figure 5.16 indicates that the observed gravity profile could be the product of basement rocks rather than large intrusive basic material. In this case, basement rocks (estimated density 2.90 g cm^{-3}) can be found at < 6 km depth within the Lundy horst and at around 7 km depth to the west of the West Lundy Fault Zone (WLFZ). The relatively low gravity signature to the east of the Sticklepath Fault (SPF) could reflect a low density sedimentary pile and/or a slightly deeper basement. Two small basic bodies at shallow depth have been included

from magnetic evidence. The net effects of these two bodies are minimal to the overall model amplitude (about a 0.6 mGal increase locally), provided that sandier units dominate in the nearby Devonian/Carboniferous sediments to give a slightly reduced density (e.g. 2.64 g cm^{-3} rather than 2.70 g cm^{-3}, as given in Table 5.1). Geological implications of this hypothesis are discussed and compared to other models in Chapter 6.

5.5 SUMMARY OF MAGNETIC AND GRAVITY MODELS

Magnetic modelling procedures indicate that the high magnetic relief around Lundy Island seen on the observed magnetic anomaly map (Figure 5.1) is not the product of one magnetic body, but rather indicates the presence of several discrete bodies. The bodies themselves can be approximately cubic or spherical, vertical columns or horizontal sill-like intrusions of either reversed or normal polarity. Despite the fact that both susceptibility (0.005 to 0.1, SI units) and NRM values (0.03 to 3 A m^{-1}) are not particularly high, there is enough contrast with the estimated background susceptibility value (0.0005) to infer that the magnetic bodies are not simply the result of magnetic variation in the undivided sedimentary pile of Devonian/Carboniferous units. The magnetic bodies are equated with basic rocks of Tertiary age and as such can be used in the interpretation of the geology of Lundy Volcano. Similarly, the Morte Point anomaly is equated with a basic Tertiary intrusion. The mean palaeomagnetic pole positions for the Upper Carboniferous-Permian was between Lat. 39.1° and 44.4°; Long. 162.7° and 166.3° with a predominantly reversed polarity (Tarling, 1980). Although the sign of Permian polarity would have been suitable for use in many of the models, the associated inclination values (-10° to -15°) would have increased amplitude and slightly lengthened wavelength values relative to the presented Tertiary models. Nevertheless, differentiating between Tertiary and Permian rocks based on theoretical modelling alone is unsound.

The observed gravity profile is a combination of a relatively flat background with a value around +18 mGal and sub-surface rocks with densities greater than a crustal average of 2.67 g cm^{-3}. Gravity modelling suggests that the observed signature can be explained by either basic intrusions at relatively shallow depth or by dense basement rocks such as pelitic gneisses at between 6 and 8 km depth. A combination of both rocks types with basement

rocks at around 6 km depth is also possible. The absence of high magnetic relief contours over the position of the gravity peak argues against the existence of shallow basic rocks, assuming that basic rocks would have a detectable induced magnetization. Gravity and magnetic models are expounded further in Chapter 6, which will discuss geological implications of the derived models.

CHAPTER 6

IMPLICATIONS FOR LUNDY VOLCANO AND TERTIARY MAGMATISM IN SOUTHWEST ENGLAND

6.1 INTRODUCTION

The evolution of the Lundy Igneous Complex has been summarized by Stone (1988), Thorpe *et al.* (1990) and Thorpe and Tindle (1991). Stone (1988) hypothesized that the Lundy granite was emplaced at a relatively high level in the upper crust and contaminated by host Devonian sediments. Thorpe *et al.* (1990) described a mixed mantle-crustal magma source for the Lundy granite, but with a different crustal source than for most of the older Cornubian granites, where the magma component may represent around 50% fractional crystallization of a basic magma to produce the required granitic melt. As basic dykes cut granite on Lundy Island, it follows that basic magma must have been available throughout the emplacement of the entire Complex. The timing of Tertiary magmatism was discussed in sections 1.1.1 and 4.1.

Thorpe *et al.* (1990) invoke the models of Huppert and Sparks (1988) to explain processes whereby granite magmas could be generated by the intrusion of basaltic magmas into the lower continental crust. In this context, Thorpe *et al.* (1990) described the emplacement of large volumes of basic magma (> 1000 km^3) into heterogeneous continental crust within the Lundy horst, so that the Lundy granite was formed by partial or total melting of relatively deep crustal rocks. Such a model would allow for interaction and potential mixing between fractionating basic magma and melt-derived granitic magma to produce the hypothesized mixed magma-crustal sourced Lundy granite. However, this would mean that Lundy Island should be underlain by a substantial body of basic rock and supportive evidence for this is not provided by either gravity or magnetic anomalies. Large volumes of basic rocks at shallow depths (~1-2 km) in particular should present some sort of magnetic signature to accompany a positive gravity anomaly, even if they have a low susceptibility.

6.1.1 Geochemical Constraints on the origin of the Lundy magmas

Thorpe and Tindle (1992) reported initial $^{87}Sr/^{86}Sr$ ratios between 0.70338 and 0.71321 for basic to acid dykes on Lundy Island, contrasting with initial $^{87}Sr/^{86}Sr$ ratios between 0.71461 ±0.00624 (Thorpe *et al.*, 1990), 0.7194 ±0.0068 (Hampton and Taylor, 1983) and 0.728 ±0.003 (Dodson and Long, 1962) for the Lundy granite itself. Such high $^{87}Sr/^{86}Sr$ ratios for the Lundy granite indicate the importance of crustal melting in the formation of the granite. Thorpe *et al.* (1990) also noted that the ε_{Nd} values for the Lundy granites (ε_{Nd} = -0.88 to -1.9) plot between contemporaneous mantle (positive ε_{Nd}), Cornubian granites (ε_{Nd} = -8 to -9) and Palaeozoic sedimentary rocks (ε_{Nd} = ~ -11), indicating that the Lundy granite was not derived solely by melting of basement rocks but that it also contains an important mantle-derived component.

McDonough *et al.* (1985) distinguished between magmatism derived from the melting of the continental lithospheric mantle ($^{87}Sr/^{86}Sr$ = 0.7035 - 0.7100; ε_{Nd} = +12 to -7) and plume-related magmatism ($^{87}Sr/^{86}Sr$ = 0.7028 - 0.7070; ε_{Nd} = +8 to -6). It is therefore not possible to characterize the source of magmatism based solely on the range of initial $^{87}Sr/^{86}Sr$ ratios of 0.70338 - 0.71321 (mean value = 0.70619) and ε_{Nd} values of 5.9 to 9.0 given by Thorpe and Tindle (1992). Nevertheless, strontium isotopes fall within the range of values given by Menzies and Halliday (1988), who noted $^{87}Sr/^{86}Sr$ values of 0.70320 - 0.07141 from mantle xenoliths derived from the continental lithosphere within Tertiary volcanics in North Scotland. Also, Rollinson (1993) noted that positive ε_{Nd} values indicate that rocks have been derived from a depleted mantle source region with Sm/Nd ratios greater than CHUR (Chondritic Uniform Reservoir, the chondritic model for the composition of the bulk earth). However, the lithosphere beneath the Lundy area is probably different from the lithosphere in Scotland.

Conversely, new data introduced in section 4.6 indicated that several trace element ratios (e.g. Zr/Nb, La/Sm, La/Ce, K/Rb and K/Ba) have more in common with plume-related magmatism than with conventional MORB activity. It thus seems likely that magmatic activity associated with the Lundy Igneous Complex was transitional between plume and

depleted N-type MORB magmatism, or that there may have been a zone of mixing between depleted and enriched mantle, with a significant contribution from the sub-continental lithospheric mantle.

At least two discrete magma populations of Si-saturated quartz tholeiites and Si-undersaturated alkaline-olivine basalts were indicated in section 4.5.1 (cf. Figure 4.10) for basic rocks on Lundy Island. The two magma populations are not simple artefacts of weathering processes. There is no evidence for mixing of these two magmas, so the two sources must have been spatially (and probably temporally) separate. The Lee Bay dykes were shown to be olivine tholeiites in section 4.5.2, although some degree of element mobility may caution against absolute definition. However, the Lee Bay dykes significantly pre-date and are more basic than their Lundy counterparts, hence they are unlikely to have originated from either of the two tholeiitic magma populations already identified for Lundy Island. Given that the entire Lundy Igneous Complex spanned a relatively short period of time (< 2 Ma; Mussett *et al.*, 1988), it also seems unlikely that the dykes were supplied by the same reservoir, even taking into account the role of fractional crystallization.

Three groups of dolerite dykes from Lundy Island were identified (Figure 4.15) based on their individual spidergram patterns. Group A corresponds to the low-Ti/low-Fe field identified by major element variations in Figure 4.11(a) and has been clearly affected by contamination by the upper continental crust (cf. Figure 4.24) with enrichment of LIL elements and showing Ti and P troughs. Fractionation of ilmenite and apatite could also cause Ti and P troughs, but optical analysis of thin sections has not revealed the presence of either mineral in the dolerite dykes and so it is assumed that this has not occurred. Although the Zr peak seen in Group A dykes is most probably caused by high Zr levels within the upper crust (Taylor and McLennan (1971), Sun (1980) suggested high Zr levels might also indicate involvement of the asthenosphere as a source material. As the Lundy Granite itself has low Zr values between 13 and 75 ppm, it is unlikely that the granite was the source of Zr in enriched-Zr spidergrams plots, despite field and thin section evidence of incorporation of granite xenoliths and feldspar xenocrysts.

Group A dolerite dykes are thus interpreted here as the product of a relatively long-lived storage body or bodies that ponded at high crustal levels to allow significant, but variable, assimilation of presumed sedimentary material. Carboniferous and Devonian silts, sands and shales (possibly up to 4 km in thickness) are the most likely host rocks for the storage bodies at high levels in the North Devon region.

Group B dykes correlate with the high-Ti/high-Fe field (Figure 4.11), but show less crustal contamination than Group A dykes. The relatively flat spidergram plot for Group B dykes (Figure 4.15) is generally less enriched in minor elements than that for Group A dykes, with the exception of Ba and Sr troughs. Barium is a reasonably mobile element and so may have been preferentially removed from the rocks by hydrothermal activity, but strontium is more immobile and would not have been affected by the same processes to the same extent. However, some strontium may have been incorporated into plagioclase phenocryst phases during protracted residence in storage reservoirs. A small trough in potassium might also indicate a fractionating phase in some of the dolerites and trachytes.

The absence of a Nb (and accompanying Ta) trough is more probably indicative of minimal crustal contamination (Weaver and Tarney, 1981) than suggesting mantle or continental lithosphere heterogeneity. Huppert and Sparks (1985) indicated that emplacement of high-temperature basic magma would be turbulent if dyke widths exceeded 3 m. Group B dykes are mostly < 2 m in width and so may have been emplaced under laminar flow conditions, which would minimize extensive wall-rock interactions and hence result in the absence of a Nb trough. Although dyke BW1 in Group B is over 4 m in width, there is field evidence of more than one intrusive phase and so each phase must have been < 2 m in width.

There is a small sample of Group C dykes, which is statistically disadvantageous. However, the data presented here indicate that Group C dykes may be the least contaminated by the continental crust, as spidergram plots are sub-horizontal and overall less enriched in trace elements than the other two groups. Such a flat profile contrasts noticeably with the saw-tooth profiles of both the lower and upper continental crusts. Group C dykes appear to be transitional between the models for OIB and P-type MORB,

but plotting closer to the P-type MORB pattern. It is also significant that there are few similarities with the spidergram pattern of the lower crust for any of the dykes (cf. Figure 4.23), suggesting at first sight that there may not have been any magma storage bodies within the lower crust above the crust-lithosphere boundary. Any deep storage bodies must have therefore have ponded below this boundary in the upper lithospheric mantle.

The spidergram plots of the Lee Bay dykes have more in common with Group C rocks than either Group A or B, but are still comparatively enriched in most trace and rare earth elements relative to Group C dykes. A distinctive Sr trough is probably due to substantial crystallization and removal of plagioclase due to fractionation and is more pronounced than for any dyke on Lundy Island. The Lee Bay dykes (up to 45 cm in width) are thus probably not derived from storage bodies associated with Lundy Island, but from a separate reservoir nearer to their outcrop.

Evidence for discrete magma sources and storage bodies is also provided by Thorpe and Tindle (1992), who demonstrated a high-Zr rhyolite (1654 ppm) and a rarer low-Zr rhyolite (294 ppm) with separate compositional and geographical characteristics. Whilst noting minimal crustal contamination in Lundy dolerites, Thorpe and Tindle (1992) envisaged that the geochemistry and petrogenesis of the bulk of the Lundy dyke association could be interpreted in terms of extensive fractional crystallization of basaltic magma in a magma chamber of complex geometry either below the presently exposed Lundy granite or within its immediate vicinity. Such an approach would encourage the concept of a Lundy volcano evolving over a period of time to form a substantial composite bimodal basalt-trachyte/rhyolite volcano above the granite in the Bristol Channel.

However, new evidence presented here indicates that there may have been several magma storage reservoirs at different depths and different geographical locations spread over the region. This argues against Lundy volcano being supplied by a single large magma chamber, as suggested by Brooks and Thompson (1973) and Thorpe and Tindle (1991; 1992), but rather by a plexus of smaller reservoirs. A cartoon of the postulated sub-surface relationships is given in Figure 6.1.

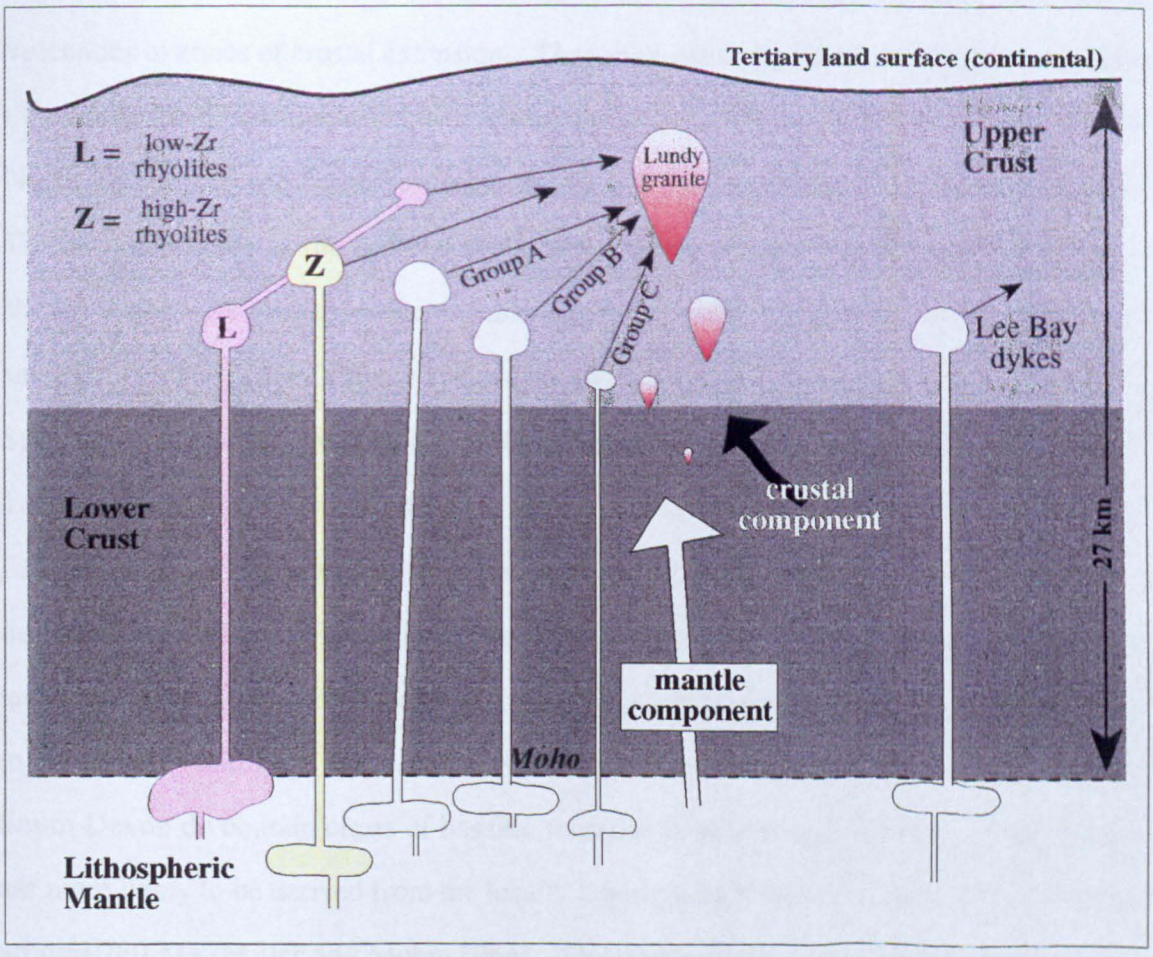

Figure 6.1: Idealized cartoon of differing sources of dykes in the Palaeogene.
Arrows emanating from magma chambers indicate emplacement of dykes. Although most dykes on Lundy Island have been sampled from the granite host, it should be noted that present-day submarine sediments up to 15 km away from the island also contain dykes. The Lundy granite is shown as having a diapiric form to simulate possible buoyancy relative to surrounding rocks. It should also be noted that erosion of an estimated 2 to 3 km of overlying sediments has exposed the Lundy granite. L and Z represent low- and high-Zr rhyolites as described by Thorpe and Tindle (1992).

Although the depth of magma chambers is schematic, their relative relationships in terms of levels within the crust are proportionate. However, lateral distances from Lundy are not real.

6.2 PHYSICAL SETTING OF MAGMATISM

Thorpe and Tindle (1991) hypothesized that Lundy was the site of a volcano around 10-20 km in diameter and composed of rhyolite and trachytic pyroclastic flows-airfalls with rhyolitic domes and basaltic scoria cones or lava flows, similar to other continental volcanoes in zones of crustal extension. They envisaged significant pyroclastic eruptions that would have been dispersed by the predominant westerly winds towards South Wales, North Devon and the Avon/Somerset region. If this hypothesis is tenable, the Lower Tertiary sediments of the Stanley Bank basin approximately 6 to 8 km east of Lundy should contain the vital evidence. Unfortunately, only the top 20 m of the basin has been sampled (to the Upper Oligocene; Fletcher,1975a) out of an estimated 120 m thickness. Supportive evidence of volcanic activity is therefore presently unavailable as the Lower Tertiary sediments in Mid and South Devon, whilst being contemporaneous with the Lundy Igneous Complex, do not contain appropriate rock clasts or weathered products indicative of sub-aerial eruptions. This may be an artefact of removal by north-flowing terrestrial river systems or indicate that prevailing winds did not carry sufficient material to the south. Although the Aller Gravels at the base of the Bovey Basin (Tertiary) in South Devon do contain clasts of basaltic material (Edwards and Freshney, 1982), these are more likely to be derived from the locally outcropping Exeter Volcanic Series, dated at around 280 Ma (Miller and Mohr, 1964). This section will examine the evidence for a Lundy volcano.

6.2.1 DISCREPANCIES IN GEOPHYSICAL MODELLING

Thorpe *et al.* (1990) noted that a positive circular gravity anomaly coincided with a positive magnetic anomaly, but comparison between Figures 5.1 and 5.6 indicates that the gravity anomaly is neither circular nor does it coincide with the magnetic anomalies. The Lundy Igneous Complex is thus atypical of other British Tertiary Volcanic Province (BTVP) centres as described by McQuillin and Tuson (1963), where circular gravity and magnetic anomalies have close inter-relationships. Bouguer anomalies for centres in the BTVP are given (in mGal) as Rhum 76, Skye 73, Mull 72, Carlingford 60, Ardnamurchan 42 and Arran 41. A Bouguer anomaly of ~ 50 mGal for Lundy Island is

thus comparable in magnitude to other BTVP centres.

Brooks and Thompson (1973) explained the positive gravity anomaly to the west and northwest of Lundy in terms of a major basic intrusion at shallow depth with a maximum thickness of 2.5 - 4 km to the west of Lundy Island. Such a body might have a volume between 1 and 2000 km^3 if a gabbro density value of 2.95 g cm^{-3} is used in modelling (Brooks and Thompson, 1973). Presumably, the volume of basic material might be argued to be greater if a lower density is used for basic rocks, assuming that the local Upper Palaeozoic density is relatively constant at 2.65 g cm^{-3}. Brooks and Thompson (1973) inferred a Tertiary age for the basic pluton and suggested a volcanic link to the Tertiary rocks of Lundy Island. Thorpe *et al.* (1990) concurred with this interpretation and noted that the position of the gravity high to the northwest was in broad agreement with the postulated NW-SE trend for the Lundy dyke swarm and postulated that this gravity high was both the source of Lundy dykes and of the heat source required to melt crustal rocks to produce in part the Lundy granite.

However, a major problem with this interpretation of the positive gravity anomaly is the absence of a coinciding magnetic signature. Such a massive basic body at shallow depths would normally be expected to produce some sort of magnetic signature, even with low susceptibility values. For example, the dyke or dyke swarm to the north of the gravity anomaly has a smaller volume than the postulated basic pluton, but is still marked magnetic by a magnetic anomaly (cf. Figure 5.6). Dolerite dykes on Lundy have a significant bimodal susceptibility distribution and also present clear field signatures. It thus seems doubtful that the parent magma chamber, particularly if lying at shallow depths, would not provide a magnetic signature.

Also, the position of the gravity high calculated in Figure 5.6 is clearly to the ***southwest*** of Lundy Island, in marked contrast to the gravity high derived by Brooks and Thompson (1973) to the northwest of Lundy (Figure 6.2). The new position of the gravity peak is not an artefact of either data processing or a function of anomalous computer plotting, as eight calculated Bouguer anomalies between 42 and 48.4 mgal occur within 5 km of the

A)

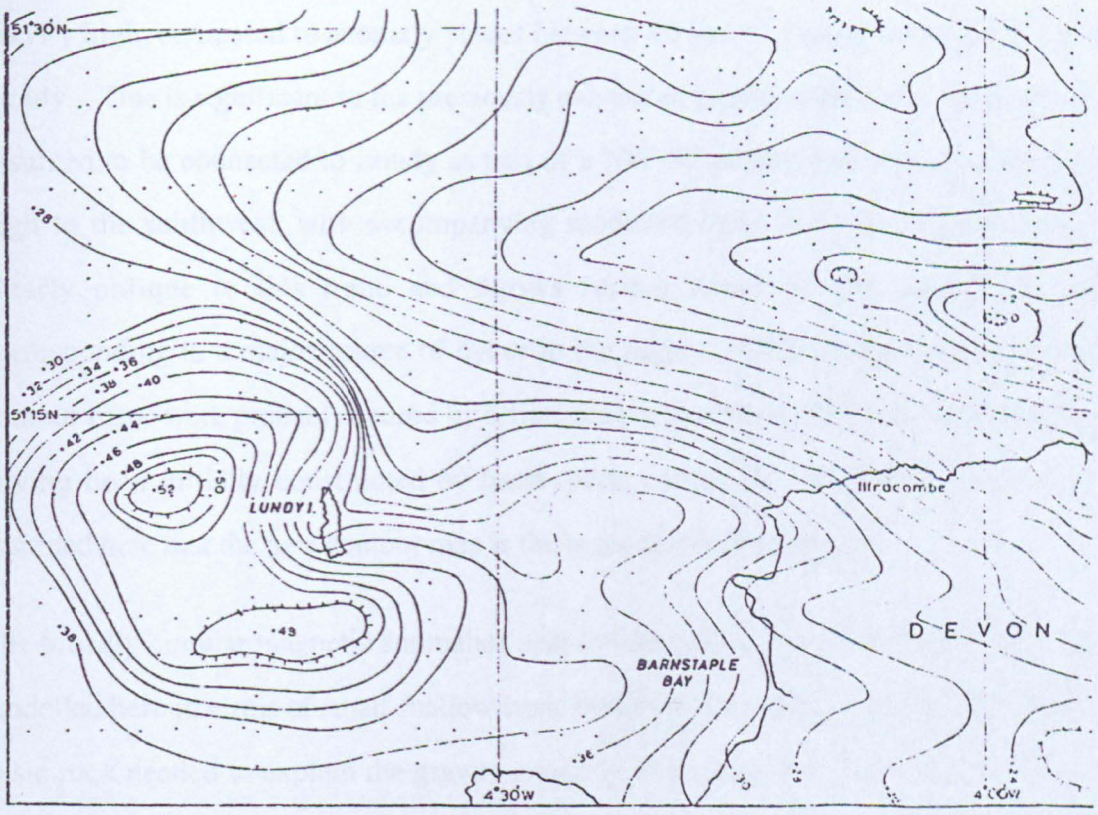

B)

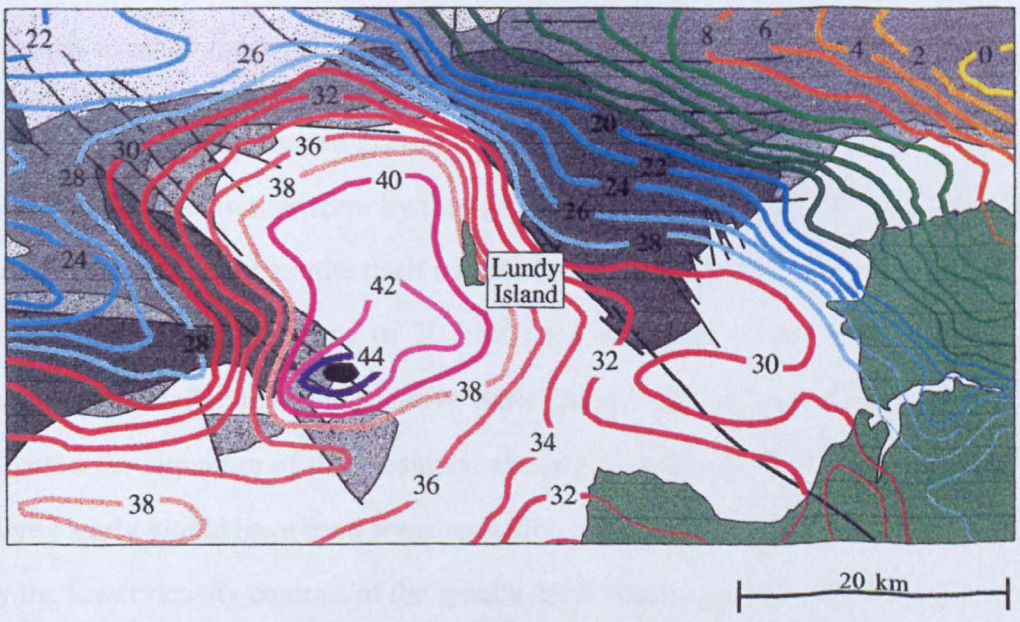

Figure 6.2: Bouguer anomaly contour maps for the Lundy area.
A) Gravity anomalies as published by Brooks and Thompson (1973). A gravity 'high' of +52 mGal is positioned to the west-northwest of Lundy Island.
B) Bouguer anomaly map for gravity data used in this thesis. The black ovoid represents the position of a gravity high greater than +46 mGal to the southwest of Lundy.
Both contour maps represent gravity data before processing the effects of the regional field. Figure 5.6 shows a larger scale version of B) with an explanation of geological units.

gravity high, compared to anomaly values between 40 and 41.5 mgal to the northwest of Lundy. This is significant as the previously calculated gravity high to the northwest was assumed to be connected to Lundy as part of a NW-SE extensional regime. A gravity high to the southwest, with accompanying modelled basic body (cf. Figure 5.14), is clearly oblique to this trend and throws further doubt on the gravity anomaly corresponding to a major source of dykes in the region. Differences between the two contour maps were probably caused by differences in plotting techniques, the earlier maps having been initially constructed by hand (pers. comm. Dr. Ian Smith, BGS). It is assumed here that the new contour map is the more objective of the two.

The broadly circular magnetic anomalies near to Lundy Island (cf. Figure 5.3) have been modelled here in terms of small shallow basic bodies and account for the large volume of basic rock needed to explain the gravity anomaly of Brooks and Thompson (1973). In any case, it is difficult to imagine how both positive and negative magnetic anomalies could be incorporated into a single basic mass, at least without implying temporal intervals to allow magnetic reversals.

Although the kidney-shaped gravity anomaly of Brooks and Thompson (1973) has been modified from a circular form by the Lundy granite (Figure 6.2), Bott (1958) suggested earlier that the Lundy granite itself had the form of a cylinder of 4.8 km diameter and 1.6 km height, giving a volume of 30 km^3 for the granite mass. This is two orders of magnitude smaller than the massive basic pluton and so the extent to which this has affected the signature of the presumed underlying basic rocks is questionable, although there clearly would have been some reduction in amplitude in the gravity anomaly caused by the lower density contrast of the granite itself with respect to surrounding rocks.

Brooks and James (1975) completed a number of seismic traverses in the Bristol Channel to enhance geological interpretation of sub-surface structures in the area. Line 73/3 was completed to investigate the cause of the postulated positive Bouguer anomaly to the northwest of Lundy Island. A two seismic layer model was derived, the uppermost layer with a seismic velocity of 4.57 ± 0.05 km s^{-1} being interpreted as about 500 m of Devonian sediments. The underlying layer was calculated as having a seismic velocity of

5.61 ± 0.09 km s-1 and this was interpreted as indicative of basic material to confirm the hypothesis of Brooks and Thompson (1973). However, the assumed seismic velocity of the basic material is relatively close to the value of 5.25 ± 0.12 km s^{-1} derived from line 73/2 to the east of Lundy Island and this velocity was interpreted as Devonian sediments. Further, Mechie (1980) and Llewellyn (1981) both interpreted seismic velocities in the region of 5.5 - 5.7 km s^{-1} within the Bristol Channel as indicating the presence of Lower Devonian sediments, whilst Al-Saadi (1976) had earlier noted that marine Devonian facies in North Devon could be characterized by seismic velocities up to 5.6 km s^{-1}. Indeed, Brooks *et al.* (1977) inferred seismic velocities in the region of 6.2 km s^{-1} as representing Lower Palaeozoic quartzitic rocks. Consequently, the conclusions of Brooks and James (1975) from the seismic evidence that basic rocks lie at shallow depth to the northwest of Lundy Island may not be justifiable, as the observed seismic velocities could simply reflect variations in either Upper or Lower Palaeozoic sediments and may not characterize basic rocks with P-wave velocities in the range 6.8 - 7.1 km s^{-1} at shallow depth (Rudnick and Fountain, 1995) and increasing to 7.2 km s^{-1} at 10 km depth.

The introduction of the basement model in Figure 5.14 and 5.16 to explain the gravity anomalies is consequently relatively attractive in terms of explaining the discrepancy between gravity and magnetic anomaly contour patterns. Not only do Bouguer anomaly contours mimic the western, northern and southern boundaries of the Lundy horst block, but the basement is also deep enough at a minimum of 6 km not to offer a significant magnetic signal at the datum. The observed negative magnetic regional field (cf. Figure 5.1) probably reflects some heterogeneity in the basement, but alternatively may be influenced by variations in the thick sedimentary pile overlying basement. There is therefore not enough corroborative geophysical evidence to indicate a shallow basic magma chamber to the west of Lundy Island. This may be a major problem for hypothesizing a volcano near to Lundy with the characteristics of other BTVP centres.

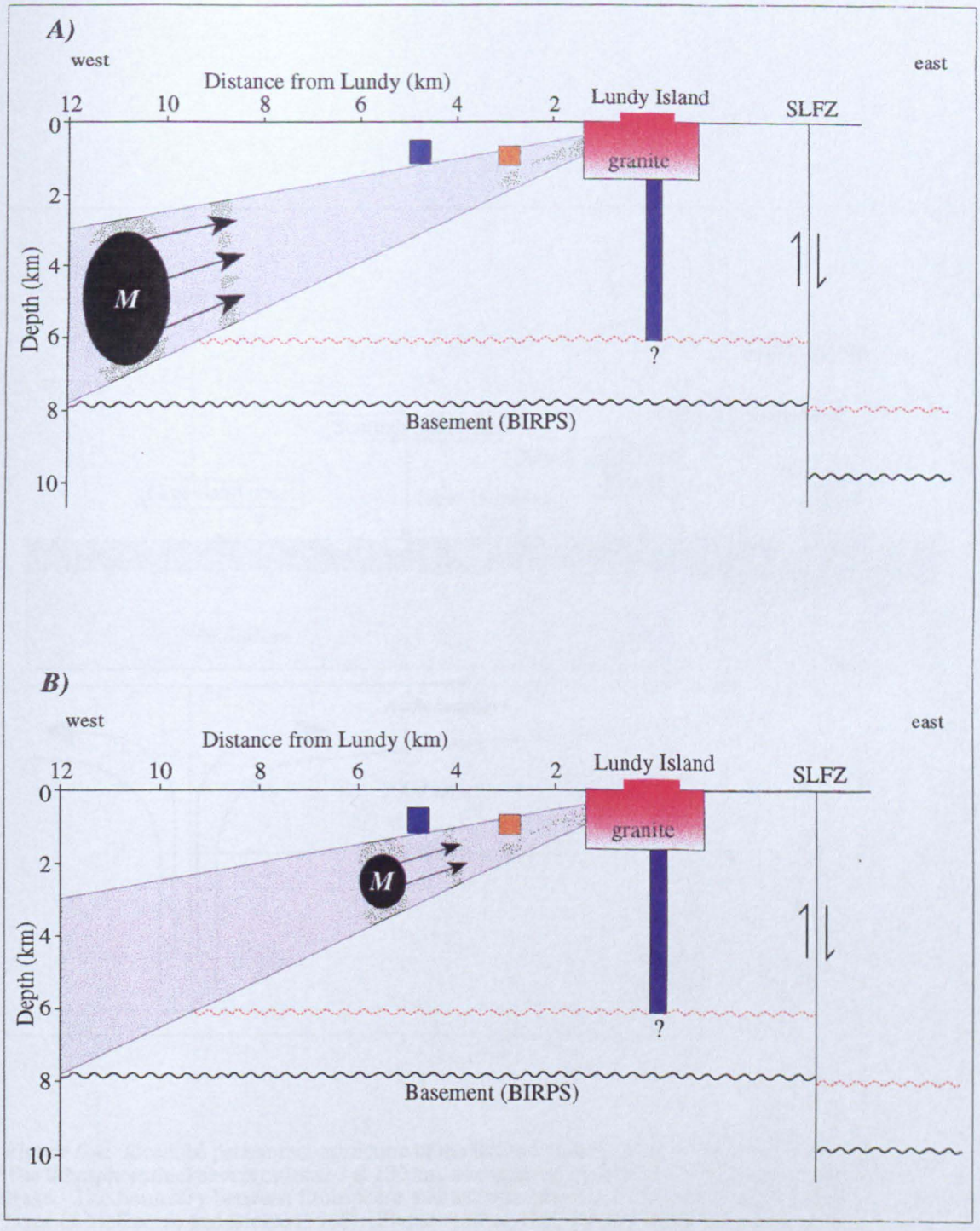

Figure 6.3: Sources of the Lundy Dyke Swarm.
Potential position of a parent magma chamber based on Walker (1993) and new AMS data. In both diagrams, the blue polygons represent positively magnetized basic bodies (cf. Figs. 5.10 + 5.12) and the pale brown square represents a negatively magnetized body (cf. Fig. 5.11). The grey zone represents the window of magma flow deduced from AMS measurements (cf. section 3.4.3.3) with an upper margin around 15^0 and a lower margin at about 35^0. SLFZ indicates the position of the Sticklepath (to Lustleigh) Fault Zone. Basement depth indicated by the black line is taken from BIRPS+ECORS (1986) and is based on line SWAT 3 (approx. 100 km to the west of Lundy), whilst the hypothetical brown basement line is derived from geophysical models shown in Figs. 5.14 + 5.16. A) calculated magma chamber position based on a total mean dyke width of 0.98 m and B) calculated magma chamber position based on a total mean dyke width of 0.53 m for radial dykes only. Note that the black ovoid shape (M) indicates the region where a potential magma chamber might occur and not the size of magma chamber itself. This region could contain more than one storage body.

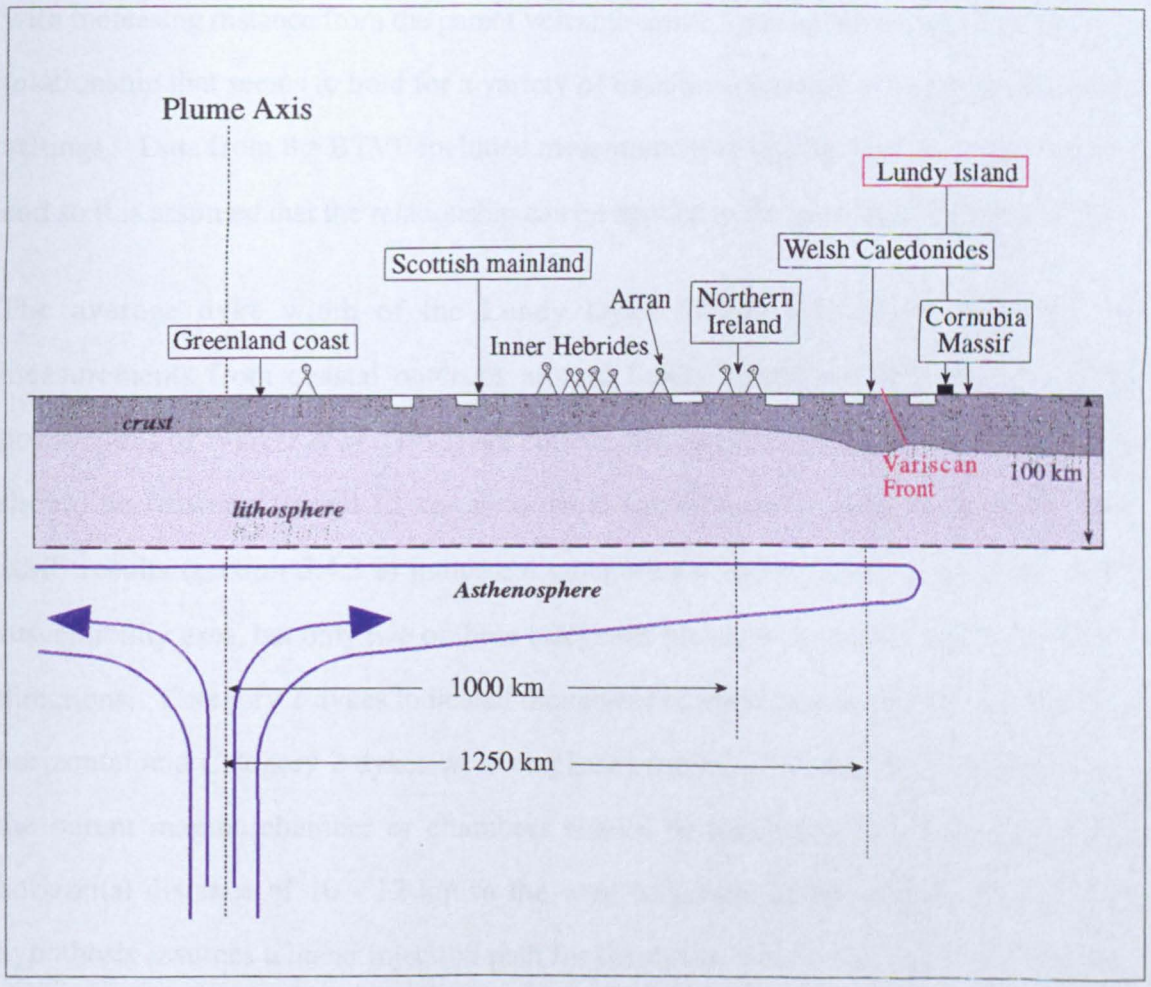

Figure 6.4: Idealized palaeo-reconstruction of the Icelandic plume prior to break-up of the North Atlantic. The lithosphere thickness is estimated at 100 km, as suggested by McKenzie (1989) for a stable Phanerozoic stage. The boundary between lithosphere and asthenosphere corresponds to the mechanical boundary layer of McKenzie and Bickle (1988). Plume radii of 1000 km and 1250 km are taken from White and McKenzie (1989) and Thompson and Gibson (1991) respectively. The black square represents the position of Lundy Island and white areas within the crust indicate pre-existing Mesozoic basins, which have a close relationship with volcanism in the BTVP (Moreton, 1987; Thompson and Gibson, 1991).

6.2.3 RELATIONSHIPS BETWEEN DYKES AND VOLCANO

Walker *et al.* (1995) described a spatial relationship between size of dyke and distance from parent magma chamber. They demonstrated that the mean dyke width increases with increasing distance from the parent volcanic centre up to a distance of about 40 km, a relationship that seems to hold for a variety of basaltic volcanoes in a variety of tectonic settings. Data from the BTVP included measurements from the Mull and Skye centres, and so it is assumed that the relationship can be applied to the postulated Lundy volcano.

The average dyke width of the Lundy Dyke Swarm is 0.98 m based on 164 measurements from coastal outcrops around Lundy Island (section 3.2.1). If the postulations of Walker *et al.* (1995) are correct, the parent magma chamber of the dykes should be between 10 and 12 km away from Lundy Island, presumably to the west. AMS results (section 3.4.3.2) indicate 4 categories of dykes based on orientations of susceptibility axes, but only two of these categories proved to be useful indicators of flow directions. Category 1 dykes indicated movement of magma between 15° and 35° from horizontal and Category 2 dykes were emplaced between 20° and 38°. Consequently, the parent magma chamber or chambers should be located at 3 - 7 km depth at a horizontal distance of 10 - 12 km to the west of Lundy Island (Figure 6.3a). This hypothesis assumes a linear injection path for the dykes, which may not be justifiable in host sediments that have suffered extensive deformation within the Variscan orogeny. Extensive faults/joints and a well developed cleavage with an east-west orientation are well displayed in host sediments, particularly the finer shales and silts. Although dyke injection pathways on Lundy Island indicated a window of 15° - 38°, this does not preclude a sub-horizontal pathway somewhere between Lundy and postulated magma chamber. Such a sill-like form would allow a magma chamber to occupy a shallower depth (Figure 6.3b) whilst having the same flow inclinations as measured by dolerite dykes on Lundy Island.

The Lundy Dyke Swarm is composed of regional and radial components (section 3.2.1), where reverse extrapolation of the radial component indicates a possible magmatic origin some 3 - 5 km to the west of Lundy Island. Magnetic modelling does indeed reveal basic

reservoirs between 3 and 5 km from the island at around 1 km depth (Figure 6.3a), but this contradicts the evidence of Walker *et al.* (1995) who predict an origin further to the west. However, the mean thickness of the radial dykes is 0.53 m which indicates a volcanic centre 5 - 6 km to the west, whereas the NW-SE regional dyke component has a thicker mean dyke width at around 1.4 m to suggest an origin some 25 - 30 km away.

Hence, the magma chambers modelled in section 5.4.1 are probably too shallow to be the focus of the observed AMS inclinations. The important corollary of this is that the shallow magma chambers modelled at a distance of 3 - 5 km from Lundy Island are probably not the magmatic source of dykes within the granite, although the smaller negative anomaly 3 km to the west could be the source of some dykes on Lundy if a strong lateral emplacement of magma is incorporated.

6.2.3 LUNDY VOLCANO?

The evidence presented thus far suggests that there may not have been a single large magma chamber within the Lundy area and hence the large composite volcano postulated by Thorpe and Tindle (1991) probably did not exist in the conventional form of a strato-volcano. Considering that around 4 km of overlying sediments may have been removed from the Lundy horst (Stone, 1988), the shallowest basic rocks modelled here by geophysical methods may have been > 4 km below ground level when still semi-molten or molten. The preferred model here is that of a number of small magma chambers, some possibly connected but others self-contained, being fed by a deeper mantle reservoir.

Rubin and Pollard (1987) quantified conditions under which dyke propagation would proceed and which criteria would need to be fulfilled before eruptions could take place. For eruptive activity to proceed at the surface, the vertical magma pressure within a chamber ($P_m(y)$) must exceed the overlying lithostatic load or weight of the rock overburden. The magma pressure is in turn partly a function of magma density, the amount of vesiculation and magma viscosity. Fujii and Kushiro (1977) calculated that typical densities for basaltic magma would be in the region of 2.6 - 2.65 g cm^{-3}, which is

similar to the host Lower Palaeozoic densities (2.62 - 2.73 g cm^{-3}) in North Devon calculated by Bott *et al.* (1958), Brooks, Bayerly and Llewellyn (1977) and Llewellyn (1981). Vesiculation can reduce density values by up to 1 g cm^{-3} which has the effect of increasing the buoyancy of the magma and making eruptions more likely. However, field evidence indicates that dykes are virtually free of vesicles apart from small trains within the chilled margins of some dykes. This is probably due to the release of small amounts of gases in the magma during high-level emplacement, where load pressure is less than the gas pressure within the magma and as such would have had minimal effect on magma density.

In the context of Lundy volcano, it seems that the overlying lithostatic load in the Lower Tertiary may have been too great to allow magma movement to the surface. The fracture toughness of the host rocks was almost certainly low enough (due to extensive Variscan deformation in predominantly argillaceous lithologies) to allow extensive lateral movement of magma in pressurized cracks formed by brittle deformation. Sediments within the Carboniferous-Devonian are neither isotropic nor homogenous and so the effects of pressure conditions could not have been in a steady state, evidenced in part by abrupt 90° directional changes of dykes on Lundy Island. However, the density and number of dykes seen on Lundy Island argues in favour of lateral emplacement being the preferred direction relative to vertical movement.

Although vertical dykes feed fissure eruptions in Iceland (Morton and Parson, 1988), new AMS evidence of magma flow indicators (cf. section 3.4.3.3) presented in this thesis do not support vertical movement of magma, although the occurrence of vertical fingers (Fig. 7 Rickwood, 1990) on the outside contact of at least two trachytic dykes along the eastern coastline indicates a degree of localized vertical movement of a viscous magma. Such localized direction indicators probably do not reflect general magma movement in the more numerous basic dykes, as viscous trachytic dykes are usually emplaced under turbulent conditions (Lister and Kerr, 1990). In conclusion, the Lundy Igneous Complex was probably not associated with sub-aerial volcanic eruptions and is more likely to be composed of several storage bodies at varying depths rather than characterized

by 1 or 2 larger magma chambers. The regional dyke swarm was probably temporally distinct from the radial dyke component and was derived from a different magmatic storage body in the crust.

6.3 TECTONIC FRAMEWORK OF THE LUNDY IGNEOUS COMPLEX

The precise siting of centres of Tertiary vulcanicity within the BTVP has been a matter of conjecture for some time. Richey (1937) supposed that plutonic centres lie at the intersection of a N-S trending lineament in basement rocks and major NE-SW trending faults. This hypothesis was partially echoed by Vann (1978) who noted that centres were positioned at the intersection of early Tertiary dyke swarms and NE-SW trending faults, although the relationship between a deep N-S lineament and NW-SE trending dykes and dyke swarms is unclear. Speight *et al.* (1982) envisaged deep-seated NW-SE trending ridges of magma as a result of the incipient extensional regime associated with the opening of the North Atlantic. Volcanic centres were thus hypothesized to be derived from the intersection of the ridge and NE-SW trending major faults.

A satisfactory explanation for the position of the Lundy Igneous Complex has not previously been offered. The distance between Lundy Island and the bulk of Tertiary activity in northwest Scotland precludes commonality in terms of tectonic setting on the grounds of increased distance from the mid-Atlantic spreading ridge (and hence probable degrees of extension), differences in basement geology and diversity in tectonic terrain. Nevertheless, Figure 5.8 derived from Meissner *et al.* (1986) presents a model of crustal thickness around ground Great Britain and indicates a crude N-S boundary at about 30 km depth - very close to the projected N-S trend of Tertiary centres. It is interesting to note that no Tertiary centres have been identified to the east of this boundary on the British mainland (i.e. at depths > 30 km), whereas conversely <u>all</u> Tertiary centres (including off-shore sites) are located to the west of this boundary at < 30 km crustal depth. Indeed, some off-shore centres to the northwest of the Scottish mainland are located very close to a crustal depth of 25 km. Overlying crustal thickness above magma

collection reservoirs at the continental crust/lithospheric mantle boundary may thus be an important factor in the siting of Tertiary vulcanicity. Deformation in crustal rocks could also be a contributory factor and so the next section will examine evidence for fracturing in host rocks.

6.3.1 IMPLICATIONS OF EARLY TERTIARY STRESS REGIMES ON THE LUNDY IGNEOUS COMPLEX

Speight et al. (1982) demonstrated that stress trajectories instrumental during dyke emplacement can be derived from the direction and distribution of dyke swarm axes, based on the underlying assumption of Anderson (1951) that dyke emplacement occurred within the plane perpendicular to the minimum principal stress (σ_3). Speight et al. (1982) ascertained that the dominant dyke swarm direction within the BTVP was northwest to southeast, indicating a dominant NE-SW extension orientation. England (1988) noted that an additional asymmetric set of sigmoidal secondary swarms linked some of the major Tertiary centres, e.g. Skye and Mull; Mull and Arran/Kintyre. The secondary swarms locally have varying strikes from NNW-SSE to N-S which suggest a component of east-west crustal extension or shear within the regional extensional field.

The number of dykes within a particular dyke swarm is closely related to the amount of crustal extension associated with each central complex and can be estimated from the relationship -

$$\text{Amount of extension (\%)} = \frac{W_d}{W} \qquad \text{equation 6.1}$$

where W_d is the total thickness of dykes normal to their margins and W is the total length of the sample traverse. This relationship only holds for dykes with similar strikes in forming a swarm axis, as dykes oblique to this trend will not be true indicators of crustal dilation for the particular swarm axis being examined, even though they may add a small extensional component to the overall effect. Sloan (1971), Knapp (1973) and Speight et al. (1982) noted that the amount of crustal extension between 5 and 10 km away from central complexes within the BTVP reduced from around a 10% average close to the centres to < 1% most swarm axes, although Speight (1972) had estimated 20% crustal

extension based on dyke measurements on Skye.

The amount of NW-SE crustal extension in the Lundy area based on the true thickness of dykes on Lundy Island with strikes of $300^{o} \pm 5^{o}$ (the largest population of dykes) is calculated at < 0.8%. However, as Lundy Island lies to the east of gravity and magnetic anomalies (interpreted in terms of basic magma chambers in Chapter 5) and hence probably > 10 km to the east of centres of magmatic activity, it appears that the regional dyke swarm has been controlled mostly by the influence of a low magnitude tensional regime rather than by doming associated with volcanic uplift. Low strain rates may indicate that crustal rocks have not been unduly softened by the injection of increased heat flow which in turn argues against large volumes of magma at relatively high crustal levels. Thus, the regional dykes were passively intruded into host rocks as opposed to forming through an active mode of emplacement, which might have embraced considerable stoping and possible assimilation of host sediments or Lundy granite. Evidence of dykes with a sub-parallel WNW-ESE strike over a horizontal distance of about 30 km (cf. Figure 1.1) is further indication that dilationary influences were not simply the response to updoming.

Nevertheless, some localized Lower Tertiary updoming in the Lundy area must have occurred to allow emplacement of the radial component of the Lundy Dyke Swarm. Such updoming may have been caused by either inflation of the upper crust in response to the upward movement of molten basic/intermediate magma or by upward buoyancy of the semi-solidified granite. Some of the radial dykes include xenoliths of solid country rocks (both granitic and sedimentary in composition) and so there must have been at least a minor degree of active emplacement with associated stoping, rather than passive emplacement into pre-existing joints as indicated by Edmonds et al. (1979) and Thorpe and Tindle (1992). The regional dyke swarm component of the Lundy Dyke Swarm is consequently temporally distinct from the radial component and probably pre-dates it, similar to the chronological relationships in other major Tertiary centres (Mussett et al., 1988; Emeleus and Gyopari, 1993). The controlling stress fields may not be entirely the product of the opening of the North Atlantic. Tectonic activity in northwest Europe also

suffered northwest-southeast directed extension in response to collision between the African and European plates (Dewey, 1988). There was consequently ample opportunity for extensional stresses to form within the Bristol Channel region from a variety of causes.

6.3.2 MAGMATIC ACTIVITY AND THE VARISCAN OROGENY

Devonian and Carboniferous rocks in Southwest England have been heavily tectonized by the Variscan Orogeny (Selwood *et al.*, 1982; Hancock *et al.*, 1983) with the most northerly expression of deformation broadly forming an east-west front through the South Wales mainland just to the north of the Welsh coastline. Four phases of deformation occurred during the orogeny which lasted between about 280 - 360 Ma (Hancock *et al.*, 1983). Hence the entire sequence of deep sedimentary rocks in North Devon up to and including Early Permian members have been affected.

The major feature of the Variscan basement in Southwest England is the development of a dominant east-west sub-vertical cleavage in host sediments and the widespread occurrence of northwest-southeast strike-slip faults. Movement along these faults was primarily dextral within the Variscan episode with some later Tertiary sinistral reactivation (Dearman, 1963; Freshney *et al.*, 1979). Although the overlying Mesozoic sediments in the South Celtic Sea/Bristol Channel Basins also suffered some tectonic uplift and subsidence (along with the underlying Palaeozoic sequences), the grade of deformation is less than that for Variscan structures.

The Sticklepath-Lustleigh Fault Zone (SLFZ) is the most important Variscan feature within the study area and was active throughout the Tertiary (Holloway and Chadwick, 1986), possibly up to and including the present time (Van Hoorn, 1987). Despite the steep easterly dip of the fault extending down into the upper crust (possibly into the lower crust), geophysical evidence suggests that magma did not utilize this obvious crustal weakness as a convenient magma conduit. This might indicate that a large voluminous magma chamber probably did not exist within the crust in the region adjacent to Lundy Island, as the magma pressure associated with such a single large body would have used

the SLFZ as a host site for magma emplacement. Although Thorpe and Tindle (1992) noted a dyke swarm to the northwest of Lundy which coincides with the SLFZ, the magnetic signature of the dyke swarm was both oblique to and displaced to the west of the SLFZ (Figure 5.1). There is therefore no evidence for any magma emplacement along the structurally mobile SLFZ and this argues in favour of the existence of several smaller bodies rather than one single large intrusion.

Blundell (1957) reported that the Lee Bay dyke and some dykes on Lundy Island were displaced by northwest-southeast faults to the same extent as country rocks and Arthur (1989) indicated a net dextral displacement of 3-8 km within the Bristol Channel region for host rocks. However, magnetic evidence presented in Chapter 3 suggested that northwest-southeast faulting is not a significant feature on Lundy Island and most dykes on Lundy are in fact undisturbed by Tertiary displacements. A fault breccia in the Lundy granite cropping out in a coastal cliff towards the northeastern end of the island does indicate at least one east-west fault, but relative displacements are impossible to determine within the locally homogenous granite. Also, inland persistence of the fault is unknown and there is no corresponding outcrop along the western coastal cliff line. Although dextral strike-slip faulting is evidenced by field observations in at least one dyke at Lee Bay, displacement is only in the order of 10-15 m and is consequently not indicative of major crustal instability.

The Lundy Horst may thus have acted as a competent block throughout the Tertiary and although bounded on all sides by significant faults (Arthur, 1989), large volumes of magma have not breached these areas of structural weakness but rather only invaded small fractures and cleavage planes within the horst itself. The dominant NW-SE strike of dykes in outcrop (Figure 3.3) broadly coincides with Variscan fault trends and these dykes are therefore again interpreted as a regional dyke swarm rather than indicating localized magmatic activity associated with the Lundy Igneous Complex. In terms of the stress regime outlined in section 6.3.1, northwest-southeast directed extension may have been facilitated by the fundamental tectonic grain created by Variscan structures, even though passive dyke emplacement in the Lundy granite was related more to cooling

fractures and cracks from Tertiary uplift. Dykes at Lee Bay were intruded parallel or sub-parallel to the dominant east-west cleavage and not along (presumably pre-existing) NW-SE faults.

The emplacement of Tertiary magmatism in the Bristol Channel was therefore facilitated by the fractured nature of the host rocks. Whilst is true that major geological units in mid- to south Devon were also tectonized by Variscan deformation, the lack of recorded Tertiary igneous rocks in those areas implies that favourable conditions in the host crust was not the only factor in controlling magmatic activity. Similarly, major geological formations on the Welsh mainland to the north were tectonized by older deformation events such as the Caledonian Orogeny, but the lack of Tertiary magmatism in this area also indicates the important role of other factors controlling emplacement of magma.

6.3.3 IGNEOUS ACTIVITY AND THE ICELANDIC PLUME

The large volumes of basalts produced within the BTVP have been explained as the product of continental rifting above an anomalously hot region - the result of growth of the present-day Icelandic plume. The characteristic form of the plume is that of a mushroom-shaped zone of anomalously hot asthenosphere beneath the lithosphere with a 2-2.5 x 10^3 km diameter in plan view (Griffiths and Campbell, 1990; Watson and McKenzie, 1991). White and McKenzie (1989) indicated a central focus for the plume under the eastern border of Greenland before the break-up of the North Atlantic plate in the Late Cretaceous/ Early Tertiary. Conversely, Duncan (1984) had earlier suggested a plume centred about 300 km further towards the northwest beneath the mainland of Greenland.

After taking palaeo-reconstruction into account, Lundy Island would have been positioned near to the southernmost extremity of the Icelandic plume at the initiation of oceanic spreading in the North Atlantic (Figure 6.4). Such a setting would have represented a centre-to-edge radius of almost 1,400 km for the plume head. This is some 150 km outside the maximum range of plume diameter given by Griffiths and Campbell (1990) as well as by Thompson and Gibson (1991), but this does not preclude the possibility of a

localized tongue of plume extending beneath the Bristol Channel area from the north. Such a feature is required to explain the plume-related signatures apparent in some of the geochemical data presented in Chapter 4. Nevertheless, plume-related magmatism cannot account for all the basic intrusions associated with Lundy Igneous Complex. As Hawkesworth and Gallagher (1993) noted, one of the distinctive features of a mantle plume is the production of large volumes of magma. The existence of voluminous basic magmas in the Lundy area is not supported thus far in this thesis.

McKenzie and Bickle (1988) quantified the thickness of a partial melt that would be generated by decompression of an upwelling asthenosphere in areas of assumed uniform stretching for a lithosphere thickness of 100 km, whilst White (1988) discussed the implications of such calculations for the BTVP (Figure 6.5). With respect to the Lundy area where ~1% crustal extension (stretching factor (β) = 1.01) is suggested by the regional dyke swarm, it seems that even when β approaches a value of 1.3, only low volumes of melt will be produced at relatively high temperatures (up to 1480 °C). Such high temperatures are more typical of the central core of the Icelandic plume, i.e. closer to the point of continental break-up, and somewhat elevated for the extreme flanks, i.e. the position of Lundy with respect to Iceland.

On the other hand, the ambient asthenosphere temperature some distance away from the influence of hot spots is around 1280 °C and Figure 6.5 indicates that melts will only be produced when β approaches 3, i.e. the lithosphere is thinned to a third of its original thickness. Even when the lithosphere is thinned to one-fifth of its original thickness (β = 5), then only ~ 2 km of melt is created (White, 1988). Figure 6.5 therefore introduces a discrepancy between ambient temperature, stretching factor and amount of melt produced. It thus seems probable that the low amount of crustal extension cannot be associated with the production of significant volumes of magma. If the conclusions of McKenzie and Bickle (1988) hold for southwest England, very small volumes of melt (or even no melt) were produced.

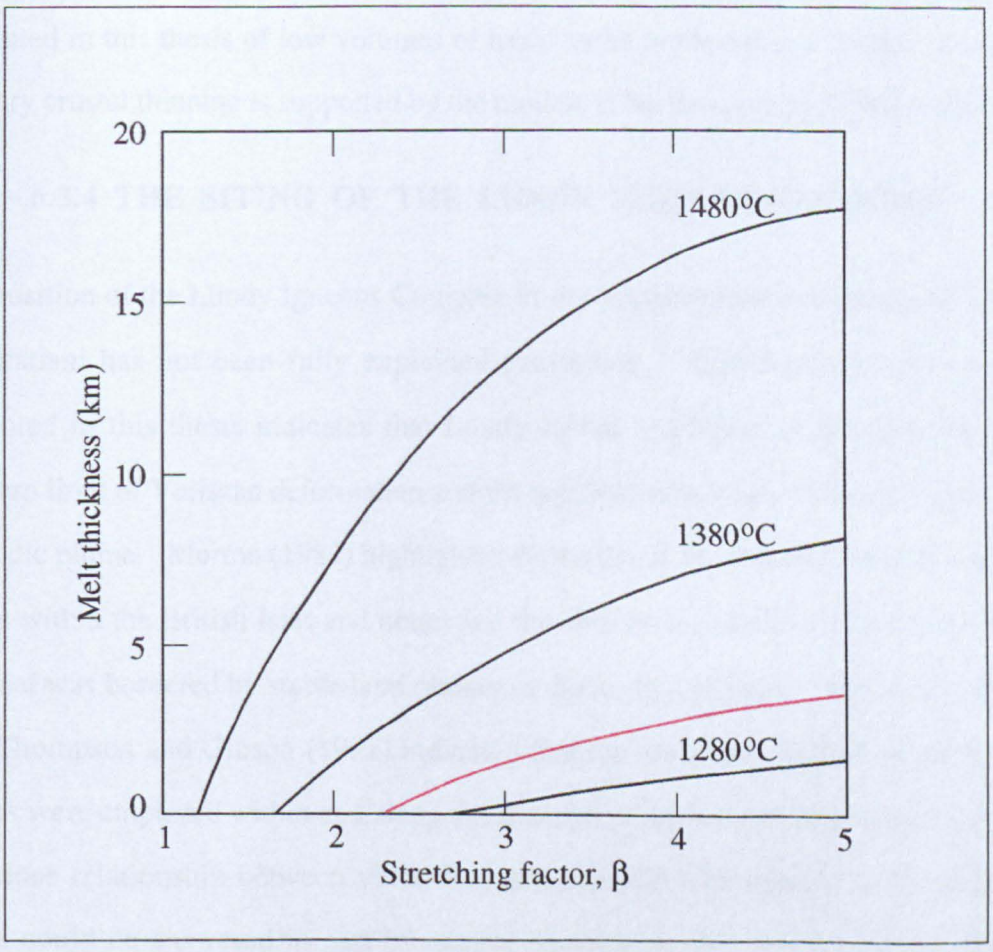

Figure 6.5: Thickness of partial melt generated by decompression melting of upwelling asthenosphere. This figure assumes a lithospheric thickness of 100 km and the three curves represent possible temperature ranges in the asthenosphere, dependant on position with respect to an underlying plume. The red line is an estimate of the temperature gradient in the mantle under the Bristol Channel area, assuming the Iceland plume had an influence that far south. After McKenzie and Bickle (1988).

Therefore although the basic rocks in the Lundy Igneous Complex appear to be transitional between plume-related magmatism and partial melts of the lithospheric mantle, it is difficult to marry the tectonic setting of the Bristol Channel area in the Lower Tertiary with the production of large volumes of magma. It thus seems likely that the hypothesis presented in this thesis of low volumes of basic melts produced in a regime of minimal Tertiary crustal thinning is supported by the models of McKenzie and Bickle (1988).

6.3.4 THE SITING OF THE LUNDY IGNEOUS COMPLEX

The position of the Lundy Igneous Complex as the southernmost occurrence of Tertiary magmatism has not been fully explained previously. However, the new evidence presented in this thesis indicates that Lundy Island is situated at the junction of the northern limit of Variscan deformation and the southernmost limits of the influence of the Icelandic plume. Morton (1987) highlighted the extent of Triassic and Jurassic subsiding basins within the British Isles and noted that the east-west subsiding basin in the Bristol Channel was bordered by stable land masses to the north and south. Following on from this, Thompson and Gibson (1991) indicated that the main lava fields and early major centres were emplaced within and along the margins of these subsiding Mesozoic basins. The close relationship between volcanism and position with respect to the Mesozoic basins could be answered in part by crustal thinning caused by extensional regimes. Although there was a substantial time gap between volcanic activity and the end of extension, Thompson and Gibson (1991) considered this indicated that crustal thinning was permanent.

Figure 5.8 showed a thickened shoulder of crust in the Welsh Caledonides area to the north of the Lundy region where the crust thickness is > 30 km. Although this area would have been a potential host for Tertiary magmatism if the influence of the Icelandic plume did extend as far as the Pembrokeshire ridge from the north, the terrain must have acted as a competent block and/or been too thick to allow easy access for migrating magma. However, any magma generated under this thick block may have migrated upwards and southwards into the Bristol Channel area if a thinned crust existed under the Mesozoic basin along the axis of the Bristol Channel. The base of the crust might also

have a local varied topography resulting in the production of a small degree of adiabatically decompressed magma.

No further Tertiary magmatism within the BTVP occurs to the south of the Lundy area due to the rigidity of the Cornubia massif and the continuation of ambient temperatures in the asthenopshere outside the influence of the Icelandic plume. The nature of the asthenosphere throughout the whole of southwest England may also have been changed by the previous phase of melting associated with the Cornubian rocks themselves. Re-melting of the asthenopshere was probably not as productive in the Tertiary compared to Permo-Carboniferous episodes.

Magmatism itself in the Lundy Igneous Complex was not only plume-related, as previously discussed, but contained abundant magma derived from partial melting of the sub-continental lithosphere. The heat source to produce this latter component was partially due to conduction through the asthenosphere and partially as a result of decompressive melting beneath the (thinned) crust. It is interesting to hypothesize the volcanic activity that might have ensued if the centre of convection in the asthenosphere which initiated the Icelandic plume had chanced to be nearer to the British Isles or if the European plate had moved westwards over the underlying hotspot at some point during the break-up of the North Atlantic. Similarly, the effects of Tertiary tectonic movements in southwest England could have been more akin to rifting forces in northeastern Europe. In either case, the eruption of a Lundy volcano might have been one of the most exciting geological occurrences in southern Britain during the last 60 Ma. Extensive plateau lavas and pyroclastic airfalls/flows might have radically changed the present-day topography and geomorphological control of the entire Southwest England.

However, evidence presented here suggests that sub-aerial eruptions were not a major feature of the postulated Lundy volcano. It seems likely that the overlying lithostatic load was enough to contain the pressure within the magma chambers, despite the relative fractured nature of the host rocks.

REFERENCES

Alexander, E.C., Mickelson, G.N. and Lanphere, M.A. (1978) MMhb-1: A new ^{40}Ar-^{39}Ar dating standard. *U.S.Geological Survey Open-File Report*, **78-701**, 6-8.

Allen, J.R.L. (1979) Old Red Sandstone facies in external basins, with particular reference to southern Britain. In: The Devonian System, (eds. M.R.House, C.T.Scrutton and M.G.Bassett). *Special Papers in Palaeontology*, **23**, 65-80.

Al-Saadi, R.H. (1976) Seismic studies of the geological structure in the inner Bristol Channel area. Unpublished Ph.D. thesis, University of Wales, Swansea.

Anderson, E.M. (1951) The dynamics of faulting and dyke formation with applications to Britain. Oliver and Boyd, Edinburgh. 206pp.

Arber, E.A.N. (1911) The coast scenery of North Devon. Dent, London. 142pp.

Arth, J.G. (1976) Behaviour of trace elements during magmatic processes - a summary of theoretical models and their applications. *Journal of Research of the U.S. Geological Survey*, **4**, 41-47.

Arthur, M.J. (1982) Investigations of geophysical anomalies in the Hereford area of the Welsh Borderland. *Institute of Geological Sciences, Applied Geophysics Unit Report 122.* 196 pp.

Arthur, M.J. (1983) Late Precambrian-Tertiary transcurrent faulting and plate margin activity in Southwest Britain. (Abstract), *2nd Deep Geology Workshop*, Cambridge University, p.11.

Arthur, M.J. (1989) The Cenozoic evolution of the Lundy pull-apart basin into the Lundy Rhomb Horst. *Geological Magazine*, **126**, 187-198.

Anderson, F.W. and Dunham, K.C. (1966) The geology of Northern Skye. *Memoir of the Geological Survey of GB*, HMSO, Edinburgh. 87 pp.

Balsley, J.R. and Buddington, A.F. (1960) Magnetic susceptibility anisotropy and fabric of some Adirondack granites and orthogneisses. *American Journal of Science*, **258A**, 6-20.

Bamford, D., Faber, S., Jacob, B., Kaminski, W., Nunn, K., Prodehl, C., Fuchs, K., King, R. and Willmore, P. (1976) A lithospheric seismic profile in Britain. *Geophysical Journal of the Royal Astronomical Society*, **44**, 145-160.

Bannerjee, S. (1991) Magnetic Granulometry. In: Environmental Magnetism Workshop Handbook, (ed. C.Hunt). *Institute of Rock Magnetism Meeting, June 1991*, University of Minnesota. 41-76.

Basaltic Volcanism Study Project (1981) Basaltic volcanism on the terrestrial planets. Pergamon Press, New York. 1286 pp.

Bell, B.R. (1982) The evolution of the Eastern Red Hills Tertiary igneous centre, Skye, Scotland. Unpublished Ph.D. thesis, University of London.

Bell, B.R. and Harris, J.W. (1986) An excursion guide to the the geology of the Isle of Skye. Geological Society of Glasgow. 317 pp.

Bell, B.R. and Emeleus, C.H. (1988) A review of the silicic pyroclastic rocks in the British Tertiary Volcanic Province. In: Early Tertiary Volcanism and the opening of the NE Atlantic, (eds. A.C.Morton and L.M.Parson). *Geological Society Special Publication No.39*, Blackwell, Oxford, 57-70.

Berggren, W.A., Kent, D.V. and Flynn, J.J. (1985) Palaeogene geochronology and chronostratigraphy. In: The chronology of the geological record, (ed. N.J.Snelling). *Memoir of the Geological Society of London*, **10**, 141-186.

Best, M.G. (1982) Igneous and metamorphic petrology. W.H.Freeman and Co., New York. 630 pp.

BIRPS and ECORS (1986) Deep seismic profiling between England, France and Ireland. *Journal of the Geological Society, London*, **143**, 45-52.

Blanchard, J.P., Boyer, P. and Gagny, C. (1979) Un nouveau critere de sens de mise en place dans une caisse filionienne: le "pincement" des mineraux aux epontes. *Tectonophysics*, **53**, 1-25.

Blundell, D.J. (1957) A palaeomagnetic investigation of the Lundy dyke swarm. *Geological Magazine*, Vol.**94**, 291-296.

Bott, M.H.P. and Tuson, J. (1973) Deep structure beneath the the Tertiary volcanic regions of Skye, Mull and Ardnamurchan, NW Scotland. *Nature*, **242**, 114-116.

Bott, M.H.P., and Tantrigoda, D.A. (1987) Interpretation of the gravity and magnetic anomalies over the Mull Tertiary intrusive complex, NW Scotland. *Journal of the Geological Society of London*, **144**, 17-28.

Bott, M.H.P., Day, A.A. and Masson Smith, D. (1958) The geological interpretations of gravity and magnetic surveys in Devon and Cornwall. *Philosophical Transactions of the Royal Society of London*, Series A, Vol.**251**, 161-191.

Breiner, S. (1973) Applications manual for portable magnetometers. Geometrics, California, 1-57.

Brooks, C., Hart, S.R. and Wendt, I. (1972) Realistic use of two-error regression treatments as applied to rubidium-strontium data. *Reviews of Geophysics and Space Geophysics*, **10**, 551-577.

Brooks, M. (1973) Some aspects of the Palaeogene evolution of Western Britain in the context of an underlying mantle hot spot. *Journal of Geology*, Vol.**81**, 81-88.

Brooks, M. and Thompson, M.S. (1973) The geological interpretation of a gravity survey of the Bristol Channel. *Journal of the Geological Society of London*, **129**, 245-274.

Brooks, M. and James, D.G. (1975) The geological results of seismic refraction surveys in the Bristol Channel, 1970-1973. *Journal of the Geological Society of London*, **131**, 163-182.

Brooks, M. and Al-Saadi, R.H. (1977) Seismic refraction studies of geological structure in the inner part of the Bristol Channel. *Journal of the Geological Society of London*, **133**, 433-445.

Brooks, M., Bayerly, M. and Llewellyn, D.J. (1977) A new geological model to explain the gravity gradient across Exmoor, north Devon. *Journal of the Geological Society, London*, **133**, 385-393.

Brooks, M., Hillier, B.V. and Miliorizos, M. (1993) New seismic evidence for a major geological boundary at shallow depth, N. Devon. *Journal of the Geological Society of London*, **150**, 131-135.

Brown, G.C. and Mussett, A.E. (1976) Evidence for two discrete centres in Skye. *Nature*, **261**, 218-220

Brown, G.M. (1980a) Bude, Sheets 307 and 308. Scale 1: 50 000. *Geological Survey of Great Britain (England and Wales).*

Brown, G.M. (1980b) Chulmleigh, Sheet 309. Scale 1: 50 000. *Geological Survey of Great Britain (England and Wales).*

Brown, G.M. (1982) Barnstaple, Sheet 283. Scale 1: 50 000. *Geological Survey of Great Britain (England and Wales).*

Burley, A.J. (1979) Geophysical Investigations. In: Geology of Bideford and Lundy Island, (eds. E.A.Edmonds, B.J.Williams and R.T.Taylor), *Memoir of the Geological Survey of GB*, Sheets 292 with 275, 276, 291 and part of 308. H.M.S.O., London. 121-124.

Butler, R.F. (1992) Palaeomagnetism. Blackwell, Oxford. 319 pp.

Butler, R.F. and Banerjee, S.K. (1975) Theoretical single-domain grain size range in magnetite and titanomagnetite. *Journal of Geophysical Research*, **80**, 4049 - 4058.

Cadogan, P.H. and Turner, G. (1977) ^{40}Ar - ^{39}Ar dating of Luna 16 and Luna 20 samples. *Philosophical Transactions of the Royal Society of London*, **A284**, 167-177.

Carmichael, R.S. (1992) Practical handbook of physical properties of rocks and minerals. CRC Press, Florida. 741 pp.

Caston, G.F. (1975) Igneous dykes and associated scour hollows of the North Channel, Irish Sea. *Marine Geology*, **18**, M77-M85.

Charoy, B. (1986) The genesis of the Cornubian batholith (southwest England): the example of the Carnmenellis pluton. *Journal of Petrology*, **27**, 571-604.

Chen, Y., Clark, A.H., Farrar, E., Wasteneys, H.A.H.P., Hodgson, M.J. and Bromley, A.V. (1993) Diachronous and independent histories of plutonism and mineralisation in the Cornubian Batholith, SW England. *Journal of the Geological Society, London*, **150**, 1183-1191.

Collinson, D.W. and Creer, K.M. (Eds.) (1967) Methods in Palaeomagnetism. Elsevier, Amsterdam. 609 pp.

Compston, W., Williams, I.S. and Meyer, C. (1984) U-Pb geochronology of zircons from lunar breccia 73217 using a sensitive high mass-resolution ion microprobe. *Journal of Geophysical Research*, **89**, 525-534.

Cook, A.H. and Thirlaway, H.I.S. (1952) A gravimeter survey in the Bristol and Somerset coal-fields. *Quarterly Journal of the Geological Society of London*, **107**, 255-286.

Cornwell, J.D. (1971) Geophysics of the Bristol Channel area. *Proceedings of the Geological Society of London*, **1664**, 286-289.

Cox, K.G. (1980) A model for flood basalt vulcanism. *Journal of Petrology*, **21**, 629-650.

Cox, A. and Dalrymple, G.B. (1967) Statistical analysis of geomagnetic reversal data and the precision of potassium-argon dating. *Journal of Geophysical Research*, **72**, 2603-2614.

Cox, K.G. and Hawkesworth, C.J. (1985) Geochemical stratigraphy of the Deccan traps at Mahabaleshwar, Western Ghats, India, with implications for open system magmatic processes. *Journal of Petrology*, **26**, 355-377.

Cox, K.G., Bell, J.D. and Pankhurst, R.J. (1979) The interpretation of igneous rocks. George Allen and Unwin, London. 450 pp.

Cross, W., Iddings, J.P., Pirsson, L.V. and Washington, H.S. (1903) Quantitative classification of igneous rocks. University of Chicago Press, Chicago.

Dagley, P. and Mussett, A.E. (1981) Palaeomagnetism of the British Tertiary Igneous Province: Rhum and Canna. *Geophysical Journal of the Royal Astronomical Society*, **65**, 475-491.

Dagley, P. and Mussett, A.E. (1986) Palaeomagnetism and radiometric dating of the British Tertiary Igneous Province: Muck and Eigg. *Geophysical Journal of the Royal Astronomical Society*, **85**, 221-242.

Dagley, P., Mussett, A.E. and Skelhorn, R.R. (1984) The palaeomagnetism of the Tertiary igneous complex of Ardnamurchan. *Geophysical Journal of the Royal Astronomical Society*, **79**, 911-922.

Dagley, P., Mussett, A.E. and Skelhorn, R.R. (1987) Polarity, stratigraphy and duration of the Mull Tertiary activity. *Journal of the Geological Society of London*, **144**, 985-996.

Dagley, P., Mussett, A.E., Wilson, R.L. and Hall, L.M. (1978) The British Tertiary Igneous Province: palaeomagnetism of the Arran dykes. *Geophysical Journal of the Royal Astronomical Society*, **54**, 75-79.

Dalrymple, G.B. and Lanphere, M.A. (1971) $^{40}Ar/^{39}Ar$ technique of K-Ar dating: a comparison with the conventional technique. *Earth and Planetary Science Letters*, **12**, 300-308.

Dalrymple, G.B. and Moore, J.G. (1968) Argon-40: excess in submarine pillow basalts from Kilauea Volcano, Hawaii. *Science*, **161**, 1132-1135.

Dalrymple, G.B., Grommé, C.S. and White, R.W. (1975) Potassium -argon age and palaeomagnetism for diabase dikes in Liberia: Initiation of central Atlantic rifting. *Geological Society of America Bulletin*, **86**, 399-411.

Dalrymple, G.B., Alexander, E.C., Lanphere, M.A. and Kraker, G.P. (1981) Irradiation of samples for $^{40}Ar/^{39}Ar$ dating using the Geological Survey TRIGA reactor. *US Geological Survey Professional Paper No. 1176.*

Damon, P.E., Laughlin, A.W. and Percious, J.K. (1967) Problem of excess argon-40 in volcanic rocks, In: Radioactive dating and methods of low level counting. International Atomic Energy Agency, Vienna, 463-481.

Davey, F.J. (1970) Bouguer anomaly map of the North Celtic Sea and entrance to the Bristol Channel. *Geophysical Journal of the Royal Astronomical Society*, **22**, 277-282.

Davies, C.M. (1987) Seismic stratigraphical sequences in the Lundy Tertiary basin, Bristol Channel. *Proceedings of the Geological Association*, Vol.**98**, part 4, 355-366.

Day, G.A. and Williams, C.A. (1970) Gravity compilation in the northeast Atlantic and interpretation of gravity in the Celtic Sea. *Earth and Planetary Science Letters*, **8**, 205-213.

Day, R., Fuller, M. and Scmidt, V.A. (1977) Hysteresis properties of titanomagnetites: grain-size and compositional dependence. *Physics of the Earth and Planetary Interior*, **13**, 260-266.

Dearman, W.R. (1963) Wrench-faulting in Cornwall and South Devon. *Proceedings of the Geologists Association*, **74**, 265-287.

Deer, W.A., Howie, R.A. and Zussman, J. (1992) An introduction to the rock-forming minerals. Longman Scientific and Technical, 696 pp.

Delaney, P.T. and Pollard, D.D. (1981) Deformation of host rocks and flow of magma during growth of minette dykes and breccia-bearing intrusions near ship Rock, New Mexico. *US Geological Survey Professional Paper*, **1202**, 1-78.

De Raaf, J.F.M., Reading, H.G. and Walker, R.G. (1965) Cyclic sedimentation in the lower Westphalian of North Devon, England. *Sedimentology*, Vol.**4**, 1-52.

Dewey, H. (1910) Notes on some igneous rocks from North Devon. *Proceedings of the Geological Association*, Vol.**21**, 429-434.

Dewey, J.F. (1988) Plate tectonics and the evolution of the British Isles. *Journal of the Geological Society of London*, **139**, 371-412.

Dickin, A.P. (1981) Isotope geochemistry of Tertiary igneous rocks from the Isle of Skye, NW Scotland. *Journal of Petrology*, **22**, 155-189.

Dineley, D.L. (1992) The Devonian. In: Geology of England and Wales, (eds. P.McL.D.Duff and A.J.Smith). Geological Society, London. 179-200.

Dobrin, M.B. and Savit, C.H. (1988) Ch.15: Magnetic prospecting - fundamental principles and instruments. In: Introduction to Geophysical prospecting. McGraw-Hill Book Company, New York. 633-675.

Dodson, M.H. and Long, L.E. (1962) Age of the Lundy granite, Bristol Channel. *Nature*, **195**, 975-976.

Dollar, A.T.J. (1941) The Lundy complex: its petrology and tectonics. *Quarterly Journal of the Geological Society of London*, **97**, 39-77.

Dollar, A.T.J. (1968) Tertiary dyke swarm of Lundy. *Proceedings of the Geological Society of London*, **1649**, 119-120.

Donovan, D.T., Lloyd, A.J. and Stride A.H. (1971) Geology of the Bristol Channel. *Proceedings of the Geological Society of London*, **1664**, 294-295.

Donovan, D.T., Savage, R.J.G., Stride, A.H. and Stubbs, A.R. (1961) Geology of the floor of the Bristol Channel. *Nature*, **189**, 51-52.

Doré, A.G. (1976) Preliminary geological interpretation of the Bristol Channel Approaches. *Journal of the Geological Society of London*, **132**, 453-459.

Duncan, R.A. (1984) Age progressive volcanism in the New England seamounts and the opening of the central Atlantic Ocean. *Journal of Geophysical Research*, **89**, 9980-9990.

Dunlop, D.J. (1981) The rock magnetism of fine-particle haematite. *Physics of the Earth and Planetary Interior*, **26**, 1-26.

Dunlop, D.J. (1986) Hysteresis properties of magnetite and their dependence on particle size: a test of pseudo-single domain remanence models. *Journal of Geophysical Research*, **91B**, 9567-9584.

Dunlop, D.J. (1990) Developments in rock magnetism. *Reprints of Progress in Physics*, **53**, 707-792.

Dunning, F.W. (ed.) (1985) Geological structure of Great Britain, Ireland and surrounding areas. *Geological Society of London Mapchart*, Geological Society, London.

Durant, G.P., Kokelaar, B.P. and Whittington, R.J. (1982) The Blackstones Bank igneous centre, Western Scotland. *Proceedings of the 6th Symposium of the Confederation Mondiale des Activites Subaquatique, Heriot-Watt University, Sept. 1980.* Natural Environment Research Council, London. 297-308.

Dymond, J. (1970) Excess argon in submarine basalt pillows. *Geological Society of America Bulletin*, **81**, 1229-1232.

Edmonds, E.A., McKeown, M.C. and Williams, M. (1975) Southwest England. *British Regional Geology, Institute of Geological Sciences*, H.M.S.O. 136 pp.

Edmonds, E.A., Williams, B.J. and Taylor, R.T. (1979) Geology of Bideford and Lundy Island. *Memoir of the Geological Survey of GB*, Sheets 292 with 275, 276, 291 and part of 308. H.M.S.O., London. 143 pp.

Edmonds, E.A., Whittaker, A. and Williams, B.J. (1985) Geology of the country around Ilfracombe and Barnstaple. *Memoir of the British Geological Survey*, Sheets 277 and 293. H.M.S.O., London. 97pp.

Edwards, R.A. and Freshney, E.C. (1982) Tertiary sedimentary rocks. In: The geology of Devon, (eds. E.M.Durrance and D.J.C.Laming). University of Exeter. 204-237.

Ellwood, B.B. (1978) Flow and emplacement directions determined for selected magnetic bodies using anisotropy of magnetic susceptibility, *Earth and Planetary Science Letters*, **41**, 254-264.

Ellwood, B.B. (1982) Estimates of flow direction for calc-alkaline welded tuffs and palaeomagnetic data reliability from anisotropy of magnetic susceptibility measurements: Central San Juan Mountains, southwest Colorado, *Earth and Planetary Science Letters*, **52**, 303-314.

Ellwood, B.B. and Fisk, M.R. (1977) Anisotropy of magnetic susceptibility variations in a single Icelandic columnar basalt, *Earth and Planetary Science Letters*, **35**, 116-122.

Ellwood, B.B., Hrouda, F. and Wagner, J.J. (1988) Symposia on magnetic fabric: introductory comments, *Physics of the Earth and Planetary Interior*, **51**, 249-252.

Emeleus, C.H. (1982) The central complexes. In: Igneous rocks of the British Isles, (ed D.S.Sutherland). Wiley, Chichester. 369-414.

Emeleus, C.H. (1985) Tertiary igneous activity. In: Geology of Scotland, (ed. G.Y. Craig, 2nd edition). Scottish Academic Press, Edinburgh. 357-398.

Emeleus, C.H. and Gyopari, M.C. (1992) British Tertiary Volcanic Province. *Geol. Conservation Review Series No.4*, Chapman and Hall, London. 259 pp.

England, R.W. (1988) The early Tertiary stress regime in NW Britain: evidence from the patterns of volcanic activity. In: Early Tertiary Volcanism and the opening of the NE Atlantic. (eds. A.C.Morton and L.M.Parson). *Geological Society Special Publication No.39*, Blackwell, Oxford, 381-390.

Ernst, R.E. and Baragar, W.R.A. (1992) Evidence from magnetic fabric for the flow pattern of magma in the Mackenzie giant radiating dyke swarm, *Nature*, **356**, 511-513.

Evans, D.J. (1973) The stratigraphy of the central part of the Bristol Channel. Unpublished Ph.D. thesis, University of Wales (Swansea).

Evans, J.W. (1922) The geological structure of the country around Combe Martin, North Devon. *Proceedings of the Geological Association of London*, **33**, 210-228.

Evans, D.J. and Thompson, M.S. (1979) The geology of the central Bristol Channel and the Lundy area, South Western Approaches, British Isles. *Proceedings of the Geological Association*, **90**, 1-14.

Fitch, F.J., Miller, J.A. and Mitchell, J. (1969) A new approach to radiometric dating in orogenic belts. In: Time and place in orogeny, (eds. P.E.Kent, G.E.Satterthwaite and A.M.Spencer). *Geological Society Special Publication No.2* , 157-195.

Fitton, J.G., Hardarson, B.S., Saunders, A.D. and Norry, M.J. (1996) Thermal and chemical structure of the Iceland plume. (abstract of meeting :Plumes - what do we know?). Leicester University, April 1996. 1-2.

Fletcher, B.N. (1975a) A new Tertiary basin east of Lundy Island. *Journal of the Geological Society of London*, **131**, 223-225.

Fletcher, B.N. (1975b) A new Tertiary basin east of Lundy Island. *Proceedings of the Geological Society of London*, **131**, 537-538.

Flinn, D. (1978) Construction and computation of three dimensional progressive deformation. *Quarterly Journal of the Geological Society of London*, **118**, 385-428.

Floyd, P.A., Exley, C.S. and Styles, M.T. (1993) Igneous rocks of southwest England. Geological Conservation Review Series No.5, Chapman and Hall, London. 256 pp.

Freshney, E.C., Beer, K.E. and Wright, J.E. (1979) The geology of the county around Chulmleigh. *Memoir of the Geological Survey of GB*, Sheet 309. H.M.S.O., London. 69pp.

Frey, F.A., Green, D.H. and Roy, S.D. (1978) Integrated models of basalt petrogenesis: a study of quartz tholeiites to olivine melilitites from southeastern Australia utilizing geochemical and experimental petrological data. *Journal of Petrology*, **19**, 463-513.

Frielander, G., Kennedy, J.W., Macias, E.S. and Miller, J.M. (1981) Nuclear and radiochemistry. Wiley, New York. 231 pp.

Fujii, K. and Kushiro, I. (1977) Melting relations and viscosity of an abyssal tholeiite. *Year Book - Carnegie Institute of Washington*, **76**, 461-465.

Fuller, A.C. (1967) The A.C. bridge method. In: Methods in palaeomagnetism, (Eds. D.W.Collinson and K.M.Creer), Elsevier, Amsterdam, 403-408.

Garner, E.L., Murphy, T.J., Gramlich, J.W., Paulsen, P.J. and Barnes, I.L. (1975) Absolute isotopic abundance ratios and the atomic weight of a reference sample of potassium. *Journal of Research of the National Bureau of Standards*, **79A**, 713-725.

Gass, I.G. and Thorpe, R.S. (1980)..Igneous case study: the Tertiary igneous rocks of Skye, NW Scotland. In: S336 Crustal and Mantle Processes, (ed. F. Aprahamian). OUP, Milton Keynes. 1-88.

Gibson, P.J. and Lyle, P. (1993) Evidence for a major Tertiary dyke swarm in County Fermanagh, Northern Ireland on digitally processed aeromagnetic imagery. *Journal of the Geological Society of London*, **155**, 37-38.

Goldring, R. (1971) Shallow-water sedimentation as illustrated in the Upper Devonian Baggy Beds. *Memoir of the Geological Society of London*, **5**, 1-80.

Goulty, N.R. (1984) Location of dykes in coalfield exploration. *First Break*, **2**, 12, 15-21.

Green, T.H. (1980) Island arc and continental magmatism: a review of petrogenetic models based on experimental petrology and geochemistry. *Tectonophysics*, **63**, 367-385.

Gribble, C.D. and Hall, A.J. (1988) A practical introduction to optical mineralogy. George Allen and Unwin, London. 249 pp.

Griffiths, R.W. and Campbell, I.H. (1990) Stirring and structure in mantle starting plumes. *Earth and Planetary Science Letters*, **99**, 66-78.

Hains, B.A., Edmonds, E.A., Briden, J.C. and Tappin, T.R. (1983) Lundy, Solid geological map, Sheet 51N-06W, (1:250 000). *Ordnance Survey for the Institute of Geological Sciences, Southampton.*

Halls, H.C. and Fahrig, W.F. (eds) (1987) Mafic dyke swarms. *Geological Association of Canada Special Paper 34*. 503 pp.

Hampton, C.M. and Taylor, P.N. (1983) The age and nature of the basement of southern Britain: evidence from Sr and Pb isotopes in granites. *Journal of the Geological Society of London*, **140**, 499-509.

Hancock, P.L., Dunne, W.M. and Tringham, M.E. (1983) Variscan deformation in southwest Wales. In: The Variscan fold belt in the British Isles, (ed. P.L.Hancock). Adam Hilger, Bristol. 47-73.

Harland, W.B., Cox, A.V., Llewellyn, P.G., Pickton, C.A.G., Smith, A.G. and Walters, R. (1982) A geological time-scale. Cambridge University Press, 128 pp.

Harrison, M. (1982) Mesozoic magmatism in the British Isles and adjacent areas. In: Igneous rocks of the British Isles, (ed D.S.Sutherland). Wiley, Chichester. 333-341.

Hart, M.B. (1982) The marine rocks of the Mesozoic. In: The geology of Devon, (eds. E.M.Durrance and D.J.C.Laming). University of Exeter, Exeter. 179-203.

Hawkes, J.R. (1982) The Dartmoor granite and later volcanic rocks. In: The geology of Devon, (eds. E.M.Durrance and D.J.C.Laming). University of Exeter, Exeter. 85-116.

Hawkes, J.R. (1985) Igneous rocks. In: Geology of the country around Ilfracombe and Barnstaple, (eds. E.A.Edmonds, A.Whittaker and B.J.Williams). *Memoir of the British Geological Survey*, H.M.S.O., London. p.57.

Hawkesworth,C.J. and Norry, M.J. (1983) Continental basalts and mantle xenoliths Shiva Geology Series, 272 pp.

Hawkesworth,C.J. and Gallagher, K. (1993) Mantle hotspots, plumes and regional tectonics as causes of intraplate magmatism. *Terra Nova*, **5**, 552-559.

Heizler, M.T. and Harrison, T.M. (1988) Multiple trapped argon isotope components revealed by $^{40}Ar/^{39}Ar$ isochron analysis. *Geochimica. Cosmochimica. Acta.*, **52**, 1295-1303.

Holloway, S. and Chadwick, R.A. (1986) The Sticklepath-Lustleigh Fault Zone: Tertiary sinistral reactivation of a Variscan dextral strike-slip fault. *Journal of the Geological Society of London*, **143**, 447-452.

Holwill, F.J.W., House, M.R., Lane, R., Gauss, G.A., Hendriks, E.M.L. and Dearman, W.R. (1969) Summer field meeting in Devon and Cornwall. *Proceedings of the Geological Association*, Vol.**80**, 43-62.

Hospers, J. and Charlesworth, H.A.K. (1954) The natural permanent magnetization of the lower basalts of Northern Ireland. *Geophysical Supplement of the Royal Astronomical Society*, Vol.**7**, 32-43.

Howell, P.M. (compiler) (1980) Lundy, Sheet 51°N - 06°W, 1: 250 000 Series, Aeromagnetic anomaly map. *Institute of Geological Sciences*, NERC.

Hrouda, F. (1982) Magnetic anisotropy of rocks and its application in geology and geophysics. *Geophysical Surveys*, **5**, 37-82.

Humphris, S.E. and Thompson, G. (1983) Geochemistry of rare earth elements in basalts from the Walvis ridge: implications for its origin and evolution. *Earth and Planetary Science Letters*, **66**, 223-242.

Humphris, S.E., Thompson, G., Schilling, J.G. and Kingsley, R.H. (1985) Petrological and geochemical variations along the mid Atlantic ridge between 46°S and 32°S: influence of the Tristan de Cunha mantle plume. *Geochimica. Cosmochimica. Acta.*, **49**, 1445-1464.

Hunt, C. (ed.) (1991) Environmental Magnetism Workshop Handbook (June, 1991). Institute of Rock Magnetism, University of Minnesota. 240 pp.

Huppert, H.E. and Sparks, R.S.J. (1985) Cooling and contamination of mafic and ultramafic magmas during ascent through the continental crust. *Earth and Planetary Science Letters*, **74**, 371-386.

Huppert, H.E. and Sparks, R.S.J. (1988) The generation of granitic magmas by intrusion of basalt into continental crust. *Journal of Petrology*, **29**, 599-624.

I.A.G. (1971) Geodetic Reference System, 1967. *Publication Speciale No.3 du Bulletin Géodésique.*

I.G.S. (1965) Aeromagnetic map of Great Britain, South Sheet, 1st edition, 1: 625 000 Series. *Institute of Geological Sciences.*, H.M.S.O., London.

I.G.S. (1981) Annual report for 1980 and 1981. *Institute of Geological Sciences*, H.M.S.O., London.

Jackson, M. (1991) Anisotropy of magnetic remanence: a brief review of mineralogical sources, physical origins, geological applications and comparison with susceptibility remanence, *Pure and Applied Geophysics*, **136**, 1, 1-28.

Jackson, M. and Tauxe, L. (1991) Anisotropy of magnetic susceptibility and remanence: a brief review of mineralogical sources, physical origins and geological applications, *Reviews in Geophysics*, **29**, 371-376.

Janák, F. (1965) Determination of anisotropy of magnetic susceptibility of rocks. Studies in Geophysics and Geodesy, 11, 419-429.

Jassim, S.Z. (1970) The Loch na Creitheach volcanic vent and the surrounding area, Isle of Skye. Unpublished Ph.D. thesis, University of Leeds.

Jelinek, V. (1981) Characterization of the magnetic fabric of rocks. *Tectonophysics*, **79**, 63-67.

Kamerling, P. (1979) The geology and hydrocarbon habitat of the Bristol Channel Basin. *Journal of Petroleum Geology*, **2**, 1, 75-93.

Kearey, P. and Brooks, M. (1984) An introduction to geophysical exploration. Blackwell, Oxford. 296 pp.

Kelling, G. and Collinson, J.D. (1992) The Silesian. In: Geology of England and Wales, (eds. P.McL.D.Duff and A.J.Smith). Geological Society, London. 239-274.

Kelley, S.P. (1995) Ar-Ar dating by laser microprobe. In: Microprobe Techniques in the Earth Sciences, (Eds. P.J.Potts, J.F.W.Bowles, S.J.B.Reed and M.R.Cave), Chapman and Hall, 327-358.

Kelley, S.P., Turner, G., Butterfield, A.W. and Shepherd, T.J. (1986) The source and significance of argon isotopes in fluid inclusions from areas of mineralisation. *Earth Planetary Science Letters*, **79**, 634-648.

Khan, M.A. (1962) Anisotropy of magnetic susceptibility of some igneous and metamorphic rocks. *Journal of Geophysical Research*, **67**, 2873-2885.

Kirton, S.R. and Donato, J.A. (1985) Some buried dykes of Britain and surrounding waters deduced by magnetic modelling and seismic reflection methods. *Journal of the Geological Society of London*, **142**, 1047-1058.

Knapp, R.J. (1973) The form and structure of Islay, Jura and Arran Tertiary basic dyke swarms. Unpublished Ph.D. thesis, University of London, London. 296 pp.

Knight, M.D. and Walker, G.P.L. (1988) Magma flow directions in dikes of the Koolau Complex, Oahu, determined from magnetic fabric studies, *Journal of Geophysical Research*, **93**, B5, 4301-4319.

Kolofíková, O. (1976) Geological interpretation of measurements of magnetic properties of basalts on example of the Chribsk Les Lava Flow of the Velky Roudny Volcano (Nízky Jeseník), *Cas. Mineral. geol.*, **21**, 387-396. (In Czech).

LaCoste, L., Clarkson, N. and Hamilton, G. (1967) LaCoste and Romberg stabilize platform shipboard gravity meter. *Geophysics*, **32**, 99-109.

Lane, R. (1965) The Hangman Grits - an introduction and stratigraphy. *Proceedings of the Ussher Society*, **1**, 166-167.

Larsen, H.C., Saunders, A.D., Clift, P.D. and the Shipboard Scientific Party (1994) Site 917. *1994 Proceedings of the Ocean Drilling Program*, Initial Reports 152, College Station TX (ODP), 107-158.

Leat, P.T., Thompson, R.N. and Morrison, M.A. (1987) Geodynamic significance of post-Variscan intrusive and extrusive potassic magmatism in SW England. *Transactions of the Royal Society of Edinburgh: Earth Sciences*, **77**, 349-360.

Lechler, P.J. and Desilets, M.O. (1987) A review of the use of loss on ignition as a measurement of total volatiles in whole rock analyses. *Chemical Geology*, **63**, 341-344.

Leeder, M.R. (1992) The Dinantian. In: Geology of England and Wales, (eds. P.McL.D.Duff and A.J.Smith). Geological Society, London. 207-238.

Le Maitre, R.W., Bateman, P., Dudek, A., Keller, J., Lameyre, S., Le Bas, M.J., Sabine, P.A., Scmid, R., Sorensen, H., Streckeisen, A., Woolley, A.R. and Zanettin, B. (1989) A classification of igneous rocks and glossary of terms. Blackwell, Oxford.

Lister, J.R. and Kerr, R.C. (1990) Fluid mechanical models of dyke propagation and magma transport. In: Mafic dykes and emplacement mechanisms, (Eds. A.J.Parker, P.C.Rickwood and D.H.Tucker). Balkema, Rotterdam, 69-80.

Llewellyn, D.J. (1981) Geophysical investigations of the deep geological structure in the Bristol Channel area. Unpublished Ph.D. thesis, University of Wales, Cardiff.

Lloyd, A.J. (1963) Upper Jurassic rocks beneath the Bristol Channel. *Nature*, **198**, 375-376.

Lloyd, A.J., Savage, R.J.G., Stride, A.H. and Donovan, D.T. (1973) The geology of the Bristol Channel Floor. *Philosophical Transactions of the Royal Society*, **274**, 1244, 595-626.

Mason, R. (1986) Petrology of metamorphic rocks. Unwin Hyman, 230 pp.

Mason, R. (1990) CIPWNorm 3.1 modelling program. University of Sydney, Sydney.

McCaffrey, R., Stewart, S., Dalzell, P., McCaffrey, L. and McElroy, J. (1993) A reconnaissance survey of the Lundy Tertiary Igneous Complex, Bristol Channel. *Proceedings of the Ussher Society*, **8**, 193-197.

McDonald, A.J.W. and Lee, M.K. (compilers) (1989) Bouguer Anomaly Map. *Regional Geophysics Group*, British Geological Survey, Keyworth.

McDonough, W.F., McCulloch, M.T., and Sun, S.S. (1985) Isotopic and geochemical systematics in Tertiary-Recent basalts from southeastern Australia and implications for the evolution of the sub-continental lithosphere. *Geochimica. Cosmochimica. Acta.*, **49**, 2051-2067.

McDougall, I. (1985) K-Ar and $^{40}Ar/^{39}Ar$ dating of the hominid-bearing Pliocene-Pleistocene sequence at Koobi Fota, Lake Turkana, northern Kenya. *Geological Society of America Bulletin*, **96**, 159-175.

McDougall, I. and Harrison, T.M. (1988) Geochronology and thermochronology by the $^{40}Ar/^{39}Ar$ method. *Oxford Monographs on Geology and Geophysics No. 9*, Oxford University Press, Oxford. 212 pp.

McFarlane, P.B. (1955) Survey of two drowned valleys in Devon. *Quarterly Journal of the Geological Society of London*, Vol.**92**, 419-429.

McKenzie, D. (1989) Some remarks on the movement of small melt fractions in the mantle. *Earth and Planetary Science Letters*, **95**, 53-72.

McKenzie, D. and Bickle, M.J. (1988) The volume and composition of melt generated by extension of the lithosphere. *Journal of Petrology*, **29**, 625-679.

McQuillin, J. and Tuson, J. (1963) Gravity measurements over the Rhum Tertiary plutonic complex. *Nature*, **199**, 1276-1277.

McQuillin, R., Bacon, M. and Binn, P.E. (1975) The Blackstones Tertiary igneous complex. *Scottish Journal of Geology*, **11**, 179-192.

Mechie, J. (1980) Seismic studies of deep geological structure in the Bristol Channel area. Unpublished Ph.D. Thesis, University of Wales, Cardiff.

Mechie, J. and Brooks, M. (1984) A seismic survey of deep geological structure in the Bristol Channel area. *Geophysical Journal of the Royal Astronomical Society*, **87**, 661-689.

Meissner, R., Matthews, D. and Wever, Th. (1986) The Moho in and around Great Britain. *Annales Geophysicae*, **6**, 659-664.

Mellor, D. and Mussett, A. E. (1975) Evidence for initial (super 36) Ar in volcanic rocks and some implications. *Earth and Planetary Science Letters*, **26**, 312-318.

Menzies, M.A. and Halliday, M. (1988) Lithospheric domains beneath Archaean and Proterozoic crust of Scotland. *Journal of Petrology*, Special Lithosphere Issue, 272-302.

Merrihue, C. and Turner, G. (1966) Potassium-argon dating by activation with fast neutrons. *Journal of Geophysical Research*, **71**, 2852-2857.

Middlemost, E.A.K. (1975) The basalt clan. *Earth Science Reviews*, **11**, 337-364.

Middlemost, E.A.K. (1989) Iron oxide ratios, norms and the classification of volcanic rocks. *Chemical Geology*, **77**, 19-26.

Miller, J.A. and Fitch, F.J. (1962) Age of the Lundy granites. *Nature*, **195**, 553-555.

Miller, J.A. and Mohr, P.A. (1964) Potassium-argon measurements on the granites and some associated rocks from southwest England. *Geophysical Journal of the Royal Astronomical Society*, **6**, 394-396.

Miller, J.A., Shibata, K. and Munro, M. (1962) The potassium-argon age of the lava of Killerton Park near Exeter. *Geophysical Journal of the Royal Astronomical Society*, **6**, 394-396.

Milsom, J. (1992) Field geophysics. Wiley, Chichester. 182 pp.

Mittermayer, E. (1969) Numerical formulas for the Geodetic Reference System 1967. *Bolletino di Geofisca Teorica ed Applicata*, **11**, 96-107.

Moorbath, S. and Bell, J.D. (1965) Strontium isotope abundance studies and rubidium-strontium age determinations on Tertiary rocks from the Isle of Skye, Northwest Scotland. *Journal of Petrology*, **6**, 37-66.

Moorbath, S. and Welke, H. (1969) Lead isotope studies on igneous rocks from the Isle of Skye, Northwest Scotland. *Earth Planetary Science Letters*, **5**, 217-230.

Morgan, W.J. (1983) Hotspot tracks and the the early rifting of the North Atlantic. *Tectonophysics*, **94**, 123-139.

Morrison, M.A., Thompson, R.N. and Dickin, A.P. (1985) Geochemical evidence for complex magmatic plumbing development of a continental volcanic centre. *Geology*, **13**, 581-584.

Morton, A.C. and Parson, L.M. (1988) Early Tertiary Volcanism and the opening of the NE Atlantic. *Geological Society Special Publication No.39*, Blackwell, Oxford, 477 pp.

Morton, N. (1987) Jurassic subsidence history in the Hebrides, NW Scotland. *Marine and Petroleum Geology*, **4**, 226-242.

Mussett, A.E, Dagley, P. and Eckford, M. (1976) The British Tertiary Igneous Province: palaeomagnetism and ages of dykes, Lundy Island, Bristol Channel. *Geophysical Journal of the Royal Astronomical Society*, **46**, 595-603.

Mussett, A.E, Dagley, P. and Skelhorn, R.P. (1980) Magnetostratigraphy of the Tertiary igneous succession of Mull. *Journal of the Geological Society of London*, **137**, 349-357.

Mussett, A.E, Dagley, P. and Skelhorn, R.P. (1988) Time and duration of activity in the British Tertiary Igneous Province. In: Early Tertiary Volcanism and the opening of the NE Atlantic, (eds. A.C.Morton and L.M.Parson). *Geological Society Special Publication No.39*, Blackwell, Oxford, 337-348.

Mussett, A.E, Dagley, P., Hodgson, B.D. and Skelhorn, R.P. (1987) Palaeomagnetism and the age of the quartz-porphyry intrusions, Isle of Arran. *Scottish Journal of Geology*, **23**, 9-22.

Nagata, T. (1964) Rock magnetism. Maruzea, Tokyo. 350 pp.

Nakamura, N. (1974) Determination of REE, Ba Fe, Mg, Na and K in carbonaceous and ordinary chondrites. *Geochimica Cosmochimica. Acta.*, **52**, 757-775.

Nathans, R., Pickart, S.J., Alperin, H.J. and Brown, P.J. (1964) Polarized-neutron study of haematite, *Physics Reviews*, **136A**, 1641.

Ofoegbu, C.O. and Bott, M.H.P. (1985) Interpretation of the Minch linear magnetic anomaly and of a similar feature on the shelf, North of Lewis by non-linear optimization. *Journal of the Geological Society of London*, **142**, 1077-1088.

Olhoeft, G.R. and Johnson, G.R. (1989) Densities of rocks and minerals. In: Practical handbook of physical properties of rocks and minerals, (ed. R.S.Carmichael). CRC Press, Florida, 141-176.

O'Reilly, W. (1984) Rock and mineral magnetism. Blackie, Glasgow. 230 pp.

Owen, T.R. (1971) The structural evolution of the Bristol Channel. *Proceedings of the Geological Society of London*, **1664**, 289-294.

Owens, W.H. (1974) Mathematical model studies on factors affecting the magnetic anisotropy of deformed rocks. *Tectonophysics*, **24**, 115-131.

Owens, W.H. and Bamford, D. (1976) Magnetic, seismic and other anisotropic properties of rock fabrics, *Philosophical Transactions of the Royal Society of London*, Series A, **283**, 55-68.

Özdemir, Ö. (1987) Inversion of titanomaghemites. *Physics of the Earth and Planetary Interior*, **46**, 184-196.

Ozima, M. and Larson, E.E. (1970) Low and high temperature oxidation of titanomagnetite in relation to irreversible changes in the magnetic properties of submarine basalts. *Journal of Geophysical Research*, **75**, 1003-1007.

Parker, A.J., Rickwood, P.C. and Tucker, D.H. (eds) (1990) Mafic dykes and emplacement mechanisms. Balkema, Rotterdam. 541 pp.

Pearce, J.A. (1976) Statistical analysis of major element patterns in basalts. *Journal of Petrology*, **17**, 15-43.

Pearce, J.A. and Norry, M.J. (1979) Petrogenetic implications of Ti, Zr, Y and Nb variations in volcanic rocks. *Contributions to Mineralogy and Petrology*, **19**, 142-157.

Peate, D.W. (1989) Stratigraphy and petrogenesis of the Parana continental flood basalts, southern Brazil. Unpublished Ph.D. thesis, Open University. 359 pp.

Peddie, N.W. (1983) International Geomagnetic Reference Field - its evaluation and the difference in total field intensity between new and old models 1965-1980. *Geophysics*, **48**, 1691-1696.

Pedley, R.C. (1991) GRAVMAG: Interactive 2.5D Gravity and Magnetic modelling program. British Geological Survey, Keyworth. 47 pp.

Potter, D.K. and Stevenson, A. (1988) Single-domain particles in rocks and magnetic fabric analysis, *Geophysical Research Letters*, **15**, 1097-1100.

Potts, P.J., Webb, P.C. and Watson, J.S. (1984) Energy-dispersive X-ray fluorescence analysis of silicate rocks for major and trace elements. *X-ray Spectrometry*, **13**, 2-15.

Potts, P.J., Bowles, .F.W., Reed, S.J.B. and Cave, M.R. (1995) Microprobe techniques in the Earth Sciences. Chapman and Hall, 419 pp.

Prentice, J.E. (1960) The stratigraphy of the Upper Carboniferous rocks of the Bideford region, North Devon. *Quarterly Journal of the Geological Society of London*, Vol.**116**, 397-408.

Ramsey, M.H., Potts, P.J., Webb, P.C., Watkins, P. Watson, J.S. and Coles, P.J, (1995) An objective assessment of analytical method precision: comparison of ICP-AES and XRF for the analysis of silicate rocks. *Chemical Geology*, **124**, 1-19.

Ramussen, R. and Pederson, L.B. (1979) End corrections in potential field modelling. *Geophysical Prospecting*, **27**, 749-760.

Readman, P.W. and O'Reilly, W. (1970) The synthesis and inversion of non-stoichiometric titanomagnetites. *Physics of the Earth and Planetary Interior*, **4**, 121-128.

Reay, D.M. and Chacksfield, B.C. (compilers) (1985) Lundy, Sheet 51°N - 06°W, 1: 50 000 Series, Bouguer gravity anomaly map. *Institute of Geological Sciences,* NERC.

Rees, A.I. (1968) The production of preferred orientation in a concentrated dispersion of elongated and flattened grains, *Journal of Geology*, **76**, 457-465.

Regelous, M. (1993) Geochemistry of dolerites from the Parana flood basalt province, southern Brazil. Unpublished Ph.D. thesis, Open University. 256 pp.

Richey, J.E. (1937) Some features of Tertiary volcanicity in Scotland and Ireland. *Bulletin Volcanologique*, séries II, tome **I**, 13-34.

Rickwood, P.C. (1990) The anatomy of a dyke and the determination of propagation and magma flow direction. In: Mafic dykes and emplacement mechanisms. (Eds. A.J.Parker, P.C.Rickwood and D.H.Tucker). Balkema, Rotterdam, 81-100.

Robson, D.A. (1964) The Acklington dyke - a proton magnetometer survey. *Proceedings of the Yorkshire Geological Society*, **34**, 293-308

Rochette, P., Jackson, M. and Aubourg, C. (1992) Rock magnetism and the interpretation of anisotropy of magnetic susceptibility, *Reviews of Geophysics*, **30**, 3, 209-226.

Roeder, P.L. and Emslie, R.F. (1970) Olivine-liquid equilibrium. *Contributions to Mineralogy and Petrology*, **29**, 275-289.

Rogers, I. (1926) On the discovery of fossil fishes and plants in the Devonian rocks of North Devon. *Transactions of the Devonian Association for the Advancement of Science, Literature and Art*, Vol.**58**, 223-234.

Rollinson, H.R. (1993) Using geochemical data: evaluation, presentation, interpretation. Longman Scientific and Technical, London. 352 pp.

Rubin, A.M. and Pollard, D.D. (1987) Origins of blade-like dikes in volcanic rift zones. In: Volcanism in Hawaii Vol.2 (Eds. T.L.Wright and P.H.Stauffer). *US Geological Survey Professional Paper*, No. 1350/2, 1449-1470.

Rudnick, R.L. and Fountain, D.M. (1995) Nature and composition of the continental crust: a lower crustal perspective. *Reviews in Geophysics*, **33**, 267-309.

Saunders, A.D. and Tarney, J. (1984) Geochemical characteristics of basaltic volcanism within back-arc basins. In: Marginal basin geology (Eds. B.P.Kokelaar and M.F.Howells). Special Publication of the Geological Society No.16, 59-76.

Selwood, E.B., Edwards, R.A., Simpson, S., Chesher, J.A., Hamblin, R.J.O., Henson, M.R., Riddolls, B.W. and Waters, R.A. (1982) Geology of the country around Newton Abbot. *Memoir of the Geological Survey of Great Britain*, 212 pp.

Schilling, J.-G., Zajac, M., Evans, R., Johnston, T., White, W., Devine, J.D. and Kingsley, R. (1983) Petrologic and geochemical variations along the Mid-Atlantic Ridge from 27°N to 73°N. *American Journal of Science*, **283**, 510-586.

Schock, H.H. (1979) Distribution of rare-earth and other trace elements in magnetites. *Chemical Geology*, **26**, 119-133.

Shearman, D.J. (1967) On Tertiary fault movements in North Devonshire. *Proceedings of the Geologists Association*, **78**, 555-566.

Shuey, R.T. and Pasquale, A.S. (1973) End corrections in magnetic profile interpretation. *Geophysics*, **38**, 507-512.

Simpson, S. (1964) The Lynton Beds of North Devon. *Proceedings of the Ussher Society*, **1**, 121-122.

Skelhorn, B.R. (1974) The Tertiary igneous geology of the Isle of Mull. Geologists' Association Guide No.20. 64 pp.

Sloan, T. (1971) The structure of the Mull Tertiary dyke swarm. Unpublished Ph.D. thesis, University of London, London. 322 pp.

Smith, R.E. and Smith, S.E. (1976) Comments on the use of Ti, Zr, Y, Sr, K, P and Nb in classification of basalts. *Earth and Planetary Science Letters*, **32**, 114-120.

Sowerbutts, W.T.C. (1987) Magnetic mapping of the Butterton Dyke: an example of geophysical surveying. *Journal of the Geological Society of London*, **144**, 29-33.

Spector, A. and Grant, F.S. (1970) Statistical models for interpreting aeromagnetic data. *Geophysics*, **35**, 293-302.

Speight, J.M. (1972) The form and structure of the Tertiary dyke swarms of Skye and Ardnamurchan. Unpublished Ph.D. thesis, University of London, 318 pp.

Speight, J.M., Skelhorn, R.R., Sloan, T. and Knapp, R.J. (1982) The dyke swarms of Scotland. In: Igneous rocks of the British Isles, (ed. D.S.Sutherland). Wiley, Chichester. 449-459.

Stacey, F.D. and Banerjee, S.K. (1974) The physical principles of rock magnetism. Elsevier, Amsterdam. 195 pp.

Stacey, F.D., Joplin, G. and Lindsay, J. (1960) Magnetic anisotropy and fabric of some foliated rocks from SE Australia. *Geophysica Pura Applica*, **47**, 30-40.

Steiger, R.H. and Jäger, E. (1977) Subcommission on geochronology: Convention on the use of decay constants in geo- and cosmochronology. *Earth and Planetary Science Letters*, **36**, 359-362.

Stille, P., Unruh, D.M. and Tatsumoto, M. (1983) Pb, Sr, Nd and Hf isotopic evidence of multiple sources for Oahu, Hawaii basalts. *Nature*, **304**, 25-29.

Stimac, J.A., Clark, A.H., Chen, Y. and Garcia, S. (1995) Enclaves and their bearing on the origin of the Cornubian batholith, southwestern England. *Mineralogical Magazine*, **59**, 273-296.

Stone, M. (1988) The significance of almandine garnets in the Lundy and Dartmoor granites. *Mineralogical Magazine*, **52**, 651-658.

Strangeway, D.W. (1965) Interpretation of the magnetic anomalies over some Precambrian dykes. *Geophysics*, **30**, 783-796.

Sun, S.S. (1980) Lead isotopic study of young volcanic rocks from mid-ocean ridges, ocean islands and island arcs. *Philosophical transactions of the Royal Society*, **A297**, 409-455.

Sutherland, D.S. (1982) The igneous rocks of the British Isles. Wiley, Chichester. 645 pp.

Tappin, D.H. (compiler) (1983) Lundy Sheet 51°N - 06°W, 1: 250 000 Series, sea bed sediments, *Ordnance Survey for the Institute of Geological Sciences, Southampton.*

Tarling, D.H. (1980) Palaeomagnetic reconstructions and the Variscan Orogeny. *Proceedings of the Ussher Society*, **4**, 233-261.

Tarling, D.H. (1983) Palaeomagnetism. Chapman and Hall, 379 pp.

Tarling, D.H. and Hrouda, F. (1993) The magnetic anisotropy of rocks. Chapman and Hall, 217 pp.

Taylor, S.R. and McLennan, S.M. (1981) The composition and evolution of the continental crust: rare earth evidence from sedimentary rocks. *Philosophical Transactions of the Royal Society of Edinburgh*, **A301**, 381-399.

Thirlwall, M.F. and Jones, N.W. (1983) Isotope geochemistry and contamination mechanics of Tertiary lavas from Skye, Northwest Scotland. In: Continental basalts and mantle xenoliths (eds. C.J. Hawkesworth and M.J. Norry). Shiva Geology Series, 186-208.

Thomas, M.D. and Brooks, M. (1973) The geological significance of a negative gravity anomaly in the South Wales coalfield. *Geology Journal*, **8**, 189-206.

Thompson, R.N. (1974) Primary basalts and magma genesis I. Skye, northwest Scotland. *Contributions to Mineralogy and Petrology*, **45**, 317-341.

Thompson, R.N. (1982) Magmatism of the British Tertiary Volcanic Province. *Scottish Journal of Geology*, **18**, 49-107.

Thompson, R.N. and Gibson, S.A. (1991) Subcontinental mantle plumes, hotspots and pre-existing thinspots. *Journal of the Geological Society, London*, **148**, 973-977.

Thompson, R.N., Esson, J, and Dunham, K.C. (1972) Major element chemical variation in the Eocene lavas of the Isle of Skye, Scotland. *Journal of Petrology*, **21**, 219-253.

Thompson, R.N., Morrison, M.A., Dickin, A.P. and Hendry, G.L. (1983) Continental flood basalts...arachnids rule OK? In: Continental basalts and mantle xenoliths (eds. C.J. Hawkesworth and M.J. Norry). Shiva Geology Series, 158-185.

Thompson, R.N., Morrison, M.A., Hendry, G.L. and Parry, S.J. (1984) An assessment of the relative roles of crust and mantle in magma genesis; an elemental approach. *Philosophical Transactions of the Royal Society*, **A310**, 549-590.

Thorpe, R.S. (1981) Classification and origin of basalts. In: Techniques Handbook (Ed. V.Russell). Open University Press, Milton Keynes. 79-96.

Thorpe, R.S. and Tindle, A.G. (1991) Lundy: remnant of a Tertiary volcano in the Bristol Channel. *Geology Today*, September-October, p.165.

Thorpe, R.S. and Tindle, A.G. (1992) Petrology and petrogenesis of a Tertiary bimodal dolerite-peralkaline/subalkaline trachyte/rhyolite dyke association from Lundy, Bristol Channel, UK. *Geological Journal*, Vol.**27**, 101-117.

Thorpe, R.S., Cosgrove, M.E. and Van Calsteren, P.W.C. (1986) Rare-earth elements, Sr- and Nd- isotope evidence for petrogenesis of Permian basaltic and K-rich volcanic rocks from southwest England. *Mineralogical Magazine*, **52**, 481-490.

Thorpe, R.S., Tindle, A.G. and Gledhill, A. (1990) The petrology and origin of the Tertiary Lundy Granite (Bristol Channel, UK). *Journal of Petrology*, Vol.**31**, Part 6, 1379-1406.

Titman, C.W., Wilkinson, I., Mitchell, J.G. and Ineson, P.R. (1989) Magnetic, chemical, petrographic and isotopic age studies of the Windy Knowe Tertiary dyke, Borders region, Scotland. *Proceedings of the Yorkshire Geological Society*, **47**, 199-205.

Townsend, H.A. and Hailwood, E.A. (1986) Magneto-stratigraphic correlation of Palaeogene sediments in the Hampshire and London basins, southern UK. *Journal of the Geological Society of London*, **142**, 957-982.

Tunbridge, I.P. (1977) Notes on the Hangman Sandstones (Middle Devonian) of North Devon. *Proceedings of the Ussher Society*, **3**, 339.

Tunbridge, I.P. (1983) The Middle Devonian shoreline of North Devon, England. *Journal of the Geological Society of London*, **140**, 147-158.

Tunbridge, I.P. (1986) Mid-Devonian tectonics and sedimentation in the Bristol Channel area. *Journal of the Geological Society of London*, **143**, 107-116.

Turner, G. (1971) Argon-40/argon-39 dating: the optimization of irradiation parameters. *Earth and Planetary Science Letters*, **10**, 227-234.

Turner, G., Huneke, J.C., Podosek, F.A. and Wasserburg, G.J. (1971) 40Ar-39Ar ages and cosmic ray exposure age of Apollo 14 samples. *Earth Science and Planetary Letters*, **12**, 19-35.

Van Hoorn, B. (1987) The South Celtic Sea/Bristol Channel Basin: origin, deformation and inversion history. *Tectonophysics*, **137**, 309-334.

Vann, I.R. (1978) The siting of Tertiary vulcanicity. In: Crustal evolution in Northwestern Britain and adjacent regions (Eds. D.R.Bowes and B.E.Leake). Geological Journal Special Issue No.10, 393-414.

Walker, G.P.L. (1993) Basaltic-volcano systems. In: Magmatic processes and plate tectonics (Eds.H.M.Pritchard, T.Alabaster, N.B.W.Harris and C.R.Neary). *Special publication of the Geological Society No.76*, Geological Society, London, 3-38.

Walker G.P.L., Eyre, P.R., Spengler, S.R., Knight, M.D. and Kennedy, K. (1995) Congruent dyke-widths in large basaltic volcanoes. In: Physics and chemistry of dykes (Eds. G.Baer and A.Heimann) - selected papers presented at the 3rd International Dyke Conference, Jerusalem, Israel, 4th-8th September 1995. Balkema, Rotterdam, 35-40.

Wasilewski, P.J. (1968) Magnetization of ocean basalts. *Journal of Geomagnetism and Geoelectricity*, **20**, 129-154.

Watson, J.S. (1996) Fast, simple method of powder pellet preparation for X-ray fluorescence analysis. X-Ray Spectrometry, 25, 173-174.

Watson, S. and McKenzie, D. (1991) Melt generation by plumes: a study of Hawaiian Islands. *Journal of Petrology*, **32**, 501-537.

Weaver, B.L. and Tarney, J. (1984) Empirical approach to estimating the composition of the continental crust. *Nature*, **310**, 575-577.

White, R.S. (1988) The Earth's crust and lithosphere. In: Oceanic and continental lithosphere - similarities and differences (eds. M.A.Menzies and K.G.Cox), Journal of Petrology, Special Lithosphere Issue, 1-10.

White, R.S. and McKenzie, D. (1989) Magmatism at rift zones: the generation of volcanic continental margins and flood basalts. *Journal of Geophysical Research*, **94**, No. B6, 7685-7729.

White, R.S., Spence G.D., Fowler, S., McKenzie, D. and Westbrook, G.K. (1987) Magmatism at rifted continental margins. *Nature*, **330**, 439-444.

Wilson, M. (1993) Igneous petrogenesis - a global tectonic approach. Unwin Hyman, London, 466 pp.

Wilson, R.L. (1961) Palaeomagnetism in Northern Ireland - thermal demagnetization of natural magnetic moments in rocks. *Geophysical Journal*, **14**, 45-58.

Wilson, R.L. (1970) Palaeomagnetic Stratigraphy of Tertiary lavas from Northern Ireland. *Geophysical Journal of the Royal Astronomical Society*, **20**, 1-9.

Wilson, R.L., Dagley. P. and Ade-Hall, J.M. (1972) Palaeomagnetism of the British Tertiary Igneous Province: the Skye lavas. *Geophysical Journal of the Royal Astronomical Society*, **28**, 285-293.

Wood, D.A., Gibson, I.L. and Thompson, R.N. (1976) Element mobility during zeolite facies metamorphism of the Tertiary basalts of eastern Iceland. *Contributions to Mineralogy and Petrology*, **55**, 241-255.

Wood, D.A., Joron, J.L., Treuil, M., Norry, M. and Tarney, J. (1979) Elemental and Sr isotope variations in basic lavas from Iceland and the surrounding ocean floor. *Contributions to Mineralogy and Petrology*, **70**, 319-339.

Woodland, A.W. (1977) Bideford and Lundy Island, Sheet 292 and parts of sheets 275, 276, 291 and 308. Scale 1: 50 000. *Geological Survey of Great Britain (England and Wales).*

York, D. (1968) Least squares fitting of a straight line with correlated errors. *Earth and Planetary Science Letters*, **5**, 320-324.

PAGE MISSING IN ORIGINAL

Appendix A1: Hysteresis loop data for samples from Lee Bay and Lundy Island.

Sample	M_{rs} (Am^2kg^{-1})	Ms (Am^2kg^{-1})	Hcr (mT)	Hc (mT)	Hcr/Hc	Mrs/Ms
Lee Bay						
CK31a	0.218	0.721	22.38	12.08	1.85	0.302
CK31b	0.168	0.720	15.11	8.71	1.73	0.233
CK30D	0.234	1.088	18.74	10.71	1.75	0.215
CK30e	0.164	0.563	20.40	11.45	1.78	0.292
CK21B5	0.132	0.498	12.06	6.67	1.81	0.265
CK21A2	0.154	0.697	14.58	8.01	1.82	0.221
CK21A4	0.143	0.501	17.62	10.01	1.76	0.287
Lundy Island						
Land1	0.078	0.966	16.51	4.25	3.88	0.081
Land2	0.107	1.042	23.96	5.62	4.27	0.102
WG1	0.101	1.072	25.09	7.93	3.16	0.094
WG2	0.187	1.883	17.50	5.46	3.21	0.099
BW1	0.182	1.561	14.85	4.99	2.97	0.115
Bat1	0.057	0.791	18.66	3.93	4.75	0.072
VC1	0.161	1.440	13.18	5.03	2.62	0.112
QB1	0.124	1.907	22.68	5.87	4.06	0.065
QB2	0.096	1.129	19.75	5.50	3.59	0.085
DK1	0.241	2.975	21.53	7.58	2.84	0.081
DK2	0.219	3.084	23.12	6.18	3.74	0.071
BW4	0.134	1.367	21.87	7.22	3.03	0.098

Appendix 2.1: Anisotropy of magnetic susceptibility (AMS) shape parameters

Dyke No.	Strike/ Dip	K_1	K_2	K_3	K_1/K_2	K_2/K_3	η_1	η_2	η_3	η_m	L	F	P_i	T
4a	308/90	0.04782	0.04716	0.04598	1.01	1.03	-3.0403	-3.0542	-3.0795	-3.0580	1.398	2.502	1.04	0.29
4b		0.04570	0.04454	0.04395	1.03	1.01	-3.0857	-3.1114	-3.1247	-3.1072	2.584	1.318	1.04	-0.32
4c		0.04520	0.05277	0.05168	1.03	1.02	-2.9151	-2.9418	-2.9627	-2.9389	2.693	2.060	1.05	-0.12
4d		0.05263	0.05125	0.05011	1.03	1.02	-2.9445	-2.9710	-2.9935	-2.9697	2.689	2.237	1.05	-0.08
4e		0.06685	0.06505	0.06237	1.03	1.04	-2.7053	-2.7326	-2.7747	-2.7375	2.788	4.138	1.07	0.21
4f		0.07353	0.06902	0.06827	1.07	1.01	-2.6101	-2.6734	-2.6843	-2.6559	6.448	1.038	1.08	-0.71
4g		0.07297	0.06863	0.06818	1.06	1.01	-2.6177	-2.6790	-2.6856	-2.6608	6.200	0.645	1.08	-0.81
4h		0.05289	0.05149	0.05047	1.03	1.02	-2.9395	-2.9664	-2.9864	-2.9641	2.703	1.976	1.05	-0.15
4i		0.05318	0.05143	0.05046	1.03	1.02	-2.9341	-2.9675	-2.9866	-2.9627	3.388	1.884	1.05	-0.27
4j		0.05792	0.05609	0.05547	1.03	1.01	-2.8487	-2.8808	-2.8919	-2.8738	3.234	1.103	1.05	-0.49
5a	312/90	0.08445	0.07791	0.07761	1.08	1.00	-2.4716	-2.5522	-2.5561	-2.5266	8.174	0.384	1.10	-0.91
5b		0.08479	0.08264	0.08133	1.03	1.02	-2.4676	-2.4933	-2.5092	-2.4900	2.598	1.583	1.04	-0.23
5c		0.08197	0.07709	0.07669	1.06	1.01	-2.5014	-2.5628	-2.5681	-2.5441	6.215	0.520	1.08	-0.84
5d		0.04986	0.04765	0.04685	1.05	1.02	-2.9985	-3.0439	-3.0608	-3.0344	4.586	1.663	1.07	-0.46
5e		0.07652	0.07510	0.07433	1.02	1.01	-2.5702	-2.5889	-2.5992	-2.5861	1.890	1.012	1.03	-0.29
5f		0.07989	0.07707	0.07641	1.04	1.01	-2.5271	-2.5630	-2.5716	-2.5539	3.623	0.844	1.05	-0.61
6a	304/86S	0.03490	0.03453	0.03410	1.01	1.02	-3.5530	-3.3659	-3.3785	-3.3666	1.093	1.496	1.02	0.08
6b		0.02748	0.02642	0.02621	1.04	1.01	-3.5943	-3.6336	-3.6416	-3.6232	3.968	0.807	1.05	-0.66
6c		0.08268	0.08073	0.07901	1.02	1.02	-2.4928	-2.5166	-2.5382	-2.5159	2.416	2.123	1.05	-0.05
6d		0.00218	0.00205	0.00199	1.06	1.03	-6.1284	-6.1899	-6.2196	-6.1793	5.942	2.859	1.10	-0.35
6e		0.00231	0.00218	0.00213	1.06	1.02	-6.0705	-6.1284	-6.1516	-6.1187	6.064	2.96	1.09	-0.43
6f		0.04718	0.04503	0.04348	1.05	1.04	-3.0538	-3.1004	-3.1355	-3.0966	4.471	3.420	1.09	-0.14
6g		0.04684	0.04535	0.04409	1.03	1.02	-3.0610	-3.0933	-3.1215	-3.0919	3.269	2.785	1.06	-0.07
6h		0.05189	0.04985	0.04846	1.04	1.03	-2.9586	-2.9987	-3.0270	-2.9948	4.072	2.779	1.07	-0.17
6i		0.05887	0.05242	0.05159	1.13	1.01	-2.8324	-2.9485	-2.9644	-2.9151	11.878	1.533	1.15	-0.76
33a	274/87N	0.00077	0.00076	0.00074	1.01	1.02	-7.1691	-7.1822	-7.2089	-7.1867	1.461	1.608	1.04	0.34
33b		.000072	0.00071	0.00070	1.03	1.01	-7.2363	-7.2502	-7.2644	-7.2503	1.988	1.334	1.03	0.01
33c		0.04685	0.04617	0.04525	1.02	1.02	-3.0608	-3.0754	-3.0956	-3.0773	1.482	1.978	1.04	0.16
33d		0.04719	0.04552	0.04900	1.04	1.01	-3.0536	-3.0896	-3.1033	-3.0822	3.661	1.352	1.05	-0.45
9	220/86N	0.04923	0.04668	0.04600	1.06	1.02	-3.0113	-3.0644	-3.0791	-3.0516	5.386	1.425	1.07	-0.57
10a	225/90	0.03282	0.03209	0.03168	1.02	1.01	-3.4167	-3.4392	-3.4521	-3.4360	2.264	1.294	1.04	-0.27

Appendix 2.1 (cont.)

Dyke No.	Strike/ Dip	K_1	K_2	K_3	K_1/K_2	K_2/K_3	η_1	η_2	η_3	η_m	L	F	P_i	T
10b		0.03696	0.03667	0.03599	1.01	1.02	-3.2979	-3.3050	-3.3245	-3.3094	0.803	1.841	1.03	0.41
10c		0.03474	0.03472	0.03401	1.00	1.02	-3.3599	-3.3604	-3.3811	-3.3671	0.059	2.057	1.02	0.95
11a	231/80N	0.04454	0.04347	0.04235	1.03	1.03	-3.1114	-3.1357	-3.1618	-3.1363	2.459	2.564	1.05	0.04
11b		0.07482	0.07304	0.07228	1.02	1.01	-2.5927	-2.6167	-2.6272	-2.6122	2.433	1.032	1.04	-0.39
11c		0.06660	0.06557	0.06391	1.02	1.03	-2.7091	-2.7246	-2.7503	-2.7280	1.577	2.537	1.04	0.24
12a	228/90	0.00063	0.00063	0.00062	1.00	1.01	-7.3657	-7.3701	-7.3811	-7.3723	0.449	1.100	1.02	0.43
12b		0.00018	0.00018	0.00017	1.02	1.07	-8.6226	-8.6405	-8.7041	-8.6557	2.012	6.274	1.09	0.56
12c		0.05090	0.05050	0.04933	1.01	1.02	-2.9779	-2.9858	-3.0092	-2.9910	0.799	2.327	1.03	0.50
13a	228/90	0.06291	0.06205	0.06038	1.01	1.03	-2.7661	-2.7797	-2.8071	-2.7843	1.396	2.700	1.04	0.33
13b		0.08200	0.07987	0.07931	1.03	1.01	-2.5010	-2.5274	-2.5344	-2.5209	2.648	0.691	1.04	-0.58
13c		0.08966	0.08780	0.08573	1.02	1.02	-2.4117	-2.4327	-2.4566	-2.4337	2.119	2.359	1.05	0.06
14a	321/80S	0.00514	0.00492	0.00489	1.05	1.01	-5.2713	-5.3155	-5.3206	-5.3024	4.467	0.502	1.06	-0.79
14b		0.00391	0.00383	0.00373	1.02	1.03	-5.5445	-5.5662	-5.5913	-5.5673	2.211	2.484	1.05	0.07
18a	270/90	0.08801	0.08447	0.08155	1.04	1.04	-2.4303	-2.4714	-2.5065	-2.4694	4.184	3.448	1.08	-0.08
18b		0.00031	0.00030	0.00030	1.01	1.01	-8.0887	-8.0985	-8.1051	-8.0974	0.837	0.686	1.02	-0.20
18c		0.00027	0.00025	0.00025	1.08	1.01	-8.2060	-8.2821	-8.2861	-8.2581	7.462	0.499	1.09	-0.90
18d		0.00897	0.00870	0.00854	1.03	1.02	-4.7143	-4.7440	-4.7625	-4.7403	2.993	1.832	1.05	-0.23
18e		0.00932	0.00912	0.00900	1.02	1.01	-4.6755	-4.6970	-4.7106	-4.6944	2.168	1.354	1.04	-0.22
18f		0.00020	0.00020	0.00020	1.01	1.01	-8.5122	-8.5272	-8.5374	-8.5256	1.323	1.177	1.03	-0.19
17	285/88N	0.00488	0.00482	0.00479	1.01	1.01	-5.3226	-5.3350	-5.3412	-5.3330	1.831	1.203	1.02	-0.33
16a	278/85S	0.01382	0.01354	0.01320	1.02	1.03	-4.2816	-4.3021	-4.3275	-4.3038	2.052	2.569	1.50	0.11
16b		0.01145	0.01132	0.01111	1.01	1.01	-4.4698	-4.4812	-4.4999	-4.4836	1.118	1.852	1.03	0.24
16c		0.01144	0.01128	0.01117	1.02	1.01	-4.4706	-4.4847	-4.4945	-4.4833	1.468	0.902	1.02	-0.18
15a	276/90	0.02071	0.02002	0.01997	1.03	1.01	-3.8770	-3.9110	-3.9135	-3.9006	3.425	1.249	1.04	-0.86
15b		0.02422	0.02398	0.02367	1.01	1.01	-3.7206	-3.7305	-3.7435	-3.7316	1.009	1.293	1.02	0.13
19	272/90	0.01727	0.01699	0.01666	1.02	1.02	-4.0588	-4.0753	-4.0947	-4.0763	1.671	1.889	1.04	0.08
23a	310/88S	0.05919	0.05888	0.05716	1.01	1.03	-2.8270	-2.8323	-2.8619	-2.8404	0.521	2.952	1.04	0.70
23b		0.01322	0.01288	0.01253	1.03	1.03	-4.3260	-4.3521	-4.3796	-4.3526	2.673	2.730	1.06	0.03
23c		0.01757	0.01701	0.01649	1.03	1.03	-4.0416	-4.0741	-4.1050	-4.0736	3.313	3.028	1.07	-0.03
23d		0.04930	0.04853	0.04699	1.02	1.03	-3.0098	-3.0256	-3.0578	-3.0311	1.588	3.184	1.05	0.34
22	308/88S	0.02929	0.02849	0.02791	1.03	1.02	-3.5305	-3.5582	-3.5788	-3.5558	2.802	2.009	1.05	-0.15

Appendix 2.1 (cont.)

Dyke No.	Strike/ Dip	K_1	K_2	K_3	K_1/K_2	K_2/K_3	η_1	η_2	η_3	η_m	L	F	P_i	T
24a	261/85S	0.01312	0.03098	0.02991	1.01	1.04	-3.4635	-3.4744	-3.5096	-3.4825	1.055	3.517	1.05	0.53
24b		0.02994	0.02918	0.02856	1.03	1.02	-3.5086	-3.5343	-3.5578	-3.5329	2.620	2.124	1.05	-0.09
24c		0.02079	0.02001	0.01943	1.04	1.03	-3.8734	-3.9115	-3.9409	-3.9086	3.857	2.899	1.07	-0.13
24d		0.02325	0.02270	0.02252	1.02	1.01	-3.7615	-3.7854	-3.7934	-3.7801	2.418	0.783	1.03	-0.50
25a	254/90	0.05530	0.05472	0.05282	1.01	1.04	-2.8950	-2.9056	-2.9407	-2.9138	1.078	3.462	1.05	0.54
25b		0.04123	0.03952	0.03892	1.04	1.02	-3.1886	-3.2309	-3.2462	-3.2219	4.300	1.511	1.06	-0.47
25c		0.00018	0.00018	0.00018	1.02	1.02	-8.6017	-8.6187	-8.6337	-8.6180	1.725	1.476	1.03	-0.06
25d		0.00019	0.00019	0.00019	1.02	1.01	-8.5674	-8.5855	-8.5952	-8.5827	1.818	0.951	1.03	-0.30
28a	298/88N	0.02423	0.02265	0.02150	1.07	1.05	-3.7202	-3.7886	-3.8397	-3.7825	6.922	5.037	1.13	-0.13
28b		0.02515	0.02314	0.02222	1.09	1.04	-3.6829	-3.7662	-3.8068	-3.7520	8.498	3.952	1.13	-0.34
28c		0.00021	0.00021	0.00021	1.02	1.02	-8.4481	-8.4696	-8.4842	-8.4674	2.163	1.449	1.04	-0.20
28d		0.02490	0.02368	0.02244	1.05	1.06	-3.6929	-3.7431	-3.7969	-3.7443	5.158	5.253	1.11	0.03
28e		0.02484	0.02449	0.02383	1.01	1.03	-3.6953	-3.7095	-3.7368	-3.7139	1.436	2.690	1.04	0.32
28f		0.02665	0.02654	0.02623	1.00	1.01	-3.6250	-3.6291	-3.6409	-3.6316	0.411	1.181	1.02	0.48
28g		0.02805	0.02447	0.02343	1.15	1.01	-3.5738	-3.7103	-3.7537	-3.6793	13.973	0.505	1.21	-0.52
27a	256/90	0.02600	0.02536	0.02465	1.03	1.03	-3.6497	-3.6746	-3.7030	-3.6757	2.559	2.788	1.05	0.07
27b		0.03416	0.03348	0.03271	1.02	1.02	-3.3767	-3.3968	-3.4201	-3.3979	2.020	2.316	1.04	0.07
27c		0.02839	0.02810	0.02679	1.01	1.05	-3.5617	-3.5720	-3.6197	-3.5845	1.062	4.723	1.06	0.65
27d		0.02532	0.02512	0.02414	1.01	1.02	-3.6762	-3.6841	-3.7239	-3.6947	0.821	3.920	1.05	0.67
27e		0.05556	0.05488	0.05412	1.01	1.01	-2.8903	-2.9026	-2.9116	-2.9032	1.241	1.392	1.03	0.06
26a	241/88S	0.02806	0.02745	0.02668	1.02	1.03	-3.5734	-3.5954	-3.6238	-3.5976	2.203	2.804	1.05	0.13
26b		0.02638	0.02566	0.02506	1.03	1.02	-3.6351	-3.6628	-3.6865	-3.6615	2.792	2.344	1.05	-0.08
26c		0.04980	0.04875	0.04462	1.02	1.09	-2.9997	-3.0211	-3.1093	-3.0434	2.265	8.634	1.12	0.61
26d		0.03397	0.03326	0.03051	1.02	1.09	-3.3823	-3.4034	-3.4898	-3.4251	2.172	8.449	1.12	0.61
26e		0.03947	0.03762	0.03575	1.05	1.05	-3.2322	-3.2802	-3.3312	-3.2812	4.913	4.975	1.10	0.03
29a	332/90	0.04418	0.04535	0.04284	1.02	1.01	-3.1195	-3.1126	-3.1031	-3.1503	1.698	1.387	1.03	-0.08
29b		0.03923	0.03871	0.03774	1.01	1.03	-3.2383	-3.2516	-3.2770	-3.2557	1.356	2.508	1.04	0.31
29c		0.04672	0.04370	0.04017	1.07	1.09	-3.0636	-3.1304	-3.2146	-3.1362	6.930	8.107	1.16	0.12
38a	297/86S	0.00562	0.00554	0.00540	1.01	1.03	-5.1814	-5.1958	-5.2214	-5.1995	1.407	2.654	1.04	0.28
38b		0.07276	0.07111	0.07072	1.02	1.01	-2.6210	-2.6435	-2.6490	-2.6379	2.273	0.543	1.03	-0.61

Appendix 2.1 (cont.)

Dyke No.	Strike/ Dip	K_1	K_2	K_3	K_1/K_2	K_2/K_3	η_1	η_2	η_3	η_m	L	F	P_i	T
38c		0.05131	0.05099	0.05026	1.01	1.01	-2.9699	-2.9761	-2.9905	-2.9789	0.631	1.428	1.02	0.39
39a	308/90	0.04126	0.03952	0.03892	1.04	1.02	-3.1879	-3.2309	-3.2462	-3.2217	4.300	1.511	1.06	-0.48
39b		0.03397	0.03326	0.03051	1.02	1.09	-3.3823	-3.4034	-3.4897	-3.4251	2.172	8.449	1.12	0.61
39c		0.03987	0.03762	0.03575	1.05	1.05	-3.2221	-3.2802	-3.3312	-3.2779	4.913	4.975	1.12	-0.07
39d		0.02423	0.02265	0.02155	1.07	1.05	-3.7202	-3.7876	-3.8374	-3.7817	6.922	5.037	1.02	-0.15
20a	264/90	0.03488	0.03382	0.03348	1.01	1.01	-3.3558	-3.3867	-3.3968	-3.3798	1.831	1.203	1.04	-0.51
20b		0.01382	0.01354	0.01320	1.02	1.03	-4.2816	-4.3021	-4.3275	-4.3038	2.051	2.569	1.05	0.11
20c		0.01145	0.01132	0.01111	1.01	1.01	-4.4698	-4.4812	-4.4999	-4.4836	1.118	1.852	1.03	0.24
20d		0.01144	0.01128	0.01117	1.02	1.01	-4.4706	-4.4847	-4.4945	-4.4833	1.468	0.902	1.02	-0.18
21a	283/80S	0.05487	0.05384	0.05331	1.01	1.01	-2.9028	-2.9217	-2.9316	-2.9187	1.831	1.203	1.03	-0.31
21b		0.05362	0.05334	0.05318	1.02	1.03	-2.9258	-2.9311	-2.9341	-2.9303	2.051	2.569	1.01	-0.27
21c		0.05125	0.05112	0.05101	1.01	1.01	-2.9710	-2.9736	-2.9757	-2.9735	1.118	1.852	1.00	-0.08
21d		0.05124	0.05108	0.05007	1.02	1.01	-2.9712	-2.9744	-2.9943	-2.9800	1.468	0.902	1.03	0.73
32a	323/90	0.08445	0.07792	0.07765	1.08	1.00	-2.4716	-2.5521	-2.5555	-2.5264	8.174	0.348	1.10	-0.92
32b		0.08459	0.08264	0.08133	1.03	1.02	-2.4699	-2.4933	-2.5092	-2.4908	2.598	1.583	1.04	-0.19
32c		0.08097	0.07709	0.07658	1.06	1.01	-2.5137	-2.5628	-2.5694	-2.5486	6.215	0.520	1.06	-0.76
41a	316/87N	0.00031	0.00030	0.00030	1.01	1.01	-8.0887	-8.0985	-8.1051	-8.0974	0.837	0.686	1.02	-0.20
41b		0.00027	0.00025	0.00025	1.08	1.01	-8.2060	-8.2821	-8.2861	-8.2581	7.462	0.499	1.09	-0.90
41c		0.00897	0.00870	0.00854	1.03	1.02	-4.7143	-4.7440	-4.7625	-4.7403	2.993	1.832	1.05	-0.23
41d		0.00932	0.00912	0.00900	1.02	1.02	-4.6755	-4.6977	-4.7106	-4.6944	2.168	1.354	1.04	-0.22
30a	058/90	0.04782	0.04716	0.04598	1.01	1.03	-3.0403	-3.0542	-3.0795	-3.0580	1.398	2.502	1.04	0.29
30b		0.04570	0.04454	0.04395	1.03	1.01	-3.0857	-3.1114	-3.1247	-3.1072	2.584	1.318	1.04	-0.32
30c		0.05420	0.05277	0.05168	1.03	1.02	-2.9151	-2.9418	-2.9627	-2.9399	2.693	2.060	1.05	-0.12
30d		0.04418	0.04345	0.04284	1.02	1.01	-3.1195	-3.1361	-3.1503	-3.1353	1.698	1.387	1.03	-0.08
1a	066/90	0.00018	0.00018	0.00018	1.02	1.02	-8.5962	-8.6187	-8.6337	-8.6162	1.725	1.476	1.04	-0.20
1b		0.00020	0.00019	0.00018	1.02	1.01	-8.5415	-8.5855	-8.6115	-8.5795	1.818	0.951	1.07	-0.26
2a	240/88S	0.02488	0.02368	0.02244	1.05	1.06	-3.6937	-3.7434	-3.7969	-3.7446	5.158	5.253	1.11	0.04
2b		0.02472	0.02449	0.02379	1.01	1.03	-3.7001	-3.7095	-3.7385	-3.7160	1.436	2.690	1.04	0.51
2c		0.02656	0.02654	0.02641	1.00	1.01	-3.6283	-3.6291	-3.6340	-3.6305	0.411	1.181	1.01	0.73
3a	245/85S	0.01382	0.01354	0.01321	1.02	1.03	-4.2816	-4.3021	-4.3275	-4.3038	2.051	2.569	1.5	0.11

Appendix 2.1 (cont.)

Dyke No.	Strike/ Dip	K_1	K_2	K_3	K_1/K_2	K_2/K_3	η_1	η_2	η_3	η_m	L	F	P_i	T
3b		0.01245	0.01232	0.01213	1.01	1.01	-4.3860	-4.3965	-4.4121	-4.3982	1.118	1.852	1.03	0.19
3c		0.01644	0.01628	0.01617	1.02	1.01	-4.1080	-4.1178	-4.1246	-4.1168	1.468	0.902	1.02	-0.18
8a	300/90	0.03488	0.03382	0.03348	1.01	1.01	-3.3558	-3.3867	-3.3968	-3.3798	1.831	1.202	1.04	-0.51
8b		0.02382	0.02354	0.02324	1.02	1.03	-3.7372	-3.7491	-3.7619	-3.7494	2.051	2.569	1.02	0.04
8c		0.02145	0.02132	0.02111	1.01	1.01	-3.8420	-3.8481	-3.8580	-3.8494	1.118	1.852	1.02	0.24
8d		0.02244	0.02128	0.02115	1.02	1.01	-3.7969	-3.8500	-3.8561	-3.8342	1.468	0.902	1.07	-0.79

N.B. The terms K_1, K_2, K_3, η_1, η_2, η_3, η_m, P_j and T are defined in Chapter 2.

Appendix 2.2: Direction of principal AMS axes

Dyke No.	K1 (maximum axis)		K2 (intermediate axis)		K3 (minimum axis)		Dyke Category
	Declination (degrees)	Inclination (degrees)	Declination (degrees)	Inclination (degrees)	Declination (degrees)	Inclination (degrees)	
4a	314.7	10.5	121.4	21.6	221.5	18.2	
4b	323.1	32.7	117.4	33.7	219.4	28.7	
4c	305.5	49.3	147.1	39.4	187.6	38.2	
4d	289.4	33.8	132.4	15.7	214.8	18.5	
4e	296.1	30.7	148.6	31.1	196.5	7.7	
4f	286.5	15.5	150.3	47.2	197.7	14.1	
4g	303.3	8.5	147.1	11.6	235.1	5.7	
4h	301.8	15.9	134.6	36.1	224.3	23.3	
4i	291.5	21.3	123.3	42.3	205.1	39.5	
4j	311.8	16.7	105.8	6.4	228.3	4.4	1
5a	318.8	17.6	140.3	23.1	228.3	11.1	
5b	303.4	8.5	117.9	29.8	218.8	42.5	
5c	304.1	26.8	136.9	23.7	233.0	21.5	
5d	299.7	20.5	144.4	23.8	212.2	25.9	
5e	320.8	10.6	142.9	12.9	205.3	3.3	
5f	294.1	11.8	137.3	36.5	228.7	4.9	1
13a	236.1	14.1	53.3	13.8	145.7	16.3	
13b	22.5	31.8	55.4	23.0	139.3	12.4	
13c	224.1	9.5	66.7	12.4	137.5	30.9	1
18a	285.0	88.5	76.6	29.6	357.4	14.2	
18b	227.1	78.1	96.5	24.8	6.2	28.3	
18c	296.5	87.4	77.0	44.9	16.1	16.4	
18d	276.6	74.8	86.4	10.8	9.1	9.8	1
24a	276.3	23.4	60.1	39.1	351.2	7.5	
24b	259.9	46.0	66.1	18.9	355.3	22.1	
24c	270.7	10.1	71.8	6.4	347.5	23.2	
24d	285.4	28.2	79.7	43.5	0.5	35.2	1
28a	304.2	12.1	104.2	47.3	218.4	18.3	
28b	306.3	23.9	110.4	51.0	201.6	41.3	
28c	286.9	4.1	126.3	33.1	200.7	26.1	
28d	294.8	7.1	141.9	21.2	226.3	12.1	
28e	291.1	17.2	135.5	42.4	180.5	10.3	
28f	284.8	9.2	110.5	42.3	195.4	9.5	
28g	300.3	7.3	95.7	28.0	225.4	22.8	1
41a	292.6	7.9	137.7	25.6	37.5	8.1	
41b	293.4	20.2	129.3	29.7	40.4	25.0	
41c	303.8	17.7	139.8	10.2	56.6	25.7	
41d	288.2	4.3	127.4	5.3	29.5	21.6	1
16a	293.7	17.7	117.8	36.4	10.6	7.6	
16b	282.9	30.4	108.9	14.7	5.5	19.3	
16c	272.4	19.6	120.7	17.2	16.3	242.5	1
10a	232.6	35.6	51.1	34.2	137.1	29.5	
10b	208.2	31.0	53.8	15.1	125.4	22.2	
10c	213.9	32.6	66.9	17.3	131.1	40.1	1
33a	285.3	26.9	88.3	29.3	358.6	11.7	
33b	268.5	45.5	101.1	14.3	16.7	26.4	
33c	257.2	29.7	107.2	37.3	188.5	5.1	
33d	252.6	41.2	113.9	12.8	205.1	9.5	1a

Dyke No.	K1 (maximum axis)		K2 (intermediate axis)		K3 (minimum axis)		Dyke Category
	Declination (degrees)	Inclination (degrees)	Declination (degrees)	Inclination (degrees)	Declination (degrees)	Inclination (degrees)	
25b	246.3	41.1	72.1	14.8	0.6	12.5	
25c	234.7	37.2	76.1	5.3	145.1	10.4	
25d	231.1	26.4	95.2	5.0	173.9	14.2	1a
21a	298.2	11.9	94.3	8.5	11.0	11.5	
21b	293.8	28.3	96.7	40.4	32.1	5.3	
21c	302.3	36.0	90.8	30.3	22.2	20.1	
21d	270.5	35.8	116.6	8.2	201.3	64.0	1a
32a	303.8	12.5	111.1	23.7	27.8	10.5	
32b	290.6	26.4	131.5	42.3	46.8	19.7	
32c	279.4	4.1	136.4	17.9	217.9	6.5	1a
38a	7.1	8.7	301.8	9.1	107.5	22.4	
38b	11.7	20.2	290.9	10.8	122.1	24.3	
38c	32.9	16.8	288.6	29.2	140.3	21.8	2
39a	216.2	11.6	308.0	25.7	109.8	22.9	
39b	191.9	14.2	313.3	5.6	104.8	9.1	
39c	208.9	7.7	318.3	21.7	103.2	9.4	
39d	192.4	17.8	321.0	33.4	124.7	29.8	2
14a	230.8	21.9	314.3	19.3	136.6	26.2	
14b	208.4	28.6	309.2	35.8	160.2	51.8	2
2a	323.1	10.7	223.8	5.6	58.9	3.7	
2b	332.6	30.7	220.0	25.4	58.2	23.8	
2c	311.8	34.2	241.7	15.1	78.4	8.2	2
3a	329.3	33.7	212.9	30.9	55.4	33.7	
3b	307.4	34.2	212.9	30.9	55.4	33.7	
3c	329.2	33.7	212.8	30.9	55.4	33.3	2
23a	31.8	14.5	320.5	12.2	119.8	38.2	
23b	36.9	35.1	298.6	9.8	146.8	51.2	
23c	229.3	38.7	297.9	34.8	149.3	37.6	
23d	204.1	41.7	304.2	6.6	142.7	10.5	2a
29a	58.7	6.5	315.6	17.3	157.8	12.3	
29b	236.1	13.3	323.9	25.8	156.4	29.1	
29c	217.9	4.9	314.7	8.4	164.9	24.1	2a
6a	309.6	9.0	123.1	19.3	234.1	10.6	
6b	68.7	78.8	115.9	68.4	191.2	12.8	
6c	320.9	36.7	148.2	25.4	231.5	32.9	
6d	328.1	58.2	142.4	41.1	239.7	2.6	
6e	136.4	7.1	308.7	17.8	210.5	22.3	
6f	116.2	13.5	304.2	14.7	207.4	26.7	
6g	298.1	61.5	124.6	33.7	200.2	41.7	
6h	139.1	35.9	317.6	44.2	228.9	11.9	
6i	111.8	51.8	263.3	70.1	228.9	11.4	3
26a	192.4	18.6	31.7	9.4	293.4	24.3	
26b	26.9	23.4	203.3	16.4	118.6	14.2	
26c	217.3	76.5	16.4	30.8	122.2	19.6	
26d	31.8	45.8	225.7	41.2	309.8	21.4	
26e	260.7	84.3	25.5	18.5	287.1	6.3	3
27a	273.1	86.1	109.4	0.3	10.1	10.8	
27b	264.8	14.3	107.5	72.4	196.3	21.4	
27c	103.2	21.8	283.4	38.6	182.9	12.3	

Dyke No.	K1 (maximum axis)		K2 (intermediate axis)		K3 (minimum axis)		
	Declination (degrees)	Inclination (degrees)	Declination (degrees)	Inclination (degrees)	Declination (degrees)	Inclination (degrees)	Dyke Category
27e	89.3	82.6	257.8	8.3	200.4	40.1	3
11a	207.4	18.6	357.4	86.1	124.5	38.1	
11b	20.2	38.6	258.4	63.7	116.3	19.4	
11c	30.7	8.3	276.5	83.4	130.6	18.7	3
12a	220.3	16.4	14.6	40.8	136.5	30.8	
12b	8.7	10.4	263.4	63.9	128.2	17.5	
12c	234.9	30.6	40.2	80.5	119.7	12.5	3
8a	103.2	6.1	321.8	80.6	119.4	12.5	
8b	88.6	85.1	273.2	14.6	210.3	29.5	
8c	319.4	48.2	86.3	41.5	193.5	20.8	
8d	283.6	18.4	116.3	50.4	221.3	30.8	3
9a	31.8	34.5	326.5	12.2	119.8	38.2	
9b	89.4	2.1	21.6	74.6	176.4	24.2	
9c	31.8	44.2	225.7	41.2	320.5	21.4	4
15a	85.4	82.6	257.8	12.5	204.1	40.1	
15b	247.3	18.7	357.4	86.1	124.8	37.4	4
20a	295.4	44.2	124.9	42.3	251.1	45.6	
20b	89.5	16.4	121.1	6.4	243.2	4.4	
20c	318.8	54.2	140.7	25.8	228.4	8.1	
20d	36.4	8.5	117.9	29.8	218.8	42.5	4
30a	147.2	35.8	320.1	87.4	5.6	11.7	
30b	18.7	51.8	263.3	70.1	217.2	14.6	
30c	191.5	18.7	35.4	47.4	114.2	24.5	
30d	277.4	23.5	213.5	16.9	114.8	24.6	4

N.B. Locations of individual dykes (as given by whole numbers in column 1) are shown in Figures 2.2 and 2.3.

Appendix A3: Relative Ar masses and ratios used in Ar-Ar dating

Sample	^{40}Ar	±	^{39}Ar	±	^{38}Ar	±	^{37}Ar	±	^{36}Ar	±
Fremington										
Frem.Ar1	9.050758	0.010730	0.138714	0.006917	0.064054	0.001703	1.607967	0.011556	0.007941	0.000225
Frem.Ar2	0.882206	0.016760	0.012253	0.000421	0.005006	0.001064	0.298993	0.008469	0.002051	0.000062
Frem.Ar3	3.825947	0.011636	0.079759	0.000480	0.001656	0.001061	0.046410	0.007533	0.003120	0.000144
Frem.Ar4	0.485583	0.007626	0.006534	0.000364	0.000983	0.001066	0.003434	0.007528	0.001082	0.000175
Frem.Ar5	0.261094	0.006290	0.002605	0.000252	0.000413	0.001053	0.000226	0.007548	0.000450	0.000219
Frem.Ar6	0.605615	0.008273	0.004633	0.001161	0.010057	0.001080	0.015893	0.007866	0.000664	0.000202
Frem.Ar7	0.611481	0.007057	0.013091	0.001004	0.008051	0.001107	0.042757	0.007574	0.000470	0.000175
Frem.Ar8	4.715285	0.030478	0.147739	0.001637	0.011381	0.001143	3.397509	0.013663	0.004470	0.000143
Lee Bay										
LB1-a	0.744414	0.013345	0.048218	0.000547	0.001920	0.001058	0.696355	0.008078	0.001605	0.000117
LB1-b	3.624999	0.006286	0.027498	0.002913	0.028094	0.001143	1.034951	0.008421	0.011540	0.000175
LB1-c	0.695082	0.012964	0.172267	0.001362	0.006228	0.001059	0.786665	0.008578	0.000751	0.000149
LB1-d	1.310037	0.009526	0.091535	0.001066	0.008061	0.001098	2.411138	0.008844	0.002508	0.000156
LB1-e	8.145397	0.020643	2.276974	0.008127	0.075226	0.001143	10.15319	0.032143	0.007467	0.000175
LB2-a	1.426116	0.008210	0.080026	0.001504	0.008947	0.001076	1.152613	0.008793	0.002934	0.000202
LB2-b	9.354474	0.008476	0.577374	0.003555	0.030630	0.001215	8.471997	0.021593	0.016813	0.000262
LB2-c	2.533265	0.018026	0.193799	0.002457	0.004578	0.001070	4.792935	0.050442	0.004188	0.000092
LB2-d	1.070748	0.010590	0.084052	0.000796	0.002317	0.001052	3.269122	0.018162	0.001900	0.000112
LB2-e	0.864862	0.011112	0.084068	0.000715	0.003377	0.001064	3.397783	0.020612	0.001550	0.000121
LB2-f	1.491741	0.009667	0.083948	0.001083	0.006075	0.001068	0.975102	0.007917	0.003041	0.000117
Horse-Shoe Rocks										
HSR1	10.355612	0.034861	0.243403	0.002476	0.027014	0.000939	1.725617	0.025736	0.005283	0.000523
HSR2	1.100754	0.003167	0.021302	0.001332	0.004303	0.000777	0.687239	0.023467	0.000713	0.000235
HSR3	2.821615	0.006904	0.044580	0.001045	0.021433	0.000825	1.013704	0.024573	0.003052	0.000312
HSR4	6.041925	0.014662	0.069588	0.001696	0.056874	0.000924	3.391520	0.030048	0.011488	0.000453

Sample	$^{40}Ar^*/^{39}Ar$	±	Age (Ma)	±	$^{39}Ar/^{40}Ar$	±	$^{36}Ar/^{40}Ar$	±
Fremington								
Frem.Ar1	48.331325	2.458339	367.18	16.96	0.015326	0.000764	0.000877	0.000025
Frem.Ar2	22.560217	2.190563	180.71	16.71	0.013889	0.000545	0.002324	0.000084
Frem.Ar3	36.409602	0.595647	283.32	4.43	0.020847	0.000141	0.000815	0.000038
Frem.Ar4	25.472290	8.121359	202.77	61.15	0.013457	0.000779	0.002224	0.000362
Frem.Ar5	49.181730	25.442816	373.01	174.32	0.009977	0.000994	0.001724	0.000384
Frem.Ar6	88.624080	25.750424	624.82	153.48	0.007652	0.000804	0.003193	0.000049
Frem.Ar7	36.101941	4.847301	281.08	34.96	0.021408	0.001665	0.000769	0.000286
Frem.Ar8	22.975663	0.435158	183.87	9.68	0.031332	0.000402	0.000948	0.000031
Lee Bay								
LB1-a	5.632996	1.079848	46.85	8.86	0.064774	0.001374	0.002149	0.000232
LB1-b	7.816323	2.066865	64.68	6.81	0.075864	0.000813	0.002038	0.000026
LB1-c	2.748393	0.266762	23.01	3.39	0.247837	0.005019	0.001079	0.000254
LB1-d	6.241204	0.517994	51.83	2.22	0.069872	0.000959	0.001908	0.000021
LB1-e	2.609151	0.026159	21.80	4.24	0.279541	0.001224	0.000916	0.000149
LB2-a	7.001459	0.757122	58.04	0.23	0.056115	0.000113	0.002055	0.000141
LB2-b	7.598396	0.143008	62.94	6.18	0.061722	0.000384	0.001797	0.000028
LB2-c	6.698033	0.188746	55.56	1.19	0.076502	0.001112	0.001650	0.000038
LB2-d	6.059338	0.416735	50.34	1.55	0.078498	0.001075	0.001774	0.000062
LB2-e	4.839360	0.446709	40.35	3.42	0.097205	0.001497	0.001792	0.000106
LB2-f	7.068874	0.847307	58.59	3.68	0.056275	0.001864	0.001863	0.000142
Horse-Shoe Rocks								
HSR1	36.130730	0.747356	281.29	5.51	0.000561	0.000051	0.023504	0.000252
HSR2	41.547426	4.169757	319.92	29.40	0.000663	0.000213	0.019353	0.001211
HSR3	42.080585	2.267975	323.68	16.23	0.001134	0.000111	0.015799	0.000373
HSR4	38.040942	2.149406	295.01	15.29	0.001901	0.000075	0.011518	0.000282

Appendix 4: Major and trace element concentrations and normative analyses.
Data for each area are presented in three blocks - major elements, trace elements and CIPW normative analyses.

Lundy Island:

Dyke	Bat 1	VC 1	BW 3	BW 4	BW 1	Land 1	Land 2
Grid Ref (SS)	12644471	13784516	132824655	13844651	13864659	14444342	14214349
SiO_2	52.23	42.55	46.04	45.52	45.86	46.53	46.12
TiO_2	1.578	2.922	2.384	3.308	3.107	1.431	1.364
Al_2O_3	16.53	13.83	15.68	14.04	14.84	18.74	15.76
Fe_2O_3	10.59	16.13	13.34	15.43	14.95	9.12	14.27
MnO	0.178	0.412	0.186	0.282	0.281	0.266	0.191
MgO	5.12	5.26	6.45	4.74	5.05	5.16	5.93
CaO	6.70	8.74	9.16	7.47	8.21	11.22	10.14
Na_2O	3.91	3.78	4.53	5.41	4.39	3.50	4.22
K_2O	1.42	0.47	0.38	0.78	0.57	0.58	0.31
P_2O_5	0.297	0.354	0.345	0.483	0.434	0.147	0.347
Loss on Ignition	1.64	5.36	2.22	3.32	2.79	3.05	3.75
Total	100.16	99.82	100.69	100.78	100.48	99.72	100.53
Rb	55.6	10.6	23.8	50.7	32.1	17.5	21.8
Sr	366	291	324	251	360	365	317
Y	65.4	49.3	40.2	60.4	54.4	34.4	39.6
Zr	264	263	217	344	301	224	248
Nb	15.2	13.8	12.9	20.9	18.3	11.9	12.4
Ba	199	148	147	169	210	104	169
Pb	4	3	3	3	4	2	3
Th	8	3	4	5	3	5	3
U	5	0	2	0	0	2	1
Sc	21	31	26	25	27	31	29
V	147	434	284	279	320	245	302
Cr	32	46	121	24	39	150	113
Co	56	45	49	35	40	34	46
Ni	92	38	70	21	34	68	71
Cu	35	83	91	56	65	85	88
Zn	72	104	78	88	87	60	73
Ga	19	21	20	22	20	19	19
Mo	0	0	0	0	0	0	0
As	12	2	6	2	1	0	5
S	954	934	1002	507	424	1041	895
Quartz	0.68	0	0	0	0	0	0
Orthoclase	8.57	2.99	2.33	4.78	3.47	3.57	2.35
Albite	33.83	23.45	25.84	30.53	30.78	22.6	25.31
Anorthite	23.88	20.75	22.01	12.18	19.82	35.1	22.67
Nepheline	0	5.84	7.17	9.18	4.16	4.45	6.27
Diopside	6.58	19.51	18.51	19.22	16.37	17.9	19.03
Hypersthene	18.88	0	0	0	0	0	0
Olivine	0	16.88	15.86	10.95	14.89	11.12	16.14
Magnetite	3.76	3.82	3.03	5.56	3.42	2.1	3.08
Ilmenite	3.06	5.94	4.65	6.52	6.11	2.83	4.52
Apatite	0.82	0.89	0.84	1.19	1.07	0.36	0.81
Fe3:Fe2 ratio	0.35	0.2	0.2	0.35	0.2	0.2	0.2
Total	100.07	100.08	100.07	100.1	100.09	100.03	100.07

Lundy Island (cont.):

Dyke	WG1	WG2	DK1	DK2	QB1	QB2
Grid Ref. (SS)	12874736	12874736	13144331	142514377	13934492	13924498
SiO_2	44.52	55.48	49.84	52.09	45.86	47.43
TiO_2	2.499	1.562	1.505	1.534	3.107	1.331
Al_2O_3	16.01	15.19	13.89	14.04	13.84	18.74
Fe_2O_3	14.78	9.42	8.61	8.94	15.95	9.12
MnO	0.314	0.152	0.249	0.234	0.281	0.266
MgO	7.47	4.85	1.82	2.18	5.05	5.16
CaO	8.56	7.00	10.96	9.54	8.31	11.22
Na_2O	3.43	3.18	3.79	3.50	4.39	3.50
K_2O	0.42	1.94	1.81	1.82	0.57	0.58
P_2O_5	0.268	0.281	0.189	0.192	0.434	0.147
Loss on Ignition	2.67	1.17	7.65	6.03	2.79	3.05
Total	100.92	100.22	100.30	100.10	100.31	99.72
Rb	8.7	51.2	76.6	83.3	32.1	17.5
Sr	284	230	286	260	360	365
Y	40.6	55.1	61.1	63.5	54.4	34.4
Zr	174	327	263	262	301	224
Nb	8.1	15.6	19.3	19.6	18.3	11.9
Ba	156	341	350	473	210	104
Pb	2	7	7	10	4	2
Th	2	10	17	18	3	5
U	1	0	3	3	0	2
Sc	29	29	34	32	27	31
V	303	201	254	259	320	245
Cr	56	64	134	137	39	150
Co	58	30	30	28	40	34
Ni	89	51	46	46	34	68
Cu	73	56	73	76	65	85
Zn	72	58	75	76	87	60
Ga	22	21	21	21	20	19
Mo	0	0	0	1	0	0
As	0	0	3	3	1	0
S	1228	393	207	257	424	1041
Quartz	0	6.82	0	4.57	0	0
Orthoclase	2.57	11.66	11.59	11.57	3.47	3.57
Albite	24.53	27.35	34.47	31.67	30.78	22.6
Anorthite	27.86	21.81	16.88	18.45	19.82	35.1
Nepheline	2.89	0	0	0	4.16	4.45
Wollastonite	0	0	4.18	0	16.37	17.9
Diopside	11.68	9.67	25.91	25.82		
Hypersthene	0	16.11	0	1.14	0	0
Olivine	21.61	0	0	0	14.89	11.12
Magnetite	3.36	2.95	3.24	3.32	3.42	2.1
Ilmenite	4.89	3.01	3.10	3.12	6.11	2.83
Apatite	0.66	0.68	0.48	0.49	1.07	0.36
Fe3:Fe2 ratio	0.20	0.20	0.20	0.20	0.2	0.2
Total	100.06	100.05	100.04	100.04	100.09	100.03

Lee Bay:

Dyke	CK21-B1	CK21-B2	CK21-B3	CK21-B4	CK21-B5	CK21-B6
Grid Ref. (SS)	47144683	47144683	47144683	47144683	47144683	47144683
SiO_2	43.75	44.22	45.70	45.57	45.11	44.99
TiO_2	2.588	2.281	2.668	2.541	2.760	2.778
Al_2O_3	16.08	16.53	15.97	16.30	15.99	16.71
Fe_2O_3	15.93	14.93	14.18	14.33	15.40	15.83
MnO	0.797	0.801	0.388	0.445	0.626	0.423
MgO	6.89	6.95	6.68	6.86	6.42	6.90
CaO	5.72	6.56	7.70	7.31	6.41	4.17
Na_2O	3.39	3.26	3.41	3.36	3.48	3.54
K_2O	0.62	0.53	0.57	0.55	0.62	0.66
P_2O_5	0.447	0.388	0.452	0.423	0.457	0.469
Loss on Ignition	4.43	4.05	2.67	3.06	3.45	4.27
Total	100.64	100.50	100.39	100.75	100.72	100.74
Rb	9.8	8.9	9.4	8.3	10.8	11.3
Sr	217	225	233	231	228	211
Y	39.9	34.5	40.4	38.5	39.8	41.7
Zr	253	219	256	238	263	263
Nb	13.3	11.4	12.1	12.7	12.9	14.2
Ba	185	136	170	167	183	203
Pb	5	2	2	3	3	3
Th	3	2	1	1	1	1
U	1	0	0	1	2	0
Sc	43	37	37	38	41	45
V	332	293	334	317	342	339
Cr	147	149	168	184	206	161
Co	70	69	61	63	66	71
Ni	95	106	82	89	86	99
Cu	91	80	93	87	96	95
Zn	108	98	105	97	112	128
Ga	20	19	21	21	19	19
Quartz	0	0	0	0	0	0
Corundum	0.42	0	0	0	0	4.08
Orthoclase	3.84	3.29	3.47	3.35	3.83	4.15
Albite	30.21	28.98	29.90	29.48	30.70	32.59
Anorthite	27.17	30.37	27.55	28.81	27.26	18.77
Nepheline	0	0	0	0	0	0
Diopside	0	1.17	7.64	5.10	2.54	0
Hypersthene	5.57	5.19	4.09	5.79	6.87	21.30
Olivine	22.70	22.09	17.83	18.24	18.75	9.78
Magnetite	3.70	3.47	3.25	3.29	3.55	3.36
Ilmenite	5.18	4.55	5.25	5.00	5.46	5.53
Apatite	1.12	0.96	1.11	1.04	1.13	1.16
Fe3:Fe2 ratio	0.20	0.20	0.20	0.20	0.20	0.20
Total	100.10	100.09	100.09	100.09	100.10	100.10

Lee Bay (cont.):

Dyke	CK30-A	CK30-B	CK30-C	CK30-D	CK30-E
Grid Ref. (SS)	47124685	47124685	47124685	47124685	47124685
SiO_2	43.32	44.09	43.26	43.52	42.96
TiO_2	2.726	2.533	2.396	2.636	2.616
Al_2O_3	16.91	16.69	16.46	17.22	16.70
Fe_2O_3	15.14	14.09	15.92	16.61	16.99
MnO	0.604	0.340	0.558	0.592	0.358
MgO	6.86	7.15	7.41	6.39	8.05
CaO	5.43	7.13	5.85	4.73	3.54
Na_2O	3.37	3.34	3.15	3.39	3.12
K_2O	0.64	0.58	0.54	0.62	0.65
P_2O_5	0.492	0.425	0.406	0.451	0.546
Loss on Ignition	4.84	4.17	4.46	4.76	4.72
Total	100.33	100.54	100.41	100.92	100.25
Rb	10.5	10.6	9.5	9.9	10.1
Sr	229	237	226	233	181
Y	44.2	36.1	34.2	35.4	46.5
Zr	261	242	226	251	253
Nb	13.2	13.6	11.4	12.8	13.2
Ba	202	174	161	186	196
Pb	1	2	2	2	4
Th	2	4	1	3	1
U	0	0	0	0	1
Sc	44	44	37	43	45
V	350	325	316	342	331
Cr	165	216	191	162	161
Co	66	65	67	68	73
Ni	82	92	94	97	90
Cu	94	87	83	93	93
Zn	96	90	89	95	103
Ga	21	20	19	20	19
Quartz	0	0	0	0	0
Corundum	1.97	0	0.98	3.53	5.96
Orthoclase	4.01	3.59	3.36	3.84	4.08
Albite	30.27	29.73	28.15	30.31	28.01
Anorthite	25.54	30.29	28.17	21.97	15.27
Nepheline	0	0	0	0	0
Wollastonite	0	0	0	0	0
Diopside	3.50	0	0	0	0
Hypersthene	8.56	0.19	7.64	14.45	24.22
Olivine	19.46	23.41	22.23	15.71	11.92
Magnetite	3.55	3.27	3.72	3.88	3.99
Ilmenite	5.50	5.05	4.81	5.25	5.28
Apatite	1.24	1.06	1.02	1.13	1.38
Fe3:Fe2 ratio	0.20	0.20	0.20	0.20	0.20
Total	100.01	100.09	100.09	100.10	100.11

Fremington Dyke:

Dyke	Frem 1	Frem 2	Frem 3	Frem 4	Frem 12	Frem 23
Grid Ref. (SS)	52073466	52073466	52073466	52073466	52073466	52073466
SiO_2	39.45	38.56	39.59	41.21	39.57	39.42
TiO_2	2.118	2.198	2.244	2.161	2.157	2.217
Al_2O_3	10.85	11.12	11.27	11.03	11.07	11.27
Fe_2O_3	10.56	11.18	10.93	10.15	10.83	11.19
MnO	0.209	0.213	0.205	0.199	0.211	0.212
MgO	6.01	6.28	6.08	5.67	6.18	6.31
CaO	12.67	12.66	12.14	12.16	12.83	12.69
Na_2O	3.26	3.27	3.29	3.33	3.28	3.53
K_2O	0.30	0.30	0.31	0.33	0.31	0.31
P_2O_5	0.514	0.548	0.552	0.531	0.540	0.561
Loss on Ignition	14.08	13.95	13.41	13.05	13.74	13.64
Total	99.92	100.28	100.02	99.82	100.7	100.34
Rb	6.0	6.3	6.1	7.1	6.7	6.7
Sr	894	894	886	893	893	895
Y	25.1	25.6	25.2	24.6	25.0	25.3
Zr	212	217	221	221	219	217
Nb	52.9	54.9	55.2	53.8	52.9	55.1
Ba	330	302	313	326	321	324
Pb	5	5	7	5	7	7
Th	6	10	8	7	6	8
U	0	4	0	2	0	4
Sc	20	23	24	20	21	23
V	237	249	247	230	243	244
Cr	336	335	350	332	334	341
Co	33	25	33	41	33	36
Ni	203	216	210	204	207	207
Cu	73	76	75	63	75	78
Zn	30	32	32	30	31	33
Ga	19	20	20	19	21	21
Mo	1	1	2	1	1	2
As	11	11	9	11	9	8
S	960	894	959	1103	918	951
Orthoclase	2.09	2.09	2.15	2.27	2.19	2.14
Albite	10.62	7.63	12.67	17.75	14.52	11.49
Anorthite	16.57	17.29	17.57	16.49	16.53	15.67
Nepheline	11.85	13.44	10.74	8.17	8.54	11.64
Diopside	44.03	42.92	40.03	40.94	43.21	43.82
Olivine	6.03	7.45	7.64	5.65	6.53	7.31
Magnetite	2.75	2.90	2.82	2.61	2.81	2.71
Ilmenite	4.73	4.89	4.97	4.78	4.74	4.86
Apatite	1.43	1.52	1.53	1.46	1.42	1.42
Fe3:Fe2 ratio	0.2	0.2	0.2	0.2	0.2	0.2
Total	100.11	100.12	100.12	100.11	100.10	100.11

Horse-Shoe Rocks:

Sample	HSR1	HSR2	HSR3	HSR4	HSR3A	HSR4A
Grid Ref. (SS)	454503	454503	454503	454503	454503	454503
SiO_2	46.80	46.60	46.98	46.56	47.12	46.43
TiO_2	1.133	1.134	1.133	1.156	1.139	1.146
Al_2O_3	16.10	16.57	16.18	16.60	16.47	16.54
Fe_2O_3	10.43	10.98	10.36	10.43	10.34	10.53
MnO	0.164	0.159	0.170	0.166	0.169	0.164
MgO	8.79	8.86	8.71	8.68	8.78	8.63
CaO	8.59	7.61	9.17	8.90	9.13	8.60
Na_2O	3.84	3.89	3.56	3.56	3.50	3.55
K_2O	0.41	0.40	0.43	0.45	0.43	0.46
P_2O_5	0.092	0.103	0.091	0.097	0.094	0.100
Loss on Ignition	4.18	3.92	3.59	3.98	3.91	3.92
Total	100.53	100.37	100.37	100.58	101.08	100.08
Rb	8.2	8.9	9.2	9.6	9.2	9.3
Sr	179	182	174	169	179	173
Y	21.3	21.7	21.2	21.8	22.1	22.2
Zr	71	72	70	70	73	77
Nb	3.3	3.4	2.8	3.5	2.8	3.5
Ba	134	139	143	149	138	150
Pb	5	3	10	5	8	5
Th	1	0	0	3	1	2
Sc	32	34	32	25	27	28
V	215	216	204	193	198	195
Cr	307	294	299	274	261	247
Co	45	50	51	45	53	47
Ni	148	149	146	148	154	149
Cu	87	85	92	80	92	83
Zn	118	120	112	118	115	118
Ga	16	18	16	18	18	18
As	10	12	13	10	10	11
S	139	193	212	128	170	128
Orthoclase	2.56	2.75	2.62	2.80	2.74	2.76
Albite	27.78	29.86	26.91	26.54	26.15	27.34
Anorthite	26.66	27.70	26.66	29.19	28.41	27.85
Nepheline	3.41	2.48	3.41	2.69	3.27	3.16
Diopside	14.12	9.12	15.26	13.25	12.67	11.92
Olivine	20.58	22.88	19.86	20.60	21.59	22.06
Magnetite	2.42	2.54	2.39	2.41	2.40	2.36
Ilmenite	2.25	2.45	2.23	2.29	2.34	2.31
Apatite	0.24	0.24	0.24	0.24	0.25	0.26
Fe3:Fe2 ratio	0.20	0.20	0.20	0.20	0.20	0.20
Total	100.02	100.02	100.02	100.02	100.02	100.02

N.B. All major and trace element analyses were obtained in three separate XRF batch runs. All trace element data have been normalised using standard reference materials at the Open University in order to obtain parity between discrete data sets. However, the values for Th, Pb and U are very low and probably unreliable when analysed by XRF apparatus. Alternatively, all major element data values are within ± 0.5% of a calibrated reference material and have thus not been corrected.

Appendix 5: Rare earth element concentrations for the Lee Bay samples

Dyke	CK21B-B2	CK21B-B6	CK30-A	CK30-B	WS	WS (expected value)
La	12.4	14.4	15.3	12.9	25.8	25.4
Ce	26.7	32.6	33.8	28.3	55.4	55.6
Nd	21.4	23.2	25.5	20.1	30.7	31.7
Sm	5.40	6.39	6.67	5.62	7.15	6.85
Eu	2.08	2.37	2.51	2.11	2.12	2.10
Tb	1.00	1.19	1.23	1.01	1.07	1.04
Yb	2.87	3.45	3.57	3.07	2.52	2.48
Lu	0.36	0.48	0.55	0.59	0.36	0.36
Th	1.20	1.47	1.48	1.32	2.81	2.92
Ta	0.63	0.77	0.76	0.70	1.19	1.17
Hf	4.88	5.94	5.61	5.31	4.81	4.79
Cs	0.30	0..39	0.54	0.35	1.16	1.08
Rb	22	15	21	29	38	33.6
Zn	99	122	101	95	107	-
Co	54.8	49.9	48.7	48.5	47.5	-
Cr	138	149	145	139	75	-
Sc	33.4	40.2	39.2	36.6	29	-
Na_2O	3.15	3.52	3.23	3.18	2.73	2.64
Fe_2O_3	14.36	14.97	14.55	13.38	13.5	-
MnO	0.16	0.17	0.16	0.15	0.15	-

N.B. Sample WS is a control sample (Whin Sill dolerite) used in the INAA apparatus at the Open University. The expected values of WS were derived from the average of 25 different analyses carried out in 1991. Zn, Co, Cr, Sc, Fe_2O_3 and MnO were not analysed at that time and so the precision of WS values for these components is unknown, but is probably within acceptable limits for the apparatus (N.Rogers, pers. comm.). Locations of dykes CK21 and CK30 are given in Figure 2.7. Samples CK21B-B2 and CK30-A were taken from dyke margins, whereas samples CK21B-B6 and CK30-B were taken from the centre of the same dykes.